NASA CR-144912

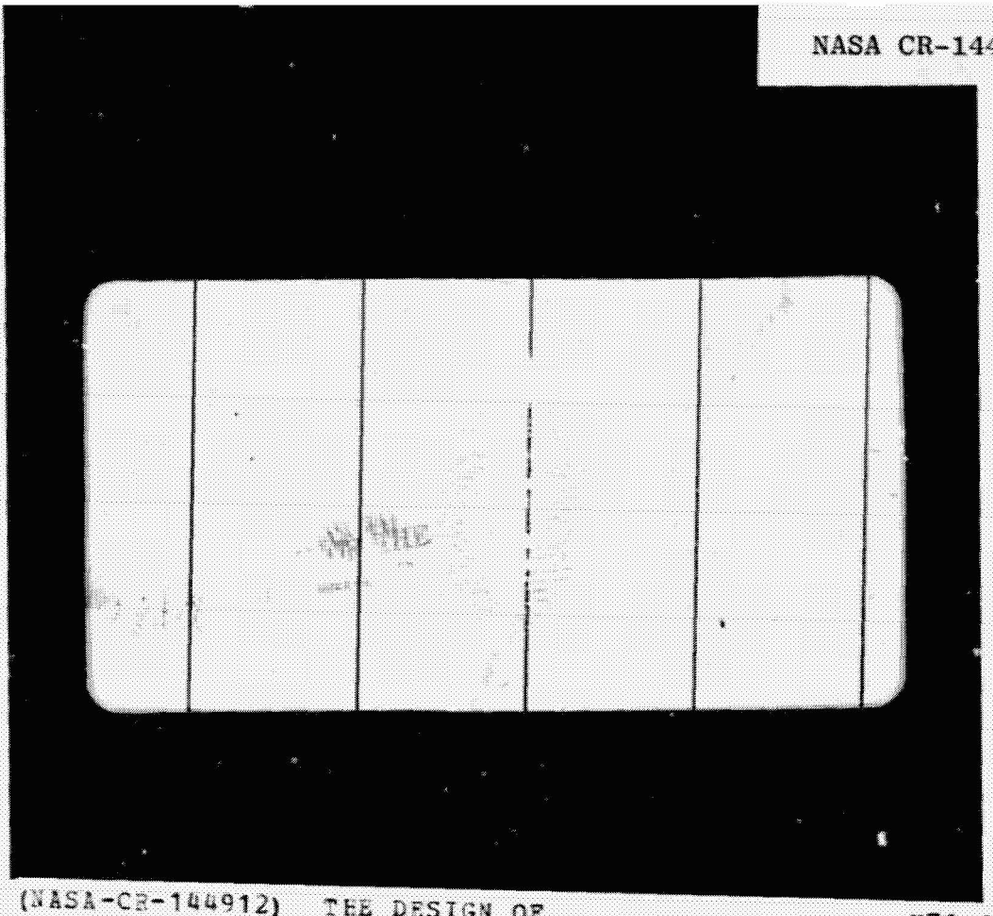

(NASA-CR-144912) THE DESIGN OF DIGITAL-ADAPTIVE CONTROLLERS FOR VTOL AIRCRAFT Final Report, 3 Mar. - 15 Nov. 1975 (Analytic Sciences Corp.) 28[illegible] p HC $9.25 CSCL 01C G3/08

N76-21215

Unclas 21515

NASA CR-144912

TR-640-1

THE DESIGN OF DIGITAL-ADAPTIVE CONTROLLERS FOR VTOL AIRCRAFT

12 March 1976

Prepared for:

NATIONAL AERONAUTICS AND SPACE ADMINISTRATION
Langley Research Center
Hampton, Virginia 23365

Prepared by:

Robert F. Stengel
John R. Broussard
Paul W. Berry

Approved by:

E. Wayne Vinje
Arthur Gelb

THE ANALYTIC SCIENCES CORPORATION
Six Jacob Way
Reading, Massachusetts 01867

FOREWORD

The investigation described in this report was performed by TASC during the period from March 3, 1975 to November 15, 1975 under Contract No. NAS1-13807 for the National Aeronautics and Space Administration. The Navigation and Guidance Research Branch of the Flight Instrumentation Division sponsored this work as a contribution to the VTOL Approach and Landing Technology (VALT) Program. Dr. David R. Downing served as Technical Monitor for this contract.

The study was directed by Dr. Robert F. Stengel of TASC. Engineering investigation was conducted by Mr. John R. Broussard and Mr. Paul W. Berry, who were assisted in computer program development by Mr. James Y. Nalbandian. Dr. Michael Athans, Professor of Electrical Engineering at the Massachusetts Institute of Technology (MIT), served as principal technical consultant. Dr. Nils R. Sandell, Jr., Assistant Professor of Electrical Engineering at MIT, also provided consulting assistance.

THE ANALYTIC SCIENCES CORPORATION

Six Jacob Way, Reading, MA 01867 tel 617-944-6850

9 April 1976

National Aeronautics and Space
Administration
Langley Research Center
Hampton, Virginia 23365

Attention: Report & Manuscript Control Office
Mail Stop 180A

Subject: Delivery of Data Item

Reference: Contract No. NAS1-13807
TASC No. J-640

Gentlemen:

In accordance with the requirements of the referenced contract The Analytic Sciences Corporation is pleased to deliver one (1) copy of the contract final report, NASA CR-144912, Data Item 7.

Very truly yours,

THE ANALYTIC SCIENCES CORP.

David E. Miller
Contract Administrator

DEM/sab

Enclosure (1)

cc: NASA/LRC
ATTN: Dr. David Downing
Mail Stop 494

DCASD, Boston (letter only)
666 Summer Street
Boston, Massachusetts 02210
ATTN: Mr. Charles E. Coveney
Code: DCRB-DBCN B4

ABSTRACT

Design procedures for VTOL automatic control systems have been developed and are presented in this report. Using linear-optimal estimation and control techniques as a starting point, digital-adaptive control laws have been designed for the VALT Research Aircraft, a tandem-rotor helicopter which is equipped for fully automatic flight in terminal area operations. These control laws are designed to interface with velocity-command and attitude-command guidance logic, which could be used in short-haul VTOL operations of the 1980's. Developments reported here include new algorithms for designing non-zero-set-point digital regulators (command response control systems), design procedures for rate-limited systems, and algorithms for dynamic control trim setting.

TABLE OF CONTENTS (Continued)

LIST OF FIGURES

LIST OF FIGURES (Continued)

LIST OF TABLES

LIST OF TABLES (Continued)

LIST OF SYMBOLS

VARIABLES	DESCRIPTION
A	• Gain matrix for control-rate-weighted PI servo • Gram matrix
a	• Inverse of a time constant • Dependent variable in a regression analysis • Accelerometer output
$\underline{a}$	Aircraft parameter vector
$\underline{b}$	• Parameter identification coefficients • Regression coefficient vector
CAS	Calibrated air speed
D	• Distance to go • Transfer function denominator
E	Gain matrix for PI servo
e	2.71828.....
F	Fundamental matrix (continuous-time system)
$\underline{f}$	• Nonlinear functions for vehicle equations of motion • Parameter identification functions
G	Control effect matrix (continuous-time system)
g	Gravitational acceleration
H	• Transformation matrix • Observation matrix
H_E^B	Transformation from earth-relative to body-axis coordinates
h	Vertical height

LIST OF SYMBOLS (Continued)

VARIABLES	DESCRIPTION
I	Identity matrix
IAS	Indicated Airspeed
J	Scalar cost function (or functional)
K	Gain matrix
L	• Disturbance effect matrix (continuous-time system) • Roll moment • Kalman filter gain
L_B	Transformation from Euler rates to body rates
M	Pitch moment
m	Dimension of control vector
$\underline{m}$	Measurement vector for gain adaptation
NGC	Navigation, guidance, and control
N	• Yaw moment • Transfer function numerator
n	Dimension of state vector
$\underline{n}$	White gaussian noise
P	• State covariance matrix • Riccati equation solution
PI	Proportional-integral
PII	Proportional-double integral
P.O.	Percentage overshoot
p	• Roll rate • Dimension of command vector
Q	State weighting matrix

LIST OF SYMBOLS (Continued)

VARIABLES	DESCRIPTION
q	• Dynamic pressure • Pitch rate
R	Control weighting matrix
r	Yaw rate
SAS	Stability augmentation system
S	Terminal state weighting matrix
S	Laplace operator (continuous-time system)
T	Transformation matrix
T_r	Rise time
T_s	Settling time
TAGS	Tactical Aircraft Guidance System
t	Time
U	Control covariance matrix
u	x-axis velocity
$\underline{u}$	Control vector
V	• Total velocity • Command velocity component (with subscript)
v	y-axis velocity
VALT	VTOL Approach and Landing Technology
VTOL	Vertical Takeoff and Landing
W	Disturbance covariance matrix
w	z-axis velocity
$\underline{w}$	Disturbance vector

LIST OF SYMBOLS (Continued)

VARIABLES	DESCRIPTION
X	Axial force
x	Axial position
$\underline{x}$	State vector
Y	Lateral force
y	Lateral position
$\underline{y}$	• Observation vector • Guidance-command vector (with subscript)
z_1	• Normal force • Attitude guidance command
z	• Normal position • Laplace operator (discrete-time)
$\underline{z}$	Measurement vector

VARIABLES (Greek)

β	Sideslip angle
Γ	Control effect matrix (discrete-time system)
γ	• Vertical flight path angle • Interpolation variable
δ	• Control displacement • Impulse function
ε	Control or guidance error
η	Azimuth angle of destination or waypoint
θ	• Pitch attitude angle • Vector of state variances
$\underline{\lambda}$	Adjoint vector

LIST OF SYMBOLS (Continued)

VARIABLES (Greek)	DESCRIPTION
μ	Wind direction
$\underline{\mu}$	Trim setting vector
ν	Observation noise variable
Ξ	Discrete process noise covariance matrix
ξ	• Horizontal flight path angle • Vector of noise variances
Σ	Summation
σ	Standard deviation
τ	• Time constant • Integration dummy variable
Υ	Discrete observation noise covariance matrix
Φ	State transition matrix (discrete-time fundamental matrix)
ρ	Correlation coefficient
ϕ	Roll attitude angle
χ	Discrete process noise covariance matrix
ψ	Yaw attitude angle
$\tilde{\omega}$	Rotational cross-product matrix
ω	• Frequency • Process noise variable

SUBSCRIPTS

a	Accelerometer measurement
B	Differential collective
b	Barometric rate-of-climb measurement

LIST OF SYMBOLS (Continued)

SUBSCRIPTS	DESCRIPTION
C	Gang collective
c	Command value
d	Desired value
E	Earth-relative
f	Final
go	Measured from final value (as t_{go} = time to go)
H	Horizontal
i	Element index for vectors and matrices
j	Element index for vectors and matrices
k	Sampling instant index
m	Measured value
N	Terminal sampling instant
n	Observation noise
p	Roll rate
q	Pitch rate
R	Differential lateral cyclic
r	• Yaw rate • Learning system parameter estimate • Radar measurement
S	Gang lateral cyclic
T	Total value
u	• Control vector gain matrix • x-axis velocity
v	• Integrated error vector gain matrix • y-axis velocity

LIST OF SYMBOLS (Continued)

SUBSCRIPTS	DESCRIPTION
w	• Wind • z-axis velocity
x	State vector gain matrix
z	Vertica
θ	Pitch attitude angle
μ	Trim effect matrix
ν	Observation noise
ϕ	Roll attitude angle
ψ	Yaw attitude angle
ω	Process noise
0	Nominal value

SUPERSCRIPTS	
j	Transfer function numerator index
T	Transpose of matrix
-1	Inverse of matrix

PUNCTUATION	
$(\dot{\ })$	Derivative of quantity with respect to time
$(\_)$	Vector quantity
$(\bar{\ })$	• Augmented quantity • Mean value
$\partial(\ )/\partial(\ )$	Partial derivative of one variable with respect to another
$\Delta(\ )$	Perturbation variable

LIST OF SYMBOLS (Continued)

PUNCTUATION	DESCRIPTION
$(\tilde{\ })$	• Error state • Model system quantity
$(\ )^*$	Reference, nominal, optimal or trim value
$(\hat{\ })$	Estimated quantity
E( )	Expected value of variable
cov( )	Covariance of variable

1. INTRODUCTION

1.1 BACKGROUND

Vertical Take-Off and Landing (VTOL) aircraft are able to operate from small landing areas and in the vicinity of natural and man-made obstacles which would prevent the operations of conventional aircraft. This capability can be used only if navigational information is adequate to identify safe and efficient flight paths, if guidance strategies can keep the vehicle on its intended path, and if control laws stabilize the vehicle and provide satisfactory response to guidance commands throughout the flight envelope. To perform these functions in all weather and with aircraft whose unaugmented flying qualities may be marginal (due to turbulence, low airspeed, steep flight paths, and/or configuration design), some degree of automatic control is required. Fully integrated navigation, guidance, and control can ease the air crew's workload, allowing more time to conduct the executive functions of mission management which are crucial to efficiency, safety, and on-time performance.

Digital systems employing adaptive concepts can be of great value in achieving the improvements in VTOL flight controls that are necessary for future operations. Digital logic facilitates many features which are desirable in advanced control systems -- e.g., branching, mode switching, gain changing, multi-loop closures, integration, multiplication, and division -- and digital control laws are readily interfaced with navigation and guidance logic. Flexibility

for design, testing, and service modification is ummatched by a comparable analog system, which is fixed once its components and circuit connections are defined. The control system's ability to adapt to dynamic variations is particularly important for VTOL aircraft, which may undergo configurational changes as well as large flight-condition variation during hover/cruise transitions.

The purpose of this investigation is to develop digital control design procedures for VTOL aircraft and to demonstrate the utility of these methods by application to a specific vehicle, the CH-47B Research Aircraft of the NASA VTOL Approach and Landing Technology (VALT) Program.

Significant features of the VTOL digital control design process, which are addressed in this report using modern estimation and control methods, include:

- Unified design of multi-input/multi-output command-response systems
- Design of discrete-time controllers to continuous-time specifications
- Selection of digital sampling interval
- Design for rate-and displacement-limited actuators
- Explicit adaptation to flight condition and vehicle configuration
- Feed-forward of dynamic trim settings for quickened response
- Links between classical response criteria and modern design techniques
- Direct evaluation of control system response on time-varying flight paths

The following sections of this chapter review the project structure, summarize its results, and outline the organization of this report.

1.2 PROJECT STRUCTURE

The VTOL Approach and Landing Technology (VALT) Program of the National Aeronautics and Space Administration is developing a technology base for the navigation, guidance, control, display, and flight management requirements of VTOL short-haul transportation systems in the 1980's time period. This program requires the development of a navigation, guidance, and control (NGC) system that permits automatic flight along complex four-dimensional (space and time) mission profiles from takeoff to landing under all weather conditions. Flight tests will be conducted at the NASA Wallops Flight Center using a CH-47B Research Aircraft, as shown in Fig. 1.2-1. This helicopter will contain standard air data sensors and gyroscopic instruments for control system measurements. Control logic will be executed in a digital flight computer, and control commands will be transmitted to the helicopter's mechanical control linkages by hydraulic actuators.

The VALT Research Aircraft, a tandem-rotor medium transport helicopter, provides a good baseline for NGC demonstration and evaluation. Its size is representative of future passenger-carrying VTOL aircraft, and its climb and descent performance is adequate for terminal-area operational studies. Prior use of this aircraft in the United States Army's Tactical Aircraft Guidance System (TAGS) program provides flight test results for comparison and flight-rated equipment for application to this NASA research.

The present investigation contributes to VALT Program objectives and has been organized to provide both theoretical and practical results to aid the design of

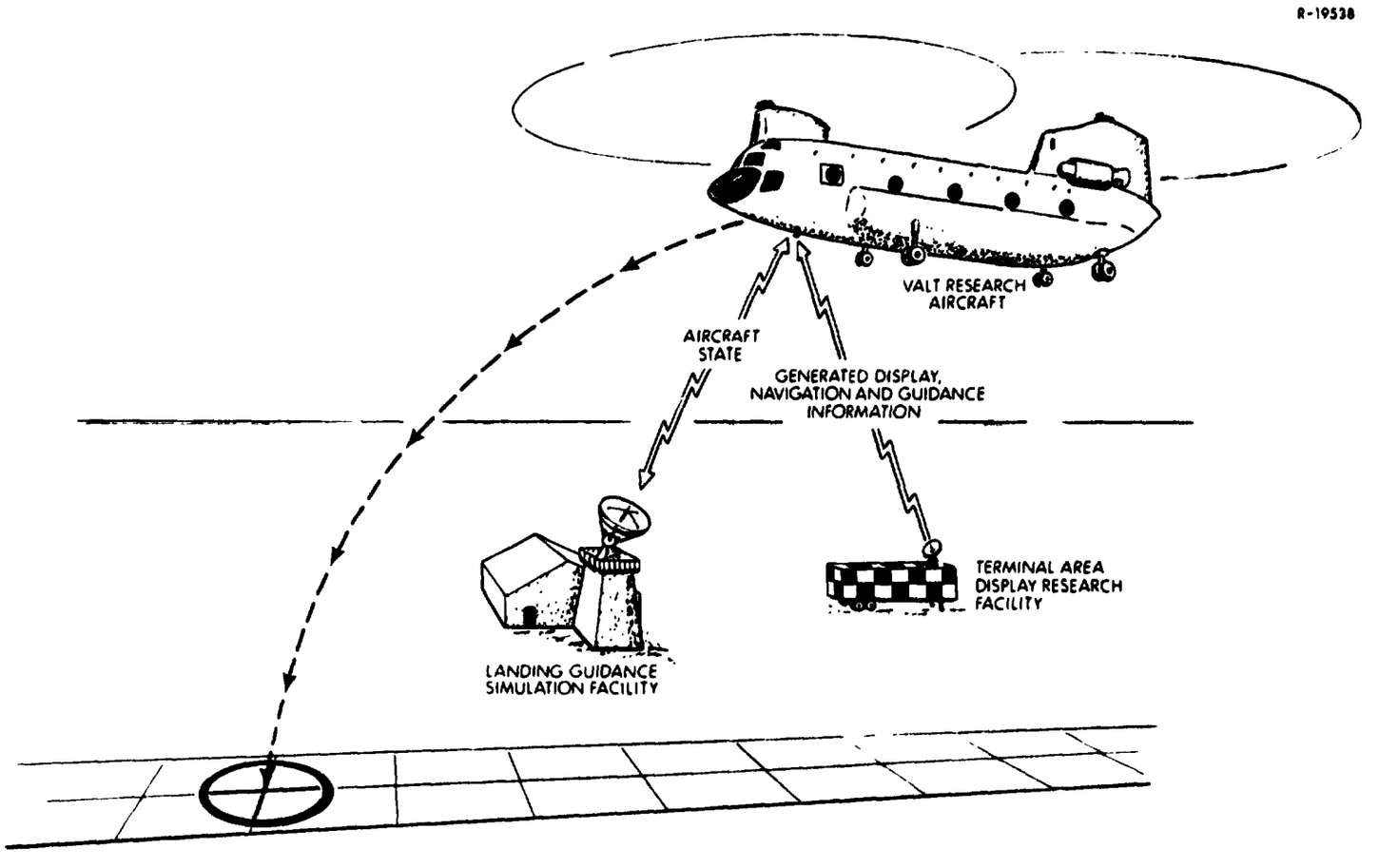

Figure 1.2-1 VALT Integrated Flight Test Facilities

fully automatic VTOL navigation, guidance, and control systems. In the course of this work, new techniques have been developed for the design of analog and digital set-point regulators, and a powerful method for explicit adaptation of control gains to predictable variations in system dynamics has been demonstrated. The latter is an extension of conventional gain scheduling techniques which does not require (but is aided by) prior knowledge of the parameter sensitivity of the system to be controlled. The design procedure is particularly valuable for identifying the control law structure required for good system response (including beneficial crossfeeds and feed-forward loops) at an early stage of the design process. By using optimal control theory, system stability margins are assured from the outset, and attention can be centered on command response and disturbance rejection. Sampling intervals of the digital system can be chosen on the basis of system performance, and the "proportional-integral" nature of the discrete-time control laws allows implementation of control logic with negligible computation transport lag. Consideration of rate and displacement limits of control actuators in the design process leads to low control gains, which in turn reduce control sensitivity to aircraft parameter variations and system nonlinearities.

The major elements of this project were defined at the outset as:

- Selection of Control Technique
- Selection of Guidance Laws
- Control Algorithm Development
- Evaluation of Control Algorithms
- Development of Design Procedure

These elements are summarized briefly. Selection of Control Technique required a review of digital-adaptive control methods to identify a method which would provide a high

probability for successful design and which could be used for both velocity-command and attitude-command control laws. Selection of Guidance Laws focussed on guidance algorithms which would be compatible with the control laws to be developed in this study, particularly those which could be used on a flight path representing conventional terminal-area operations as well as an experimental spiral descent. Control Algorithm Development consisted of the formulation of design equations, the preparation of necessary computational tools, and the generation of control system gains which are specific to the VALT Research Aircraft. Evaluation of Control Algorithms included the comparison of closed-loop system performance at design working points and along time-varying reference flight paths. The latter was accomplished for the new control laws alone and for integrated guidance and control (using previously defined guidance logic). The steps in control system design are described in Development of Design Procedure, which is reported here and in the documentation of computer design tools (Ref. 1).

1.3 SUMMARY OF RESULTS

A comprehensive procedure for designing digital-adaptive control laws for VTOL (and other) aircraft has been developed and is presented in this report. Velocity-command and attitude-command control laws have been designed for the VALT Research Aircraft, a CH-47B helicopter equipped for flight testing new navigation, guidance, and control concepts. These digital control laws are derived using optimal estimation and control methods; the resulting control laws correspond to classical control laws in their use of proportional-integral compensation, command pre-filtering, feed-forward, and linear feedback/crossfeed loops.

Air data and gyroscopic measurements are processed by a constant-gain Kalman filter for noise rejection and blending, and the result is seen to be equivalent to a bank of complementary and low-pass filters. While the linear-optimal may appear, at first glance, to be more complex than "classical" control laws, they are designed with considerably less effort and reliance on the designer's intuition. They can operate at lower sampling rates, and they achieve equivalent or superior performance in command response and disturbance rejection.

An open-loop-explicit technique is used for control law adaptation to variations in flight condition.* Initially, steady-state control gains are computed at a number of design points throughout the flight envelope. Once suitable quadratic-synthesis weighting matrices are found for a single flight condition, satisfactory gains can be found for all flight conditions with little change in the weightings. The gains are correlated with flight variables to establish functional relationships for gain scheduling. Gain schedules then are formed by regression analysis, resulting in a control law with essentially invariant dynamics at all flight conditions. Gains which can be considered constant or zero are identified at this point.

The linear-optimal design algorithms provide feedback paths from all state variables to all control variables (uncoupled state-control pairs have zero gains, and inconsequential gains can be eliminated from the final design.) As a consequence, the basic velocity-command

*"Open-loop" refers to the adaptive mechanism for changing gain values -- the primary control loops use feedback and are, therefore, "closed-loop."

and attitude-command control laws have the same number of gains before scheduling. In addition, the control laws have four control trim settings, each consisting of a static and a dynamic component.

The fact that linear-optimal control system design begins by feeding all states to all controls is useful, because it allows the designer to evaluate the relative importance of all possible control signal paths. The classical approach begins by defining a simple control structure; if testing proves that the structure is not good enough, a new control path may be considered, but the correct choice is not always obvious. The result is that classical designs tend toward simplicity but may require a great deal of intuition and testing. The linear-optimal approach begins with the most complex structure, in order to achieve optimal performance. The challenge to the practical designer is to eliminate those elements which contribute little to system response. The subtleties and counter-intuitive elements are presented to the designer from the beginning, rather than in later stages of development. From the designer's point of view, the difference between linear-optimal and classical control system design is identical to the difference between "top-down" and "bottom-up" planning. The former identifies the goals and overall structure first, while the latter gives preliminary attention to the details of implementation.

1.4 ORGANIZATION OF THE REPORT

Each of the next four chapters is directed at a specific phase of control system technique, application or evaluation. Chapter 2 presents the foundations of helicopter control system design, separation of guidance and control

functions, alternatives for adaptive control, and particulars of the VALT Research Aircraft. Theoretical concepts for linear-optimal control system design are developed in Chapter 3. Chapter 4 deals with control adaptation, the determination of trim settings, the correlation of system gains with flight condition, and state estimation. The application of these techniques to velocity-command and attitude-command control laws for the VALT Research Aircraft is treated in Chapter 5. Chapter 6 discusses the evaluation of these control laws on various mission profiles using a linear-time-varying simulation. Conclusions are presented in Chapter 7. Computational details are given in the Appendices, including descriptions of the major design tools and a mathematical model of the VALT Research Aircraft.

2. FUNDAMENTAL ISSUES IN THE DESIGN OF VTOL CONTROL SYSTEMS

2.1 OVERVIEW

This chapter is directed to the antecedents of advanced digital control system development for VTOL aircraft in the VALT Program -- the design techniques which have been applied to date, particulars regarding the VALT Research Aircraft, a methodology for partitioning guidance and control functions within the NGC system, and the alternatives for adaptive control system structures. The purpose of this chapter is to establish a framework within which the developments of later chapters can be interpreted. Section 2.2 reviews the structure of a stability augmentation system for a tandem-rotor helicopter, the structure of the TAGS control system, and experimental developments in helicopter control. Section 2.3 summarizes characteristics of the VALT Research Aircraft. Section 2.4 treats the selection of guidance logic, the separation of guidance and control functions, and adaptive control structures.

2.2 PRIOR DEVELOPMENTS IN THE DESIGN OF HELICOPTER CONTROLLERS

The open-loop (or unaugmented) dynamic characteristics of VTOL aircraft are adverse in comparison with conventional aircraft. This is a consequence of the dynamic coupling, low natural damping and control power, and/or flow interference effects which occur at low forward speed and hover. Configurational modifications which improve low-speed flying

qualities frequently contribute to adverse characteristics at high speed. The need for stability augmentation of some sort became apparent in the early phases of design of most of these VTOL aircraft. Mechanical design has achieved limited successes in improving helicopter stability (including the "δ_3" blade-flapping hinge, the Bell "stabilizer bar," and the Hiller "control rotor"), but acceptable flying qualities over the entire flight envelope on most helicopters require some form of electronic motion sensing and feedback to powered control actuators (Ref. 2). Hence, high-performance VTOL aircraft suitable for future short-haul transportation systems require (at a miminum) feedback control, even for manual operation.

Reference 3 contains numerous papers related to helicopter guidance and control technology; these are primarily devoted to sensor, actuator, and analog computer hardware. Guidance and control algorithm development is discussed in Refs. 4 to 7. Such algorithms typically are of the "PID-type" (proportional-integral-differential compensation), and classical analytical techniques are used, with allowance made for control gain scheduling. More recent developments, including the XV-14B variable-stability VTOL Program (Ref. 8), the early phases of the VALT Program (Ref. 9), and the U.S. Army Tactical Aircraft Guidance System (TAGS) Program (Ref. 10), generally have relied on classical analysis and have included model-following concepts. (Modern control theory was used in the initial phases of the variable-stability XV-14B program (Ref. 11)). Additional information on recent guidance and control implementations can be found in Ref. 12.

Modern control theory has been applied successfully in several VTOL control studies, all of which are based upon continuous-time implementations (Refs. 13 to 15). An

analysis of control laws for the X-22A ducted-fan VTOL aircraft (Ref. 13) used three modern approaches (root-square locus, model-in-the-performance index, and a pilot command technique), and a command-augmentation system for the SH-3D helicopter is designed in Ref. 14. The effects of rotor dynamics are considered in Ref. 15, observer theory is used in Ref. 16, and a helicopter with suspended load is stabilized in Ref. 17.

In the remainder of this section, two flight-tested automatic control systems for the CH-47B tandem-rotor helicopter are discussed. The first is the operational stability augmentation and trim system used on the production aircraft. The second is the experimental Tactical Aircraft Guidance System (TAGS) developed by the U.S. Army. General characteristics of the CH-47B aircraft are discussed in Section 2.3.

2.2.1 Control Systems for the Production CH-47 Aircraft

The CH-47's basic flight control systems are representative of the stability augmentation and trim capabilities deemed necessary or sufficiently useful to be included in the basic equipment for an operational VTOL aircraft. The systems are not intended for direct interface with automatic navigation and control systems, nor do they provide dynamic "shaping" (or pre-filtering) of pilot commands; however, they augment helicopter stability to provide acceptable flying qualities, and they trim rotor settings to reduce vibration, to improve nominal performance, and to achieve desirable stick-force gradients for the pilot (Ref. 18).

Each of the tandem-rotor helicopter's two rotors has three degrees of control freedom, for a total of six possible control effects of varying utility and authority.

A collective increase in the incidence of each blade of a single rotor modulates its thrust magnitude. Longitudinal cyclic variation of rotor blade incidence tilts the net thrust vector forward or backward, while lateral cyclic variation rotates the thrust vector to the left or right. Gang commands cause both rotors to change incidence in similar fashion, and differential commands provide rotor motions of opposite sense. Thus, gang collective control (δ_C) primarily effects vertical acceleration, and differential collective control (δ_B) produces a significant pitching moment. Gang lateral cyclic control (δ_S) provides a rolling moment, and differential lateral cyclic control (δ_R) produces a yawing moment.

The CH-47B is equipped with two separate pitch trim systems and three dual-redundant stability augmentation systems (Ref. 18). These systems are: longitudinal cyclic trim; differential collective pitch trim; and longitudinal, lateral, and directional stability augmentation. There are no automatic roll or yaw trim systems. In addition, rotor RPM in this turbine-powered aircraft is maintained by a separate system. All systems use analog electronics and have been designed using classical methods.

The longitudinal cyclic trim system commands the rotor planes to minimize vibration, stress, drag and fuselage attitude variation as a function of indicated airspeed (IAS). The cyclic commands to the rotors are not identical; hence, the net motion is both "gang" and "differential." This system has limited authority, low rates, and no direct inputs from the pilot or angular motion sensors. The system commands rotor swash plates directly through dedicated actuators (See Fig. 2.3-2).

The differential collective pitch trim system also is scheduled against IAS, improving handling qualities by providing stabilizing stick-force gradients at the pilot's station. The system input is to the lower-boost pitch actuator (See Section 2.3) through an actuator which is in series with the mechanical linkage from the cockpit.

The longitudinal stability augmentation system (SAS) operates on the lower-boost actuator pitch command (δ_B) with pitch-rate feedback. System gain is constant, and compensation includes low-pass, lead-lag, and "washout" (high-pass) filters.

The lateral SAS operates on the roll command (δ_S) and uses roll-rate feedback. As its primary function is to increase roll damping, system gain is constant, and the only compensation is a noise-rejecting low-pass filter.

The directional SAS is the most complex of the primary automatic control systems, feeding yaw-rate, roll-rate, and sideslip-angle inputs to the yaw command (δ_R). Yaw-rate compensation has constant gain, a low-pass filter, and "washout." Roll rate and sideslip angle both have low-pass compensation, and the latter has a velocity-dependent gain.

These systems are seen to be quite similar to the corresponding systems in conventional aircraft. There is no coupling of longitudinal information into lateral-directional systems (or vice versa), and only the trim settings and a single gain are scheduled. The independent variable for scheduling is indicated airspeed in all cases. The sideslip feedback, which is derived from differential pressure ports mounted on the nose, is the only unusual SAS feature by

conventional aircraft standards. The sideslip measurement is used to provide directional static stability, which is usually adverse on tandem-rotor helicopters (Section 2.3).

2.2.2 Control Systems for the TAGS Program

The Tactical Aircraft Guidance System (TAGS) provided three-axis velocity command and yaw-rate command in response to manual control inputs, and it incorporated comprehensive sensor information and computer processing in the control of a CH-47B helicopter (Ref. 19). The system, designed using classical control techniques, received extensive flight testing, during which time significant configuration changes were made in the control logic (Ref. 20). Objectives of the program were to demonstrate precise flight control under all weather conditions, as well as to reduce pilot workload.

Important new features for automatic helicopter control were demonstrated in the TAGS Program, including the use of a digital computer for flight control, velocity-command control, automatic trim in all axes, automatic mode switching, gust rejection, improved control coordination, and redundant system operation. Major elements of the TAGS avionics were the digital computer, inertial reference unit, rate gyros, accelerometers, airspeed indicator, barometric and radar altimeters, utility data sensors, and control actuators. Although sideslip angle was measured initially, it was eliminated due to difficulties associated with redundancy management.

The TAGS control structure consisted of four command-control systems plus rotor torque management. The command channels, operating at a sampling interval of 55 msec,

provided direct pilot control of longitudinal velocity, vertical velocity, lateral velocity, and yaw rate (for turn coordination). The basic elements of each command-control axis were:

- Inner Stability Loop
- Outer Stability Loop
- Command Input Loop
- Crossfeed Terms
- Trim

In order to provide reversion to the safety pilot with minimum transients (should a TAGS failure occur or be simulated), the production SAS remained operational. SAS signals were fed to the TAGS computer and subtracted from TAGS commands; hence, the helicopter appeared to be under TAGS control alone but could be switched to conventional control with the SAS actuators appropriately displaced. The production pitch trim was disconnected, but its logic was implemented within the TAGS computer.

The longitudinal velocity-command system illustrates the level of control structure detail which was found useful in the TAGS Program. The system is designed with the hierarchy listed above, and it provides a differential pitch collective command output (Ref. 20).

The inner control loop stabilizes the short-period mode by feeding back body-axis pitch rate and the pitch Euler angle. The former passes through a low-pass filter and a pure-time delay, and its control gain is dependent on calibrated airspeed (CAS), i.e., IAS with corrections for instrument error. The pitch attitude is biased for trim by a CAS-dependent term and a term which accounts for proper fuselage attitude during ground contact.

The outer control loop provides speed stability with velocity feedback. Its use of proportional-integral compensation leads to zero steady-state tracking error for step changes in commanded velocity. The velocity feedback signal has three components. Near hover, ground-relative velocity is obtained from the inertial reference unit. In cruise, a complementary filter blends calibrated airspeed with pitch attitude to form an air-relative velocity reference which attentuates pitch upsets due to gusts. The velocity reference is phased between ground- and air-relative signals during transition.

The command input loop is a third-order filter which shapes the velocity command and which generates equivalent pitch acceleration, rate, and attitude commands. The latter signals are formed between the integration states of the filter and are differenced with feedback signals in the inner loop. The equivalent angular commands improve system step response and are viewed as cancelling helicopter stability derivatives and adjusting trim setting. These terms serve the same purpose as the secondary commands and dynamic trim compensation developed in the present investigation (Section 2.4).

There are four crossfeed terms in the longitudinal command system. The body pitch-rate signal which occurs in steady turns is cancelled by a nonlinear yaw-rate/roll-angle crossfeed. Further lateral turn coordination is provided by a yaw-rate signal to pitch attitude, while transient turn compensation is derived from yaw-acceleration input to δ_B. Helicopter aerodynamics cause a nose-down pitching moment in right turns and a nose-up pitching moment in left turns. This effect is cancelled by a yaw-rate input to δ_B.

The δ_B command is scaled and limited before being transmitted to the actuator. Rate and displacement limits are imposed on the signal, and gain factors account for weight and altitude variations.

In summary, the longitudinal velocity-command system has a single command input and a single command output (Ref. 20). In addition, it uses eight separate measurements of flight variables. There are four integrators, 16 nonlinear elements, 20 gains, two pure lags, and a washout filter in the primary digital control logic. Additional elements are required for synchronization with the redundant control strings, for SAS cancellation, and for ground contact logic. The vertical, lateral, and directional command channels have corresponding sophistication in structure.

2.3 CHARACTERISTICS OF THE VALT RESEARCH AIRCRAFT

Before discussing the VALT Research Aircraft, some general comments on the control characteristics of tandem-rotor helicopters are appropriate. The strong pitching moment afforded by separate rotors allows large variation of center-of-gravity (a useful feature for transport aircraft), and two rotors provide a large load capacity. The thrust interference of the two rotors can degrade stability and flying qualities of the unaugmented airframe (Refs. 2 and 21). In forward flight, the short period and Dutch roll modes may be statically unstable (resulting in real, rather than complex, roots), and roll damping is low. Speed stability can be negative during cruise and too positive at hover. As a consequence of synchronized counter-rotating rotors, net angular momentum is low, and the gyroscopic coupling of longitudinal and lateral-directional motions is small.

Aerodynamic coupling can result from rotor disc loading distributions and from asymmetric downwash on the fuselage. It generally proves desirable to provide automatic stability augmentation for the tandem-rotor helicopter, and the use of dual-redundant systems on the CH-47B (Section 2.2.1) indicates that substantial flying qualities improvements are obtained from an operating SAS.

2.3.1 Vehicle Characteristics

The CH-47B helicopter, shown in Fig. 2.3-1, is a medium transport vehicle which carries an 8,850-lb payload (approximately 30 passengers) at a normal operating weight of 33,000 lb. Maximum airspeed ("never-exceed velocity") is 160 kt, while lateral and aft velocities are limited to 35 and -30 kt, respectively; normal cruise speed is 140 kt. Maximum sea-level climb rate is 2,000 ft/min, and service ceiling is 14,000 ft.

2.3.2 Elements of the Control System

This section summarizes the mechanical elements, the actuators, the computer, and the sensors to be used for flight control in this investigation.

A schematic of the mechanical elements of the VALT Research Aircraft, adopted from Ref. 18, is shown in Fig. 2.3-2. Pilot commands enter the mechanical system through the lower-boost hydraulic actuators, which are physically located near the cockpit. VALT computer commands drive the same actuators used in the TAGS, and the TAGS actuator outputs drive the lower-boost actuators. Operational SAS inputs are in series with the lower-boost outputs. The combined signals are mixed (Fig. 2.3-2) before

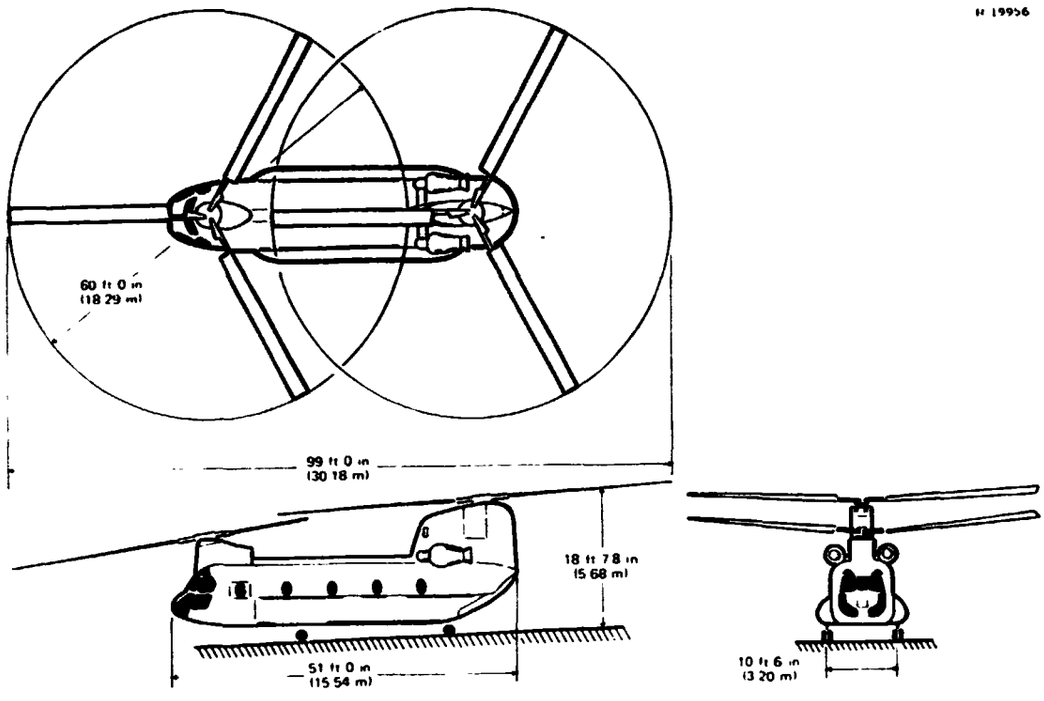

Figure 2.3-1 Basic Features of the VALT Research Aircraft

commanding the upper-boost actuators that drive the two rotor swash plates. (The swash plates control rotor blade incidence).

The TAGS actuators are the limiting dynamic elements between the VALT computer and the rotors. Each actuator has a time constant of 0.0125 sec, a rate limit of ±3 in/sec, and a displacement limit of ±2 in. Rotor dynamic response can be modeled as that of a second-order system with a natural frequency of 24 rad/sec and a damping ratio of 0.6.

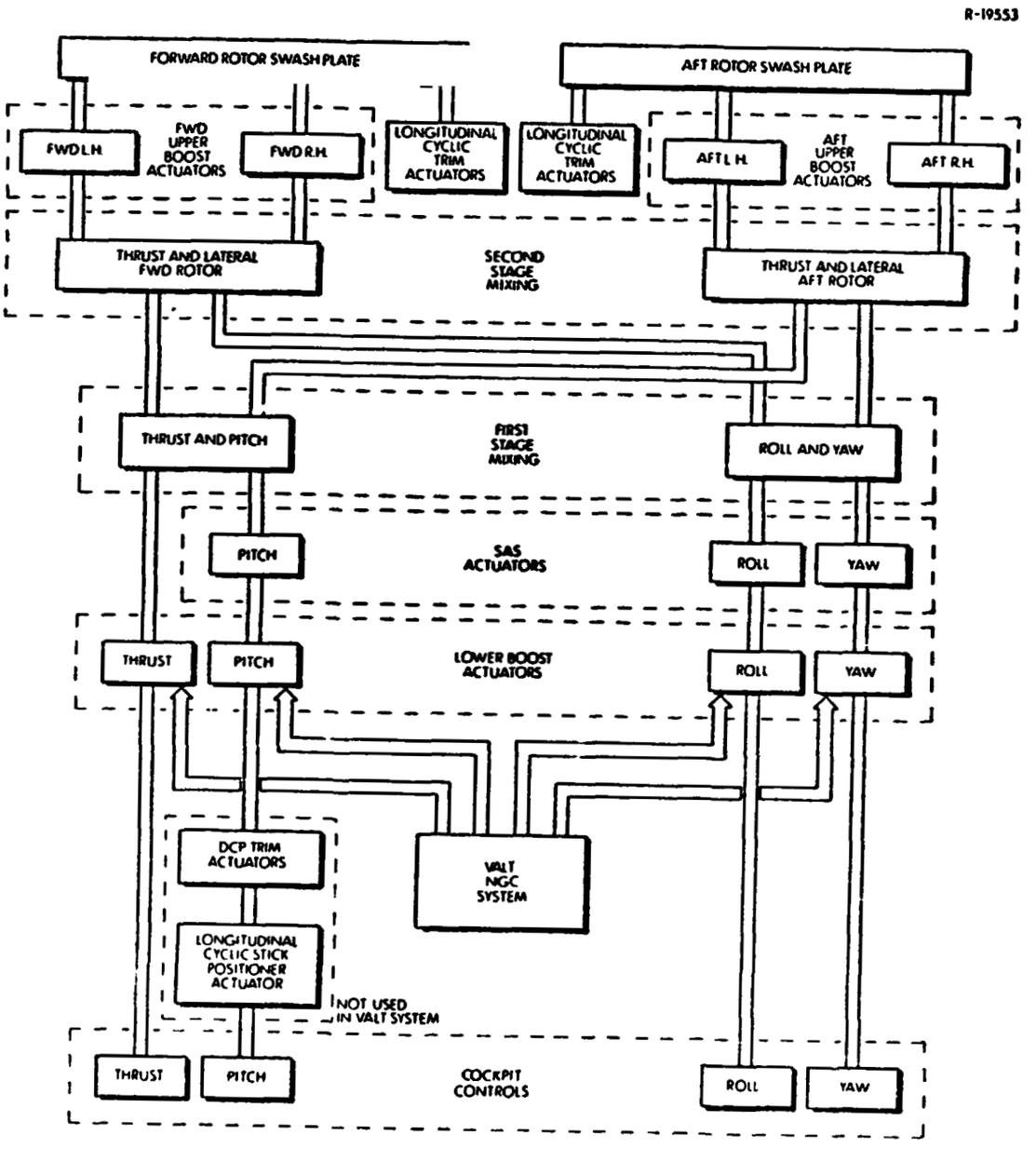

Figure 2.3-2 Elements of the CH-47B Control System

Control sensors include airspeed indicator, barometric altimeter, vertical gyro, rate gyros, and linear accelerometers.

2.4 SELECTION OF GUIDANCE LAWS AND CONTROL TECHNIQUE

Before a control system is designed, its objectives and candidate methods for accomplishing these objectives must be defined. The first area of concern is how to distinguish between functions which relate to "guidance" and those which are properly termed "control". Because the guidance and control logic must interact, and because the guidance function precedes the control function in planning and execution, Section 2.4.1 examines guidance law structures which are appropriate for VTOL aircraft, a definition of the guidance/control interface, and the corresponding control structures. Section 2.4.2 reviews control design techniques which could be applied to the VTOL aircraft.

2.4.1 Guidance and Control Structures

Guidance and control systems are regulating mechanisms which are required to keep the vehicle on its intended flight path. The difference between the two rests in their inputs and outputs. Guidance is associated with the translational motions of the vehicle in an earth-relative frame; position inputs and velocity- (or acceleration-) command outputs are expressed accordingly. Guidance laws can be formulated with rudimentary descriptions of vehicle dynamic characteristics, as, for example in Ref. 22. The time scale of related motions is slow, and the magnitude of motions is often large, in the sense that nonlinearities in the equations

of motion must be considered. Control is more closely allied with angular motions of the vehicle, expressed in body-axis or velocity-axis coordinates. Rotational stability and mechanisms for producing forces and moments are of particular concern. The time scale of associated motions is fast and the magnitude of motions is often small, in the sense that linear equations of motion can be employed.

The objective in distinguishing between guidance and control should be to make a partitioning of design functions possible, as illustrated by Fig. 2.4-1. Part (a) of the figure identifies some components of the guidance and control problem, as well as inter-relationships between system variables. The guidance law accepts mission objectives and defines desired values of the total state vector, $\underline{x}_0$, or some subset of its components (which include position, velocity, angle, and angle rate). A closed-loop guidance law must "know" the vehicle's position and may require its velocity. The control law accepts guidance commands and forms a set of total actuator commands, $\underline{u}_T$. A closed-loop control law requires angular measurements and may use translational acceleration and velocity. Given the desired state, x_0, there are corresponding nominal control settings, $\underline{u}_0$, which would cause the vehicle to follow the desired path in the absence of disturbances and dynamic uncertainties; thus, $\underline{u}_0$ provides an open-loop control which can augment the closed-loop control. In most cases, the guidance and control feedback paths are concentric, i.e., they evidence the inner-to-outer-loop structure shown by Fig. 2.4-1(a). With this structure it is possible to conduct the major portion of guidance and control design separately, using the structures of Fig. 2.4-1(b) and (c).

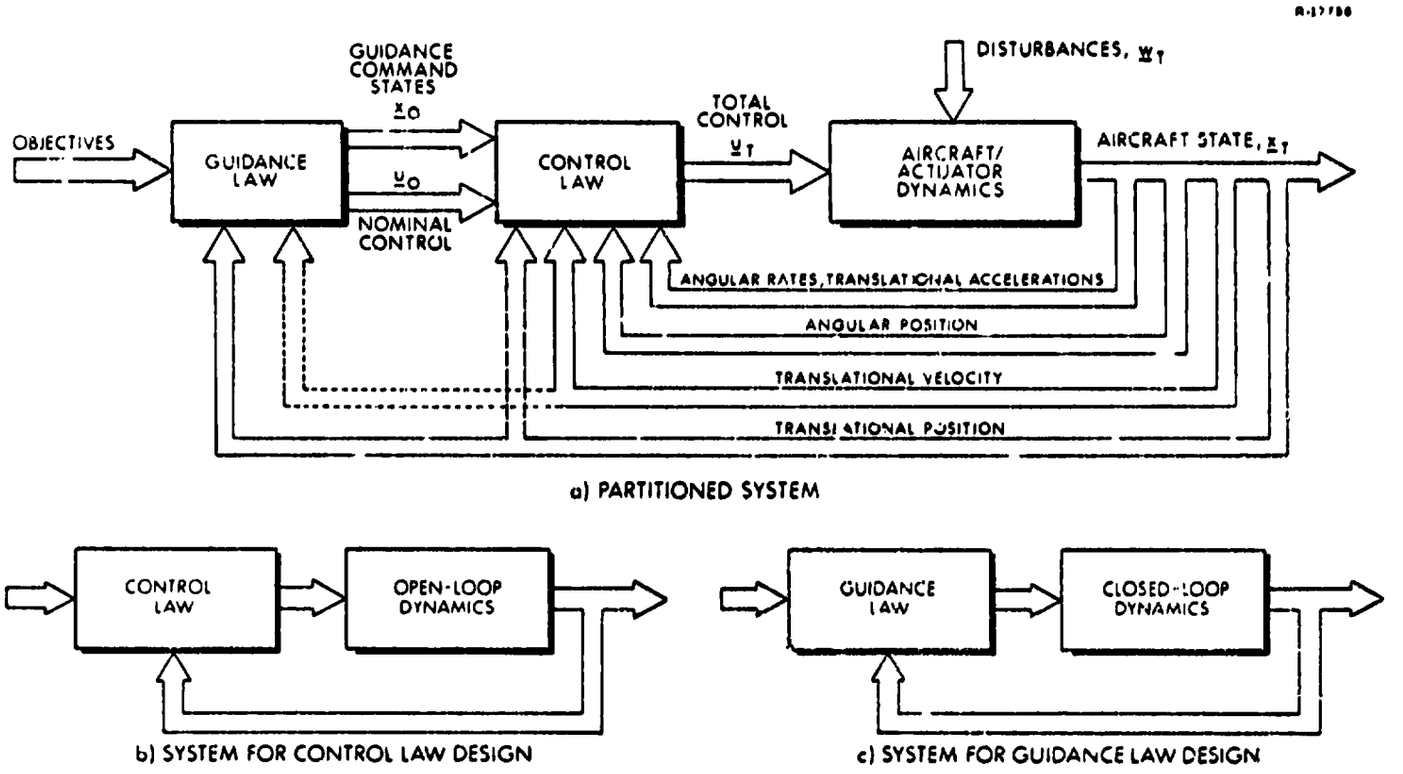

Figure 2.4-1 Separation of Guidance and Control Functions for Algorithm Development

Alternatives for guidance law outputs include velocity commands, acceleration commands, and vehicle attitude commands.

The velocity-command law is formulated with a third-order dynamic model in which translational position is a pure integral of translational velocity and dynamic coupling with other vehicle states is assumed negligible. The guidance/control partition is obvious in this case: the 12 rigid-body vehicle states are separated into three guidance-law states (three components of translational position) and nine control-law states (three components each of translational velocity, vehicle attitude, and angular rate). Because the guidance state is independent of vehicle dynamics, the velocity-command guidance law could tend to violate vehicle dynamic constraints, so limitations of the vehicle must be taken into account in the guidance formulation. The velocity-command law must be augmented by yaw command to maintain proper vehicle direction during cruise.

An acceleration-command law would increase the guidance-law state dimension to six (translational position and velocity), and it would introduce the vehicle's point mass dynamics into the guidance model; therefore, some vehicle dynamic constraints can be considered directly. Under some conditions, the corresponding control law could be simpler; however, translational velocity affects angular motion and could be required in the control design model as well. In such instance, guidance/control partitioning is made more complex.

Many VTOL vehicles (the helicopter included) obtain horizontal accelerations by tilting the vehicle; therefore, an attitude-command law is equivalent to an acceleration-

command law in the horizontal plane. The attitude-command law must be augmented by commanding either vertical acceleration or velocity.

The remainder of this section is devoted to a methodology for separating linear and nonlinear elements of guidance and control logic; this leads to the structures selected for study in this contract.

Linear and Nonlinear Models - The nonlinear equations which govern vehicle motion can be written as the vector first-order differential equation

$$\dot{\underline{x}}_T(t) = \underline{f}[\underline{x}_T(t), \underline{u}_T(t), \underline{w}_T(t)] \qquad (2.4\text{-}1)$$

The total state, control, and disturbance vectors can be divided into nominal and perturbation components as follows:

$$\underline{x}_T(t) = \underline{x}_0(t) + \underline{x}(t) \qquad (2.4\text{-}2)$$

$$\underline{u}_T(t) = \underline{u}_0(t) + \underline{u}(t) \qquad (2.4\text{-}3)$$

$$\underline{w}_T(t) = \underline{w}_0(t) + \underline{w}(t) \qquad (2.4\text{-}4)$$

A first-order Taylor series expansion of Eq. (2.4-1) leads to a nonlinear equation for the nominal flight path,

$$\dot{\underline{x}}_0(t) = \underline{f}[\underline{x}_0(t), \underline{u}_0(t), \underline{w}_0(t)] \qquad (2.4\text{-}5)$$

and a linear equation for perturbations about the nominal path

$$\dot{\underline{x}}(t) = F(t)\underline{x}(t) + G(t)\underline{u}(t) + L(t)\underline{w}(t) \qquad (2.4\text{-}6)$$

where the time-varying linear system matrices are

$$F(t) = \left.\frac{\partial \underline{f}}{\partial \underline{x}}\right|_{\substack{\underline{x}_0(t) \\ \underline{u}_0(t) \\ \underline{w}_0(t)}} \tag{2.4-7}$$

$$G(t) = \left.\frac{\partial \underline{f}}{\partial \underline{u}}\right|_{\substack{\underline{x}_0(t) \\ \underline{u}_0(t) \\ \underline{w}_0(t)}} \tag{2.4-8}$$

$$L(t) = \left.\frac{\partial \underline{f}}{\partial \underline{w}}\right|_{\substack{\underline{x}_0(t) \\ \underline{u}_0(t) \\ \underline{w}_0(t)}} \tag{2.4-9}$$

A guidance and control design procedure based upon Eqs. (2.4-5) and (2.4-6) is readily formed and is most easily described by considering a single flight:

- Define the mission objective (e.g., fly from $\underline{x}(0)$ to $\underline{x}(t_f)$).
- Define the nominal path ($\underline{x}_0(t)$, $0 \le t \le t_f$) which satisfies the objective and observes constraints (e.g., air traffic control and operating procedures).
- Compute the corresponding nominal control ($\underline{u}_0(t)$, $0 \le t \le t_f$) which satisfies Eq. (2.4-5).
- Design closed-loop guidance and control algorithms which keep the vehicle on the nominal path (in the presence of unmodeled disturbances, dynamic uncertainties, and measurement errors) by generating the appropriate $\underline{u}(t)$ as the flight progresses. Describe vehicle dynamics by the linear model (Eq. (2.4-6) in the guidance and control design.

- The control command is then the sum of open-loop and closed-loop components, i.e., $\underline{u}_T(t) = \underline{u}_0(t) + \underline{u}(t)$.

This procedure identifies the elements of unified guidance and control algorithm design concisely, but it is not to be taken literally. Repeating the process for every possible flight profile is undesirable and unnecessary; however, the most useful elements of the procedure can be retained by recognizing three important points. The first is that the nominal control, $\underline{u}_0(t)$, serves the purpose of a dynamic control trim setting in the guidance and control system. It need not attempt to provide exact open-loop control -- in fact, the closed-loop system should adjust to follow the path even if $\underline{u}_0(t)$ is incorrect, as variations in trim settings due to weight, center-of-gravity location, aircraft-to-aircraft variations, etc., can be expected. Practical methods of computing $\underline{u}_0(t)$ are discussed in Section 4.3. The second point is that the time-varying matrices, F(t), G(t), and L(t), used in Eq. (2.4-6) are slowly varying, and they are explicit functions of flight condition rather than time; therefore, the values necessary for guidance and control design can be generated without reference to a fixed flight path. The third point is that guidance/control partitioning is desirable and further simplifies the design procedure. With these observations, techniques for separately defining guidance and control logic are discussed below.

Velocity-Command Guidance Structure - Figure 2.1-2 illustrates a guidance law structure which incorporates both linear and nonlinear elements. It consists of nonlinear logic for transforming mission objectives into desired present position, nominal velocity, and nominal control, as well as a linear perturbation guidance law. (In this

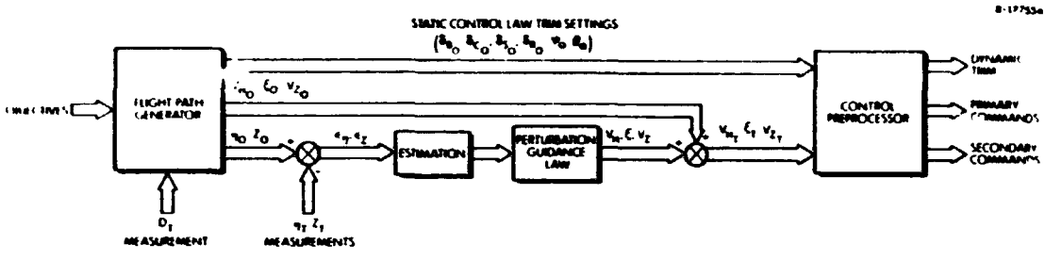

Figure 2.4-2 Elements of a Velocity-Command Guidance Law

respect, the structure is similar to that proposed in Refs. 22 to 24.) Position and velocity are expressed in cylindrical coordinates. Altitude (Z), distance-to-go (D), and azimuth angle (η) are referenced to the destination, or to an intermediate waypoint. Vertical velocity (V_Z), horizontal velocity magnitude (V_H), and horizontal direction (ξ) are referenced to North and the local vertical. It is convenient to use the measured distance-to-go, D_T, as an independent variable for guidance. This reduces the problem dimension by one, and it references desired position and velocity to the destination: $\eta_0(D_T)$, $Z_0(D_T)$, $V_{Z_0}(D_T)$, $\xi_0(D_T)$, and $V_{H_0}(D_T)$. For 4-D navigation, in which time-to-go also is important, the time variable can be added explicitly (by specifying $t_{go}(D_T)$) or implicitly (by revising $V_{H_0}(D_T)$ to reflect the time constraint). The generation of desired and nominal values may require nonlinear operations; however, the nonlinear operations may be essentially static, as the guidance law is separated from complex vehicle dynamics.

As shown in Fig. 2.4-2, measurements of Z_T and η_T allow the guidance error, ε_Z and ε_η, to be formed, either with state estimation (as shown) or without. These errors are processed by the perturbation guidance law, which can be designed by the same procedure used to design control

laws in this report. The outputs of the perturbation guidance law (V_Z, V_H, ξ) are summed with the nominal values to form the total velocity commands (V_{Z_T}, V_{H_T}, ξ_T). These commands and the static trim settings are the basic outputs of the guidance law and are converted to corresponding control actuator commands in the control law which follows.

It will be seen in Section 4.3 that the static trim settings are dependent on velocity; hence, they can be based on either V_{Z_0}, V_{H_0}, and ξ_0 or on V_{Z_T}, V_{H_T}, and ξ_T. The former approach would be independent of the perturbation guidance law and, therefore, less sensitive to position measurement errors. The latter approach could provide a small performance advantage, in that the trim settings are based on the total desired velocity vector.

Before the earth-referenced guidance commands can be used by the body-referenced control law, additional computations are required; these are performed in the control preprocessor shown in Fig. 2.4-2. The control preprocessor performs several functions including:

- Transformation of commanded velocity vector (primary command) to body-axes
- Generation of secondary command variables
- Correction for steady winds
- Computation of dynamic trim compensation

Transformation of the velocity command to body axes is necessary because the control law is most naturally derived in the body-axis frame; i.e., V_{H_T}, V_{Z_T}, and ξ_T are converted to the body-axis commands u_T, v_T, w_T. The transformation requires knowledge of the vehicle's earth-referenced Euler roll, pitch, and yaw angles, ϕ, θ, and ψ.

Assuming the conventional yaw-pitch-roll sequence for defining these angles, the Euler angle transformation matrix, H_E^B, can be written as the product of three rotational matrices:

$$H_E^B = \begin{bmatrix} 1 & 0 & 0 \\ 0 & \cos\phi & \sin\phi \\ 0 & -\sin\phi & \cos\phi \end{bmatrix} \begin{bmatrix} \cos\theta & 0 & -\sin\theta \\ 0 & 1 & 0 \\ \sin\theta & 0 & \cos\theta \end{bmatrix} \begin{bmatrix} \cos\psi & \sin\psi & 0 \\ -\sin\psi & \cos\psi & 0 \\ 0 & 0 & 1 \end{bmatrix} \tag{2.4-10}$$

(The transformation can be simplified as appropriate, e.g., by using small-angle assumptions or eliminating the ψ rotation when using a two-axis vertical gyro.) Assuming that the earth-relative velocity vector is expressed in cylindrical coordinates, it must be transformed to cartesian coordinates before applying Eq. (2.4-10).

If vehicle velocity is more easily measured in an earth-referenced frame than a body-axis frame, this transformation should be applied to the velocity error in the control law rather than in the preprocessor. The present development assumes that velocity is measured in body-axes.

Secondary commands are required for much the same reason that they were included in the TAGS (Section 2.2.2). Control feedback will tend to produce sluggish transient response if the variations in angular rates which accompany a commanded velocity maneuver are neglected. In addition, yaw angle, ψ_T, can be commanded to orient the vehicle centerline along the direction of travel during cruise. In the no-wind case, $\psi_T = \xi_T$. Near hover, ψ_T should be commanded separately to meet touchdown constraints and to avoid large heading changes for small velocity changes. Secondary angular-rate commands can be computed as

$$\begin{bmatrix} p_T \\ q_T \\ r_T \end{bmatrix} = L_B \begin{bmatrix} \dot{\phi}_T \\ \dot{\theta}_T \\ \dot{\psi}_T \end{bmatrix} \tag{2.4-11}$$

where $\dot{\psi}_T = 0$, $\dot{\theta}_T = \dot{\gamma}$, and

$$\gamma_T = \tan^{-1}(V_{Z_T}/V_{H_T}) \tag{2.4-12}$$

and the discrete-time equivalents of $\dot{\gamma}_T$ and $\dot{\psi}_T$ are generated by back-differencing. The matrix, L_B, is

$$L_B = \begin{bmatrix} 1 & \sin\phi\tan\theta & \cos\phi\tan\theta \\ 0 & \cos\theta & -\sin\phi \\ 0 & \sin\phi\sec\theta & \cos\phi\sec\theta \end{bmatrix} \tag{2.4-13}$$

Note that Eq. (2.4-11) compensates the angular rates for steady turns, quickens turn entry, and coordinates rate changes during steep ascent or descent.

Correction for a steady, horizontal wind also can be provided. With wind speed (V_w) and direction (μ), the following yaw-angle command provides zero sideslip angle:

$$\psi_T = \xi_T + \tan^{-1}\left[\frac{\sin(\mu-\xi_T)}{V_H/V_w+\cos(\mu-\xi_T)}\right] \tag{2.4-14}$$

The yaw angle correction term also could be obtained from a wind estimate, which could be an integral part of the perturbation guidance law as in Ref. 25, or sideslip angle can be nulled directly in the control law. The principal advantage in correcting the yaw guidance command for cross winds is that this approach is less sensitive to gusts than feedback nulling alone.

Section 4.3 shows that $\underline{u}_0(t)$ is not sufficient to produce force and moment equilibrium; the angles ϕ_0 and θ_0 must be defined as well. Figure 2.4-2 illustrates the six static trim settings and the dynamic trim compensation of these variables in the control preprocessor. The latter accounts for the rate and acceleration effects on the proper choice of $\underline{u}_0(t)$, $\phi_0(t)$, and $\theta_0(t)$,which corresponds to open-loop control of maneuvers.

Velocity-Command Control Structure - Figure 2.4-3 outlines the control structure, which will be examined in detail in later chapters. The essential information in this figure is that control trim settings coming from the control preprocessor are summed with the linear control law output to form the total control command, $\underline{u}(t)$, and that estimation may be required to minimize the effects of measurement error. The linear control law generates corrections to the open-loop command which null steady-state following error through the "Type 1" design described in the next chapter. The control law also provides stability augmentation.

Attitude-Command Guidance and Control Structure - The design philosophy applied to the velocity-command system also is appropriate to an attitude-command system. The principal differences lie in the guidance state dimension and in the details of preprocessor function. Trim settings are defined as before, except that explicit control of ϕ and θ eliminates them as trim variables.

The attitude-command system considered here uses ϕ and θ to provide horizontal acceleration, nulls sideslip angle through ψ command, and commands vertical velocity directly (as in the velocity-command system). Again using

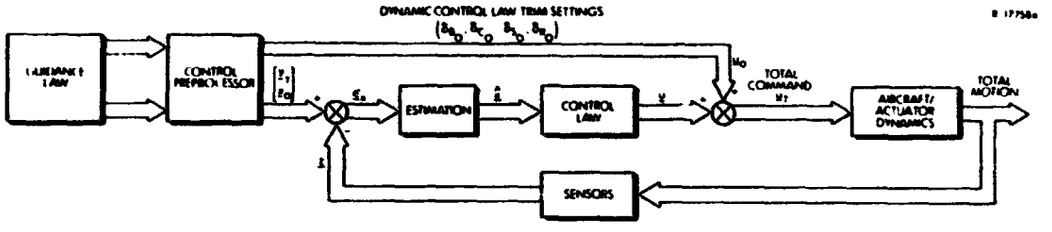

Figure 2.4-3 Primary Elements of the Control Law

D_T as the independent variable, the guidance input states include position, $\eta_0(D_T)$ and $Z_0(D_T)$, and horizontal velocity, $\xi_0(D_T)$ and $V_{H_0}(D_T)$. Whereas the latter two quantities contribute to velocity-command output, they are internal to the attitude-command law. The attitude law computes output values of ϕ_T, θ_T, ψ_T and V_{Z_T} by summing the nominal values with the outputs of the perturbation guidance law.

The control preprocessor performs the following functions:

- Transformation of velocity and angular rates to body axes
- Correction for steady winds
- Computation of dynamic trim compensation

The control preprocessor transmits the ϕ and ϑ commands without change. The velocity vector, consisting of two nominal components and one command component, is transformed to body coordinates by

$$\begin{bmatrix} u_T \\ v_T \\ w_T \end{bmatrix} = H_E^B \begin{bmatrix} V_{H_0} \cos\xi_0 \\ V_{H_0} \sin\xi_0 \\ V_{Z_T} \end{bmatrix} \qquad (2.4\text{-}15)$$

Body-axis angular rates are

$$\begin{bmatrix} p_T \\ q_T \\ r_T \end{bmatrix} = L_B \begin{bmatrix} \dot{\phi}_T \\ \dot{\theta}_T \\ \dot{\psi}_T \end{bmatrix} \qquad (2.4\text{-}16)$$

where the Euler angle rates are determined by back-differencing. Steady-wind correction and dynamic trim are computed as before, and the basic components of the control law are unchanged (although gains and the locations of integrators are altered).

Manual-Control Entry Points - From the standpoint of control law design, it is best to think of manual inputs as an alternate set of guidance commands. There should be no change to the control laws unless the manual intervention also implies a mode change for such reason as failed sensors. Thus, the pilot commands are interpreted as total velocity or total attitude commands to the control preprocessor, as appropriate. Corresponding control trim settings are computed directly from the commands in the first case and from airspeed measurements in the second.

Summary - This section has presented guidance and control structures which are appropriate for VTOL automatic system design, in preparation for the detailed developments of the following chapters. The next section presents the candidate design techniques which were considered for control law development.

2.4.2 Control Design Techniques

This section provides a summary of adaptive control techniques that are potentially applicable for digital VTOL

flight control systems. The functional diagram in Fig. 2.4-4 is used as a general representation for a flight control system. A particular design may consist of only a few of the functions indicated; however, the complete diagram is useful for categorizing control law design techniques.

The solid, dashed, and broken lines in Fig. 2.4-4 define three control loops, whose functions are as follows:

- The main control loop provides the airframe feedback control signals needed to achieve desired response to pilot inputs. For nominal airframe dynamics, the command prefilter, forward compensation, and feedback compensation blocks can be designed using either conventional or optimal control techniques. The additional functions of input shaping and actuator prefiltering can be used to provide desirable command response. The response transformation selects an appropriate combination of the airframe states as the response.

- The explicit-adaptive control loop identifies the airframe dynamic parameters as flight conditions change, making use of airframe sensor and/or air data. The resulting parameter estimates are utilized to adjust gains in the main control loop according to an explicit-adaptation algorithm. This gain adjustment is designed to maintain desired response characteristics.

- The implicit-adaptive control loop detects airframe parameter changes by analyzing the difference between actual airframe response and desired response. The response error is processed by an implicit-adaptation algorithm, which adjusts the main control loop gains to reduce a performance measure.

If the main control loop can be designed with fixed gains so that satisfactory performance is achieved over all

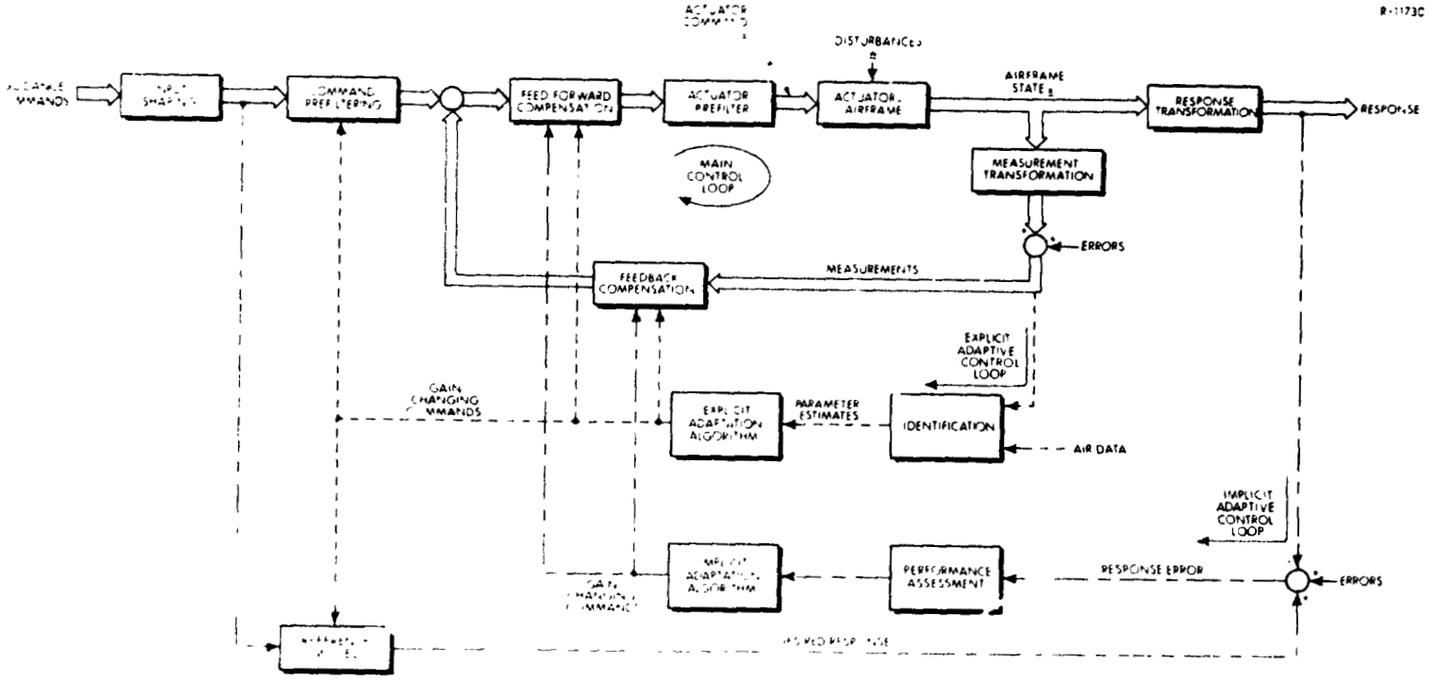

Figure 2.4-4 Functional Diagram for an Adaptive Flight Control System

flight conditions without gain adjustment, the system is said to be insensitive rather than adaptive. The definitions of explicit- and implicit-adaptive control techniques are taken from Ref. 26 and are useful for distinguishing between those systems which identify airframe parameters and those which do not. Usually an adaptive control system is thought of as either explicitly or implicitly identifying the unknown parameters; however, it is conceivable that both types of adaptation can be present in the same system design. In addition, an explicit loop may adjust design parameters in an implicit control loop -- e.g., in the reference model.

Alternatives for control system design are discussed in the remainder of this section. After introducing some basic concepts for fixed-gain systems, several approaches to adaptive control are discussed, including explicit-adaptive control, parameter identification for explicit-adaptive control, implicit-adaptive control, and learning (or self-organizing) control systems.

Fixed-Gain Control Laws - In a fixed-gain control law, only the main control loop in Fig. 2.4-4 is operative. The design principle is to choose compensation such that the system response is reasonably insensitive to airframe parameter variations. Techniques for fixed-gain control law design, including both classical and modern control methods, also form the basis for adaptive control design.

When using classical control techniques, linear system dynamics are transformed from the time domain of ordinary differential (or difference) equations to the frequency-domain equivalent (Ref. 27). Normally, it is assumed that the coefficients of these equations are constant during

some time span of interest. The Laplace transform then converts the time-domain vector differential equation

$$\dot{\underline{x}}(t) = F\underline{x}(t) + G\underline{u}(t) \qquad (2.4\text{-}17)$$

to the frequency-domain equation

$$(sI-F)\underline{x}(s) = G\underline{u}(s) \qquad (2.4\text{-}18)$$

where $\underline{x}(t)$ is the vector of motion variables (including rigid-body motions, aeroelastic variables, etc.), and $\underline{u}(t)$ is the vector of control variables; the Laplace transforms of these vectors are $\underline{x}(s)$ and $\underline{u}(s)$, respectively. The corresponding system coefficients are contained in the matrices F and G which, being constant, are identical in the time and frequency domains. Differentiation with respect to time, represented by ($\dot{}$), is transformed to the operator sI, where s is the Laplace operator and I is the identity matrix. Pre-multiplying Eq. (2.4-18) by the inverse of (sI-F) provides the transfer matrix form

$$\underline{x}(s) = (sI-F)^{-1}G\,\underline{u}(s) \qquad (2.4\text{-}19)$$

from which any scalar transfer function of interest (for example, the effect of the i^{th} control on the j^{th} motion variable) can be obtained as

$$\frac{x_j(s)}{u_i(s)} = \frac{N_i^j(s)}{D(s)} \qquad (2.4\text{-}20)$$

Here, D(s) is the characteristic equation of (sI-F), i.e., its determinant, and $N_i^j(s)$ is the appropriate transfer function numerator (Ref. 28). Equation (2.4-18) is the preferred form for classical continuous-time ("analog") control system design.

The equivalent discrete-time equations, required for classical digital control system design, can be derived

from the foregoing equations. As described in later sections, the system state can be described at sampling instants (k) by the difference equation

$$\underline{x}(k+1) = \Phi\underline{x}(k) + \Gamma\underline{u}(k) \qquad (2.4\text{-}21)$$

and scalar transfer functions can be written as

$$\frac{x_j(z)}{u_i(z)} = \frac{N_i^j(z)}{D(z)} \qquad (2.4\text{-}22)$$

where z is a discrete-time Laplace operator.

The classical approach to control system design is to achieve insensitivity to parameter variations through the use of output feedback, together with high-gain forward loop compensation, in the manner originally advocated by Bode, Nyquist, and Evans. Conventional synthesis procedures, which are analogous to the familiar s-plane techniques for continuous systems, exist for linear digital systems. These include the use of z-plane root loci and Bode-diagram synthesis in the w-plane, which are useful for positioning closed-loop poles and achieving desired stability margins. In addition, design criteria that are associated with the sampled nature of the system can be imposed. These include ripple-free* response and finite settling time for specific test inputs -- step, ramp, etc. In order to achieve a response that is insensitive to the input type, it is generally necessary to design for a damped-exponential response tolerating some ripple. Conventional digital design techniques are well documented (Refs. 29 to 33).

*Ripple refers to the output response error at times between samples.

Modern control theory, which is based on time-domain, state-space models for system dynamics, offers a number of systematic procedures for designing sampled-data feedback control systems (Refs. 34 and 35) and receives major emphasis in this report. State-space methods are particularly advantageous for control of systems with multiple inputs and multiple outputs.

In a digital flight control system, the airframe response at discrete instants of time, t_1, t_2, ..., is of principal interest in the design of stability augmentation. Therefore, Eq. (2.4-21) is an appropriate format for representing the airframe dynamics. If the sampling interval is of uniform width, Δt, and the airframe dynamics are constant, Φ and Γ also are constant (independent of k). The values of these matrices are determined from the continuous airframe dynamics by well-known techniques for forming difference equation solutions from differential equations (Ref. 34).

The objective in linear-quadratic control design ("quadratic synthesis") is to determine the control law which minimizes a quadratic performance index of the form

$$J = \underline{x}_N^T S_N \underline{x}_N + \sum_{k=0}^{N-1} (\underline{x}_k^T Q_k \underline{x}_k + \underline{u}_k^T R_k \underline{u}_k) \qquad (2.4\text{-}23)$$

where the sampling index is now represented as a subscript. In Eq. (2.4-23), N denotes a specified terminal time, t_N, and the quantities S_N, Q_k, and R_k are positive-definite weighting matrices. For steady tracking, terminal error is neglected in the performance index, and Q and R are constant, leaving

$$J = \sum_{k=0}^{\infty} (\underline{x}_k^T Q \underline{x}_k + \underline{u}_k^T R \underline{u}_k) \qquad (2.4\text{-}24)$$

In the following chapters, methods for choosing the discrete-time cost function to minimize continuous-time criteria (thereby minimizing "ripple") are presented.

If the control commands, $\underline{u}_k$, are chosen to minimize J, it is found that good system response in terms of classical performance measures (overshoot, rise time, etc.) generally can be achieved. The weighting on the state in Eq. (2.4-24) tends to reduce transient effects; the weighting on the control tends to prevent the use of excessive control levels.

The control law for the linear-optimal regulator takes the form

$$\underline{u}_k = -K\underline{x}_k \qquad (2.4\text{-}25)$$

where K is determined from the steady-state solution of a matrix Riccati difference equation (Chapter 3).

It is tacitly assumed in the above discussion that measurements of the airframe state vector, $\underline{x}_k$, are available for mechanizing the feedback control law. Such measurements can be obtained from air data and body-mounted gyros and accelerometers; however, they may be corrupted by additive measurement noise. If the measurements are modeled as linear functions of the state corrupted by additive gaussian noise, an optimal estimate of the state can be obtained by mechanizing a Kalman filter, as described in Ref. 36. Alternatively, if some measurements are obtained with negligible error, it may be more convenient to mechanize an observer (Ref. 37), which does not require any assumptions about the noise statistics. Although the regulator control law is developed without any specific consideration of the effect of airframe parameter variations, the optimal control law is found to have low sensitivity to such variations (Refs. 38 and 39).

Another approach to the design of optimal control laws is the use of model-following techniques. These are particularly attractive when a desired dynamic response is specified for the flight control system in terms of the known model,

$$\tilde{\underline{x}}_{k+1} = \tilde{\Phi}\underline{x}_k + \tilde{\Gamma}\underline{u}_{c_k} \qquad (2.4\text{-}26)$$

That is, it is desired to force the airframe response, $\underline{y}_k$, to follow a model output

$$\tilde{\underline{y}}_k = \tilde{H}\,\tilde{\underline{x}}_k \qquad (2.4\text{-}27)$$

This objective is stated in precise terms by defining an appropriate error function, $\underline{e}_k$, substituting the latter for $\underline{x}_k$ in the performance index given in Eq. (2.4-24), and minimizing the index with respect to the sequence of controls, $\underline{u}_k$. If we define

$$\underline{e}_k = \tilde{\underline{y}}_k - \underline{y}_k \qquad (2.4\text{-}28)$$

the resulting control problem is referred to as explicit model-following control* (Ref. 40) and results in a control law of the form

$$\underline{u}_k = -K_1\underline{x}_k - K_2\tilde{\underline{x}}_k + K_3\underline{u}_{c_k} \qquad (2.4\text{-}29)$$

where K_1 to K_3 are obtained as steady-state solutions to a matrix Riccati equation. Alternatively, if we define the error function to be

*The terms explicit and implicit model following are not to be confused with the explicit and implicit adaptive control loops in Fig. 2.4-4. The former are alternate names for the model-in-the-system and model-in-the-performance-index concepts, respectively, described by Tyler (Refs. 26 and 42) for continuous systems.

$$\underline{e}_k = \tilde{H}\left[\tilde{\Phi}\underline{x}_k\right] - \underline{y}_{k-1} \qquad (2.4\text{-}30)$$

the control problem is referred to as implicit model-following, which yields the control law (Ref. 41)

$$\underline{u}_k = -K_4\underline{x}_k + K_5\underline{u}_{c_k} \qquad (2.4\text{-}31)$$

The implicit technique in Eq. (2.4-31) has the same structure as the regulator control law in Eq. (2.4-25), whereas the explicit method is more complex, in that it requires computation of the model state, $\tilde{\underline{x}}_k$.

One disadvantage of the methods described above is that the steady-state response of the resulting flight control system depends upon knowledge of the airframe parameters, through the gains of Eqs. (2.4-25), (2.4-29) and (2.4-31). This sensitivity will tend to be high if the feedback gains are low. Optimal control laws tend to be low-gain compensation techniques (compared with classical methods); hence, the steady-state response sensitivity to parameter variations may be significant, as shown in Section 3.5.1.

Steady-state response can be improved by introducing integral compensation. This compensation is introduced by augmenting the airframe state vector with a new set of state variables, $\underline{y}^*$, defined by the equation

$$\dot{\underline{y}}^* = \underline{x}(t) - \underline{x}_c \qquad (2.4\text{-}32)$$

where the pilot input command, $\underline{x}_c$, is assumed to be constant. When $\underline{y}_k^*$ is included in the state vector discrete-time model for the airframe dynamics, then

$$\lim_{t\to\infty} \underline{x}(t) = \underline{x}_c \qquad (2.4\text{-}33)$$

for the optimal control laws described above, regardless of the airframe parameter variations. That is, the control law has the property of being a Type "1" Servo. This concept is pursued in later sections of this report.

Another method that can be used to select feedback gains in a digital flight controller is the so-called pole-assignment technique. In this approach, it is assumed that an accurate estimate of the state vector is available and that the equations of motions (Eq. (2.4-17)) are controllable in the sense that a sequence, $\underline{u}_k$, can be chosen to achieve any desired final value of $\underline{x}_k$ in a finite number of steps. On this basis, it is possible to select a set of feedback gains so that the closed-loop poles of the stability augmentation system have desired values.

Explicit-Adaptive Control Techniques - Perhaps the simplest explicit-adaptive control technique is gain scheduling, in which control gains are stored as functions of the observed flight condition. The gains are computed by applying one of the control design procedures described earlier, assuming fixed values of the airframe parameters. This is done for a number of flight conditions, and curve-fitting is used to define the relationship between gains and flight variables. This is referred to as an open-loop adaptive technique (Ref. 26) because it depends upon prior knowledge of airframe dynamics as a function of flight condition. Once the gain schedule is chosen, no automatic means is available for correcting the control law on-line in response to new estimates of airframe parameters.

Another form of explicit adaptive control can be derived by noting that many fixed-gain methods yield the control-law gain matrix as a function of the known air-

frame parameters, $\underline{a}$, written symbolically as $K(\underline{a})$. This relationship may be quite complicated in the case of optimal control laws, where K is the solution of a matrix Riccati equation, or it may be relatively simple in the case of the pole-assignment technique, where the functional form of $K(\underline{a})$ often can be derived analytically. In either case, if $\underline{a}$ is unknown, it can be estimated on-line by processing measurement data obtained from the flight control sensors (rate gyro, accelerometer, etc.,), and the control gain can be determined by calculating $K(\hat{\underline{a}})$, where ($\hat{}$) denotes an estimated quantity. This differs from the open-loop technique described above in that the control gains are updated by the current parameter estimates rather than by the indirectly related flight condition variables. This form of the explicit-adaptive control loop is mechanized in Fig. 2.4-4 by combining the calculation of $K(\hat{\underline{a}})$, i.e., the explicit adaptation algorithm, with one of the parameter identification techniques discussed below.

Parameter Identification Methods - One direct method of estimating the airframe parameters in flight is to assume that the parameter values are known as functions of altitude and Mach number from flight test or wind tunnel data. These functions can be stored either in tabular form or as fitted functions, such that it is a simple matter to compute the parameter on-line from flight data. This is analogous to gain scheduling, in that it requires detailed information about the relationship between aircraft parameters and flight condition; however, it has the advantage of providing effectively instantaneous identification, and little or no filtering of the air data measurement errors is required. In addition, the identification does not require command or gust inputs to excite the airframe, as do the techniques described below.

The concept of estimating airframe parameters by processing flight test data has received considerable attention (Ref. 43). Recursive parameter estimation, performed by processing the same type of data in real time within the flight control system, is one method of identifying the airframe dynamics on-line for the purpose of adaptive control. A number of these techniques are reviewed in Ref. 26, including Lion's method, recursive least squares, and the method of instrumental variables. A digital mechanization of Lion's method is discussed in Ref. 44.

The problem also can be formulated as a recursive nonlinear state estimation problem, where the unknown parameters are viewed as state variables. Nonlinear filtering algorithms, such as the extended Kalman filter (Ref. 45) or recursive maximum likelihood estimator (Ref. 46), can be applied to estimate the system state vector, which includes the airframe parameters.

Implicit-Adaptive Control Techniques - Parameter-adaptive control systems with implicit plant identification operate on indirect measures of flight conditions, such as airframe output-error signals. These measures provide indications of variations in airframe dynamics and can be used for adjusting feedback gains. Typically, output error signals are obtained by comparing the control system output with that of a reference model, as illustrated in the broken line portion of Fig. 2.4-4. Techniques include gradient gain adjustment, Liapunov design methods, and dither-adaptive techniques (Ref. 26).

An important factor influencing the suitability of these methods for aircraft flight control is the question of whether or not the significant aircraft transfer functions have dominant right-half-plane zeros that vary with changes in flight condition. For example, the transfer function between tail-surface inputs and the normal acceleration output of a conventional aircraft has right-half-plane zeros. In this situation, none of the implicit-adaptive control methods are well suited for providing desired autopilot performance over a wide range of rapidly varying flight conditions. This is true because these methods either employ high-gain compensation in the adaptive loop or in the main control loop to achieve desired performance, or because they attempt to cancel any right-half-plane zero in the airframe transfer function with a corresponding pole. The latter approach definitely produces an unstable system, and the former yields a design that tends to become unstable when parameter variations cause changes in the right-half-plane zeros. By comparison, those adaptive control techniques which employ explicit parameter identification are capable of providing desired control system response characteristics at all flight conditions, assuming accurate parameter estimates can be obtained.

When the transfer function of interest has only left-half-plane zeros, as in the case of pitch rate control, implicit-adaptive control has demonstrated good performance. The Liapunov design method is particularly attractive, since it can be chosen to guarantee asymptotically stable response error for fixed (but unknown) airframe parameters; an application of th· ·pproach to aircraft flight control is described in Refs and 48.

Dither-adaptive systems operate on the principle of maintaining constant flight control system bandwidth over all flight conditions by adjusting the control loop gain as flight conditions change. This is accomplished by inducing a high-frequency, low-amplitude oscillation in the airframe response through the use of a nonlinear controller, through high-gain compensation, or by introducing a test signal, and adjusting the loop gain to maintain constant oscillation amplitude -- i.e., to maintain constant high-frequency gain.

The dither-adaptive concept is important, both historically and in terms of current applications. It was among the first types of implicit adaptive systems to be developed, and it has found the widest usage in flight tests and in operational aircraft and missiles (Refs. 49, 50, 51, 52, and 53). Its advantages are that the adaptive mechanism is usually quite simple, involving no more than one or two controller gains, and it usually relies on straightforward synthesis techniques; however, there is little experience available for applying these techniques to situations where several adaptive parameters are necessary to compensate for changes in plant dynamic characteristics. Furthermore, there is some evidence that this type of control can contribute to unstable behavior when unexpected flight conditions are encountered (Ref. 54).

Learning Systems - The foregoing concepts can be employed in the design of a control system which trains itself to use appropriate gains as a mission progresses. To illustrate the concept of a learning system, consider an application where a set of aircraft parameters, $\underline{a}$, is identified using a functional fit to air data measurements, $\underline{m}$. The set of numerical coefficients $\underline{b}$ associated with the

fit are based upon wind tunnel data and prior flight test data. In flight, the parameter vector is computed in the form

$$\hat{\underline{a}} = \underline{f}(\underline{m},\underline{b}) \qquad (2.4\text{-}34)$$

where $\underline{b}$ is stored in the computer. As mentioned earlier, this provides rapid identification of $\underline{a}$, since little or no data processing (filtering) of the measurements, $\underline{m}$, is required, and it does not require excitation of the airframe. It has the disadvantage that any errors made in calculating the values of $\underline{b}$, due to prior data imperfections, will never be corrected. Consequently, one could develop an algorithm (say, an extended Kalman or maximum likelihood filter) to independently identify $\underline{a}$ from the flight control sensor outputs, $\hat{\underline{z}}$, and to use the resulting independent set of parameter estimates, $\hat{\underline{a}}_r$, to obtain improved values of $\underline{b}$.

The utility of the learning concept is that it permits rapid calculation of $\hat{\underline{a}}$, which is needed for adaptive control, using the functional approximation, $\underline{f}$. The computation required to obtain $\underline{b}$ and $\hat{\underline{a}}_r$ might be much more time consuming, but this could be done at a slow sampling rate. The concept is characterized by the fact that $\underline{f}$ retains the results of previous corrections, provided $\underline{b}$ is optimized using all past data, as well as the most recent value of $\hat{\underline{a}}_r$. Ultimately, when $\underline{f}$ has been sufficiently "trained", the learning functions could be removed, leaving only the direct calculation of $\hat{\underline{a}}$.

Selected Design Technique - A comprehensive gain scheduling procedure was chosen for further study on the basis of simplicity, control precision for a dynamic system of known structure, compatibility with the design techniques

of modern control theory, and high probability of achieving a successful, practical design. As defined earlier, this is a realization of open-loop explicit adaption. The resulting control laws possess the following attributes:

- System gains adapt to flight condition without forcing by gust disturbances, control inputs, or dithering.
- On-board computations for gain adaptation are minimal.
- Adaptation time for changing flight conditions is fixed and rapid
- Structure of the Linear-Quadratic-Gaussian (LQG) control problem is maintained.
- Design procedures are readily applied to VTOL configurations other than the tandem-rotor helicopter used as a design base in this report and can be extended to include the effects of aeroelasticity, rotor dynamics, ground effects, powered lift/vehicle interactions, etc.

Details of this control design procedure are contained in following sections.

2.5 CHAPTER SUMMARY

This chapter has presented foundation material in the development of control systems for VTOL aircraft, including a review of past developments, characteristics of the VTOL aircraft that is investigated here, an overall structure for designing a guidance and control system, and a survey of adaptive control design techniques.

3. THE LINEAR-OPTIMAL CONTROLLER

3.1 OVERVIEW

In the previous chapter, the nonlinear dynamic equation

$$\dot{\underline{x}}(t) = \underline{f}(\underline{x}(t),\underline{u}(t)) \qquad (3.1\text{-}1)$$

was separated into a nonlinear nominal equation and an equation of the form

$$\dot{\underline{x}}(t) = F\underline{x}(t) + G\underline{u}(t) \qquad (3.1\text{-}2)$$

This chapter presents methods for determining control laws which stabilize and command dynamic systems described by Eq. (3.1-2). The primary method of development is quadratic synthesis, which seeks to minimize an infinite-time quadratic cost functional. Quadratic synthesis provides a control structure which is consistent with classical principles of good control system design. An infinite-time cost functional is used because it results in a constant-gain control law which is easily implemented. In addition, the optimal feedback solution has desirable insensitivity to system parameter perturbations, and the resulting closed loop system is asymptotically stable (Ref. 57).

Section 3.2 discusses three continuous-time linear-optimal regulators which can be designed using infinite-time quadratic cost functions. (A regulator is defined as a controller which returns the linear system of Eq. (3.1-2) to zero equilibrium from an initial offset.) Two of the regulators derived in Section 3.2 have

the additional feature that the controller will return the system to zero equilibrium in the presence of a constant disturbance, while the third design requires that no continuing disturbance be present.

Section 3.3 presents three continuous-time linear-optimal servos. (A servo is a controller which tracks arbitrary (vector) reference inputs.) The dynamic controller of Section 3.3.1 provides zero tracking error under certain conditions and is derived for comparison with "Type 1" servos. The servos of Sections 3.3.2 and 3.3.4 are proportional-integral (PI) and proportional-double integral (PII) controllers. They have the additional property that control rates are weighted, and they provide command response features which are important in flight control system design.

Sections 3.4 and 3.5 present similar results for discrete-time control systems, which are of practical significance for digital flight control systems. Section 3.4 develops the sampled-data regulator, a discrete-time controller for a continuous-time system. The controller accepts sampled information about the system and uses this to construct piecewise-constant control inputs to the system. This way, many of the ideas developed in the continuous-time case carry-over to the discrete-time case. Section 3.5 presents sampled-data equivalents to the PI and PII controllers of Section 3.3. The resulting discrete-time servo controllers serve as candidates for the controllers in the digital-adaptive control law. Section 3.6 summarizes the chapter.

3.2 CONTINUOUS-TIME REGULATOR

The regulator designs are presented in this section. The first is the well-known basic linear-optimal regulator, which is discussed in many texts (e.g., Refs. 55, 56, and 58). The second regulator, the control-rate weighted regulator, uses the theory of the basic regulator to design a controller which simultaneously regulates the state while keeping the control rates at low values. The third design (Ref. 55), a control-rate-weighted proportional-plus-integral regulator, extends the second design to account for the case in which a constant disturbance affects the system. The accommodation of the disturbance is achieved by integral action. The fourth design (Ref. 58), a proportional-plus-integral regulator, uses the theory of the basic regulator to accommodate a constant disturbance but does not require that the control rate be weighted, as in the third design.

3.2.1 Basic Linear-Optimal Regulator

Given the linear-time-invariant system

$$\dot{\underline{x}}(t) = F\underline{x}(t) + G\underline{u}(t) \qquad (3.2\text{-}1)$$

where $\underline{x}(t)$ is an (n x 1)-dimensional state vector and $\underline{u}(t)$ is an (m x 1)-dimensional control vector, the object of control is to find the time function, $\underline{u}(t)$, that stabilizes the system without undue movement of the controls and states. This requirement can be achieved by determining $\underline{u}(t)$ such that the quadratic cost functional

$$J = \int_0^\infty \{\underline{x}^T(t) Q \underline{x}(t) + \underline{u}^T(t) R \underline{u}(t)\} dt \qquad (3.2\text{-}2)$$

is minimized. The matrices Q and R are, respectively, the state-weighting matrix and the control-weighting matrix.

The solution to this problem is a linear feedback control law given by

$$\underline{u}(t) = -K\,\underline{x}(t) \qquad (3.2\text{-}3)$$

where K is a constant (m x n) feedback gain matrix. The gain matrix is expressed by

$$K = R^{-1}G^{T}P \qquad (3.2\text{-}4)$$

P is a constant, symmetric positive-definite (n x n) matrix which is the solution to the algebraic matrix Riccati equation

$$0 = PF + F^{T}P + Q - PGR^{-1}G^{T}P \qquad (3.2\text{-}5)$$

This solution exists and is unique provided that the matrices [F,G] form a controllable pair and $[F,Q^{\frac{1}{2}}]$ form an observable pair* (Ref. 77). Under these mild assumptions, eigenvalues of the closed-loop system given by

$$\dot{\underline{x}}(t) = (F-GK)\underline{x}(t) \qquad (3.2\text{-}6)$$

all lie in the left-half complex plane.

The optimal regulator structure is analogous to conventional stability augmentation systems, as shown in Fig. 3.2-1. The feedback gain, K, is adjusted by choosing Q and R matrices to obtain desirable initial condition response subject to allowable control usage. In general, all states are fedback to all controls, although many feedback paths may have negligible effect. Full state feedback provides compensation without actually increasing the order of the system, as indicated by Eq. (3.2-6).

*$Q^{\frac{1}{2}}$ is defined so that $Q = (Q^{\frac{1}{2}})^{T}(Q^{\frac{1}{2}})$.

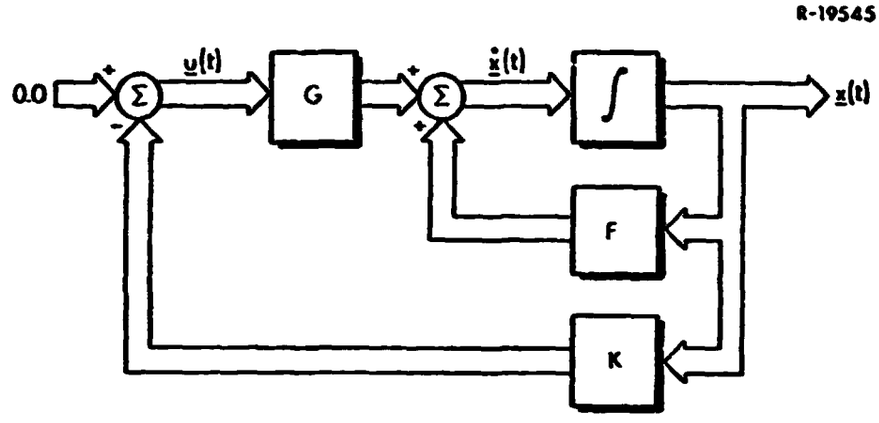

Figure 3.2-1 The Basic Linear-Optimal Regulator

3.2.2 Control-Rate-Weighted Regulator

Suppose another requirement in the design of a controller is that the control rate not be unduly large. This new requirement can be reflected in the cost functional by adding a control-rate term, $\dot{\underline{u}}(t)$:

$$J = \int_0^\infty \left\{ \underline{x}^T(t)Q\underline{x}(t) + \underline{u}^T(t)R\underline{u}(t) + \dot{\underline{u}}^T(t)S\dot{\underline{u}}(t) \right\} dt \qquad (3.2\text{-}7)$$

where S is an positive-definite, symmetric, (m x m) matrix. To solve this problem, let

$$\underline{u}_1(t) = \dot{\underline{u}}(t) \qquad (3.2\text{-}8)$$

and define the system matrices as

$$F_1 = \begin{bmatrix} F & G \\ 0 & 0 \end{bmatrix} \qquad (3.2\text{-}9)$$

$$G_1 = \begin{bmatrix} 0 \\ I \end{bmatrix} \qquad (3.2\text{-}10)$$

$$R_1 = S \tag{3.2-11}$$

$$Q_1 = \begin{bmatrix} Q & 0 \\ 0 & R \end{bmatrix} \tag{3.2-12}$$

$$\underline{x}_1(t) = \begin{bmatrix} \underline{x}(t) \\ \underline{u}(t) \end{bmatrix} \tag{3.2-13}$$

The problem can be reformulated as follows:

$$\dot{\underline{x}}_1(t) = F_1\underline{x}_1(t) + G_1\underline{u}_1(t) \tag{3.2-14}$$

$$J = \int_0^\infty \{\underline{x}_1^T(t)Q_1\underline{x}_1(t) + \underline{u}_1^T(t)R_1\underline{u}_1(t)\}dt \tag{3.2-15}$$

The system has the same form as in the previous section, and the solution is analogous to Eq. (3.2-3):

$$\underline{u}_1(t) = \dot{\underline{u}}(t) = -K\underline{x}_1(t) = [-K_1 \ -K_2]\begin{bmatrix} \underline{x}(t) \\ \underline{u}(t) \end{bmatrix} \tag{3.2-16}$$

The gains are computed from Eqs. (3.2-4) and (3.2-5), with the system matrices redefined as above. The closed-loop form of the system is

$$\begin{bmatrix} \dot{\underline{x}}(t) \\ \dot{\underline{u}}(t) \end{bmatrix} = \begin{bmatrix} F & G \\ -K_1 & -K_2 \end{bmatrix}\begin{bmatrix} \underline{x}(t) \\ \underline{u}(t) \end{bmatrix} \tag{3.2-17}$$

The block diagram of the control-rate-weighted regulator is shown in Fig. 3.2-2.

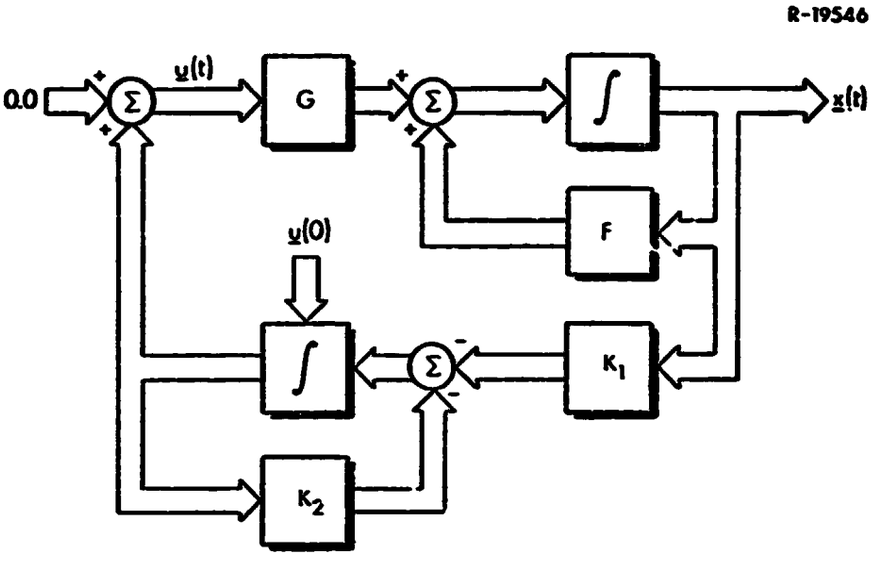

Figure 3.2-2 A Control-Rate-Weighted Regulator

Figure 3.2-2 shows that including control-rate weighting in the cost functional introduces a low-pass filter between the states which are fedback and the actual control inputs to the system. In the figure, the integrators associated with the controller are shown with the initial condition, $\underline{u}(0)$. For aircraft applications, the value of $\underline{u}(0)$ is unimportant, and the integrators usually have zero initial condition. Mathematically, however, $\underline{u}(0)$ is significant, as different values of $\underline{u}(0)$ will result in different values of the cost functional (Eq. (3.2-15)). (Ref. 79) There is an "optimum" value of $\underline{u}(0)$ which gives the lowest value of the cost function. This point is noted because the control-rate-weighted servos of later sections will put the unconstrained nature of $\underline{u}(0)$ to good use. The primary use of the regulator is to counteract external disturbances (such as the wind) whose timing cannot be predicted. In addition to wind gusts, constant disturbances can affect the system. The previous two regulators are not able to

counteract constant disturbances because they do not have integral compensation. The next two control laws have integral compensation and will return a system to a zero set point or zero equilibrium from any initial offset and with certain types of constant disturbances. The final form will be the familiar porportional-plus-integral ("Type 1") regulator.

3.2.3 Control-Rate-Weighted Proportional-Integral Regulator

The purpose of this section is to extend the regulator developed in Section 3.2.2 so that certain types of constant disturbances are accommodated by the control law. In order to show the effect of the disturbance on the system, the constant disturbance is included in the system equation.

Consider the system

$$\dot{\underline{x}}(t) = F\underline{x}(t) + G\underline{u}(t) + D\underline{w} \qquad (3.2\text{-}18)$$

where $\underline{w}$ is a constant disturbance vector of dimension (p x 1), and D is a constant (n x p) matrix. Assume that there exists a constant (m x 1) vector, $\underline{u}^*$, such that

$$G\underline{u}^* = D\underline{w} \qquad (3.2\text{-}19)$$

Then Eq. (3.2-18) can be rewritten as

$$\dot{\underline{x}}(t) = F\underline{x}(t) + G(\underline{u},t)+\underline{u}^*) \qquad (3.2\text{-}20)$$

What is required is a control, $\underline{u}(t)$, which counteracts $\underline{u}^*$ and provides regulatory action for the system. One way of specifying this control would be to build an estimator which estimates the value of $\underline{u}^*$ (Ref. 25). Another way, which

follows, results in a proportional-integral (PI) system (Ref. 55).

Let

$$\underline{u}_2(t) = \underline{u}(t) + \underline{u}^* \tag{3.2-21}$$

and assume that the control derivative is weighted as in the previous section. By taking the derivative of Eq. (3.2-21), it follows that

$$\dot{\underline{u}}_2(t) = \dot{\underline{u}}(t) \tag{3.2-22}$$

Using Eqs. (3.2-8) and Eq. (3.2-13).

$$\underline{u}_1(t) = \dot{\underline{u}}(t) = \dot{\underline{u}}_2(t) \tag{3.2-23}$$

$$\underline{x}_1(t) = \begin{bmatrix} \underline{x}(t) \\ \underline{u}_2(t) \end{bmatrix} \tag{3.2-24}$$

and defining the system by Eqs. (3.2-9) to (3.2-12), the problem is reduced to standard-form (Eqs. (3.2-14) and (3.2-15)). The control solution obtained from Eqs. (3.2-4) and (3.2-5) is

$$\dot{\underline{u}}(t) = -K_1\underline{x}(t) - K_2\underline{u}_2(t) \tag{3.2-25}$$

The rate command is converted to a displacement command as follows: Equation (3.2-20) can be used to obtain an alternate expression for $\underline{u}_2(t)$, given by

$$\underline{u}_2(t) = \underline{u}(t) + \underline{u}^* = (G^TG)^{-1}G^T(\dot{\underline{x}}(t)-F\underline{x}(t)) \tag{3.2-26}$$

The matrix $(G^TG)^{-1}G^T$ is called the pseudo-inverse of G, which exists if G is of full rank m (Ref. 36). Substituting Eq. (3.2-26) into Eq. (3.2-25) results in

$$\dot{\underline{u}}(t) = -K_1\underline{x}(t) - K_2[(G^TG)^{-1}G^T(\dot{\underline{x}}(t)-F\underline{x}(t))] \qquad (3.2\text{-}27)$$

Notational simplification can be provided in Eq. (3.2-27) by defining the (m x n) gain matrices

$$K_3 = K_1 - K_2(G^TG)^{-1}G^TF \qquad (3.2\text{-}28)$$

$$K_4 = K_2(G^TG)^{-1}G^T \qquad (3.2\text{-}29)$$

and integrating both sides of the equation, this results in the following form for the optimal control solution:

$$\underline{u}(t) = -K_4\underline{x}(t) - \int_0^t K_3\underline{x}(\tau)d\tau + \underline{u}(0) + K_4\underline{x}(0) \qquad (3.2\text{-}30)$$

Note that Eq. (3.2-30) contains m scalar integrators, since $K_2\underline{x}(\tau)$ is a vector of order m. Figure 3.2-3) shows the optimal control law in block diagram form and displays the desired proportional-plus-integral structure. In Eq. (3.2-30), the initial condition on the state, $\underline{x}(0)$, is an unknown and cannot be changed. The value of $\underline{u}(0)$ in Eq. (3.2-30) is a parameter which can be set at any desired value. The discussion of $\underline{u}(0)$ in the last section is applicable here, and no initial condition is placed on the integral in Eq. (3.2-30); hence, $\underline{u}(0) = -K_4\underline{x}(0)$ is a reasonable choice.

3.2.4 Direct Proportional-Integral Regulator

In the previous section, the integral action of the control law was obtained by weighting $\dot{\underline{u}}$ in the cost function. This section presents an alternate PI regulator where the integral action is achieved without $\dot{\underline{u}}$ being weighted, as derived in Ref. 60. The integral action is attained by introducing integrators directly into the system. Let $\underline{y}(t)$

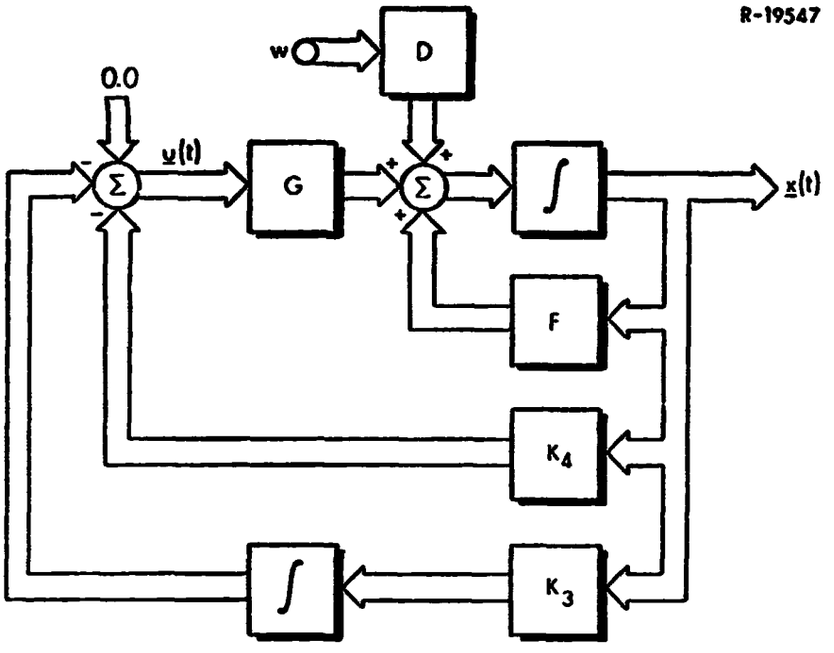

Figure 3.2-3 A Control-Rate-Weighted Proportional-Integral Regulator

be a (p x 1) output vector that is the integral of linear combinations of the states, $\underline{x}(t)$, i.e.,

$$\dot{\underline{y}}_I(t) = T\underline{x}(t) \tag{3.2-30}$$

In Eq. (3.2-30), T is a constant (p x n) transformation matrix mapping a subset of the vector, $\underline{x}(t)$, into the vector space of $\dot{\underline{y}}_I(t)$. Equation (3.2-30) can be combined with the system Eq. (3.2-1) to produce the composite system

$$\begin{bmatrix} \dot{\underline{x}}(t) \\ \dot{\underline{y}}_I(t) \end{bmatrix} = \begin{bmatrix} F & 0 \\ T & 0 \end{bmatrix} \begin{bmatrix} \underline{x}(t) \\ \underline{y}_I(t) \end{bmatrix} + \begin{bmatrix} G \\ 0 \end{bmatrix} \underline{u}(t) \tag{3.2-31}$$

The following cost function is defined for the composite system:

$$J = \int_0^\infty \left\{ [\underline{x}^T(t) \;\; \underline{y}_I^T(t)] Q \begin{bmatrix} \underline{x}(t) \\ \underline{y}_I(t) \end{bmatrix} + \underline{u}^T(t) R \underline{u}(t) \right\} dt \qquad (3.2\text{-}32)$$

A control, $\underline{u}(t)$, which minimizes Eq. (3.2-32) can be found provided the matrices $\begin{bmatrix} F & 0 \\ T & 0 \end{bmatrix}$ and $\begin{bmatrix} G \\ 0 \end{bmatrix}$ form a completely controllable pair. Reference 62 shows that the above pair is completely controllable provided that

$$\text{rank} \begin{bmatrix} F & G \\ T & 0 \end{bmatrix} = n + p \qquad (3.2\text{-}33)$$

Equation (3.2-33) implies that there must be at least as many controls as there are integrators, i.e., $p \leq m$. If they are equal in number ($m = p$), then the ability to invert the matrix in Eq. (3.2-33) specifies whether or not the system is controllable.

Using Eq. (3.2-4) and (3.2-5) the control which minimizes the cost function (Eq. (3.2-32)) is given by

$$\underline{u}(t) = [-K_5 - K_6] \begin{bmatrix} \underline{x}(t) \\ \underline{y}_I(t) \end{bmatrix} \qquad (3.2\text{-}34)$$

which can be written as

$$\underline{u}(t) = -K_5 \underline{x}(t) - K_6 \int_0^t T\underline{x}(\tau) d\tau \qquad (3.2\text{-}35)$$

The block diagram for this regulator is shown in Fig. 3.2-4.

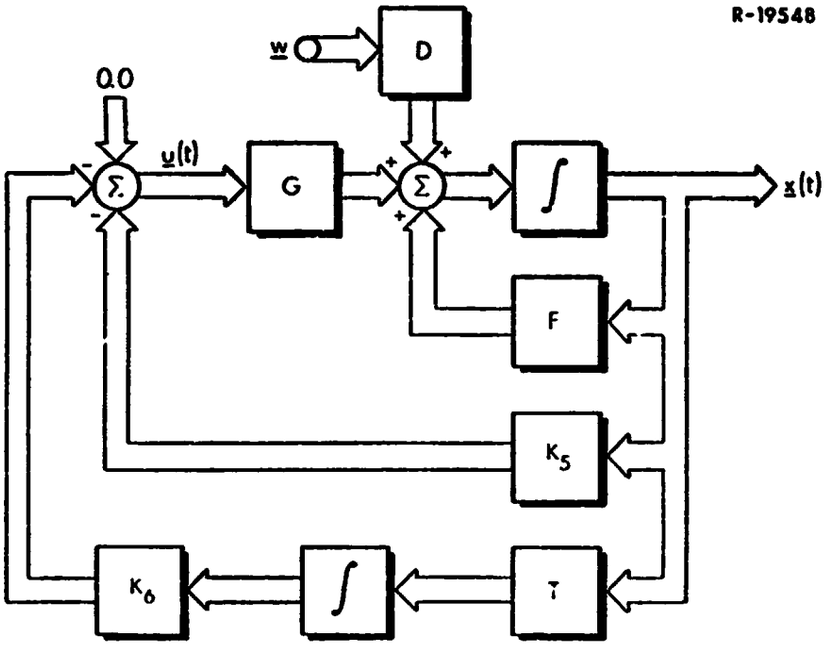

Figure 3.2-4 A Proportional-Integral Regulator

With a constant disturbance present, the closed-loop system appears as

$$\begin{bmatrix} \dot{\underline{x}}(t) \\ \dot{\underline{y}}_I(t) \end{bmatrix} = \begin{bmatrix} (F-GK_5) & -GK_6 \\ T & 0 \end{bmatrix} \begin{bmatrix} \underline{x}(t) \\ \underline{y}_I(t) \end{bmatrix} + \begin{bmatrix} D \\ 0 \end{bmatrix} \underline{w} \qquad (3.2\text{-}36)$$

Since the constant disturbance does not affect the asymptotic stability of the system, Eq. (3.2-36) reduces to the following, as $t \to \infty$:

$$\begin{bmatrix} 0 \\ 0 \end{bmatrix} = \begin{bmatrix} F-GK_5 & -GK_6 \\ T & 0 \end{bmatrix} \begin{bmatrix} \underline{x}^* \\ \underline{y}_I^* \end{bmatrix} + \begin{bmatrix} D \\ 0 \end{bmatrix} \underline{w} \qquad (3.2\text{-}37)$$

In Eq. (3.2-37), $\underline{x}^*$ and $\underline{y}_I^*$ are the steady-state values of the aircraft states and integrator states, respectively. From Eq. (3.2-37), it follows that

$$T\underline{x}^* = 0 \tag{3.2-38}$$

The steady-state error of linear combinations of the state is zero in the presence of a constant disturbance. The two PI regulators presented here and in the previous section have different asymptotic properties. The control law in Section 3.2.3 forces

$$\lim_{t\to\infty} \underline{x}(t) = 0 \tag{3.2-39}$$

provided the disturbance, $D\underline{w}$, is in the range space of the control matrix G (Ref. 55). Only a subspace of dimension m (at most) of the states can be returned to zero given any general disturbance. The control law in this section forces

$$\lim_{t\to\infty} T\underline{x}(t) = 0 \tag{3.2-40}$$

whether or not $D\underline{w}$ is in the range space of G. In other words, the control law of Section 3.2 3 cannot do better than the control law derived in this section, while the control law in this section can accommodate disturbances that are in the null space of the G matrix.

For the VALT Research aircraft considered in this report, either control law could be used as a regulator, although neither can entirely eliminate generalized disturbance effects. Wind disturbances can cause three forces and three moments, thus affecting six state rate components. There are four independent control variables; therefore, these disturbances exceed the range space of the G matrix. This problem is discussed further in Section 4.3.

3.3 CONTINUOUS-TIME SERVO

Section 3.2 dealt with the regulator problem, which involved returning a linear-time-invariant system to equilibrium from some initial offset. Attention is now turned to the servo problem, where certain system outputs are required to attain input (or "command") values. For design purposes, the command inputs are constant values, and the problem can be restated as the accommodation of a non-zero regulation set point.

Consider the system presented in Section 3.2.1:

$$\dot{\underline{x}}(t) = F\underline{x}(t) + G\underline{u}(t) \qquad (3.3\text{-}1)$$

In this section, the purpose of the control, $\underline{u}(t)$, will be to stabilize Eq. (3.3-1) while at the same time forcing a certain output of the states given by

$$\underline{y}(t) = T\underline{x}(t) \qquad (3.3\text{-}2)$$

to attain an arbitrary constant reference, $\underline{y}_d$, such that

$$\lim_{t\to\infty} \underline{y}(t) = \underline{y}_d \qquad (3.3\text{-}3)$$

The next sections present four control laws which achieve this requirement. They are the

- Control-Rate-Weighted Dynamic Controller
- Control-Rate-Weighted Proportional-Integral (PI) Servo
- Proportional-Integral Servo
- Proportional-Double Integral (PII) Servo

The first control law can provide the reference output, $\underline{y}_d$, under special circumstances, while the last three are "Type 1" systems with broader capabilities.

The servo is an important control law for VTOL aircraft, since the reference vector, $\underline{y}_d$, can be the output of a guidance law which is steering the aircraft (Fig. 2.4-2). The last two control laws, the PI and PII controllers, are continuous-time servos, whose discrete-time versions serve as the primary candidates for the VALT Research Aircraft control laws developed in this report.

3.3.1 Control-Rate-Weighted Dynamic Servo

The theory of the control-rate-weighted regulator in Section 3.2.2 is used in this section to determine a control law which has the ability to force $\underline{y}(t)$ to the reference, $\underline{y}_d$. This control law was developed by Athans in Ref. 59.

Let $\underline{x}^*$ and $\underline{u}^*$ be the steady-state values of the states and controls, given the value of $\underline{y}_d$. The variables, $\underline{x}^*$ and $\underline{u}^*$, must satisfy the following equations:

$$0 = F\underline{x}^* + G\underline{u}^* \tag{3.3-4}$$

$$T\underline{x}^* = \underline{y}_d \tag{3.3-5}$$

Equation (3.3-4) is a consequence of the fact that in steady-state, $\dot{\underline{x}}(t) = 0$. Equation (3.3-5) follows from the steady-state assumption and from Eq. (3.3-2). Define the following variables:

$$\tilde{\underline{x}}(t) = \underline{x}(t) - \underline{x}^* \tag{3.3-6}$$

$$\tilde{\underline{u}}(t) = \underline{u}(t) - \underline{u}^* \tag{3.3-7}$$

Using Eqs. (3.3-6) and (3.3-7), the system equation takes the following form:

$$\dot{\underline{x}}(t) = \dot{\tilde{\underline{x}}}(t) = F\underline{x}(t) + G\underline{u}(t) = F\tilde{\underline{x}}(t) + G\tilde{\underline{u}}(t) \qquad (3.3\text{-}8)$$

In order to find the control law, $\underline{u}(t)$, in Eq. (3.3-8) using quadratic synthesis, a cost functional must be specified. The cost functional includes weighting on $\dot{\underline{u}}(t)$, as in Section 3.2.2:

$$J = \int_0^\infty \left\{ \tilde{\underline{x}}^T(t) Q \tilde{\underline{x}}(t) + \tilde{\underline{u}}^T(t) R \tilde{\underline{u}}(t) + \dot{\underline{u}}(t) S \dot{\underline{u}}(t) \right\} dt \qquad (3.3\text{-}9)$$

In Eq. (3.3-9), Q is positive semi-definite, $[F, Q^{\frac{1}{2}}]$ is a completely observable pair, and the matrices R and S are positive definite. Define the same variables as in Eqs. (3.2-8) and (3.2-13):

$$\underline{u}_1(t) = \dot{\underline{u}}(t) = \dot{\tilde{\underline{u}}}(t) \qquad (3.3\text{-}10)$$

$$\underline{x}_1(t) = \begin{bmatrix} \tilde{\underline{x}}(t) \\ \tilde{\underline{u}}(t) \end{bmatrix} \qquad (3.3\text{-}11)$$

The problem has been reduced to the same two equations given by Eq. (3.2-14) and Eq. (3.2-15). The solution is as before and is given by

$$\dot{\underline{u}}(t) = \dot{\tilde{\underline{u}}}(t) = [-K_1 \; -K_2] \begin{bmatrix} \tilde{\underline{x}}(t) \\ \tilde{\underline{u}}(t) \end{bmatrix} \qquad (3.3\text{-}12)$$

or, integrating to obtain the control displacement,

$$\underline{u}(t) = -K_1 \int_0^t \underline{x}(\tau)d\tau - K_2 \int_0^t \underline{u}(\tau)d\tau + \underline{u}(0) \qquad (3.3\text{-}13)$$

In closed-loop form, the system can be described as

$$\begin{bmatrix} \dot{\underline{x}}(t) \\ \dot{\underline{u}}(t) \end{bmatrix} = \begin{bmatrix} F & G \\ -K_1 & -K_2 \end{bmatrix} \begin{bmatrix} \underline{x}(t) \\ \underline{u}(t) \end{bmatrix} + \begin{bmatrix} 0 \\ I \end{bmatrix} [K_1 \; K_2] \begin{bmatrix} \underline{x}^* \\ \underline{u}^* \end{bmatrix} \qquad (3.3\text{-}14)$$

Equation (3.3-14) can be simplified if it is assumed that the number of outputs in $\underline{y}(t)$ equal the number of controls and that the matrix $\begin{bmatrix} F & G \\ T & 0 \end{bmatrix}$ is invertible. With these assumptions, the conditions given by Eq. (3.3-4) and Eq. (3.3-5) can be combined to form

$$\begin{bmatrix} 0 \\ 0 \end{bmatrix} = \begin{bmatrix} F & G \\ T & 0 \end{bmatrix} \begin{bmatrix} \underline{x}^* \\ \underline{u}^* \end{bmatrix} + \begin{bmatrix} 0 \\ I \end{bmatrix} \underline{y}_d \qquad (3.3\text{-}15)$$

and $\underline{x}^*$ and $\underline{u}^*$ can be determined by

$$\begin{bmatrix} \underline{x}^* \\ \underline{u}^* \end{bmatrix} = \begin{bmatrix} F & G \\ T & 0 \end{bmatrix}^{-1} \begin{bmatrix} 0 \\ I \end{bmatrix} \underline{y}_d = \begin{bmatrix} S_{11} & S_{12} \\ S_{21} & S_{22} \end{bmatrix} \begin{bmatrix} 0 \\ I \end{bmatrix} \underline{y}_d \qquad (3.3\text{-}16)$$

or

$$\underline{x}^* = S_{12} \, \underline{y}_d \qquad (3.3\text{-}17)$$

$$\underline{u}^* = S_{22} \, \underline{y}_d \qquad (3.3\text{-}18)$$

Define the matrix, L, as

$$L = K_1 S_{12} + K_2 S_{22} \qquad (3.3\text{-}19)$$

The closed-loop system then can be stated as

$$\begin{bmatrix} \dot{\underline{x}}(t) \\ \dot{\underline{u}}(t) \end{bmatrix} = \begin{bmatrix} F & G \\ -K_1 & -K_2 \end{bmatrix} \begin{bmatrix} \underline{x}(t) \\ \underline{u}(t) \end{bmatrix} + \begin{bmatrix} 0 \\ L \end{bmatrix} \underline{y}_d \qquad (3.3\text{-}20)$$

The block diagram of the control-rate-weighted dynamic controller is shown in Fig. 3.3-1. The figure shows that

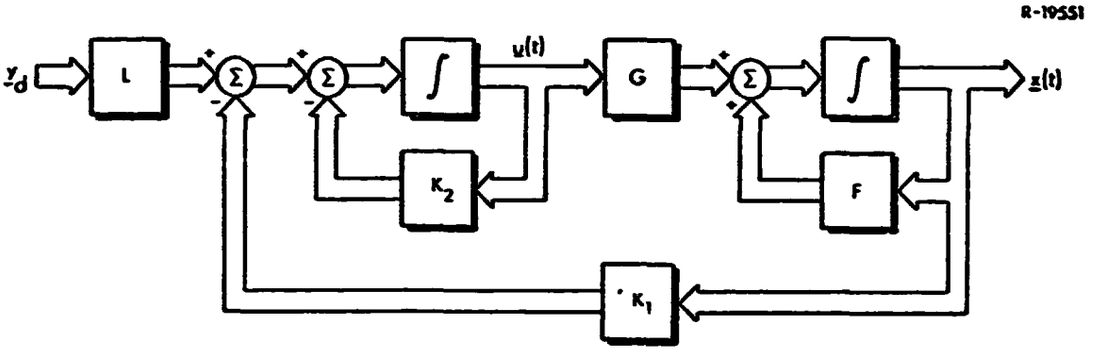

Figure 3.3-1 A Control-Rate-Weighted Dynamic Servo

although there is an integration in the control law, there is control variable feedback around the integrator, and its primary purpose is to provide low-pass filtering so that $\dot{\underline{u}}(t)$ is moderated. Note that the invertibility of the composite matrix enters the problem in Eq. (3.3-16). A discussion of the implications of this is presented in Section 3.3.3.

In Eq. (3.3-20), if the system matrices F and G have actual values which are different from the ones used in the design, the steady-state value of $\underline{y}(t)$ will not necessarily approach $\underline{y}_d$. This is because the system in Fig. (3.3-1) is not "Type 1". A Type 1 system contains one pure integration in series with the control actuator (Ref. 78). Sandell, using the Type 1 definition, produced the control law which is shown next.

3.3.2 Control-Rate-Weighted Proportional-Integral (PI) Servo

The following derivation of a proportional-integral (PI) servo is based on weighting $\dot{\underline{u}}$ in the cost-functional and is taken from Ref. 61. The discrete-time version of this servo is a candidate for implementation on VTOL aircraft.

The derivation proceeds as in Section 3.3.1, from Eq. (3.3-4) to Eq. (3.3-12). An additional assumption is used, i.e., that the following matrix is invertible:

$$\begin{bmatrix} F & G \\ T & 0 \end{bmatrix}^{-1} = \begin{bmatrix} S_{11} & S_{12} \\ S_{21} & S_{22} \end{bmatrix} \qquad (3.3\text{-}21)$$

This assumption implies that the number of reference outputs equals the number of controls, where T is defined in as in Eq. (3.3-5). Since the control law is determined by quadratic synthesis, the basic requirements that [F,G,T] is minimal (completely controllable and observable), $[F,Q^{\frac{1}{2}}]$ is a completely observable pair, R and S are positive definite, and Q is positive semi-definite. R, S, and Q have the same definition as in Eq. (3.3-9). The derivation is modified beginning at Eq. (3.3-12), which is restated as

$$\dot{\underline{u}}(t) = -K_1\tilde{\underline{x}}(t) - K_2\tilde{\underline{u}}(t) \qquad (3.3\text{-}22)$$

The derivation uses the idea developed in Section 3.2.3, in which a substitution is made for $\tilde{\underline{u}}(t)$. Instead of using the pseudo-inverse of G, it is assumed that there exists an (m x n) matrix B such that

$$BG = I \qquad (3.2\text{-}23)$$

where I is the (m x m) identify matrix. There are an infinite number of B matrices which could satisfy Eq. (3.3-23), provided G is full rank m and m < n. Using Eq. (3.3-23) and Eq. (3.3-8), an alternate expression for $\underline{\tilde{u}}(t)$ is obtained:

$$\underline{\tilde{u}}(t) = B\dot{\underline{\tilde{x}}}(t) - BF\underline{\tilde{x}}(t) \qquad (3.3\text{-}24)$$

Substituting Eq. (3.3-24) into Eq. (3.3-22) results in

$$\dot{\underline{\tilde{u}}}(t) = (-K_1+K_2BF)\underline{\tilde{x}}(t) - K_2B\dot{\underline{\tilde{x}}}(t) \qquad (3.3\text{-}25)$$

There are unique matrices, L and B, such that Eq. (3.3-23) is satisfied, and the following is true:

$$-K_1 + K_2BF = -LT \qquad (3.3\text{-}26)$$

Equations (3.3-26) and (3.3-23) then can be combined to produce

$$[K_2B \;\; L]\begin{bmatrix} F & G \\ T & 0 \end{bmatrix} = [K_1 \;\; K_2] \qquad (3.3\text{-}27)$$

Post-multiplying both sides of the equation by $\begin{bmatrix} F & G \\ T & 0 \end{bmatrix}^{-1}$ and using Eq. (3.3-21), it can be seen that the expressions for L and B are uniquely given by

$$L = K_1S_{12} + K_2S_{22} \qquad (3.3\text{-}28)$$

$$B = K_2^{-1}K_1S_{11} + S_{21} \qquad (3.3\text{-}29)$$

Substituting Eq. (3.3-26) into Eq. (3.3-25) produces

$$\dot{\underline{\tilde{u}}}(t) = L(\underline{y}_d-\underline{y}(t)) - K_2B\,\dot{\underline{\tilde{x}}}(t) \qquad (3.3\text{-}30)$$

Integrating Eq. (3.3-30), the control law can be written as

$$\underline{u}(t) = \int_0^t L(\underline{y}_d - \underline{y}(\tau))d\tau - K_2 B\underline{\tilde{x}}(t) + K_2 B\underline{\tilde{x}}(0) + \underline{u}(0) \quad (3.3\text{-}31)$$

where $\underline{u}(0)$ is unspecified. A substitution for $\underline{u}(0)$, which reduces the structure of Eq. (3.3-31), is

$$\underline{u}(0) = A\underline{y}_d - K_2 B\underline{x}(0) \quad (3.3\text{-}32)$$

where the matrix, A, is defined by

$$A = S_{22} + K_2^{-1} K_1 S_{12} \quad (3.3\text{-}33)$$

Substituting Eq. (3.3-32) into Eq. (3.3-31) produces

$$\underline{u}(t) = \int_0^t L(\underline{y}_d - \underline{y}(\tau))d\tau - K_2 B(\underline{x}(t) - \underline{x}^*) + K_2 B(\underline{x}(0) - \underline{x}^*)$$

$$+ A\underline{y}_d - K_2 B\underline{x}(0) + AT\underline{x}(t) - AT\underline{x}(t) \quad (3.3\text{-}34)$$

Equation (3.3-34) can be reduced by defining

$$N = -K_2 B + AT \quad (3.3\text{-}35)$$

Substituting Eq. (3.3-35) into Eq. (3.3-34) and reducing,

$$\underline{u}(t) = \int_0^t L(\underline{y}_d - T\underline{x}(\tau))d\tau + N\underline{x}(t) + A(\underline{y}_d - T\underline{x}(t)) \quad (3.3\text{-}36)$$

This control law (Fig. 3.3-2)) resembles a classical PID controller, where the derivative feedback has been replaced by feedback of the entire state (Ref. 59). Note that to obtain the value of $\underline{u}(0)$ given by Eq. (3.3-32), the initial condition on the integrator must be set to 0. The matrix, A, is chosen to give optimal cost in Eq. (3.3-9), i.e., this is the optimal $\underline{u}(0)$ when $\underline{x}(0) = 0$.

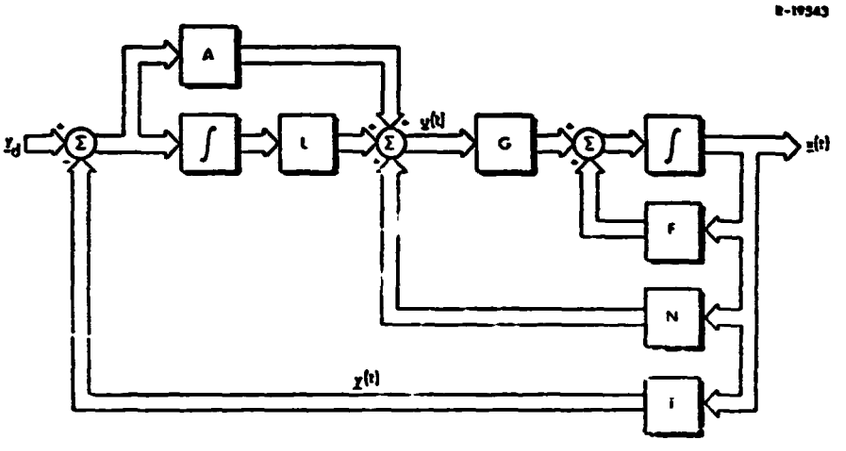

Figure 3.3-2 A Control-Rate-Weighted Proportional-Integral Servo

This section has presented a servo for which the integral action was obtained by weighting $\dot{\underline{u}}(t)$ in the cost functional. The next section presents a servo design which does not require that $\dot{\underline{u}}(t)$ be weighted.

3.3.3 Proportional-Integral Servo

This section presents a proportional-plus-integral servo which introduces the required integration states directly into the system structure. This development was reported by Young and Willems in Ref. 62. The basic idea is to use the theory developed in Section 3.2.4 (which counteracts constant disturbances) to accommodate the non-zero set point. In Section 3.2.4, if integration variables are defined as

$$\dot{\underline{x}}_I(t) = T\underline{x}(t) \tag{3.3-37}$$

then in the limit, as $t \to \infty$, $T\underline{x}(t) \to 0$. The integration variables given by Eq (3.3-37) are defined in this section by

$$\dot{\underline{y}}_I(t) = T\underline{x}(t) = \underline{y}_d \qquad (3.3\text{-}38)$$

In this case, if the system is designed using quadratic synthesis, it is expected that

$$\lim_{t\to\infty} \dot{\underline{y}}_I(t) = 0$$

which implies that

$$\lim_{t\to\infty} T\underline{x}(t) = \underline{y}_d \qquad (3.3\text{-}39)$$

the desired result.

Formally, the system Eq. (3.2-1) is combined with Eq. (3.3-38) to produce

$$\begin{bmatrix} \dot{\underline{x}}(t) \\ \dot{\underline{y}}_I(t) \end{bmatrix} = \begin{bmatrix} F & 0 \\ T & 0 \end{bmatrix} \begin{bmatrix} \underline{x}(t) \\ \underline{y}_I(t) \end{bmatrix} + \begin{bmatrix} G \\ 0 \end{bmatrix} \underline{u}(t) + \begin{bmatrix} 0 \\ -I \end{bmatrix} \underline{y}_d \qquad (3.3\text{-}40)$$

The following variables are defined:

$$\lim_{t\to\infty} \underline{x}(t) = \underline{x}^* \qquad (3.3\text{-}41)$$

$$\lim_{t\to\infty} T\underline{x}(t) = T\underline{x}^* = \underline{y}_d \qquad (3.3\text{-}42)$$

$$\lim_{t\to\infty} \underline{u}(t) = \underline{u}^* \qquad (3.3\text{-}43)$$

$$\tilde{\underline{x}}(t) = \underline{x}(t) - \underline{x}^* \qquad (3.3\text{-}44)$$

$$\tilde{\underline{u}}(t) = \underline{u}(t) - \underline{u}^* \qquad (3.3\text{-}45)$$

With these definitions, Eq. (3.3-40) can be rewritten as

$$\begin{bmatrix} \dot{\tilde{\underline{x}}}(t) \\ \dot{\underline{y}}_I(t) \end{bmatrix} = \begin{bmatrix} F & 0 \\ T & 0 \end{bmatrix} \begin{bmatrix} \tilde{\underline{x}}(t) \\ \underline{y}_I(t) \end{bmatrix} + \begin{bmatrix} G \\ 0 \end{bmatrix} \tilde{\underline{u}}(t) \qquad (3.3\text{-}46)$$

where the control $\tilde{\underline{u}}(t)$ must minimize the following cost functional:

$$J = \int_0^\infty \left\{ [\tilde{\underline{x}}^T(t) \; \underline{y}_I^T(t)] Q \begin{bmatrix} \tilde{\underline{x}}(t) \\ \underline{y}_I(t) \end{bmatrix} + \tilde{\underline{u}}^T(t) R \tilde{\underline{u}}(t) \right\} dt \qquad (3.3\text{-}47)$$

Equations (3.3-46) and (3.3-47) are in the same form as the basic linear optimal regulator, which was shown in Section 3.2.1. The answer for $\underline{u}(t)$ is given by Eq. (3.2-3) and is

$$\underline{u}(t) = -K_1 \underline{x}(t) - K_2 \underline{y}_I(t) + K_1 \underline{x}^* + \underline{u}^* \qquad (3.3\text{-}48)$$

In order for Eq. (3.3-48) to be true, Eq. (3.3-46) must be a completely controllable system. Reference 62 shows that the system is completely controllable provided

$$\text{rank} \begin{bmatrix} F & G \\ T & 0 \end{bmatrix} = n + p \qquad (3.3\text{-}49)$$

where p is the dimension of $\underline{y}_d$. The structure of the control law given by Eq. (3.3-48) can be reduced if a matrix can be found which maps the $\underline{y}_d$ vector into the corresponding $\underline{x}^*$ and $\underline{u}^*$ vectors. Section 3.3.1 showed that the mappings exist if the matrix in Eq. (3.3-49) is invertible. The matrix maps are given, in that case, by Eqs. (3.3-17) and (3.3-18). If the matrix in Eq. (3.3-49) is not invertible but Eq. (3.3-49) is satisfied, some of the states of the system are unconstrained, given the set point, $\underline{y}_d$. One way of resolving the problem is to add further constraints (other than $\underline{y}_d$) until the states become uniquely specified. This is done

in Ref. 25 by requiring that the states and controls accommodate $\underline{y}_d$ and at the same time minimize a linear combination of the steady-state values of the states and controls. The minimization provides the additional constraint, so that the matrix mappings S_{12} and S_{22} in the following are unique:

$$\underline{x}^* = S_{12}\,\underline{y}_d \tag{3.3-50}$$

$$\underline{u}^* = S_{22}\,\underline{y}_d \tag{3.3-51}$$

By making the substitution

$$E = K_1 S_{12} + S_{22} \tag{3.3-52}$$

the expression for the control (Eq. (3.3-48)) can be reduced to the following closed-loop expression:

$$\begin{bmatrix} \dot{\underline{x}}(t) \\ \dot{\underline{y}}_I(t) \end{bmatrix} = \begin{bmatrix} (F-GK_1) & -GK_2 \\ T & 0 \end{bmatrix} \begin{bmatrix} \underline{x}(t) \\ \underline{y}_I(t) \end{bmatrix} + \begin{bmatrix} GE \\ -I \end{bmatrix} \underline{y}_d \tag{3.3-53}$$

A block diagram of the control law is shown in Fig. 3.3-3. It exhibits the integral action necessary to make the control law a Type 1 system. Feedforward of the command, $\underline{y}_d$, results in the steady-state value of the integrator state, $\underline{y}_I(t)$, being zero if F and G are known perfectly. If there is a constant disturbance present, then

$$\lim_{t\to\infty} T\underline{x}(t) = \underline{y}_d \tag{3.3-54}$$

is true, but the value of $\underline{y}_I(t)$ in steady-state is no longer zero. The steady-state value of the integrator states will be effectively used in the next section, which extends the results of this section to the case where the control rate is weighted.

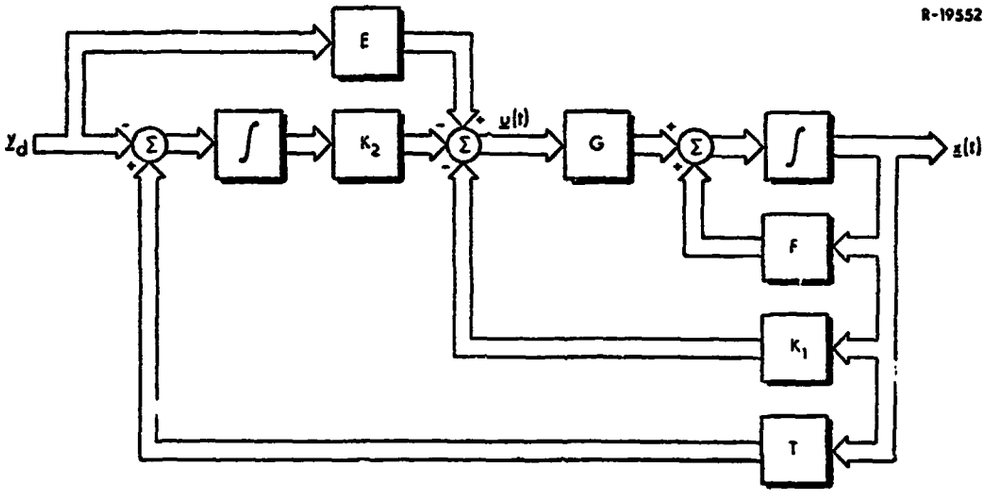

Figure 3.3-3 A Proportional-Integral Servo

3.3.4 Proportional-Plus-Double Integral (PII) Servo

This final section combines the control-rate weighting of Section 3.3.1 with the integration states of Section 3.3.3 to produce a servo which has integral action and limits the control rate. This design can be considered an alternative to the design in Section 3.3.2.

The development is straightforward, proceeding exactly as in Section 3.3.3, except that there are m additional states in the system. Combining Eqs. (3.3-37) to (3.3-45) with Eqs. (3.3-6) to (3.3-11), the system and cost function for this section are

$$\begin{bmatrix} \dot{\underline{\tilde{x}}}(t) \\ \dot{\underline{\tilde{u}}}(t) \\ \dot{\underline{\tilde{y}}}_I(t) \end{bmatrix} = \begin{bmatrix} F & G & 0 \\ 0 & 0 & 0 \\ T & 0 & 0 \end{bmatrix} \begin{bmatrix} \underline{\tilde{x}}(t) \\ \underline{\tilde{u}}(t) \\ \underline{\tilde{y}}_I(t) \end{bmatrix} + \begin{bmatrix} 0 \\ I \\ 0 \end{bmatrix} \dot{\underline{u}}(t) \qquad (3.3\text{-}55)$$

$$J = \int_0^\infty \left\{ [\tilde{\underline{x}}^T(t), \tilde{\underline{u}}^T(t), \tilde{\underline{y}}_I^T(t)] Q \begin{bmatrix} \tilde{\underline{x}}(t) \\ \tilde{\underline{u}}(t) \\ \tilde{\underline{y}}_I(t) \end{bmatrix} + \dot{\underline{u}}^T(t) R \dot{\underline{u}}(t) \right\} dt \quad (3.3\text{-}56)$$

The variable, $\tilde{\underline{y}}_I(t)$, is defined as

$$\tilde{\underline{y}}_I(t) = \underline{y}_I(t) - \underline{y}_I^* \quad (3.3\text{-}57)$$

where $\underline{y}_I^*$ is the steady-state value of the integrator states, as $t \to \infty$. If the controllability and observability requirements are satisfied for Eqs. (3.3-55) and (3.3-56), then the control, $\underline{u}(t)$, is given by

$$\underline{u}(t) = -K_1\underline{x}(t) - K_2\underline{u}(t) - K_3\underline{y}_I(t) + K_1\underline{x}^* + K_2\underline{u}^* + K_3\underline{y}_I^* \quad (3.3\text{-}58)$$

Equation (3.3-58) is obtained from Eq. (3.2-3) because Eqs. (3.3-55) and (3.3-56) are in the regulator form of Eqs. (3.2-1) and (3.2-2). In Eq. (3.3-58), $\underline{x}^*$ and $\underline{u}^*$ are determined by the set point vector, $\underline{y}_d$, but $\underline{y}_I^*$ is not constrained. A useful way of determining $\underline{y}_I^*$, if $p = m$, is given by the next equation:

$$\underline{y}_I^* = -K_3^{-1}K_1\underline{x}^* - K_3^{-1}K_2\underline{u}^* \quad (3.3\text{-}59)$$

If $p < m$, then $\underline{y}_I^*$ can be found by introducing a minimization constraint, as discussed in Section 3.3.3, so that

$$K_1\underline{x}^* + K_2\underline{u}^* + K_3\underline{y}_I^* = 0 \quad (3.3\text{-}60)$$

Using Eq. (3.3-59) or Eq. (3.3-60), the feedforward of the set point, $\underline{y}_d$, is not needed, as shown in Fig. 3.3-4, which is a block diagram of the control law given by Eq. (3.3-58). In Fig. 3.3-4, the implementation of the control law does not require that $\underline{y}_I^*$, $\underline{x}^*$ and $\underline{u}^*$ be calculated, since the

system approaches these values in steady-state automatically. The closed-loop form of the system is given by

$$\begin{bmatrix} \dot{\underline{x}}(t) \\ \dot{\underline{u}}(t) \\ \dot{\underline{y}}_I(t) \end{bmatrix} = \begin{bmatrix} F & G & 0 \\ -K_1 & -K_2 & -K_3 \\ T & 0 & 0 \end{bmatrix} \begin{bmatrix} \underline{x}(t) \\ \underline{u}(t) \\ \underline{y}_I(t) \end{bmatrix} + \begin{bmatrix} 0 \\ 0 \\ -I \end{bmatrix} \underline{y}_d \qquad (3.3\text{-}61)$$

This control law is competitive with the one in Section 3.3.2, in that they both require the same number of gains.

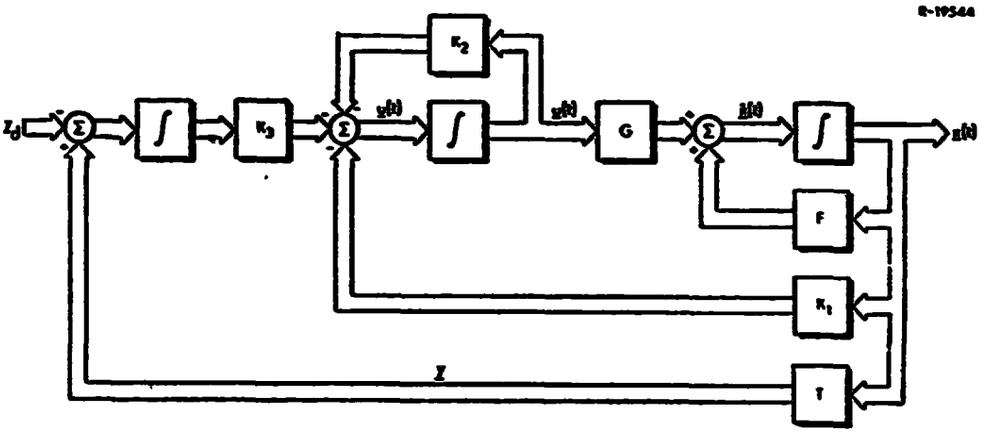

Figure 3.3-4 A Proportional-Plus-Double Integral Servo

This section ends the discussion of continuous-time regulators and servos which can be solved using quadratic synthesis. The next section introduces ways of designing discrete-time control laws which are equivalent to these continuous-time designs.

3.4 DISCRETE-TIME-EQUIVALENT OF THE CONTINUOUS-TIME REGULATOR

The goal of this section is to present a method for obtaining a discrete-time version of the continuous-time regulator shown in Section 3.2.1. If this can be done, then all of the control laws in Section 3.2 and 3.3 possess discrete-time versions, since in all cases they eventually reduce to Eqs. (3.2-1) and (3.2-2).

The method chosen comes from Ref. 63, and it results in a so-called sampled-data regulator. A sampled-data regulator consists of a control law which drives a continuous system using piecewise-constant inputs that change only at sampling intervals. The objective of a sampled-data regulator is to control a system along a trajectory that is as close as possible to the trajectory obtained by using a continuous controller. The derivation proceeds as follows.

Let the continuous-time dynamical system be modeled by

$$\dot{\underline{x}}(t) = F\underline{x}(t) + G\underline{u}(t) \qquad (3.4\text{-}1)$$

where $\underline{x}(t)$ is an n-dimensional state vector, $\underline{u}(t)$ is an m-dimensional control vector, and F and G are compatible, constant matrices. The cost function is given by

$$J = \int_0^\infty \left\{ \underline{x}^T(t)Q\underline{x}(t) + \underline{u}^T(t)R\underline{u}(t) \right\} dt \qquad (3.4\text{-}2)$$

with $Q \geq 0$ and $R > 0$. A control, $\underline{u}(t)$, is to be determined that changes only at the sampling times given by

$$\{t_k\} = \{t_k : t_k = k\Delta t;\ k=0,1,2,\ldots\} \qquad (3.4\text{-}3)$$

and that minimizes Eq. (3.4-2) subject to Eq. (3.4-1). In Eq. (3.4-3), Δt is the sampling interval. To find $\underline{u}(t)$, the continuous-time system is transformed into a discrete-time system using the following equation:

$$\underline{x}(t) = e^{[Ft]}\underline{x}(0) + \int_0^t e^{[F(t-\tau)]}\, G\underline{u}(\tau)d\tau \qquad (3.4\text{-}4)$$

which is the solution for $\underline{x}(t)$ in Eq. (3.4-1), given $\underline{u}(t)$. Using the superposition principle of linear systems and the fact that $\underline{u}(t)$ is constant between sampling intervals, Eq. (3.4-4) can be reduced to the following discrete-time system:

$$\underline{x}_{k+1} = \underline{x}(t_{k+1}) = \Phi(\Delta t)\underline{x}_k + \Gamma(\Delta t)\underline{u}_k \qquad (3.4\text{-}5)$$

where $\Delta t = t_{k+1} - t_k$ for $k = 0,1,\ldots$. The state-transition matrix, $\Phi(\Delta t)$, in Eq. (3.4-5) is given by

$$\Phi(\Delta t) = e^{[F\Delta t]} = \Phi(t_{k+1}, t_k) \qquad (3.4\text{-}6)$$

The control-effect matrix, $\Gamma(\Delta t)$, is given by

$$\Gamma(t_{k+1}, t_k) = \left[\int_{t_k}^{t_{k+1}} \Phi(t_{k+1}, t)dt\right]G = \left[\int_0^{\Delta t} e^{[Ft]}dt\right]G = \Gamma(\Delta t) \qquad (3.4\text{-}7)$$

The cost functional becomes

$$J = \sum_{k=0}^{\infty} [x_k^T \hat{Q}\, \underline{x}_k + 2\, \underline{x}_k^T M\, \underline{u}_k + \underline{u}_k^T \hat{R}\, \underline{u}_k] \qquad (3.4\text{-}8)$$

where

$$\hat{Q} = \int_{t_k}^{t_{k+1}} \phi^T(t,t_k) Q\, \phi(t,t_k) dt$$

$$= \int_0^{\Delta t} e^{[F^T t]} Q\, e^{[Ft]} dt \qquad (3.4\text{-}9)$$

$$M = \int_{t_k}^{t_{k+1}} \phi^T(t,t_k) Q\, \Gamma(t,t_k) dt$$

$$= \int_0^{\Delta t} e^{[F^T t]} Q \left[\int_0^t e^{[Fs]} ds \right] dt\, G \qquad (3.4\text{-}10)$$

$$\hat{R} = \int_{t_k}^{t_{k+1}} [R + \Gamma^T(t,t_k) Q\, \Gamma(t,t_k)] dt$$

$$= \Delta t R + G^T \int_0^{\Delta t} \left[\int_0^t e^{[F^T s]} ds \right] Q \left[\int_0^t e^{[F\tau]} d\tau \right] dt\, G$$

(3.4-11)

To simplify the optimization, the following matrices are defined:

$$\Theta = \Phi - \Gamma M^T \qquad (3.4\text{-}12)$$

$$\chi = \hat{Q} - M \hat{R}^{-1} M^T \qquad (3.4\text{-}13)$$

The matrices $\hat{Q}$ and $\hat{R}$, are respectively, positive semi-definite and positive definite. (Ref. 63)

The optimal control law can be found assuming, that the discrete-time system Eq. (3.4-5) is controllable and is given by

$$\underline{u}_i = -K\underline{x}_i, \quad i = 0,1,2,... \tag{3.4-14}$$

where

$$K = \hat{R}^{-1} M^T + (\hat{R}+\Gamma^T P \Gamma)^{-1} \Gamma^T P \Theta \tag{3.4-15}$$

In Eq. (3.4-15), P is the steady-state solution to the discrete Riccati equation,

$$P = \Theta^T P \Theta - \Theta^T P \Gamma (\hat{R}+\Gamma^T P \Gamma)^{-1} \Gamma^T P \Theta + \chi \tag{3.4-16}$$

Resorting to the original matrices, Eq. (3.4-16) and (3.4-15) become

$$P = \Phi^T P \Phi - (\Gamma^T P \Phi + M^T)^T (\hat{R}+\Gamma^T P \Gamma)^{-1} (\Gamma^T P \Phi + M^T) + \hat{Q} \tag{3.4-17}$$

$$K = (\hat{R}+\Gamma^T P \Gamma)^{-1} (\Gamma^T P \Phi + M^T) \tag{3.4-18}$$

In general, P is positive semi-definite. but if the system is observable, i.e., if $(F, Q^{\frac{1}{2}})$ is an observable pair, then it is positive definite.

In summary, this section has provided a way of controlling a continuous-time system with a discrete-time controller. The feedback gain of this controller is given by Eq. (3.4-18) and is obtained by solving a discrete Riccati equation. The advantages are clear: Q and R matrices can be specified for a continuous-time cost function and evaluated with the discrete-time control law, Eq. (3.4-14). This is a simpler approach than trying to specify $\hat{Q}$, M, and $\hat{R}$ directly, since values in Q and R can be found based on an intuitive understanding of the continuous-time problem. The next section applies the results in this section to two of the servos in Section 3.3.

3.5 DISCRETE-TIME SERVO

This section applies the results of Section 3.4 to the continuous-time PI servo of Section 3.3.3 and the continuous-time PII servo of Section 3.3.4. No similar derivations have been found in the literature, and the results can be considered new.

A simplified discrete version of the PI servo of Section 3.3.3 is derived here. The derivation is not as straightforward as the approach in Section 3.4 implies. Some simplifications are used in order to obtain control laws which can be programmed on a digital computer. The simplifications which lead to Eq. (3.5-24) help explain why digital control systems tend to oscillate or "ring" (Ref. 64), while continuous control laws do not. The terms that are neglected in the simplification would have provided dampin, and there would have been no delay in the response of the discrete law for both controllers.

3.5.1 Dynamic and Proportional-Integral Servos

This section derives the simplified discrete-time version of the continuous-time PI servo. The continuous-time system and cost are repeated below. In the two equations, the variable, $\underline{v}(t)$, replaces the variable $\underline{u}_1(t)$ in Eq. (3.2-8) to distinguish between the two systems. The system is (Eq. (3.2-14)), or

$$\begin{bmatrix} \dot{\underline{x}}(t) \\ \dot{\underline{u}}(t) \end{bmatrix} = \begin{bmatrix} F & G \\ 0 & 0 \end{bmatrix} \begin{bmatrix} \underline{x}(t) \\ \underline{u}(t) \end{bmatrix} + \begin{bmatrix} 0 \\ I \end{bmatrix} \underline{v}(t) \qquad (3.5\text{-}1)$$

and the cost function is given by

$$J = \int_0^\infty \left\{ [\underline{x}^T(t)\ \underline{u}^T(t)] \begin{bmatrix} Q & 0 \\ 0 & R \end{bmatrix} \begin{bmatrix} \underline{x}(t) \\ \underline{u}(t) \end{bmatrix} + \underline{v}(t)^T R_1 \underline{v}(t) \right\} dt \tag{3.5-2}$$

Using the sampling interval Δt, the discrete-time equations corresponding to Eq. (3.5-1) and (3.5-2) are

$$\begin{bmatrix} \underline{x} \\ \underline{u} \end{bmatrix}_{k+1} = \begin{bmatrix} \Phi & \Gamma \\ 0 & I \end{bmatrix} \begin{bmatrix} \underline{x} \\ \underline{u} \end{bmatrix}_k + \begin{bmatrix} \Gamma_1 \\ \Gamma_2 \end{bmatrix} \underline{v}_k \tag{3.5-3}$$

$$J = \sum_{k=0}^{\infty} \left\{ [\underline{x}^T \underline{u}^T]_k \hat{Q} \begin{bmatrix} \underline{x} \\ \underline{u} \end{bmatrix}_k + [\underline{x}^T \underline{u}^T]_k M \underline{v}_k + \underline{v}_k^T \hat{R} \underline{v}_k \right\} \tag{3.5-4}$$

The problem which was mentioned in the introduction has developed at this point. The matrix Γ_1 has no counterpart in a physical situation since there is no direct control path betwen $\underline{v}_k$ and $\underline{x}_{k+1}$ in the digital system. The problem is by-passed (but not eliminated) if the state and subsystems of Eq. (3.5-1) are transformed separately:

$$\underline{x}_{k+1} = \Phi\ \underline{x}_k + \Gamma\ \underline{u}_k \tag{3.5-5}$$

$$\underline{u}_{k+1} = \underline{u}_k + \Gamma_3\ \underline{v}_k + \Gamma_4\ \underline{v}_{k+1} \tag{3.5-6}$$

The matrices, Γ_3 and Γ_4, are determined by digital integration. Using Euler integration, the matrices become

$$\Gamma_3 = \Delta t I \tag{3.5-7}$$

$$\Gamma_4 = 0 \tag{3.5-8}$$

The discrete system given by Eq. (3.5-5) and (3.5-6) can be rewritten as

$$\begin{bmatrix} \underline{x} \\ \underline{u} \end{bmatrix}_{k+1} = \begin{bmatrix} \phi & \Gamma \\ 0 & I \end{bmatrix} \begin{bmatrix} \underline{x} \\ \underline{u} \end{bmatrix}_{k} + \begin{bmatrix} 0 \\ \Delta t I \end{bmatrix} \underline{v}_k \tag{3.5-9}$$

where I is the (m x m) identity matrix. It is interesting to compare this approach with the rigorous expression given by Eq. (3.5-3). Expanding the expressions for Γ_1 and Γ_2 results in

$$\Gamma_1 = \frac{G\Delta t^2}{2!} + \frac{FG\Delta t^3}{3!} + \frac{F^2 G\Delta t^4}{4!} + \ldots \approx 0. \tag{3.5-10}$$

$$\Gamma_2 = \Delta t I \tag{3.5-11}$$

The term, Γ_2, equals its counterpart, Γ_3. If Δt is small, Γ_1 is very close to zero; hence the simplification is usually a very good one. The development proceeds with Eq. (3.5-3) replaced by Eq. (3.5-9) and leaving the cost functional, Eq. (3.5-4), the same.

The objective of this section is to find a control law for the discrete system which will cause certain system outputs, $\underline{y}_k$, to reach the set point, $\underline{y}_d$, in steady state, where $\underline{y}_d$ is an (m x 1) constant vector. The set point, $\underline{y}_d$, has the same number of variables as the control, $\underline{u}_k$. The output, $\underline{y}_k$, is given by

$$\underline{y}_k = T\, \underline{x}_k \tag{3.5-12}$$

where T is the same (m x n) constant transformation matrix as in Eq. (3.3-2).

It is assumed that $[\phi, \Gamma, T]$ is minimal, i.e., that this matrix set is completely controllable and observable.

It is also assumed that

$$\begin{bmatrix} F & G \\ T & 0 \end{bmatrix}^{-1} = \begin{bmatrix} S_{11} & S_{12} \\ S_{21} & S_{22} \end{bmatrix} \text{ exists and} \tag{3.5-13}$$

$$\begin{bmatrix} \Phi & \Gamma \\ T & 0 \end{bmatrix}^{-1} = \begin{bmatrix} A_{11} & A_{12} \\ A_{21} & A_{22} \end{bmatrix} \text{ exists.} \tag{3.5-14}$$

From Eq. (3.3-50) and (3.3-51), if Eq. (3.5-13) is true, the following occurs:

$$\lim_{k\to\infty} \underline{x}_k = \underline{x}^* = S_{12}\, \underline{y}_d \tag{3.5-15}$$

$$\lim_{k\to\infty} = \underline{u}_k = \underline{u}^* = S_{22}\, \underline{y}_d \tag{3.5-16}$$

Substituting x^* and u^* into Eq. (3.5-5) results in

$$\underline{x}^* = \Phi \underline{x}^* + \Gamma \underline{u}^* \tag{3.5-17}$$

which is an alternate definition of the variables, $\underline{x}^*$ and $\underline{u}^*$. Define the error variables,

$$\tilde{\underline{x}}_k = \underline{x}_k - \underline{x}^* \tag{3.5-18}$$

$$\tilde{\underline{u}}_k = \underline{u}_k - \underline{u}^* \tag{3.5-19}$$

Then Eq. (3.5-5) can be written as

$$\begin{aligned} \tilde{\underline{x}}_{k+1} &= \Phi \tilde{\underline{x}}_k + \Gamma \underline{u}_k + (\Phi - I)\underline{x}^* \\ &= \Phi \tilde{\underline{x}}_k + \Gamma \tilde{\underline{u}}_k \end{aligned} \tag{3.5-20}$$

Equation (3.5-6), with assumptions Eq. (3.5-7) and (3.5-8), can be written as

$$\underline{u}_{k+1} - \underline{u}^* = \underline{u}_k - \underline{u}^* + \Gamma_2 \underline{v}_k \qquad (3.5\text{-}21)$$

$$\tilde{\underline{u}}_{k+1} = \tilde{\underline{u}}_k + \Gamma_2 \underline{v}_k \qquad (3.5\text{-}22)$$

The vector, $\underline{v}_k$, can be considered the discrete-time version of the continuous-time commanded control-rate, i.e.,

$$\underline{u}_{k+1} - \underline{u}_k = \Gamma_2 \underline{v}_k = \Delta t \, \underline{v}_k \qquad (3.5\text{-}23)$$

It is the difference between control actions. Weighting $\underline{v}_k$ in the cost functional weights this difference and does not allow large jumps in the control law output to occur. The discrete system, Eq. (3.5-9), can be written as

$$\begin{bmatrix} \tilde{\underline{x}}_{k+1} \\ \tilde{\underline{u}}_{k+1} \end{bmatrix} = \begin{bmatrix} \Phi & \Gamma \\ 0 & I \end{bmatrix} \begin{bmatrix} \tilde{\underline{x}}_k \\ \tilde{\underline{u}}_k \end{bmatrix} + \begin{bmatrix} 0 \\ \Gamma_2 \end{bmatrix} \underline{v}_k \qquad (3.5\text{-}24)$$

with the cost functional

$$J = \sum_{k=0}^{\infty} \left\{ [\tilde{\underline{x}}^T \; \tilde{\underline{u}}^T]_k \, \hat{Q} \begin{bmatrix} \tilde{\underline{x}} \\ \tilde{\underline{u}} \end{bmatrix}_k + [\tilde{\underline{x}}^T \; \tilde{\underline{u}}^T]_k \, M \, \underline{v}_k + \underline{v}_k^T \hat{R} \, \underline{v}_k \right\} \qquad (3.5\text{-}25)$$

The servo problem has been transformed into a regulator problem which was solved in Section 3.4, viz. Eq.(3.4-5) and Eq. (3.4-8). The control, $\underline{v}_k$, which minimizes the cost functional, Eq. (3.5-25), is given by

$$\underline{v}_k = -K_1 \tilde{\underline{x}}_k - K_2 \tilde{\underline{u}}_k \qquad (3.5\text{-}26)$$

where K_1 and K_2 are the gains obtained using the discrete Riccati equation (Eq. (3.4-18)). Various matrix manipulations can be performed on Eq. (3.5-26) to obtain the final expression for the control law, as shown below.

It is known that if Γ is of full rank m, there exists an (m x n) matrix B such that

$$B\Gamma = I \tag{3.5-27}$$

where I is the (m x m) identity matrix. Together with Eq. (3.5-20), this implies that

$$\underline{\tilde{u}}_k = B\,\underline{\tilde{x}}_{k+1} - B\Phi\,\underline{\tilde{x}}_k \tag{3.5-28}$$

Substituting this equation into Eq. (3.5-26) leads to an expression for the command in terms of the error state variables:

$$\underline{v}_k = (-K_1+K_2B\Phi)\underline{\tilde{x}}_k - K_2\,B\underline{\tilde{x}}_{k+1} \tag{3.5-29}$$

Further simplifications are possible. Assume that one can choose an (m x m) matrix, L, such that

$$-LT = (-K_1+K_2B\Phi) \tag{3.5-30}$$

Then Eq. (3.5-29) can be rewritten as

$$\begin{aligned}\underline{v}_k &= -LT(\underline{\tilde{x}}_k) - K_2B\,\underline{\tilde{x}}_{k+1} \\ &= -L(T\underline{x}_k-\underline{y}_d) - K_2B\,\underline{\tilde{x}}_{k+1}\end{aligned} \tag{3.5-31}$$

It remains to be shown that L and B exist. Equation (3.5-30) can be combined with the expression for B, Eq. (3.5-27), to yield

$$[K_2B \quad L]\begin{bmatrix}\Phi & \Gamma \\ T & 0\end{bmatrix} = [K_1 \quad K_2] \tag{3.5-32}$$

The matrix $\begin{bmatrix}\Phi & \Gamma \\ T & 0\end{bmatrix}$ was assumed invertible at the start of the problem in Eq. (3.5-14). The reason is that multiplying both sides of Eq. (3.5-32) by its inverse provides unique solutions for L and B, i.e.,

$$L = K_1A_{12} + K_2A_{22} \tag{3.5-33}$$

$$B = K_2^{-1}K_1A_{11} + A_{21} \tag{3.5-34}$$

Equation (3.5-14) can be considered as the discrete-time controllability requirement. The control command has been simplified to Eq. (3.5-31), which is necessary to solve the discrete-time servo problem. At this point there are two directions which can be taken in order to reach the objective of a physically implementable discrete control law. The first approach results in the discrete-time version of the dynamic controller, which does not have the integral compensation property of a PI controller. The second approach does have integral compensation and is the discrete-time version of the proportional-integral servo of Section 3.3.2.

Discrete Dynamic Controller - In Eq. (3.5-31), replace $\underline{x}_{k+1}$ with the system Eq. (3.5-5):

$$\begin{aligned}\underline{v}_k &= -L(\underline{y}_k-\underline{y}_d) - K_2B(\Phi\underline{x}_k+\Gamma\underline{u}_k-\underline{x}^*) \\ &= L(\underline{y}_d-T\underline{x}_k) + (-K_2B\Phi+K_2BS_{12}T)\underline{x}_k \\ &\quad + (K_2BS_{12})(\underline{y}_d-T\underline{x}_k) - K_2\underline{u}_k\end{aligned} \tag{3.5-35}$$

By defining the following matrices,

$$N_1 = L + K_2 B S_{12} \tag{3.5-36}$$

$$N_2 = -K_2 B\Phi + K_2 B S_{12} T \tag{3.5-37}$$

$$N_3 = -K_2 \tag{3.5-38}$$

and employing the expression for the control, $\underline{u}_k$, (Eq. (3.5-9)) the control law for the discrete dynamic controller becomes

$$\underline{u}_{k+1} = \underline{u}_k + \Delta t\, N_3\, \underline{u}_k + \Delta t\, N_1(\underline{y}_d - T\underline{x}_k) + \Delta t\, N_2(\underline{x}_k) \tag{3.5-39}$$

If the model of the system were known precisely, then the control law given by Eq. (3.5-39) would provide the constant $\underline{y}_d$ with no error. This rarely happens in practice, and it is the reason for the next derivation.

Discrete Proportional-Integral Controller - The analysis begins with Eq. (3.5-31); the vector $K_2 B\, S_{12}\, T\, \underline{x}_{k+1}$ is added and subtracted as follows:

$$\begin{aligned}\underline{v}_k &= L(\underline{y}_d - T\underline{x}_k) - K_2 B\, \underline{x}_{k+1} + K_2 B\, S_{12}\, \underline{y}_d \\ &\quad - K_2 B\, S_{12}\, T\underline{x}_{k+1} + K_2 B\, S_{12}\, T\underline{x}_{k+1} \\ &= L(\underline{y}_d - T\underline{x}_k) + K_2 B\, S_{12}(\underline{y}_d - T\underline{x}_{k+1}) \\ &\quad + (K_2 B\, S_{12}\, T - K_2 B)\underline{x}_{k+1}\end{aligned} \tag{3.5-40}$$

Equation (3.5-40) can be simplified by defining the following matrices:

$$N_4 = K_2 B\, S_{12} \tag{3.5-41}$$

$$N_5 = K_2 B\, S_{12} T - K_2 B \tag{3.5-42}$$

Substituting the expression for $\underline{v}_k$ into Eq. (3.5-9), the discrete PI control and system become

$$\underline{x}_{k+1} = \Phi \underline{x}_k + \Gamma \underline{u}_k \qquad (3.5\text{-}43)$$

$$\underline{u}_{k+1} = \underline{u}_k + \Delta t L(\underline{y}_d - T\underline{x}_k) + \Delta t N_4(\underline{y}_d - T\underline{x}_{k+1}) + \Delta t N_5(\underline{x}_{k+1}) \qquad (3.5\text{-}44)$$

At the starting instant (k=0), the control law produces

$$\underline{u}_1 = \underline{u}_0 + \Delta t L(\underline{y}_d - T\underline{x}_0) + \Delta t N_4(\underline{y}_d - T\underline{x}_1) + \Delta t N_5(\underline{x}_1) \qquad (3.5\text{-}45)$$

where $\underline{u}_0$ is unconstrained, in the same way that $\underline{u}(0)$ in Eq. (3.3-31) was unconstrained. It is not possible to determine $\underline{u}_1$, since the measured value of $\underline{x}_1$ is not available at k=0. In order to eliminate the problem, a number of procedures are available. The primary goals are: preserve the integration action, have a physically realizable control law, and minimize the cost function, Eq. (3.5-25).

The last requirement provides the means of determining $\underline{u}_1$. The control law which satisfies the above is given by delaying Eq. (3.5-44) by one time step,

$$\underline{u}_k = \underline{u}_{k-1} + \Delta t L(\underline{y}_d - T\underline{x}_{k-1}) + \Delta t N_4(\underline{y}_d - T\underline{x}_k) + \Delta t N_5(\underline{x}_k) \qquad (3.5\text{-}46)$$

and requiring that the current value of $\underline{y}_d$ always be used to determine the next control value. To see why Eq. (3.5-46) is the answer, Eq. (3.5-45) first must be reviewed.

In Eq. (3.5-45), one choice of $\underline{u}_0$ could be

$$\underline{u}_0 = 0 \qquad (3.5\text{-}47)$$

Then the value of $\underline{u}_1$ given by Eq. (3.5-44) would be (for x(0)=0)

$$\underline{u}_1^* = \Delta t L\, \underline{y}_d + \Delta t\, N_4\, \underline{y}_d \qquad (3.5\text{-}48)$$

However, another choice of $\underline{u}_0$ which minimizes the cost functional given by Eq. (3.5-25) even further is

$$\underline{u}_0 = \underline{u}_1^* = \Delta t L \underline{y}_d + \Delta t N_4 \underline{y}_d \qquad (3.5\text{-}49)$$

since these are all available at k = 0. Returning to Eq. (3.5-46), the value of $\underline{u}_0$ is specified at k = 0 and is given by

$$\underline{u}_0 = \underline{u}_{-1} + \Delta t L(\underline{y}_d - T\underline{x}_{-1}) + \Delta t N_4(\underline{y}_d - T\underline{x}_0) + \Delta t N_5(\underline{x}_0) \qquad (3.5\text{-}50)$$

One can assume

$$\underline{u}_{-1} = 0 \qquad (3.5\text{-}51)$$

$$\underline{y}_{d_{-1}} = 0 \qquad (3.5\text{-}52)$$

$$\underline{x}_{-1} = \underline{x}_0 = 0 \qquad (3.5\text{-}53)$$

or any other combination which is in steady state, but the above yields the simplest analysis. The choice for $\underline{u}_0$ in Eq. (3.5-50) could have been

$$\underline{u}_0 = \Delta t L(\underline{y}_{d-1}) + \Delta t N_4(\underline{y}_{d_0}) = \Delta t N_4 \underline{y}_d \qquad (3.5\text{-}54)$$

or the one deemed desirable by Eq. (3.5-46):

$$\underline{u}_0 = \Delta t L(\underline{y}_{d_0}) + \Delta t N_4(\underline{y}_{d_0})$$
$$= \Delta t L\, \underline{y}_d + \Delta t N_4 \underline{y}_d \qquad (3.5\text{-}55)$$

Of the two choices, the latter equals the previous expression for $\underline{u}_0$, Eq. (3.5-49), and it results in the smaller cost function.

This explains why the latest value of $\underline{y}_d$ should be used in Eq. (3.5-46). In a physical implementation of the

control law, the reasons are more obvious. The zeroth sampling instant occurs whenever $\underline{y}_d$ changes (from the standpoint of the control law structure). The matrices, ΔtL and ΔtN_4, are large, but their sum is small. The $\underline{u}_0$ of Eq. (3.5-54) could saturate all the controllers whenever $\underline{y}_d$ changes, while Eq. (3.5-55) gives well-behaved transients. The final expression for the discrete PI controller is

$$\underline{u}_k = \underline{u}_{k-1} + \Delta tL(\underline{y}_{d_k} - T\underline{x}_{k-1}) + \Delta tN_4(\underline{y}_{d_k} - T\underline{x}_k) + \Delta tN_5(\underline{x}_k) \tag{3.5-56}$$

This is a physically realizable control law. Interestingly, the multivariable expression given by Eq. (3.5-56), which was brought about by a series of matrix manipulations on the quadratic synthesis solution, resembles the velocity form of the classical discrete-time PI controller. In the velocity form of the classical single-input/single-output discrete PI controller, however, the second term in Eq. (3.5-56) would be $\Delta tL(\underline{y}_{d_{k-1}} - T\underline{x}_{k-1})$ (Ref. 64).

3.5.2 Discrete-Time PII Controller

The purpose of this section is to derive a discrete-time version of the continuous-time PII control law developed in Section 3.3.4.

The continuous-time system used in Section 3.3.4 is given by

$$\begin{bmatrix} \dot{\underline{x}}(t) \\ \dot{\underline{u}}(t) \\ \dot{\underline{y}}_I(t) \end{bmatrix} = \begin{bmatrix} F & G & 0 \\ 0 & 0 & 0 \\ T & 0 & 0 \end{bmatrix} \begin{bmatrix} \underline{x}(t) \\ \underline{u}(t) \\ \underline{y}_I(t) \end{bmatrix} + \begin{bmatrix} 0 \\ I \\ 0 \end{bmatrix} \underline{v}(t) + \begin{bmatrix} 0 \\ 0 \\ -I \end{bmatrix} \underline{y}_d \tag{3.5-57}$$

where $\underline{v}(t)$ replaces $\dot{\underline{u}}(t)$. The corresponding cost functional is

$$J = \int_0^\infty \left\{ [\underline{x}^T(t)\ \underline{u}^T(t)\ \underline{y}_I^T(t)]\, Q \begin{bmatrix} \underline{x}(t) \\ \underline{u}(t) \\ \underline{y}_I(t) \end{bmatrix} + \underline{v}^T(t) R \underline{v}(t) \right\} dt \tag{3.5-58}$$

As in Section 3.4, the discrete-time equivalent of Eq. (3.5-57) is

$$\begin{bmatrix} \underline{x} \\ \underline{u} \\ \underline{y}_I \end{bmatrix}_{k+1} = \begin{bmatrix} \Phi & \Gamma & 0 \\ 0 & I & 0 \\ \Phi_1 & \Phi_2 & I \end{bmatrix} \begin{bmatrix} \underline{x} \\ \underline{u} \\ \underline{y}_I \end{bmatrix}_k + \begin{bmatrix} \Gamma_1 \\ \Gamma_2 \\ \Gamma_3 \end{bmatrix} \underline{v}_k + \begin{bmatrix} 0 \\ 0 \\ -\Delta t\, I \end{bmatrix} \underline{y}_d \tag{3.5-59}$$

The same problem that occurred with Γ_1 in Section 3.5.1 occurs here, and it is compounded by the additional matrices, Φ_2 and Γ_3. Treating the individual subsystems separately and using Euler discrete integration leads to the approximate system,

$$\begin{bmatrix} \underline{x} \\ \underline{u} \\ \underline{y}_I \end{bmatrix}_{k+1} = \begin{bmatrix} \Phi & \Gamma & 0 \\ 0 & I & 0 \\ \Delta t T & 0 & I \end{bmatrix} \begin{bmatrix} \underline{x} \\ \underline{u} \\ \underline{y}_I \end{bmatrix}_k + \begin{bmatrix} 0 \\ \Delta t I \\ 0 \end{bmatrix} \underline{v}_k + \begin{bmatrix} 0 \\ 0 \\ -\Delta t I \end{bmatrix} \underline{y}_d \tag{3.5-60}$$

The quantities that have been neglected in Eq. (3.5-60) are given below:

$$\Phi_1 = \Delta t T + \overbrace{\frac{\Delta t^2}{2!} TF + \frac{\Delta t^3}{3!} TF^2 + \ldots}^{\approx 0} \tag{3.5-61}$$

$$\Phi_2 = TG \frac{\Delta t^2}{2!} + TFG \frac{\Delta t^3}{3!} + TF^2G \frac{\Delta t^4}{4!} + \ldots \approx 0 \tag{3.5-62}$$

$$\Gamma_1 = G\frac{\Delta t^2}{2!} + FG\frac{\Delta t^3}{3!} + F^2G\frac{\Delta t^4}{4!} + \ldots \approx 0 \qquad (3.5\text{-}63)$$

$$\Gamma_2 = \Delta t I \qquad (3.5\text{-}64)$$

$$\Gamma_3 = TG\frac{\Delta t^3}{3!} + TFG\frac{\Delta t^4}{4!} + TF^2G\frac{\Delta t^5}{5!} + \ldots \approx 0 \qquad (3.5\text{-}65)$$

Comparing Eqs. (3.5-61) through (3.5-65) with Eq. (3.5-60) shows that all terms with Δt of order two and higher are neglected when Euler integration is used. If the sampling interval is small, this is a reasonable assumption.

It is assumed that the matrix $\begin{bmatrix} F & G \\ T & 0 \end{bmatrix}$ has rank n + p, where p is the dimension of the commanded set point, $\underline{y}_d$, and $p \leq m$. It is further assumed that $[\Phi,\Gamma,T]$ is minimal, i.e., completely controllable and observable. Let $\underline{x}^*$, $\underline{u}^*$, $\underline{y}_I^*$ be the steady-state value of the system, given a $\underline{y}_d$ command, and define the following error variables:

$$\tilde{\underline{x}}_k = \underline{x}_k - \underline{x}^* \qquad (3.5\text{-}66)$$

$$\tilde{\underline{u}}_k = \underline{u}_k - \underline{u}^* \qquad (3.5\text{-}67)$$

$$\tilde{\underline{y}}_{I_k} = \underline{y}_{I_k} - \underline{y}_I^* \qquad (3.5\text{-}68)$$

Then, the system equation (3.5-6) can be rewritten as

$$\begin{bmatrix} \tilde{\underline{x}} \\ \tilde{\underline{u}} \\ \tilde{\underline{y}}_I \end{bmatrix}_{k+1} = \begin{bmatrix} \Phi & \Gamma & 0 \\ 0 & I & 0 \\ \Delta t T & 0 & I \end{bmatrix} \begin{bmatrix} \tilde{\underline{x}} \\ \tilde{\underline{u}} \\ \tilde{\underline{y}}_I \end{bmatrix}_k + \begin{bmatrix} 0 \\ \Delta t I \\ 0 \end{bmatrix} \underline{v}_k \qquad (3.5\text{-}69)$$

The servo problem has again been reduced to a regulator problem. The discrete-time feedback gains are found using Eq. (3.4-18), resulting in the following control law:

$$\underline{v}_k = -K_1\tilde{\underline{x}}_k - K_2\tilde{\underline{u}}_k - K_3\tilde{\underline{y}}_{I_k} \tag{3.5-70}$$

$$\underline{v}_k = -K_1\underline{x}_k - K_2\underline{u}_k - K_3\underline{y}_{I_k} + K_1\underline{x}^* + K_2\underline{u} + K_3\underline{y}_I^* \tag{3.5-71}$$

At this point, as in the continuous case, let $\underline{y}_I^*$ be such that

$$K_1\underline{x}^* + K_2\underline{u}^* + K_3\underline{y}_I^* = 0 \tag{3.5-72}$$

The total closed-loop system becomes

$$\underline{x}_{k+1} = \Phi\underline{x}_k + \underline{u}_k \tag{3.5-73}$$

$$\underline{u}_{k+1} = \underline{u}_k - \Delta tK_1\underline{x}_k - \Delta tK_2\underline{u}_k - \Delta tK_3\underline{y}_{I_k} \tag{3.5-74}$$

$$\underline{y}_{I_{k+1}} = \underline{y}_{I_k} + \Delta t(T\underline{x}_k - \underline{y}_d) \tag{3.5-75}$$

In actual implementation, $\underline{y}^*$ need not be calculated, since the discrete integrators reach this value automatically.

3.5.3 Design With the Discrete-Time Servos

In the previous two sections, two types of multivariable discrete servo designs were presented. Each was a successful attempt to design a system based on the sampled-data regulator theory of Ref. 63, and summarized in Section 3.4. To accomplish the derivation, certain matrices in the rigorous expressions for the discrete-time systems were neglected. All the quantities neglected were shown to contain higher-order Δt terms. This was shown to be equivalent to the situation which would occur if each subsystem

was integrated separately and Euler integration was used to approximate the discrete control effect. The problem solved is an approximation to the rigorously defined sampled-data regulator, although the cost functional was not changed when the system matrices were changed.

The derivations in Section 3.5.1 and 3.5.2 could have been done without the approximations, yielding essentially the same control laws but with more effort. In the program DIGADAPT (Appendix A), the control gains are obtained with the rigorously discretized system, control, and cost function, but time responses are simulated with these gains in the simplified system equations. Figure (5.9-1) of Section 5.8 compares this approach for the discrete PII system with the theoretical response. The theoretical response has slightly less overshoot and a slower rise time, but the two curves do not differ significantly. In addition, the faster rise time of the simplified control law was deemed desirable. Finally, the gains chosen this way are independent of the digital integration; hence, a method other than Euler integration could be used for control implementation. In summary, the control gains are obtained using Eq. (3.5-59) and implemented using Eq. (3.5-60).

3.6 CHAPTER SUMMARY

This chapter has presented eleven linear-optimal control laws for continuous-time and discrete-time systems. Each control law has been determined by defining a quadratic cost function and solving a matrix Riccati equation. The controllers and their control law equations are listed below.

Continuous-Time Control Laws

- Basic Feedback Regulator

$$\underline{u}(t) = -K\underline{x}(t) \qquad (3.6\text{-}1)$$

- Control-Rate-Weighted Regulator

$$\dot{\underline{u}}(t) = -K_2\underline{u}(t) - K_1\underline{x}(t) \qquad (3.6\text{-}2)$$

- A Control-Rate-Weighted Proportional-Integral Regulator

$$\underline{u}(t) = -K_3\underline{x}(t) - \int_0^t K_4\underline{x}(\tau)d\tau \qquad (3.6\text{-}3)$$

- A Proportional-Integral Regulator

$$\underline{u}(t) = -K_5\underline{x}(t) - K_6\int_0^t T\underline{x}(\tau)d\tau \qquad (3.6\text{-}4)$$

- A Control-Rate-Weighted Dynamic Controller

$$\dot{\underline{u}}(t) = -K_1\underline{x}(t) - K_2\underline{u}(t) + L\,\underline{y}_d \qquad (3.6\text{-}5)$$

- A Control-Rate-Weighted Proportional-Integral Servo

$$\underline{u}(t) = N\underline{x}(t) + \int_0^t L(\underline{y}_d - T\underline{x}(\tau))d\tau + A(\underline{y}_d - T\underline{x}(t)) \qquad (3.6\text{-}6)$$

- A Proportional-Integral Servo

$$\underline{u}(t) = -K_1\underline{x}(t) - K_2\int_0^t (T\underline{x}(\tau) - \underline{y}_d)d\tau + E\,\underline{y}_d \qquad (3.6\text{-}7)$$

- A Proportional-Plus-Double Integral Servo

$$\underline{u}(t) = -K_1\underline{x}(t) - K_2\underline{u}(t) - K_3\int_0^t (T\underline{x}(\tau) - \underline{y}_d)d\tau \qquad (3.6\text{-}8)$$

Discrete-Time Control Laws

- A Discrete Feedback Regulator

$$\underline{u}_k = -K\underline{x}_k \tag{3.6-9}$$

- A Discrete Control-Rate-Weighted Proportional-Integral Servo

$$\underline{u}_k = \underline{u}_{k-1} + \Delta t L(\underline{y}_{d_k} - T\underline{x}_{k-1}) + \Delta t N_4(\underline{y}_{d_k} - T\underline{x}_k) + \quad ;(\underline{x}_k) \tag{3.6-10}$$

- A Discrete Dynamic Controller

$$\underline{u}_{k+1} = \underline{u}_k + \Delta t N_1 \underline{u}_k + \Delta t N_2(\underline{y}_d - T\underline{x}_k) + \Delta t N_3(\underline{x}_k) \tag{3.6-11}$$

- A Discrete Proportional-Plus-Double Integral Servo

$$\underline{u}_{k+1} = \underline{u}_k - \Delta t K_1 \underline{x}_k - \Delta t K_2 \underline{u}_k - \Delta t K_3 \underline{y}_{I_k} \tag{3.6-12}$$

$$\underline{y}_{I_{k+1}} = \underline{y}_{I_k} + \Delta t(T\underline{x}_k - \underline{y}_d) \tag{3.6-13}$$

The discrete-time servos, Eqs. (3.6-10) and (3.5-12,13) are two good candidates for the control system of VTOL aircraft. Each system has its advantages and drawbacks. Both systems are Type 1 controllers and will accept any set point and changes in that set point. Both systems require the same number of gains, and each can adapt to any guidance system simply by changing the T matrix. Both systems have weighting on the control rate in their continuous versions, producing control laws which should not drive an actuator beyond its rate limits for expected magnitudes of command and feedback.

The first of those controllers, given by Eq. (3.6-10), can be considered to have feed-forward of the set

point, as shown in Fig. 3.6-1. There are no delays between commands and the system. This system responds immediately to changes in the command, $\underline{y}_d$; however, the controller could be susceptible to noise because of its fast response. The gains N_4 and L are very large, but they tend to cancel. This is not desirable from a noise suppression point of view

The second controller of Eqs. (3.6-12,13) does not have a direct feed-forward of the command $\underline{y}_d$; hence, it has a more sluggish response than the PI controller. Feed-forward command could have been included by choosing $\underline{y}_I^*$, the integrator steady-state value, to be zero. This would have added more gains to the PII system. The sluggishness of the system can be advantageous if noise suppression is desired, since the system has a low-pass filtering effect in the state feedback path. As shown in Fig. 3.6-2, the PII controller has two sampling-time delays between commands and the control actuators, but only one delay between the feedback variables and the actuators. This does not hinder its response, however, as shown in Chapter 5. The gains calculated for the discrete PII controller should stand up well under the gain-scheduling algorithms of Chapter 4; the gains are determined by the Riccati equation and have parameter insensitivity properties which allow for gain and system variations to occur without destabilizing the aircraft.

A further discussion of each controller and how it is mated with velocity-command and attitude-command control structures is given in Chapter 5, along with some simulation comparisons.

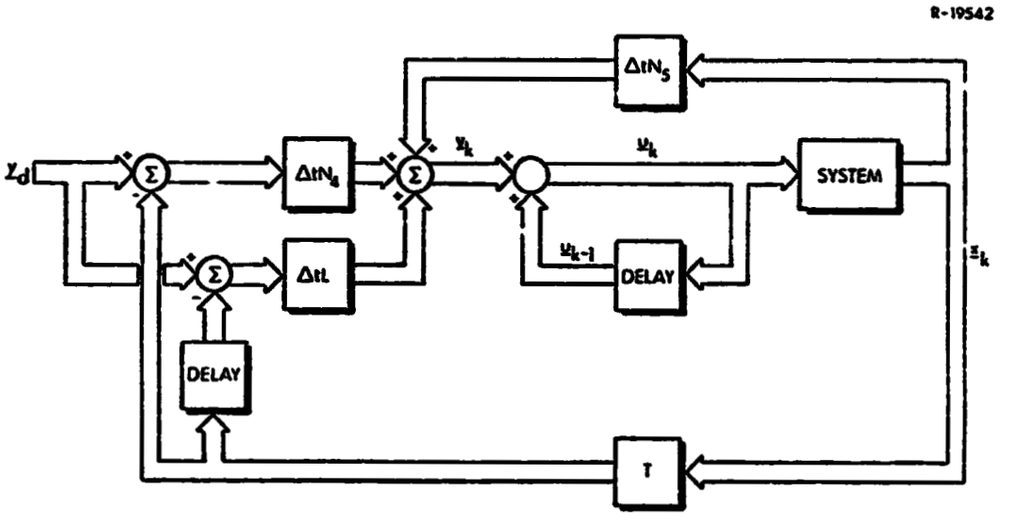

Figure 3.6-1 The Discrete PI Controller

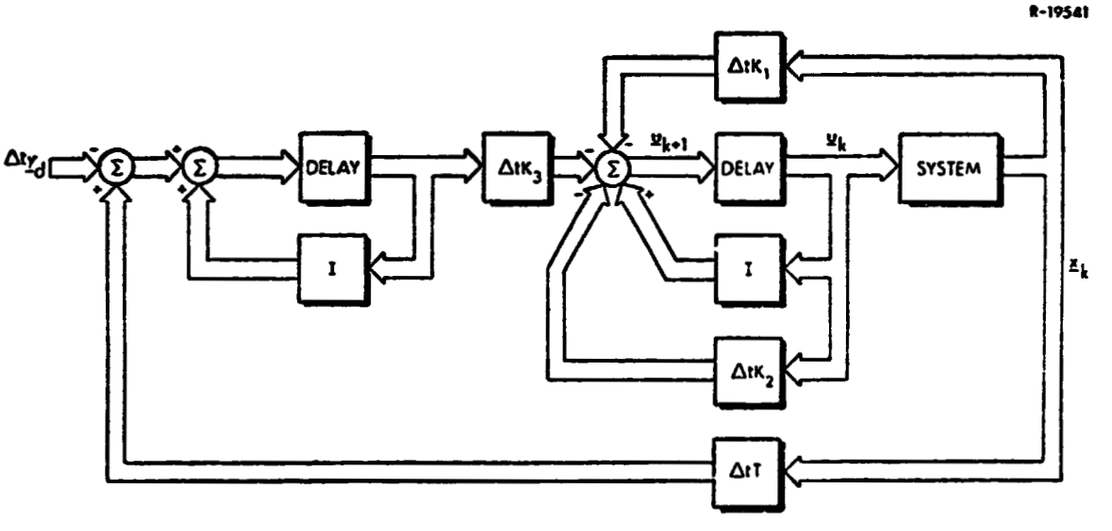

Figure 3.6-2 The Discrete PII Controller

4. DIGITAL-ADAPTIVE CONTROL LAW DEVELOPMENT

4.1 OVERVIEW

The control law forms a set of total actuator commands from guidance commands and augments system stability. It must perform these functions throughout the flight envelope in an efficient manner. Chapter 2 developed the overall functions of the linear control law, its interface with the guidance law, its use of nominal control settings, and its possible need for state estimation. The chapter also indicated alternatives for adapting control gains to changing flight conditions. Chapter 3 presented a number of control law structures based upon quadratic synthesis, beginning with continuous-time control laws and extending these results to sampled-data systems using discrete-time design principles. Important details which supplement the earlier chapters are presented in this chapter.

This chapter presents methods for sampling interval determination, trim computation, gain scheduling, and state estimation. As shown in Section 4.2, the sampling interval can be specified in such a way that system dynamics, disturbance environment, and state estimation errors are considered. The control trim problem is shown to separate into static and dynamic elements in Section 4.3, which also indicates that preferred attitudes may have to be specified to achieve force and moment equilibrium. A three-step procedure for scheduling control gains is desired in Section 4.4. The procedure, which includes evaluation of means and standard deviations, correlation coefficients, and regression

coefficients also is applicable to scheduling trim settings and dynamic trim compensation. Section 4.5 describes the general theory of linear-optimal state estimation and presents several simplified Kalman filters, including low-pass, complementary, and reduced-order filters. The chapter is summarized in Section 4.6.

4.2 DETERMINATION OF CONTROL SAMPLING INTERVAL

This section presents a technique for choosing a digital sampling interval which allows flight control to be maintained with as few computations as possible, subject to the designer's evaluation of error growth between control commands. The method is adapted from Ref. 65, which provides design techniques for a STOL flight control system.

Past methods for determining sampling interval have been based on frequency-domain concepts of the information content of a signal and of the equivalent phase lag introduced by sampling. In the first approach, Shannon's information theorem is invoked loosely (Ref. 80). It will be recalled that a noise-free periodic signal with frequency ω_n can, in principle, be reconstructed perfectly from samples collected at a rate of $2\omega_n$ samples per sec. A logical application of this theorem is to sample at a rate which is sufficient to capture the highest significant frequency in a given system, e.g., some multiple of the rot RPM in a helicopter or a bending-mode frequency in an elastic vehicle. Recognizing that errors in measurement are inevitable, the designer may choose to sample at a faster rate -- 4, 6 or even 10 times per cycle of the highest important mode. The trouble with this approach is that it may be unduly conservative, leading to computer usage for flight control which is much higher than necessary.

The second approach is associated with control laws which are designed for continuous systems and then simply sampled at a high rate (without major modification to the control gains) in the digital implementation (Ref. 81). The sample-and-hold process introduces a phase lag which could be sufficient to destabilize the system (or at least lower the effective damping ratio of significant oscillatory modes of the system). The procedure followed is to define an allowable phase lag for the limiting mode -- say 5 to 10 deg -- and to choose the sampling rate accordingly. Again, the result is conservative and computationally inefficient.

A method which eliminates this conservatism and provides a direct engineering measure of sampling errors is potentially more valuable than either previous method. The procedure is to specify sampling interval as a function of error covariance propagation between control commands. The error propagation takes system dynamics into account, and it indicates the rate at which information concerning the system state is degraded; hence, the motivation is similar to the information-theoretic approach. Since linear-optimal control theory assures stability, phase margin considerations need not dominate the choice of sampling interval for the discrete-time controller. Reference 82 indicates that differences between assumed and actual aircraft dynamics have greater effect on closed-loop response at low sampling rates. Such differences can be treated as "process noise" in the procedure developed below.

Before applying error covariance propagation to sampling interval determination, consider a simple example of the evolution of system state under purely deterministic conditions. A first-order linear system described by the differential equation

$$\dot{x} + ax = au \tag{4.2-1}$$

has the solution

$$x(t) = e^{-a(t-t_0)}\, x(t_0) + \int_{t_0}^{t} e^{-a(t-\tau)}\, au(\tau)d\tau \tag{4.2-2}$$

The only unknown is $x(t_0)$, and u(t) is arbitrary. One sample is all that is needed to completely specify x(t) for all time, once the choice of u(t) is made. If u(t) is the output of a linear regulator, it is a function of x(t), and a closed-form solution for x(t) can be based upon a single sample, i.e., x(0). If the system is subject to disturbances or a is imprecisely known, additional sampling will be required to specify x(t).

Next, consider a similar system with disturbances, process noise, and measurement noise. The first-order system is described by

$$\dot{x} + ax = au + w_1 \tag{4.2-3}$$

where w_1 represents the disturbance input plus the known input multiplied by uncertainties in a. The state measurement, y, is corrupted by measurement noise, w_2:

$$y = x + w_2 \tag{4.2-4}$$

A measurement of this system should be made when the future behavior of the system can no longer be predicted with certainty. Knowing or assuming statistics for the noise processes, w_1 and w_2, the sampling interval can be selected on the basis of limiting the growth of uncertainty in the knowledge of x(t). This error growth concept is illustrated

by Fig. 4.2-1, which is adapted from Ref. 65. Since the purpose of the digital control system is to maintain outputs within specified bounds, the sampling rate should be chosen to allow the controller to issue commands often enough so that the open-loop error propagation between control instants does not exceed the allowable error.

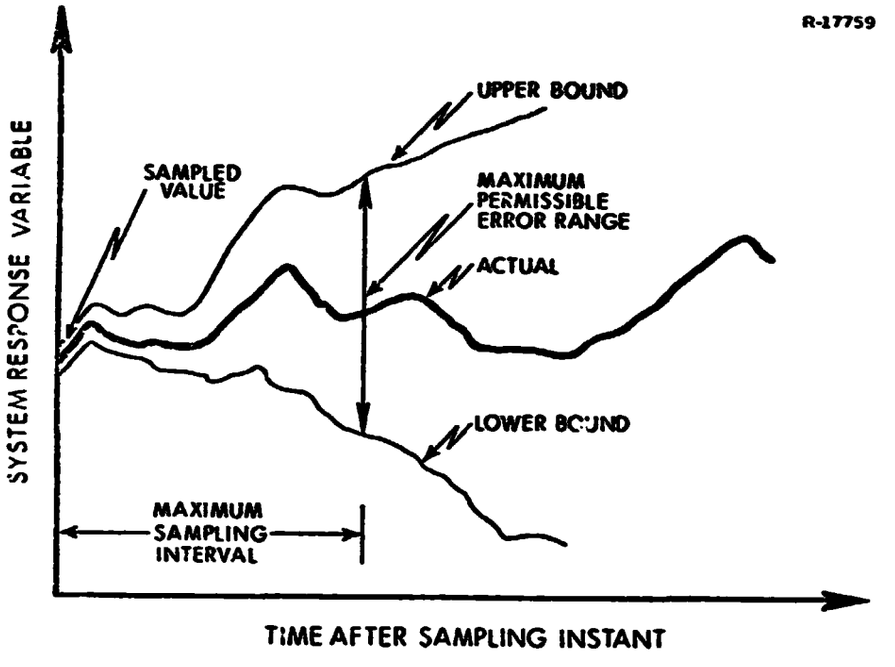

Figure 4.2-1 Propagation of Uncertainty

Propagation of the state covariance matrix, P(t), of a multivariable linear system is governed by the equation

$$\dot{P}(t) = FP(t) + P(t)F^T + W \qquad (4.2\text{-}5)$$

Here, F is a linear system matrix, as used in Eq. (3.1-2), and W is the covariance matrix of a process noise vector, $\underline{w}_1$. The process noise vector contains disturbance inputs and system modeling uncertainties, as does the scalar, w_1, in

Eq. (4.2-3). P(0), the state uncertainty at the beginning of a sampling interval, can be chosen as the covariance matrix of the measurement error vector, $\underline{w}_2$, which is defined as in the scalar Eq. (4.2-4). The control sampling interval is determined by integrating Eq. (4.2-5) from t = 0 until the time at which some element of P(t) equals or exceeds an acceptable value. The time at which this occurs is the sampling interval required for flight control. In practice, the sampling interval can be specified at a "worst case" flight condition to obtain a single acceptable value for all flight conditions.

This sampling interval selection process has several advantages over the earlier approaches. The system matrix F can include all significant aeroelastic and rotor modes for a VTOL aircraft. Consequently, the control designer need not decide beforehand which higher frequency modes should or should not be considered in choosing sampling interval. In so far as they affect the flight variable uncertainties to be bounded, all dynamic modes contribute to the selection. Unlike the information-theoretic approach, the damping ratios as well as the natural frequencies contribute to the selection, as both affect the growth of the state covariance matrix. It is noted that large values of W and P(0) each can reduce the time it takes for P(t) to reach its limit. If the aircraft is expected to fly in extreme turbulence, this can be anticipated in the choice of W. Uncertainties in aircraft parameters also cause W to increase. Noisy flight data measurements provide non-zero initial uncertainties in the state, and therefore, in P(0). Each of these conditions can cause the control sampling rate to increase.

This method can be extended to include allowable uncertainties in control actuator commands once the continuous-time regulator has been defined. With control-gain matrix, K, the control-deflection covariance, U, is

$$U(t) = KP(t)K^T \qquad (4.2\text{-}6)$$

and the sampling interval can be chosen to limit diagonal elements of U. U is only an approximation to the actual discrete-time control covariance, since it is derived using the continuous-time gain matrix; however, this matrix should suffice for choice of sampling interval. Alternatively, an iterative procedure using discrete-time gains could be employed.

In summary, the sampling interval can be chosen on the basis of state or control (whichever is limiting), and it can be chosen before the discrete-time control gains are generated.

4.3 TRIM CONTROL SETTINGS

An aircraft is in the trimmed condition when its controls are set to produce equilibrium in the equations of motion. Static trim occurs when the aircraft is in flight with zero state rates, i.e., when translational and rotational velocities are constant. For flight within the atmosphere, aerodynamic effects further require rotational velocity to meet algebraic constraints (as in a steady turn) to avoid varying specific forces which would destroy the static equilibrium. The trim concept can be extended to non-zero state rate flight by defining dynamic trim as the condition in which control settings produce desired values of states and state rates.

Trim setting is an important factor in aircraft control. Static trim control settings are required for steady flight maneuvers, e.g., cruise, hover, climb, descent, and coordinated turn. Dynamic trim control settings provide open-loop control of transient maneuvers, e.g., cruise-hover transition, turn entry and exit, and VTOL configuration transition. In general, the determination of trim requires the solution of a subset of the nonlinear equations of motion, although small variations from a known trim setting should follow the same linear patterns which are assumed throughout the literature of aircraft stability and control.

Command augmentation control systems, such as the proportional-integral controllers developed in the preceding chapter, provide an automatic trim feature. In a sense, the linear control logic performs a sweep solution of the nonlinear dynamic equations (as realized by the aircraft's actual motions) until a trim control setting is found and held by the control system's integrator. It is reasonable to question the need for explicit trim computation in a guidance and control system, especially when the many factors which can alter the control trim point are noted. For example, weight, center-of-gravity location, and airspeed all affect the control setting required for static equilibrium in a VTOL aircraft, and storing trim settings as functions of many variables may not be feasible.

The true value of explicit trim setting in a control system with integral compensation is in the ability to feed forward control settings which correspond (approximately) to the flight variables commanded by the guidance law, thereby enhancing the transient response of the closed-loop system. In effect, the static trim setting anticipates the proper value to be held by the control system's integrator,

and the dynamic trim setting compensates for the vehicle's inertial and aerodynamic resistance to changes in flight condition. If trim settings were computed with a perfect model of the aircraft and if there were no external disturbances, the closed-loop guidance and control laws would see no error and provide no control. To the extent that the model is not known precisely, explicit trim settings are in error; hence, caution must be exercised in placing too much emphasis on explicit trim control.

The following sections discuss methods for determining trim control settings. A technique which combines nonlinear static trim with linear dynamic trim compensation is developed.

4.3.1 Nonlinear Trim Solutions

The general trim problem can be defined as finding the control solution, $\underline{u}_T$, which provides equilibrium in the aircraft dynamic equation,

$$\dot{\underline{x}}_T = \underline{f}(\underline{x}_T, \underline{u}_T, \underline{w}_T) \qquad (4.3\text{-}1)$$

for given values of the state and disturbance, $\underline{x}_T$ and $\underline{w}_T$, and for desired values of the state rate, $\dot{\underline{x}}_T$. Assuming that the components of $\dot{\underline{x}}_T$ are non-zero and linearly independent, $\underline{u}_T$ must span the state space for the general trim solution to exist. The control also must possess sufficient range to assure solutions for the domain of possible $\dot{\underline{x}}_T$, $\underline{x}_T$, and $\underline{w}_T$. In other words, every system rate must be directly affected by a control, and the controls must possess sufficient authority to force a solution.

Unfortunately, the rigid-body equations of motion cannot meet these criteria, as the kinematic state variables

(translational and angular position) are not directly forced by the controls. The controls generate forces and moments; hence, they are felt only by the translational and rotational acceleration, and it is possible to provide acceleration trim precisely. Equation (4.3-1) can be partitioned as

$$\dot{\underline{x}}_1 = \underline{f}_1(\underline{x}_1, \underline{x}_2) \tag{4.3-2}$$

$$\dot{\underline{x}}_2 = \underline{f}_2(\underline{x}_1, \underline{x}_2, \underline{u}, \underline{w}) \tag{4.3-3}$$

where the subscript T is implied. The kinematic variables are

$$\underline{x}_1^T = [x \; y \; z \; \phi \; \theta \; \psi] \tag{4.3-4}$$

and the dynamic variables are

$$\underline{x}_2^T = [u \; v \; w \; p \; q \; r] \tag{4.3-5}$$

Thus, the revised general trim problem is to find the control, $\underline{u}$, which satisfies Eq. (4.3-3) for given values of $\underline{x}_1$, $\underline{x}_2$, and $\underline{w}$ and for desired values of $\dot{\underline{x}}_2$. Six control variables are required; they must span the space of $\underline{x}_2$ and have adequate authority for the domain of possible states, state rates, and disturbance inputs.

For aircraft with less than six independent control variables, trim equilibrium can be achieved only if elements of $\underline{x}_1$ can be treated as trim parameters, i.e., if the control deficiency can be overcome through force- and moment-producing effects of the kinematic variables. For example, the VALT Research Aircraft employs four control variables; two additional trim parameters must be specified.* Since x, y, and ψ have no dynamic effect, and z (whose only

*Note that active control of longitudinal cyclic trim would reduce this requirement to a single additional parameter.

significant effect is on the scaling of aerodynamic forces and moments) can not be specified arbitrarily, the trim parameters must be ϕ and θ. Roll-angle trim accounts for the fact that δ_R and δ_S alone cannot trim $\dot{v}$, $\dot{p}$, and $\dot{r}$; pitch-angle trim assists δ_B and δ_C in simultaneously trimming $\dot{u}$, $\dot{w}$, and $\dot{q}$. (Although not pursued here, the roles of ϕ and v could be interchanged in the trim process, i.e., roll angle could be specified and sideslip angle, which is proportional to v, could be treated as a trim parameter.)

The revised general trim problem for the tandem-rotor helicopter can be summarized as follows:

Given the parameter, z^*, and the reduced state vector, $\underline{x}_2^*$, find the trim vector, $\underline{\mu}^*$, which yields the desired reduced state rate, $\dot{\underline{x}}_2^*$, where

$$\underline{x}_2^{*T} = [u\ v\ w\ p\ q\ r]^* \tag{4.3-6}$$

and

$$\underline{\mu}^{*T} = [\delta_B \delta_C \delta_R \delta_S\ \phi\ \theta] \tag{4.3-7}$$

Numerical solutions to this problem include optimal path-following and functional minimization, both of which are discussed below.

Optimal Path-Following - One approach to determining trim settings corresponds to the first three steps of the guidance and control design procedure presented in Section 2.4.1. A nominal path, $\underline{x}^*(t)$, between origin and destination is defined, and open-loop controls which produce this path are computed using numerical optimization algorithms (as contained, for example, in Ref. 34). As shown below, the entire state vector need not be defined to compute the nominal path and associated control. The ability to specify only a

subset of the nominal state histories is the primary advantage in using this approach to obtain trim settings.

Consider an example in which the flight occurs during the time interval $[0,t_f]$ and the nominal translational position subset, $\underline{y}^*(t)$, of the state is specified. Define the error between a computed trial trajectory, $\underline{y}(t)$, and the nominal value, $\underline{y}^*(t)$, as $\Delta\underline{y}(t)$; a scalar cost function which measures a norm of the path-following error is then formed. For example, a quadratic penalty of errors along the path and at the terminal point is appropriate:

$$J = \Delta\underline{y}(t_f)^T S \Delta\underline{y}(t_f) + \int_0^{t_f} \Delta\underline{y}(t)^T Q \Delta\underline{y}(t) dt \qquad (4.3\text{-}8)$$

Here, S and Q are positive-definite matrices which cause J to increase when $\Delta\underline{y}(t)$ is non-zero. The vehicle's dynamic constraints in following the flight path, expressed by Eq. (4.3-1), are included in the augmented cost function,

$$\bar{J} = \Delta\underline{y}(t_f)^T S \Delta\underline{y}(t_f) + \int_0^{t_f} \{\Delta\underline{y}(t)^T Q \Delta\underline{y}(t) + \underline{\lambda}^T [\dot{\underline{x}}(t) - \underline{f}(\underline{x}(t), \underline{u}(t), \underline{w}(t))]\} dt \qquad (4.3\text{-}9)$$

where $\underline{\lambda}$ is the necessary adjoint (or co-state) vector (Ref. 34). $\bar{J}$ is minimized with respect to $\underline{u}(t)$, $0 \le t \le t_f$, by successive iterations (e.g., steepest-descent or accelerated gradient algorithms). When $\bar{J}$ has converged to a minimum value, the associated $\underline{u}^*(t)$ is the necessary open-loop control for following $\underline{y}^*(t)$; therefore, it is the dynamic trim setting which corresponds to the nominal flight path. In the process, all elements of $\underline{x}^*(t)$ are computed; hence, trim values of $\phi^*(t)$ and $\theta^*(t)$, as well as $\delta_B^*(t)$, $\delta_C^*(t)$, $\delta_S^*(t)$, and $\delta_R^*(t)$, are obtained, fully defining $\underline{u}^*(t)$.

The difficulties with this method of computing trim settings are that the procedure is computationally expensive and time-consuming. Results are obtained for a single path and must be generalized to all feasible paths.

Functional Minimization - This approach, also called parametric optimization, requires all elements of $\underline{x}_2^*$ and $\dot{\underline{x}}_2^*$ to be specified as given or desired, but it is not tied to any particular flight path. In this case, Eq. (4.3-3) is solved directly using an iterative process, e.g., a steepest-descent or accelerated gradient algorithm (Ref. 34). A scalar cost function, J, measures error in $\dot{\underline{x}}_2$ matching; a quadratic form is appropriate for computing a norm of the vector error,

$$J = \Delta\dot{\underline{x}}_2^T \, Q \, \Delta\dot{\underline{x}}_2 \qquad (4.3\text{-}10)$$

where

$$\Delta\dot{\underline{x}}_2 = \dot{\underline{x}}_2^* - \underline{f}_2(\underline{z}^*, \underline{x}_2^*, \underline{\mu}, \underline{w}^*) \qquad (4.3\text{-}11)$$

As in the previous case, the trim value of $\underline{\mu}^*$ is determined when J reaches a minimum.

The principal difficulty with this approach is that the six trim settings are functions of 13 variables (plus disturbances, weight variations, etc., if considered); thus, exhaustive function evaluations are required, and direct storage of the results would be difficult.

One response to this quandry is to ignore some trim settings altogether or to investigate trim settings as functions of fewer flight variables. (Recall that the TAGS scheduled static trim values of δ_B and θ as functions of calibrated airspeed (CAS) alone.) Several alternatives can

be considered, including elimination of weight, center-of-gravity location, and explicit altitude dependence (by using CAS rather than true airspeed). In addition, there are the following possibilities:

- Quasi-Static Trim: Assume $\dot{\underline{x}}_2^* = 0$.
- Non-Rotating Static Trim: Assume p*, q*, and r* are zero.
- Symmetric Static Trim: Assume v* is zero.
- Longitudinal Static Trim: Neglect lateral-directional trim settings.

The potential disadvantage in providing simplified trim is that valuable feed-forward commands could be lost, although this must be judged on a case-by-case basis. This disadvantage can be overcome to a large extent by adding linear dynamic trim compensation to static trim settings computed from one of the simplified nonlinear equations sets considered above. This option is discussed below.

4.3.2 Linear Dynamic Trim Compensation

First-order corrections to static trim settings can account for dominant dynamic effects, particularly those due to accelerations and angular rates. For this development, disturbances are neglected, and it is assumed that Eq. (4.3-3) can be expanded into nonlinear and linear parts. We begin by assuming that $\dot{\underline{x}}_2^*$ is sufficiently small that it can be considered a perturbation only. Then Eq. (4.3-3) can be written as

$$0 = \underline{f}_2(z_0^*, \underline{x}_{2_0}^*, \underline{\mu}_0^*) \tag{4.3-12}$$

and

$$\dot{\underline{x}}_2^* = F_2 \underline{x}_2^* + G_\mu \underline{\mu}^* \tag{4.3-13}$$

where F_2 and G_μ are defined as in Eq. (2.4-7) and (2.4-8). Using functional minimization, the nonlinear equation (Eq. (4.3-12)) provides a quasi-static trim setting

$$\underline{\mu}_0^* = \underline{\mu}_0^*(z_0^*, \underline{x}_{2_0}^*) \tag{4.3-14}$$

The linear equation (Eq. (4.3-13)) allows state/state-rate corrections to the trim setting to be computed as

$$\underline{\mu}^* = G_\mu^{-1}(\dot{\underline{x}}_2^* - F_2 x_2^*) \tag{4.3-15}$$

where G_μ is a square matrix and is assumed to possess an inverse. If the quasi-static trim is complete and precise, then $F_2 x_2^* = 0$, and the linear trim compensation is simply

$$\underline{\mu}^* = G_\mu^{-1}\, \dot{\underline{x}}_2^* \tag{4.3-16}$$

The total trim setting is

$$\underline{\mu}_T^* = \underline{\mu}_0^* + \underline{\mu}^* \tag{4.3-17}$$

The states and state rates used to compute trim settings are obtained from the primary and secondary guidance commands. Back-differencing is used to provide the necessary derivatives. Recognizing again that the prime function of explicit trim setting is to improve transient response to guidance commands, simplifications are justified. These include decoupling of the longitudinal and lateral-directional quasi-static trim, elimination of v and $\dot{v}$ trim, and selection of conservative values of G_μ^{-1} and F_2. The TAGS results suggest that quasi-static trim could be reduced to

$$\delta_{B_0}^* = \delta_{B_0}^* \text{ (CAS)} \tag{4.3-18}$$

$$\theta_0^* = \theta_0^* \text{ (CAS)} \tag{4.3-19}$$

Linear dynamic trim compensation then could take the form

$$\begin{bmatrix} \delta_B^* \\ \delta_C^* \\ \delta_R^* \\ \delta_S^* \\ 0 \\ 0 \end{bmatrix} = G_\mu^{-1} \begin{bmatrix} \dot{u}^* \\ 0 \\ \dot{w}^* \\ \dot{p}^* \\ \dot{q}^* \\ \dot{r}^* \end{bmatrix} - G_\mu^{-1} F_2 \begin{bmatrix} 0 \\ 0 \\ 0 \\ p^* \\ q^* \\ r^* \end{bmatrix} \tag{4.3-20}$$

It is assumed here that dynamic corrections to trim values of ϕ and 0 can be neglected. In a practical implementation, rows and columns of G_μ^{-1} and F_2 are eliminated as appropriate for computational efficiency.

4.4 GAIN SCHEDULING

This section presents a three step procedure for scheduling the control gains of a VTOL aircraft discrete controller. The gains are scheduled by finding functional relationships between certain flight conditions of the VTOL aircraft and the control gains at those flight conditions.

Previous methods for scheduling control gains have been successful and indicate that gain scheduling is a sound approach, (Ref. 26 and 68). The methodologies typically are based on single input/single output concepts (e.g.,

maintaining constant loop gain). For example, the TAGS program (Ref. 19) used the scheme shown in Fig. 4.4-1 as one means for gain adaptation: The net gain changes with air speed. Other flight variables which have been used for gain scheduling in other aerodynamic vehicles include Mach number, angle of attack, and dynamic pressure. Although these flight conditions and scheduling techniques have worked well, they provide inadequate insight for gain scheduling in a multivariable system.

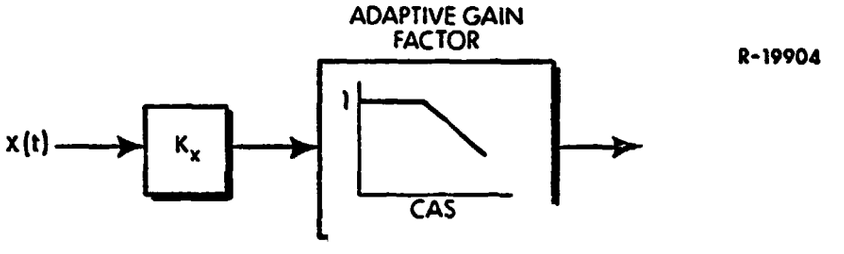

Figure 4.4-1 Gain Changing With a Flight Condition

The method developed here is a logical extension of previous work to multivariable systems. It involves three steps and places minimum reliance on past experience and intuition. The three steps are:

- The determination of a mean-standard deviation table which aids in finding which gains should be kept constant instead of being scheduled.
- The determination of a correlation coefficient table which aids in specifying the flight variables that should be used in gain scheduling algorithms.
- The determination of relationships (or curve fits) between chosen flight conditions and gains.

This new gain scheduling procedure is simple to use, the results are easily implementable on a digital computer, and the procedure has broad application. Other applications in this report include the scheduling of estimation gains, trim settings, and dynamic trim coefficients.

4.4.1 Correlation Between Control Gains and Flight Conditions

This section illustrates a computationally efficient method of determining which flight parameters can be used as independent variables in gain-scheduling algorithms. The gain-scheduling algorithm does not depend on the method used for computing gains -- it can be used as well with conventional or linear-optimal point design techniques. The system matrices for VTOL aircraft vary in a complex but deterministic way with flight conditions. If the closed-loop dynamics of the aircraft are maintained essentially invariant by automatic control, it is reasonable to assume that the necessary control gains also vary in a particular manner. It would be expected that if the control gains are determined based on the same criterion of performance at each flight condition, the gains and flight conditions should be correlated.*

The search for gain/flight variable dependencies begins by determining which gains need not be scheduled.

*Two variables are correlated if by observing the value of one variable, one is able to draw some kind of conclusion about the value of the other variable.

This is done by investigating features of the gain itself. Two features which suggest that a gain be held constant are its standard deviation and mean value. Certain gains do not exhibit wide variations as the flight conditions change. This can be determined by constructing a table of means and standard deviations for the gains. An example of a table obtained for the VALT Research Aircraft using the PII discrete control law is shown in Table 4.4-1. In the table, Gain 52 displays a very low standard deviation. This indicates the gain probably need not be scheduled but left at its mean value.

TABLE 4.4-1
EXAMPLE OF MEAN-STANDARD DEVIATION TABLE

	Mean	Standard Deviation	S.D. Per Cent of Mean
etc.			
Gain 50	-.00598	.0269	449.0
Gain 51	-.1013	.032	31.7
Gain 52	2.55	.046	1.82
etc.			

The other feature of gains is the relative magnitude of a gain compared to other gains of a similar class. Gains 50, 51, and 52, shown above, are coupling gains between controllers (K_2 of Eq. (3.5-74)). Gain 50 is small compared to Gain 52 and also exhibits a wide variation in magnitude. It may be desirable to set such a gain to zero. Simulations should be done, however, to fully determine a zeroed gain's effect on controlling the VTOL aircraft. Gain 51 is an example of a logical candidate for scheduling. The gain is of sufficient magnitude and displays enough variation to warrant scheduling.

The second step determines correlation coefficients between the gains and all available flight variables. One method of determining the correlation coefficients between a set of gains (dependent variables) and flight conditions (independent variables) is given by the following (Ref. 72):

$$\rho(a,m) = \frac{|\mathrm{cov}[a,m]|}{\sigma(a)\,\sigma(m)} = \frac{\left|\sum_{i=1}^{k}(a_i-\bar{a})(m_i-\bar{m})\right|}{\sqrt{\sum_{i=1}^{k}(a_i-\bar{a})^2}\sqrt{\sum_{i=1}^{k}(m_i-\bar{m})^2}} \qquad (4.4\text{-}1)$$

In Eq. (4.4-1), k is the number of flight conditions for which the gains are known, a_i is the value of the gain observed at flight point i, and m_i is the measured value of the flight condition at flight point i. The variable $\bar{a}$ is the mean value of the gain given by

$$\bar{a} = \frac{\sum_{i=1}^{k} a_i}{k} \qquad (4.4\text{-}2)$$

and $\bar{m}$ is the mean value of the flight condition. The closer the value of the correlation coefficient, ρ, is to one, the better the correlation between the gain and the flight condition. Independent variables which can be considered for gain scheduling include body-axis velocities (u,v,w), earth-relative velocities (V_x,V_y,V_z), Euler angles (θ,ϕ,ψ) and control trim positions. These variables can be inverted, squared, and so on, in the search for high correlation. To determine the important independent variables for a particular gain, a correlation coefficient table is constructed. A typical example of part of a table obtained by the program SCHED (Appendix A-2) for control gains using the PII

TABLE 4.4-2
EXAMPLE OF CORRELATION COEFFICIENTS TABLE

	u	u^2	$1/u$	V^2	$1/V^2$	θ	ϕ	w	....etc.
Gain 1	.838	(.939)	.297	(.939)	(.912)	.804	.018	.0359	
Gain 2	(.879)	.743	.168	.745	.541	(.890)	.028	.245	
Gain 3	.672	.786	.069	.782	(.904)	.724	.447	.339	
⋮									
etc.									

discrete servo is shown in Table 4.4-2. The circled values are the high correlation coefficients between gains and independent variable functions. After the highly correlated flight variables for a gain are found, the third step is initiated.

4.4.2 Curve Fitting

The third step in the gain-scheduling procedure is to construct a smooth curve relationship between the gains which are to be scheduled and the most highly correlated flight conditions. Referring to Section 2.4.2, the smooth curve snould be in the form of Eq. (2.4-34). Two particularly desirable curve-fitting techniques, which produce equations like Eq. (2.3-34), are multiple and polynomial regressions, i.e.,

$$\hat{a} = b_0 + b_1 m_1 + b_2 m_2 + \ldots + b_n m_n \qquad (4.4\text{-}3)$$

and

$$\hat{a} = b_0 + n_1 m_i + b_2 m_i^2 + \ldots + b_n m_i^n \qquad (4.4\text{-}4)$$

In the multiple regression, Eq. (4.4-3), n flight variables,

m_i, i=1 to n, are combined linearly to produce an estimate, $\hat{a}$, of the gain a. In the polynomial regression, Eq. (4.4-4), powers of the flight variable, m_i, are combined linearly to estimate a. A method for determining the regression coefficients, b_i, i=1 to n, is shown next.

Multiple Regression - A multiple regression analysis determines the regression coefficients, b_0, b_1, ..., b_n, in Eq. (4.4-3) so that the sum of the squared error between the regression estimate, $\hat{a}$, and the true value of a is minimum. The error function, J, which is to be minimized is given by

$$J = \sum_{i=1}^{k} (a_i - \hat{a}_i)^2 \qquad (4.4\text{-}5)$$

In Eq. (4.4-5), a_i is the value of the gain at flight point, i, and there are k flight points. To minimize J, set

$$\frac{\partial J}{\partial b_0} = \frac{\partial J}{\partial b_1} = \cdots \frac{\partial J}{\partial b_n} = 0 \qquad (4.4\text{-}6)$$

Then the expressions for the regression coefficients form a set of simultaneous linear equations, which in matrix notation are

$$A\,\underline{b} = \underline{c} \qquad (4.4\text{-}7)$$

Solving for $\underline{b}$ in Eq. (4.4-7) results in

$$\underline{b} = A^{-1}\underline{c} \qquad (4.4\text{-}8)$$

The vector, $\underline{b}$, is an (n x 1) vector containing the regression coefficients. The matrix, A, is known as the Gram matrix, (Ref. 77).

To determine just how good the b_i values are, the correlation coefficient for the multiple regression fit can be found, as in Eq. (4.4-1):

$$\rho(a,\hat{a}) = \frac{\left|\sum_{i=1}^{k}(a_i-a)(\hat{a}_i-\bar{\hat{a}})\right|}{\sqrt{\sum_{i=1}^{k}(a_i-\bar{a})^2}\sqrt{\sum_{i=1}^{k}(\hat{a}_i-\bar{\hat{a}})^2}} \qquad (4.4\text{-}9)$$

The closer ρ is to one, the better the fit of the multiple regression model. When using a multiple regression, the more independent variables chosen, the higher the value of ρ, until n=k and ρ=1. In order to avoid using a large number of independent variables, the maximum number used for scheduling the gains in this report is three. An effort is always made to have as few independent variables as possible in the gain schedule, since this saves on-board computer storage and duty cycle time. An alternate way of estimating gain values is to use only one of the flight variables and to perform a polynomial regression. A method for determining the regression coefficients, b_i, for the polynomial regression is shown next.

Polynomial Regression - An n^{th}-order polynomial regression analysis determines the regression coefficients, $b_0, b_1, \ldots, b_n$, in Eq. (4.4-4) so that the sum of the squared error between the regression estimate, $\hat{a}$, of Eq. (4.4-3) and the true value of a is minimum. In this case, there is only one kind of independent variable, m_i, for each gain value, but it is raised to various powers. One can define the following variables:

$$
\begin{aligned}
m_i &= m_1 \\
m_i^2 &= m_2 \\
&\vdots \\
m_i^n &= m_n
\end{aligned}
\qquad (4.4\text{-}10)
$$

The analysis for the polynomial regression would proceed as in the multiple regression, starting at Eq. (4.4-5). The polynomial regression can be considered a special case of the multiple regression. This is reflected in the fact that one of the functions in the program SCHED (Appendix A) is squaring. SCHED can perform a simple or second-order polynomial regression by using the variable or the variable and its square function in a multiple regression.

Summary - This section has presented a new method for adapting control gains to the changing conditions of a VTOL aircraft. The method is simple, efficient, and provides schedules which are easily implemented on an on-board computer. The basic feature of the technique is that regression coefficients which relate measured flight conditions to control gain values can be found. The adaptive scheme in this section will be shown to be useful for not only control gain scheduling but for other control system variables as well, including discrete Kalman filter gains, static trim parameters (Table 5.8-15), discrete-time linear system and control matrices used in the Kalman filter, and continuous-time linear system and control matrices used in dynamic trim (Table 5.8-17).

4.5 STATE ESTIMATION FOR CONTROL

One of the basic requirements for the controllers determined by the quadratic synthesis technique of Chapter 3 is that all states must be fedback for real-time control of the aircraft. State values are measured by such sensors as attitude gyros, angular rate gyros, barometric altimeters, radar measurements, airspeed indicators, and accelerometers. The output of each sensor can be assumed to have the form

$$z(t) = x_T(t) + n(t) \qquad (4.5\text{-}1)$$

In Eq. (4.5-1), $z(t)$ is the sensor output, $x_T(t)$ is the true state, and $n(t)$ is an additive measurement noise. The statistical properties of $n(t)$, which define the accuracy of the sensor, could be modelled in many ways; from a mathematical and physical point of view, white Gaussian noise is a logical choice. Noise is considered white if past values of $n(t)$ do not aid in predicting future values of $n(t)$. This means that any two values of $n(t)$ are uncorrelated. Noise that is Gaussian has a probability density function which is uniquely defined by its mean and covariance. The mean and covariance of $n(t)$ are

$$E\{n(t)\} = 0 \quad \text{for all } t \qquad (4.5\text{-}2)$$

$$\text{cov}[n(t),n(\tau)] = \sigma_n^2 \delta(t-\tau) \qquad (4.5\text{-}3)$$

σ_n^2 is called the intensity of the noise and it is assumed constant for stationary white noise. The intensity of stationary white noise is constant at all frequencies. The larger the value of σ_n^2, the larger the power level of the noise at each frequency.

There are many ways to extract the state, $\underline{x}_T(t)$, from the measurement $\underline{z}(t)$, but the most general is the linear-optimal filter developed by Kalman in Refs. 73 and 74. The Kalman filter is formulated for multivariable systems; hence, it can operate on all the sensor outputs in a unified manner. Equations for the steady-state continuous- and discrete-time filters are given in Section 4.5.1. Estimates for a class of nonlinear systems can be made using an adaptive Kalman filter (Ref. 75). An open-loop adaptive Kalman filter is presented in Section 4.5.2. The filter is open-loop adaptive because it uses the scheduling algorithms developed in Section 4.4 to determine its gains. A simplification of the Kalman filter for estimating aircraft states is given in Section 4.5.3; it is based on results by Higgens on complementary filters (Ref. 67). Section 4.5.4 further simplifies the Kalman filter estimate of aircraft states, resulting in the discrete form of the low-pass filter (Ref. 36). Section 4.5.5 presents the reduced-order filter and applies it to estimating the lateral velocity of an aircraft.

4.5.1 Kalman Filter

This section presents the basic equations of steady-state continuous- and discrete-time Kalman filters. The Kalman filter provides a precise way of obtaining a "best" estimate of states based on sensor measurements. The Kalman filter enables prior information about a system to be used to produce estimation algorithms. This information includes the aircraft dynamics which produce the state, the statistics of the noise that perturbs the aircraft, and the statistics of the noise that corrupts the sensor measurements. Derivations of the basic algorithms can be found in Refs. 36, 56, and 58.

Continuous-Time Filter Problem - Given the linear system,

$$\dot{\underline{x}}(t) = F\underline{x}(t) + G\underline{u}(t) + \underline{\omega}(t) \qquad (4.5\text{-}4)$$

and the linear measurement equation,

$$\underline{z}(t) = H\underline{x}(t) + \underline{\nu}(t) \qquad (4.5\text{-}5)$$

find an estimate of $\underline{x}(t)$ which is optimal in a statistical sense, as defined below. In Eqs. (4.5-4) and (4.5-5), H, F and G are constant matrices. $\omega(t)$ and $\underline{\nu}(t)$ are zero-mean white Gaussian noise processes with covariances

$$\text{cov}[\underline{\omega}(t),\underline{\omega}(\tau)] = Q_F\delta(t-\tau) \qquad (4.5\text{-}6)$$

$$\text{cov}[\underline{\nu}(t),\underline{\nu}(\tau)] = R_F\ (t-\tau) \qquad (4.5\text{-}7)$$

Using a least-squares error minimization criterion, the estimate, $\hat{\underline{x}}(t)$, is generated by

$$\dot{\hat{\underline{x}}}(t) = F\hat{\underline{x}}(t) + G\underline{u}(t) + L[\underline{z}(t)-H\hat{\underline{x}}(t)] \qquad (4.5\text{-}8)$$

where L is the Kalman filter gain given by

$$L = PH^T R_F^{-1} \qquad (4.5\text{-}9)$$

and P is the solution to the algebraic Riccati equation

$$0 = PF^T + FP + Q_F \cdot PH^T R_F^{-1} HP \qquad (4.5\text{-}10)$$

P in Eq. (4.5-10) is the steady-state error covariance matrix. The steady-state Kalman filter gain is constant because it is tacitly assumed the observations have started in the distant past, approaching $t\to-\infty$ in the limit.

Discrete-Time Filter Problem - Consider the discrete-time linear dynamic system whose state at the $k+1^{st}$ sampling instant is generated by the difference equation

$$\underline{x}_{k+1} = \Phi\underline{x}_k + \Gamma\underline{u}_k + \underline{\omega}_k \qquad (4.5\text{-}11)$$

with sensor output at discrete intervals given by

$$\underline{z}_k = H\underline{x}_k + \underline{\nu}_k \qquad (4.5\text{-}12)$$

The discrete-time filtering problem is to find the best linear estimate of the state at the $k+1^{st}$ instant based on the output sequence $(\underline{x}_k, \underline{x}_{k-1}, \underline{x}_{k-2} \cdots)$, which is the set of previous state values of the discrete system up to the instant, k. The disturbances, $\underline{\omega}_k$ and $\underline{\nu}_k$, are assumed to be white, zero-mean random sequences with covariances given by

$$\text{cov}[\underline{\omega}_k, \underline{\omega}_j] = \Xi\ \delta_{kj} \qquad (4.5\text{-}13)$$

$$\text{cov}[\underline{\nu}_k, \underline{\nu}_j] = T\ \delta_{kj} \qquad (4.5\text{-}14)$$

The two sequences are assumed to be uncorrelated, i.e.,

$$\text{cov}[\underline{\omega}_k, \underline{\nu}_j] = 0 \qquad (4.5\text{-}15)$$

for all k and j. The matrices ϕ, Γ, and H are constant and have dimensions which are appropriate to the state, control, and disturbance effects.

There are two steps in the steady-state Kalman filtering process for producing the state estimate at k:

- Extrapolate the state estimate from k-1 to k
- Update the state estimate by the measurement at k using the optimal gain matrix

The state estimate extrapolation for use at k is obtained with the state transition matrix and the control action by the equation

$$\underline{\hat{x}}_{k/k-1} = \phi\, \underline{\hat{x}}_{k-1} + \Gamma\, \underline{u}_{k-1} \qquad (4.5\text{-}16)$$

where $\underline{\hat{x}}_{k-1}$ is the state estimate at k-1. After the observation, $\underline{z}_k$, is obtained, $H\, \underline{x}_{k/k-1}$ is subtracted from the observation to produce the estimation error. This is combined with the state estimate extrapolation to produce the state estimate at k:

$$\underline{\hat{x}}_k = \underline{\hat{x}}_{k/k-1} + L(\underline{z}_k - H\, \underline{\hat{x}}_{k/k-1}) \qquad (4.5\text{-}17)$$

L is the steady-state Kalman filter gain given by

$$L = PH^T[HPH^T+T]^{-1} \qquad (4.5\text{-}18)$$

where the matrix, P, is the steady-state covariance of the estimation error:

$$\mathrm{cov}[(\underline{x}_k - \underline{\hat{x}}_{k/k-1}) \,,\, (\underline{x}_k - \underline{\hat{x}}_{k/k-1})] = P \qquad (4.5\text{-}19)$$

P is determined by solving the following discrete algebraic Riccati equation:

$$P = \phi P \phi^T + \phi P H^T [HPH^T+T]^{-1}\, HP\phi^T + \Xi \qquad (4.5\text{-}20)$$

For the next state estimate (at k+1), the process repeats itself starting at Eq. (4.5-16). If a controller is using the output of the filter to control an aircraft, it could use $\underline{\hat{x}}_k$ at time k. The references previously cited contain general derivations of the Kalman filter for finite sequences of observation.

The discrete Kalman filter equations are easy to compute on a digital computer. The program DIGADAPT

(Appendix A) solves Eq. (4.5-20) for p and generates Kalman filter gains.

4.5.2 Adaptive Filter

The total aircraft states, $\underline{x}_T(t)$, are generated by the nonlinear dynamic equation,

$$\dot{\underline{x}}_T(t) = f(\underline{x}_T(t), \underline{u}_T(t), \underline{w}_T(t)) \qquad (4.5\text{-}21)$$

which is Eq. (2.4-1) of Section 2.4.1. The deterministic controllers of Chapter 3 use the perturbation state, $\underline{x}(t)$, where

$$\underline{x}(t) = \underline{x}_T(t) - \underline{x}_0(t) \qquad (4.5\text{-}22)$$

and $\underline{x}_0(t)$ is the nominal state of the aircraft coming from the primary and secondary commands (Chapter 2). This section presents a digital-adaptive filter which uses the discrete Kalman filter of Section 4.5.1 to estimate the perturbation state, $\underline{x}(t)$, from the sensor measurement, $\underline{z}(t)$ (Ref. 75). It will be shown that not all of the states need be measured to produce the estimate.

The structure of the filter is shown in Fig. 4.5-1. The sensor, $\underline{z}_T(t)$, may represent the actual state, a combination of states, a subset of the states, or redundant observations of the states. The nominal measurement values are subtracted from the output of the sensors yielding the perturbation measurements. The nominal measurement values are derived from the command signals, the scheduled static trim values, and the computed dynamic trim values. The output perturbation values are assumed to be the states generated by

$$\underline{x}_{k+1} = \Phi_k \underline{x}_k + \Gamma_k \underline{u}_k + \underline{\omega}_k \qquad (4.5\text{-}23)$$

$$\underline{z}_k = H\underline{x}_k + \underline{\nu}_k \qquad (4.5\text{-}24)$$

Assuming that Φ_k and Γ_k are known, a steady-state discrete Kalman filter gain is calculated using Eq. (4.5-18). The matrices L_k, Φ_k, Γ_k, and H are used to calculate the perturbation state estimate $\hat{\underline{x}}_{k+1/k}$. The value of $\hat{\underline{x}}_{k+1/k}$ is the value which would be used by the controller for feedback.

The values of Φ_k and Γ_k may not be known at the k^{th} instant. Using the scheduling procedure of Section 4.4, however, Φ_k, L_k, and Γ_k can be estimated from the flight variables. An application of a reduced-order estimator of this type which estimates lateral velocity is shown in Section 4.5.5.

The estimator in Fig. 4.5-1 may be unnecessarily complex. Simpler estimators are derived in following sections.

4.5.3 Complementary Filter

This section develops two types of complementary filters which can be useful in estimating the states of a VTOL aircraft. The complementary filter is derived using the general theory of Kalman filters and can be considered to be a special case of a continuous-time steady-state Kalman filter. The derivations presented summarize results shown by Higgens in Ref. 67. Using an earlier result by Brown (Ref. 76), Higgens shows that the complementary filter (normally designed in the frequency domain) can be written in state-space notation and expressed as a Kalman filter. The complementary filter is useful when certain states of the aircraft are measured (directly or

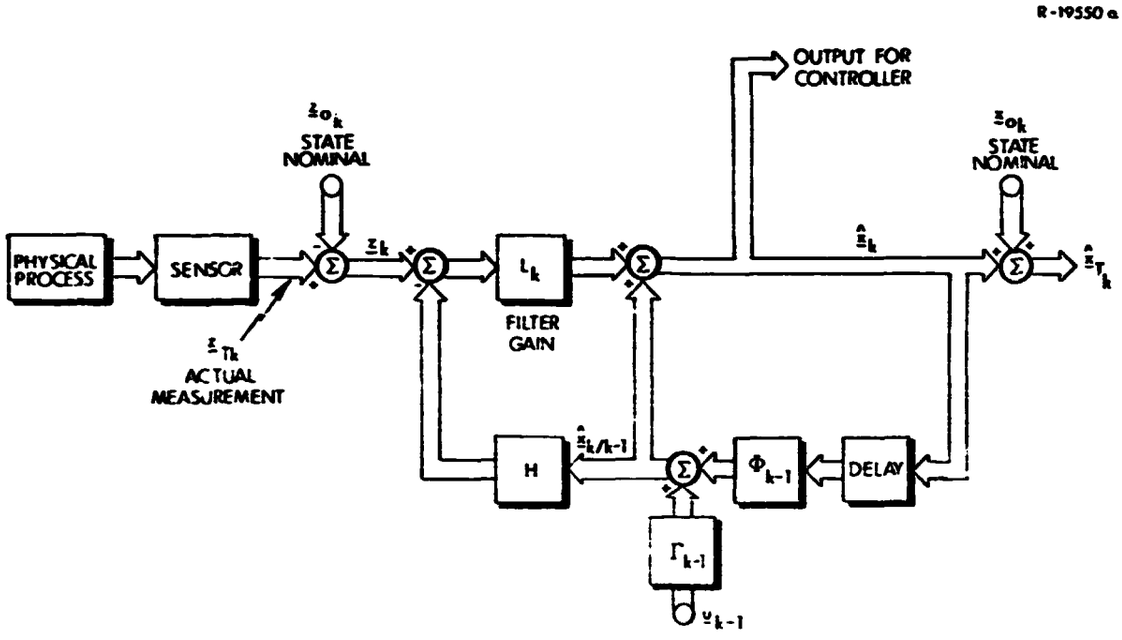

Figure 4.5-1 Discrete Linearized Kalman Filter

indirectly) by more than one sensor. It provides a way of combining these measurements to produce an optimal estimate of the state. The discrete equations for the complementary filter are shown to be much simpler than the filter of the previous section.

The basic complementary filter, shown in Fig. 4.5-2, receives two noise-corrupted versions, x and y, of the same signal, z. One (x) contains low-frequency noise, and the other (y) contains high-frequency noise. The transfer function H(s) is designed to filter out the high-frequency noise in y and is called a low-pass filter. If H(s) is a low-pass filter, [1-H(s)] is its complement, a high-pass filter, and it is used to filter out the low-frequency noise in the measurement, x. The two filtered variables are combined to

produce an estimate of z. Classical derivations of H(s) can proceed without a detailed description of the noise process, although the filter often is adjusted through trial-and-error.

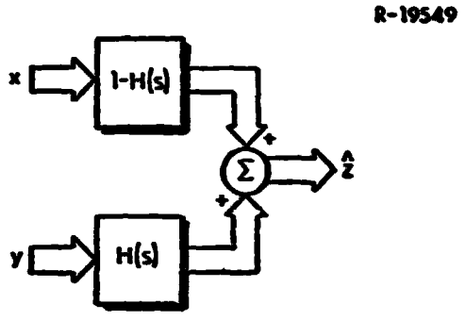

Figure 4.5-2 Basic Complementary Filter

Two examples of a complementary filter derived using Kalman filter theory are shown next. To aid in understanding the concept, the derivations are presented for the estimation of vertical velocity, first from accelerometer and climb rate measurements, then from accelerometer and altimeter measurements.

Application 1: Acceleration and Velocity Measurements - It is assumed that the two available measurements are vertical acceleration, $\ddot{h}_a$, from an accelerometer and vertical velocity, $\dot{h}_b$, obtained from a barometric rate-of-climb meter. If the output of the accelerometer is assumed corrupted by white Gaussian noise, then the integrated accelerometer signal contains low-frequency noise. In a complementary filter, the integrated accelerometer signal is processed by a high-pass filter and the climb-rate signal is processed by a low-pass filter, the results then are combined to produce an estimate of vertical velocity. To develop the corresponding Kalman filter, let the variable

$\dot{h}$ be the true vertical velocity. Then a process equation for $\dot{h}$, with $z = \dot{h}$, is

$$\dot{z} = \ddot{h}_a = Fz + G\ddot{h} + \omega \qquad (4.5\text{-}25)$$

$$y = \dot{h}_b = z + \nu = \dot{h} + \nu \qquad (4.5\text{-}26)$$

where y is the observation, F is the system matrix and G is the control matrix. In this case, F is zero, G is one, and the variables ω and ν are assumed to be zero-mean white Gaussian noise processes with covariances given by

$$\text{cov}[\omega(t),\omega(\tau)] = \sigma_\omega^2\, \delta(t-\tau) \qquad (4.5\text{-}27)$$

$$\text{cov}[\nu(t),\nu(\tau)] = \sigma_\nu^2\, \delta(t-\tau) \qquad (4.5\text{-}28)$$

Equations (4.5-25) and (4.5-26) are in the correct form for a Kalman filter application. Using Eq. (4.5-8), the dynamic equation for the estimate of $\dot{h}$ is

$$\dot{\hat{z}} = L[y-\hat{z}] + \ddot{h}_a \qquad (4.5\text{-}29)$$

where the Kalman filter gain L is given by

$$L = P\,\frac{1}{\sigma_\nu^2} \qquad (4.5\text{-}30)$$

and the algebraic Riccati equation becomes

$$0 = \sigma_\omega^2 - P^2\,\frac{1}{\sigma_\nu^2} \qquad (4.5\text{-}31)$$

Equation (4.5-31) is solved to obtain

$$P = \sqrt{\sigma_\omega^2 \sigma_\nu^2} = \sigma_\omega\, \sigma_\nu \qquad (4.5\text{-}32)$$

$$L = \sigma_\omega/\sigma_\nu \tag{4.5-33}$$

Substituting this in Eq. (4.5-29) results in

$$\dot{\hat{z}} = \ddot{h}_a + \frac{\sigma_\omega}{\sigma_\nu}\,[\dot{h}_b - \hat{z}] \tag{4.5-34}$$

$$\dot{\hat{z}} = -\frac{\sigma_\omega}{\sigma_\nu}\,\hat{z} + \frac{\sigma_\omega}{\sigma_\nu}\,\dot{h}_b + \ddot{h}_a \tag{4.5-35}$$

Typically, the barometric rate-of-climb signal is noisier than the accelerometer signal and a value of $\sigma_\nu/\sigma_\omega = 4$ can be used. A similar analysis could be done if the measurements were lateral velocity from a sideslip angle sensor and a lateral accelerometer.

Equation (4.5-35) gives the filter in continuous time. For digital flight control applications, a suitable discrete-time version of Eq. (4.5-35) must be developed. A difference equation obtained directly from Eq. (4.5-34) is

$$\hat{z}(k\Delta t) = \hat{z}[(k-1)\Delta t] + \int_{(k-1)\Delta t}^{k\Delta t} (L[\dot{h}_b(t) - \hat{z}(t)] + \ddot{h}_a(t)\,dt \tag{4.5-36}$$

where Δt is the sampling interval of the discrete filter. Assuming that $[\dot{h}_b(t) - \hat{z}(t)]$ and $\ddot{h}_a(t)$ are constant over the sampling interval, Eq. (4.5-37) becomes

$$\hat{z}(k\Delta t) = \hat{z}[(k-1)\Delta t] + \Delta t\{L[\dot{h}_{b\,(k-1)\Delta t} - \hat{z}_{\,(k-1)\Delta t}] + \ddot{h}_a[(k-1)\Delta t]\} \tag{4.5-37}$$

Substituting $\dot{h}$ for z and representing the sampling index as a subscript, Eq. (4.5-37) can be arranged as

$$\hat{\dot{h}}_k = \hat{\dot{h}}_{k-1} + \Delta t \frac{\sigma_\omega}{\sigma_\nu}\left[\dot{h}_{b_{k-1}} - \hat{\dot{h}}_{k-1}\right] + \Delta t \ \ddot{h}_{a_{k-1}} \qquad (4.5\text{-}38)$$

The complementary filter shown next uses a measurement of the variable derivative and variable integral to produce an estimate of the variable. The estimation of vertical velocity is used as an example.

Application 2: Acceleration and Position Measurements - It is assumed that two measurements which are available to estimate velocity are a position measurement, z_p, which is obtained from a radar or barometric altimeter, and acceleration, $\ddot{z}_a$, which is obtained from an on-board accelerometer. The position measurement is differentiated to produce velocity. The differentiation increases the high-frequency noise content in the signal. The integration of $\ddot{z}_a$ enhances the low-frequency noise in the velocity measurement derived from the accelerometer.

The process equations for this system are

$$\begin{bmatrix}\dot{z}_1\\ \dot{z}_2\end{bmatrix} = \begin{bmatrix}z_2\\ \ddot{z}_a\end{bmatrix} = \begin{bmatrix}0 & 1\\ 0 & 0\end{bmatrix}\begin{bmatrix}z_1\\ z_2\end{bmatrix} + \begin{bmatrix}0\\ 1\end{bmatrix}\ddot{z}_a + \begin{bmatrix}0\\ \omega\end{bmatrix} \qquad (4.5\text{-}39)$$

and the observation equation is

$$y = z_p = z_1 + \nu \qquad (4.5\text{-}40)$$

where z_1 is true position and z_2 is true velocity. The variables ω and ν are zero-mean, white Gaussian noise processes with the same definitions as Eqs. (4.5-29 and 4.5-30). Define the following:

$$F = \begin{bmatrix} 0 & 1 \\ 0 & 0 \end{bmatrix} \tag{4.5-41}$$

$$G = \begin{bmatrix} 0 \\ 1 \end{bmatrix} \tag{4.5-42}$$

$$H = [1\ 0] \tag{4.5-43}$$

Then the process equation is in the same form as Eq. (4.5-4), and linear-optimal estimation theory can be used to produce the estimation equation

$$\begin{bmatrix} \dot{\hat{z}}_1 \\ \dot{\hat{z}}_2 \end{bmatrix} = \begin{bmatrix} 0 & 1 \\ 0 & 0 \end{bmatrix} \begin{bmatrix} \hat{z}_1 \\ \hat{z}_2 \end{bmatrix} + \begin{bmatrix} 0 \\ 1 \end{bmatrix} \ddot{z}_a + L \begin{bmatrix} (z_p - \hat{z}_1) \end{bmatrix} \tag{4.5-44}$$

In the above, L is the Kalman filter gain and is given by

$$L = P \begin{bmatrix} 1 \\ 0 \end{bmatrix} \frac{1}{\sigma_\nu^2} \tag{4.5-45}$$

where P is the solution to the algebraic Riccati equation

$$FP + PF^T + \begin{bmatrix} 0 & 0 \\ 0 & \sigma_\omega^2 \end{bmatrix} - P \begin{bmatrix} 1 \\ 0 \end{bmatrix} \frac{1}{\sigma_\nu^2} [1\ 0]P = 0 \tag{4.4-46}$$

Solving Eq. (4.5-46) for P, the Kalman filter gain becomes

$$L = \begin{bmatrix} \sqrt{2\sigma_\omega/\sigma_\nu} \\ \sigma_\omega/\sigma_\nu \end{bmatrix} \tag{4.5-47}$$

Equation (4.5-44) gives the continuous-time filter equation. The filter uses the accelerometer and altitude measurements to produce estimates of position and velocity. A difference equation obtained from Eq. (4.5-44), required for digital implementation, is

$$\underline{\hat{z}}(k\Delta t) = e^{F\Delta t}\underline{\hat{z}}([k-1]\Delta t) + \int_{(k-1)\Delta t}^{k\Delta t} e^{F(t-\tau)}(L[z_p(t)-\hat{z}_1(t)] + G\ddot{z}_a(t))dt \tag{4.5-48}$$

If $(z_r(t)-\hat{z}_1(t))$ and $\ddot{z}_a(t)$ are assumed constant over the sampling interval, Δt, then Eq. (4.5-48) can be rewritten as

$$\begin{bmatrix} \hat{z}_1 \\ \hat{z}_2 \end{bmatrix}_k = \begin{bmatrix} 1 & \Delta t \\ 0 & 1 \end{bmatrix} \begin{bmatrix} \hat{z}_1 \\ \hat{z}_2 \end{bmatrix}_{k-1} + \begin{bmatrix} \Delta t^2/2 \\ \Delta t \end{bmatrix} \ddot{z}_{a_{k-1}}$$

$$+ \begin{bmatrix} 1 & \Delta t/2 \\ 0 & 1 \end{bmatrix} L\Delta t(\hat{z}_{p_{k-1}} - \hat{z}_{1_{k-1}}) \tag{4.5-49}$$

where $\hat{z}_1$ is the estimated position and $\hat{z}_2$ is the estimated velocity.

This section has presented two complementary filters which provide estimates of a state when more than one measurement is available. If there is only one sensor measurement and it has low sensor noise, a simple Kalman filter can be used to obtain an estimate of the true state. This is done in the next section.

4.5.4 The Low-Pass Filter

Many aircraft states are measured by single sensors. For example the Euler angles (θ, ϕ, ψ) are measured by attitude gyros, and the angular rates (p, q, r) are measured by the rate gyros. The measurements usually contain little noise, and a full Kalman filter estimator, as in Section 4.5.2, may be more complicated than necessary. A much simpler discrete-time estimator which incorporates the knowledge that sensor noise is low is derived next. The discrete-time estimator that results is shown to be a low-pass filter.

Consider a single aircraft state, x. The discrete-time state equation for x is

$$\begin{bmatrix} x \\ \vdots \end{bmatrix}_{k+1} = \left[\begin{array}{c|ccc} \Phi_{11} & \cdot & \cdot & \cdot \\ \hline \cdot & \cdot & & \\ \vdots & & \ddots & \\ \cdot & & & \end{array}\right] \begin{bmatrix} x \\ \vdots \end{bmatrix}_{k} + \Gamma \underline{u}_k + \underline{\omega}_k \qquad (4.5\text{-}50)$$

where x is written as the first component of the vehicle state, and the remaining states are positioned accordingly. In many instances, the value of Φ_{11} is very close to one because the dynamic effect of x_k on x_{k+1} (i.e., the internal damping effect) is small compared to the forcing of x_{k+1} by disturbances, control, and other states. A reasonable simplification of Eq. (4.5-50) occurs by assuming that Φ_{11} is one and that all the other quantities which affect the state are combined in one driving noise. The process equation for the state, x, under these assumptions, becomes

$$x_{k+1} = x_k + \omega_k \qquad (4.5\text{-}51)$$

which is a random-walk process. Let the measurement of x be given by

$$z_k = x_k + \nu_k \tag{4.5-52}$$

In Eqs. (4.5-51) and (4.5-52), ω and ν are modeled as white Gaussian noise sequences with covariances

$$E\{\omega_k \omega_j\} = \sigma_\omega^2 \, \delta_{kj} \tag{4.5-53}$$

$$E\{\nu_k \nu_j\} = \sigma_\nu^2 \, \delta_{kj} \tag{4.5-54}$$

The steady-state discrete Kalman filter for this case is

$$\hat{x}_k = \hat{x}_{k-1} + L(z_k - \hat{x}_{k-1}) \tag{4.5-55}$$

where the Kalman filter gain, L, is given by

$$L = \frac{P}{P+\sigma_\nu^2} \tag{4.5-56}$$

P, the steady-state error covariance, satisfies the following Riccati equation (taken from Eq. (4.5-20)):

$$P = P - \frac{P^2}{P+\sigma_\nu^2} + \sigma_\omega^2 \tag{4.5-57}$$

Solving for P in Eq. (4.5-57) and substituting into Eq. (4.5-56) leads to

$$P = \frac{\sigma_\omega^2}{2} \left\{ 1 + \left[1 + 4 \left(\frac{\sigma_\nu^2}{\sigma_\omega^2} \right) \right]^{\frac{1}{2}} \right\} \tag{4.5-58}$$

$$L = \frac{\sigma_\omega^2}{\frac{\sigma_\omega^2}{2}\left\{1+\left[1+4\left(\frac{\sigma_\nu^2}{\sigma_\omega^2}\right)\right]^{\frac{1}{2}}\right\}} \qquad (4.5\text{-}59)$$

The filter gain then can be written as

$$L = \frac{2}{1+\left[1+\left(\frac{2\sigma_\nu}{\sigma_\omega}\right)^2\right]^{\frac{1}{2}}} \qquad (4.5\text{-}60)$$

An alternate form of the Kalman filter equation, which is useful for comparison with a classical digital low-pass filter, is

$$\hat{x}_k = \left[\frac{-1+\left[1+\left(\frac{2\sigma_\nu}{\sigma_\omega}\right)^2\right]^{\frac{1}{2}}}{1+\left[1+\left(\frac{2\sigma_\nu}{\sigma_\omega}\right)^2\right]^{\frac{1}{2}}}\right]\hat{x}_{k-1} + \frac{2}{1+\left[1+\left(\frac{2\sigma_\nu}{\sigma_\omega}\right)^2\right]^{\frac{1}{2}}}\hat{z}_k \qquad (4.5\text{-}61)$$

A classical low-pass filter can be derived as follows. In the frequency domain, a continuous-time low-pass filter can be written as

$$\hat{x}(s) = \frac{1}{\tau s+1}\, z(s) \qquad (4.5\text{-}62)$$

The corresponding differential equation,

$$\dot{\hat{x}}(t) = -\frac{1}{\tau}\hat{x}(t) + \frac{1}{\tau}z(t) \qquad (4.5\text{-}63)$$

has the solution,

$$\hat{x}_k = e^{-\frac{1}{\tau}\Delta t}\hat{x}_{k-1} + (1-e^{-\frac{1}{\tau}\Delta t})z_k \qquad (4.5\text{-}64)$$

It is easily shown that for every σ_v and σ_ω which produces the filter given by Eq. (4.5-61), there is a time constant, τ, which produces the same filter using Eq. (4.5-64). For example let Δt equal one, σ_v equal $\sqrt{3}$, and σ_ω equal 2. Equation (4.5-61) then produces

$$\hat{x}_k = \frac{1}{3}\hat{x}_{k-1} + \frac{2}{3}\hat{z}_k \qquad (4.5\text{-}65)$$

The same filter equation can be produced using Eq. (4.5-64) if the time constant, τ, is assumed to be $1/\ln 3$. Substituting Δt and τ into Eq. (4.5-64) results in

$$\hat{x}_k = \frac{1}{3}\hat{x}_{k-1} + \frac{2}{3}\hat{z}_k \qquad (4.5\text{-}66)$$

The two filters are the same.

4.5.5 A Reduced-Order Suboptimal Filter

This section presents a procedure for determining a discrete-time, reduced-order, suboptimal Kalman filter for estimating the lateral velocity of a VTOL aircraft. In the design of a full-order Kalman filter, as in Section 4.5.1, the Kalman gain matrix, L, sometimes has elements that are small in comparison to other elements. This means that some states do not contribute significantly in the estimate of other states. If it is known which states do not aid in estimating desired states, they can be eliminated from the filter structure. This is the concept of a reduced-order, suboptimal filter (Ref. 36). The filter is suboptimal

because the full-order Kalman filter is, by theory, the optimal design, and any simplifications, however slight, degrade performance. The advantage to be gained is a simpler filter with almost optimal performance.

The low-pass filter in Section 4.5.4 is an example of the suboptimal filter in the extreme, where no other state, other than the one being estimated, is used to determine the filter equation. The complementary filters in Section 4.5.3 also are reduced-order filter designs. The filter developed in this section is an example of a reduced-order, suboptimal filter for estimating the lateral velocity, v, where v is not a measured variable but the lateral acceleration, $\dot{v}$, is. The following discussion motivates the order reduction for this filter example.

A common simplification in specifying aircraft dynamic models is to decouple the longitudinal states (u,w,q,θ) from the lateral states (v,p,r,ϕ,ψ). The decoupling is a good approximation for helicopters at low forward velocities, but at high forward velocities, asymmetrical rotor loading becomes more pronounced, and a decoupled system is no longer a valid representation of system dynamics.

Using this information, the dynamic system chosen for estimating v is

$$\underline{x}_{k+1} = \Phi_1 \underline{x}_k + \Gamma_1 \underline{u}_k + \underline{\omega}_k \qquad (4.5\text{-}67)$$

where Φ_1, Γ_1 are (7x7) and (7x4) matrices, respectively, that result when the u and w rows and columns are removed from the full-order Φ and Γ matrices of the aircraft. The effects of q and θ are retained to account for the increased coupling at high forward speeds. The available measured states for the system given by Eq. (4.5-67) are assumed to be

$$\underline{z}^T = [\dot{v}_m \; p_m \; q_m \; r_m \; \theta_m \; \phi_m \; \psi_m] \qquad (4.5\text{-}68)$$

where the measurements in $\underline{z}$ come from on-board sensors (discussed in Section 5.7.1). The observation matrix for Eq. (4.5-68) is given by

$$H = \left[\begin{array}{c|cccccc} f_{vv} & f_{vp} & f_{vq} & f_{vr} & f_{v\theta} & f_{v\updownarrow} & f_{v\psi} \\ \hline 0 & 1 & & & & & \\ 0 & & 1 & & 0 & & \\ 0 & & & 1 & & & \\ 0 & & & & 1 & & \\ 0 & 0 & & & & & \\ 0 & & & & & 1 & \\ 0 & & & & & & 1 \end{array}\right] \qquad (4.5\text{-}69)$$

The elements in the first row of H come from the lateral velocity row of the F matrix system dynamics. Using Eq. (4.5-68) and (4.5-69), the measurement equation for the system becomes

$$\underline{z}_k = H\underline{x}_k + \underline{\nu}_k \qquad (4.5\text{-}70)$$

The control effect on v is included in the observation noise. The variables ω and ν in Eqs (4.5-67) and (4.5-70) are white Gaussian noise processes and have covariances given by Eqs. (4.5-13) and (4.5-14), respectively. The discrete system for this example has the form necessary to apply the discrete Kalman filter. Using Section 4.5.1, the filter is given by

$$\hat{\underline{x}}_k = \hat{\underline{x}}_{k/k-1} + L(\underline{z}_k - H\hat{\underline{x}}_{k/k-1}) \qquad (4.5\text{-}71)$$

$$\hat{\underline{x}}_{k+1/k} = \Phi_1 \, \hat{\underline{x}}_k + \Gamma_1 \, \underline{u}_k \qquad (4.5\text{-}72)$$

where L is the (7x7) Kalman filter gain given by Eq. (4.5-18).

In Section 5.7-2 it is shown that p, q, r, θ, ϕ, and ψ are estimated using low-pass filters. This can be incorporated into Eq. (4.5-72) by writing only the estimate equation for v in Eq. (4.5-71).

$$\hat{v}_k = \hat{v}_{k/k-1} + L_1 \begin{bmatrix} \dot{v}_{mk} - (f_{vv}\hat{v}_{k/k-1} + f_{vp}\hat{p}_k + f_{vq}\hat{q}_k + f_{vr}\hat{r}_k + f_{v\theta}\hat{\theta}_k + f_{v\phi}\hat{\phi}_k + f_{v\psi}\hat{\psi}_k) \\ (p_m - \hat{p}_k) \\ (q_m - \hat{q}_k) \\ (r_m - \hat{r}_k) \\ (\theta_m - \hat{\theta}_k) \\ (\phi_m - \hat{\phi}_k) \\ (\psi_m - \hat{\psi}_k) \end{bmatrix} \tag{4.5-73}$$

Using the same idea, Eq. (4.5-72) can be reduced to

$$\hat{v}_{k+1/k} = \Phi_{11} \begin{bmatrix} \hat{v}_k \\ \hat{p}_k \\ \hat{q}_k \\ \hat{r}_k \\ \hat{\theta}_k \\ \hat{\phi}_k \\ \hat{\psi}_k \end{bmatrix} + \Gamma_{11}\, u_k \tag{4.5-74}$$

The outputs of the low-pass filters at k are used to produce the residuals at k in Eq. (4.5-73) along with the residual for $\dot{v}$. The residuals are multiplied by the first row in L denoted as L_1, and the result is summed with the update, $\hat{v}_{k/k-1}$. The summation produces the best estimate of v at k

given by $\hat{v}_k$. The low-pass filters do not have separate update equations, but the update for $\hat{v}_k$ can be given by Eq. (4.5-74), where Φ_{11} is the first row of Φ_1 and Γ_{11} is the first row of Γ_1.

In summary, this section has specified a reduced-order, suboptimal Kalman filter that estimates the lateral velocity using other states and an accelerometer measurement. Implementation of the filter requires that L_1, Φ_{11}, Γ_{11}, and the elements of F be scheduled like the gains in Section 4.4. Some of the assumptions used in this section are demonstrated in Section 5.7.

The other parts of Section 4.5 presented three types of Kalman filters which can be used to estimate aircraft states. Each of the other three filters is a simplification of a full-order Kalman filter, and all three are discrete-time filters with constant gains and simple structures.

4.6 CHAPTER SUMMARY

Methods for using the digital PI controller and digital PII controller for VTOL aircraft have been shown The methods consist of adapting the linear controllers to varying flight conditions using gain scheduling techniques. The primary results obtained are the following:

- By propagating the noise covariances at different flight conditions, a minimal sampling time for a controller can be obtained.
- It is expected that the integrating action of the digital controllers will adapt to varying trim. To aid the response time of the controllers, two trim setting techniques are developed.

- The static trim values for the aircraft are correlated and scheduled against the flight conditions.
- Linear dynamic trim compensation can be computed from

$$\begin{bmatrix} \delta_B^* \\ \delta_C^* \\ \delta_R^* \\ \delta_S^* \\ 0 \\ 0 \end{bmatrix} = G_\mu^{-1} \begin{bmatrix} \dot{u}^* \\ 0 \\ \dot{\omega}^* \\ \dot{p} \\ \dot{q} \\ \dot{r} \end{bmatrix} - G_\mu^{-1} F_2 \begin{bmatrix} 0 \\ 0 \\ 0 \\ p^* \\ q^* \\ r^* \end{bmatrix} \qquad (4.6\text{-}1)$$

  where G_μ^{-1} and F_2 can be scheduled with flight conditions. Under static conditions the left side of Eq. (4.6-1) is zero.
- The control gains are found for a finite set of points in the flight envelope. The gains are correlated and scheduled according to flight conditions.
- For those sensors which have low additive noise and negligible bias error, a low-pass filter can estimate the state.
- A discrete-time complementary filter estimates a state when more than one sensor (each with different additive noise) provides measurements of the state value.
- A reduced-order, discrete-time Kalman filter can estimate measured and unmeasured states where the Kalman gains and discrete system and control matrices are scheduled.

5. APPLICATIONS OF THE CONTROL DESIGN TECHNIQUE

Chapter 5 describes the design of digital controllers with open-loop explicit adaptation for the VALT Research Aircraft using the techniques presented in Chapters 3 and 4. A summary of the technique is given in Section 5.10.

5.1 OVERVIEW

The control laws developed for VTOL aircraft in Chapter 3 are narrowed down to the discrete PI and PII servos shown in Sections 3.5 and 3.6. Both are determined by quadratic synthesis, have the same number of gains, and have the same number of delays in their structure. Each of the control laws is used in the design of command-control systems in this chapter.

The first effort of the design is to determine the sampling times for the controllers, which is done in Section 5.2. Section 5.3 presents the two command-response systems which are to be designed for the VALT Research Aircraft. The flight conditions which are used to design the control laws are given in Section 5.4. Section 5.5 presents the criteria used for the control system designs, including classical step response criteria and quadratic cost criteria. Section 5.6 describes design procedures for each of the control systems. The process of choosing the correct quadratic response criteria to meet the classical response criteria is shown. Section 5.7 presents simplified discrete-time Kalman filters using a typical set of motion sensors. Section 5.8

presents the regression coefficients for the controller design. Section 5.9 provides a representative number of simulations obtained in the design work of Section 5.6. The overall design procedure and a chapter summary are contained in Section 5.10.

5.2 SAMPLING INTERVAL

The control sampling interval of 12 computational frames per sec has been determined using the state error covariance propagation method described in Section 4.2. As in Ref. 66 , the wind is assumed to be the primary disturbance input, and parameter uncertainties and measurement errors are not considered directly. Atmospheric turbulence is modeled as three independent, exponentially-correlated Gauss-Markov processes, defined by

$$\dot{w}_x = -\frac{1}{\tau_x} w_x + w_{x_0} \qquad (5.2\text{-}1)$$

$$\dot{w}_y = -\frac{1}{\tau_y} w_y + w_{y_0} \qquad (5.2\text{-}2)$$

$$\dot{w}_z = -\frac{1}{\tau_z} w_z + w_{z_0} \qquad (5.2\text{-}3)$$

The wind-velocity components (w_x, w_y, w_z) force the aircraft and are themselves forced by the uncorrelated, zero-mean random processes (w_{x_0}, w_{y_0}, w_{z_0}). The correlation times of the turbulence components are τ_x, τ_y, and τ_z. The covariance matrix associated with the turbulence driving terms is

$$W_0 = \begin{bmatrix} \frac{2\sigma_x^2}{\tau_x} & 0 & 0 \\ 0 & \frac{2\sigma_y^2}{\tau_y} & 0 \\ 0 & 0 & \frac{2\sigma_z^2}{\tau_z} \end{bmatrix} \qquad (5.2\text{-}4)$$

where σ_x, σ_y, and σ_z represent the rms-levels of the turbulence. The correlation times and turbulence levels are assumed to be 1 sec and 20 fps, respectively, for all three axes; thus the helicopter is forced by a rapidly varying, high-gust environment.

In solving for the state covariances, Eq. (4.2-5) is used. The initial values of the state covariances are set to zero. The wind equations, (Eq. (5.2-1) to (5.2-3)) are adjoined to the helicopter equations for the solution, and the entire set is driven by Eq. (5.2-4). The bounds on helicopter motion variables are taken to be 0.5 deg for angles, 5 deg/sec for angular rates, and 2 fps for translational velocities. The worst-case flight condition (hover) produced a 0.16-sec sampling interval, the result of lateral velocity reaching its bounding value. At this point, the maximum angle uncertainty is less than 0.2 deg in all axes, and the roll rate uncertainty is 2.6 deg/sec.

Assuming no computational delays, this result indicates an allowable sampling rate of about 6 frames per sec; however, a sampling rate of 12 frames per sec has been used here. The integral compensation of the PII controller, developed in Chapter 3 and used in the design of the velocity-command control law, imposes a delay of one sampling

interval between feedback measurement and control command; therefore, errors which begin to grow immediately following a control action are measured at the next sampling instant but are not reflected in control commands until the following sampling instant, i.e., errors continue to grow over two sampling periods. Consequently, the velocity-command control law was assumed to require the 12 frames-per-sec rate, and the same rate was used for the attitude-command law to provide commonality.

5.3 CONTROL MODES

In Section 3.5 two kinds of discrete command-response control laws, the PI and PII controllers, were derived. Both will accept any set point command if the number of commands equal the number of controls. The PII controller has a distinct advantage if the number of set points or command inputs is less than the number of controls. The PI controller can handle this case, but not as efficiently. As an example, the velocity-command system for the VALT Research Aircraft could have been designed with only three commands, whereas the aircraft has four controls. The choice of command variables determines the transformation matrix, T, in the command-input segment of each control law (see, for example, Fig. 3.6-1).

5.3.1 Velocity-Command Control Law

The velocity guidance law, as explained in Chapter 2, commands the translational velocities of the VTOL aircraft. V_x, V_y, V_z are the velocities of the craft along the earth-relative x, y, and z axes, respectively. The guidance system gives earth-relative velocity commands to the controller

which depend on where the craft is at present and where it should be, as a function of range to go.

The (3 x 9) transformation matrix, T, for this system is

$$T = \left[H_B^E \,\middle|\, 0 \right] \tag{5.3-1}$$

where H_B^E is the transpose of the matrix H_E^B given by Eq. (2.4-10), which converts the body-frame reference velocities to the earth-relative velocities. Equation (5.3-1) indicates that the PII controller should be used for this guidance system, because three command variables are specified, and there are four control variables. The fourth state, which is not a primary guidance command, is yaw. Section 2.4 explained how yaw can and should be used as a fourth (secondary) command. With yaw added, the dimension of the transformation matrix increases, and T has the following structure, where the states are arranged, u, v, w, p, q, r, θ, ϕ, ψ:

$$T = \left[\begin{array}{ccc|cccccc} & & & 0 & 0 & 0 & 0 & 0 & 0 \\ & H_B^E & & 0 & 0 & 0 & 0 & 0 & 0 \\ & & & 0 & 0 & 0 & 0 & 0 & 0 \\ \hline 0 & 0 & 0 & 0 & 0 & 0 & 0 & 0 & 1 \end{array}\right] \tag{5.3-2}$$

The expression for yaw angle with no horizontal wind can be calculated from Eq. (2.4-13) and is given by

$$\psi + \beta = \tan^{-1} \frac{V_y}{V_x} \tag{5.3-3}$$

Figure 5.3-1 shows an earth-relative frame, a body reference frame, and the velocity vector orientated with a non-zero sideslip.

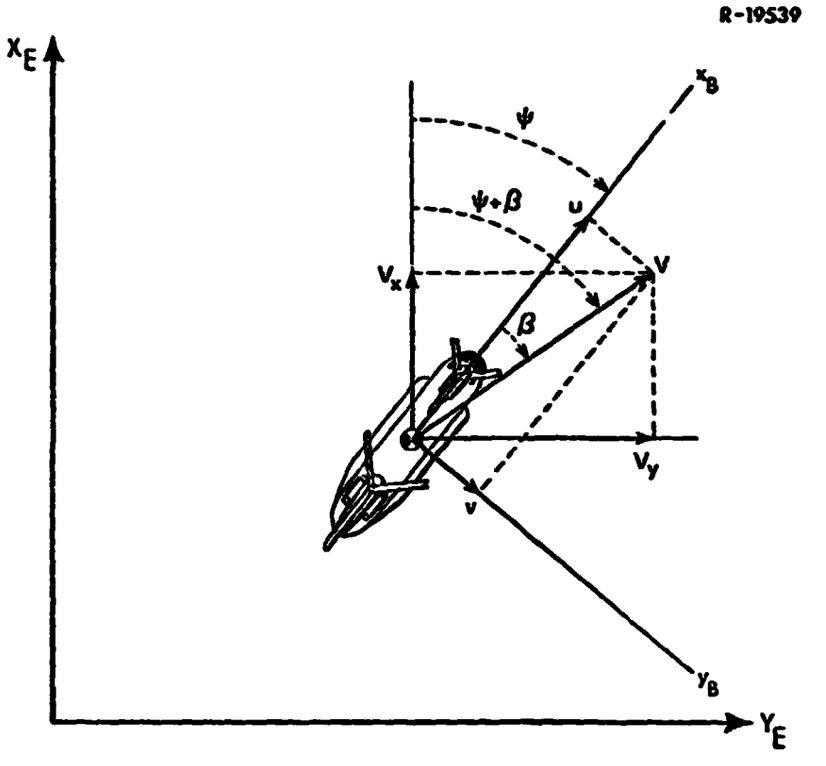

Figure 5.3-1 Coordinate Frame of the VALT Research Aircraft

Later sections show that the PII control law is chosen to accept the commands from the velocity-command guidance system. Referring to Fig. 3.6-2, the PII block diagram, the matrix T of Eq. (5.3-2) converts the body-axis aircraft states to the earth-relative guidance-command reference frame. The value of the guidance command, $\underline{y}_d$, is subtracted from $T\underline{x}$ to produce the error between the commanded values of velocity and yaw and the actual aircraft velocity and yaw angle. The errors are accumulated, and the output of the accumulator drives the remainder of the control law. The accumulator drives the remainder of the control law. The accumulator output will continually drive the control dynamics until there is no longer an error between $\underline{y}_d$ and $T\underline{x}$, and the aircraft holds trim.

The control dynamics form a combination regulator and low-pass filter. The regulator part is associated with the feedback of all the states to the summation block which determines $\underline{u}_{k+1}$. Since all the states are fedback, there are longitudinal/lateral-directional crossfeeds present. The low-pass filtering effect is produced by the feedback of $\underline{u}_k$ to the summation block for $\underline{u}_{k+1}$. The low-pass filter is due to the weighting of $\dot{\underline{u}}$ in the cost functional for the PII control law, and it helps keep actuator rates and positions below their limits. The output of the control dynamics, $\underline{u}_k$, enters the system as shown at the bottom of Fig. 2.3-2.

5.3.2 Attitude-Command Control Law

The attitude-command guidance law commands the three Euler angles (θ, ϕ, and ψ) and vertical velocity, as discussed in Chapter 2. The (4 x 9) transformation matrix, T, between attitude guidance commands and body-axis states is given by

$$T = \begin{bmatrix} 0 & 0 & 0 & 0 & 0 & 0 & 1 & 0 & 0 \\ 0 & 0 & 0 & 0 & 0 & 0 & 0 & 1 & 0 \\ 0 & 0 & 0 & 0 & 0 & 0 & 0 & 0 & 1 \\ H_B^E(3,1) & H_B^E(3,2) & H_B^E(3,3) & 0 & 0 & 0 & 0 & 0 & 0 \end{bmatrix} \quad (5.3\text{-}4)$$

The bottom row of T converts the u, v, w body-axis velocities to the earth-relative velocity command, V_{Z_E}, and it contains the bottom three elements of the matrix H_B^E in Eq. (5.3-2).

Later sections show that the PI control law is chosen to accept the commands from the attitude-command guidance system. This choice is made because angle commands require fast responses, and the PI control law has little

delay between commands and control input. Referring to Fig. 3.6-1, the PI block diagram, the body reference states are transformed by the T matrix given in Eq. (5.3-4), then subtracted from the $\underline{y}_d$ command which comes from the attitude guidance law. There is also a delayed $T\underline{x}$ which is subtracted from the current $\underline{y}_d$ command. The delayed error and current error are summed with the regulating state feedback to produce the control command which drives the system. This controller tends to have low control rates, because $\dot{\underline{u}}$ is weighted in its cost function. The control rate is governed by the difference between the two gain matrices which feedforward the error variables. The PI control law drives the system as long as there is an error between the commands of the guidance law and the feedback term, $T\underline{x}$.

5.4 FLIGHT CONDITIONS FOR POINT DESIGN

The next element in the design is the determination of the flight conditions at which the control gains are computed. At this point in the application of the control design technique, the command laws, transformation matrices and sampling time have been determined.

The design points in the flight envelope where the servo gains are determined should meet the following requirements:

- The points should represent normal takeoff, climb, cruise, descent, and landing flight conditions.
- Regions of instability should be included even if normal flight operations rarely occur there.

Figure 5.4-1 shows the 19 points that were chosen for the VALT Research Aircraft using these guidelines. The normal flight modes -- hover, ascent, level flight, and descent -- were considered for points in the x-z plane. Inside this region, the area near hover contains a concentration of points, as take-off and landing maneuvers are critical. As the forward velocity increases, the points fan out to provide the gain scheduling algorithm with a representative number of conditions. Vehicle dynamics are computed for sea level altitudes, and ground effects are not considered.

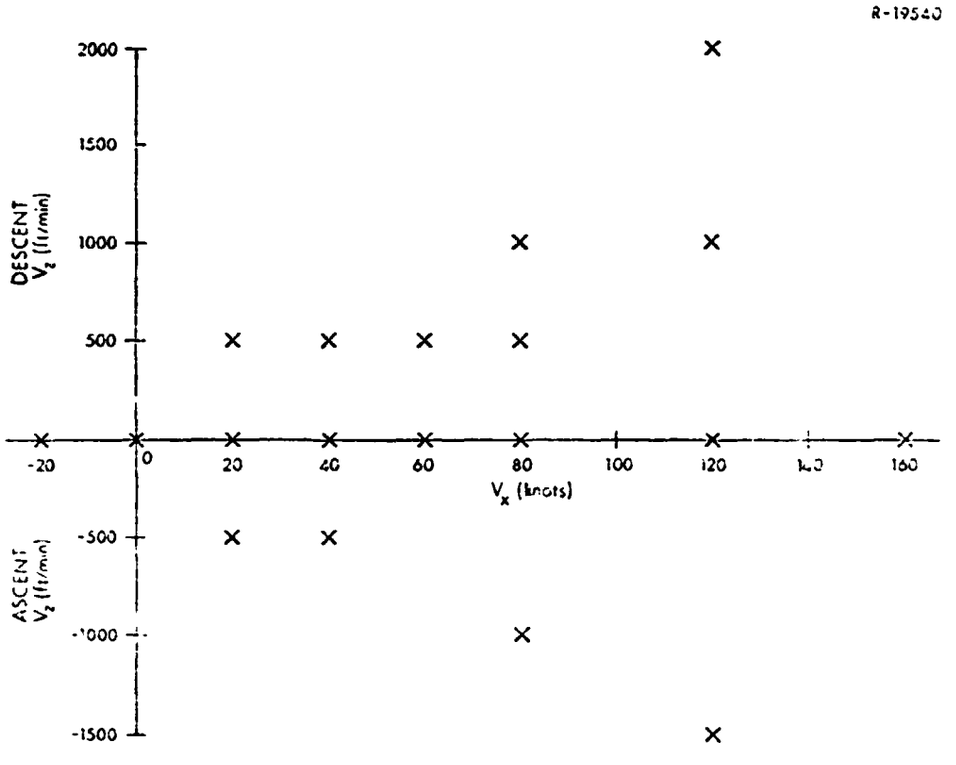

Figure 5.4-1 Flight Conditions for Point Design

5.5 CRITERIA FOR CONTROL SYSTEM DESIGN

Both classical and modern response criteria have proven valuable in the design and evaluation of control systems, and both criteria are used in the design of the current example. Basic response criteria are expressed in terms of the step response, which must stay within certain limits. With a step input at t = 0.

- The rise time (T_r), the value at which the response first meets a certain percent of the step, must be achieved;
- The Percent Overshoot (P.O.) must not be exceeded; and
- The response should be within a specified percent of the final value after the settling time (T_s) is exceeded.

Linear-optimal design is based on quadratic response criteria. In this method, the Q and R weighting matrices of a quadratic cost functional, J, are specified so that the system has acceptable response to commands and disturbances with acceptable control usage. Cost functionals for the PI and PII control laws are given by Eq. (3.5-2) and Eq. (3.5-58). Although the control laws are discrete, the cost functionals initially are specified in the continuous-time domain.

For the PI control law, the states, control positions, and control rates are weighted. For the PII control law, the states, control positions, integrator states, and control rates are weighted. Each of the continuous-time cost functionals can be placed in the more general format,

$$J = \int_0^\infty (\underline{x}^T Q \underline{x} + \underline{u}^T R u) dt \qquad (5.5\text{-}1)$$

which is Eq. (3.2-3). The states, $\underline{x}$, and controls, $\underline{u}$, in Eq. (5.5-1) depend on the control structure.

There are two systematic ways of determining Q and R in Eq. (5.5-1). One way is to specify the maximum values of the states and control which are acceptable under normal operating conditions (Ref. 56). The elements of Q and R can be specified by the following equations:

$$r_{ii} = 1/u_{i_{max}}^2 \quad , \; i = 1 \text{ to } m \tag{5.5-2}$$

$$q_{jj} = 1/x_{j_{max}}^2 \quad , \; j = 1 \text{ to } n \tag{5.5-3}$$

Note that the non-diagonal elements of Q and R are zero in this tradeoff between state and control disturbances. An alternate way of choosing Q and R is to vary individual elements of the weighting matrices until a desired response is obtained from the resulting closed-loop system. In practice, once acceptable values of Q and R are obtained for a single flight condition, solutions at other flight conditions are readily obtained. The control designer thus has a choice in interpreting Q and R effects on design as either trading off state and control motions or as providing a means of obtaining stable systems with desirable command response.

5.5.1 Classical Response Criteria

Classical response criteria have been specified for the VALT Research Aircraft's two command systems. For the velocity-command system specifications are:

- V_Z Command:

  Rise time criterion: Amplitude >90% of the final value with . 2 sec

  Overshoot criterion: Overshoot <5% of the final value for $0<V_X<10$ kt

  Overshoot $<0.5V_X$% of the final value for $10<V_X<40$ kt

  Overshoot <20% of the final value for $V_X>40$ kt

- V_X, V_y Commands:

  Rise time criterion: Amplitude >80% of the final value within 5 sec

  Overshoot criterion: Overshoot $<(4+.4V_X)$% of the final value for $0<V_X<40$ kt

  Overshoot <20% of the final value for $V_X>40$ kt

A settling time is not specified for the commands. Since there is no yaw angle response specification given, a suitable quadratic response criteria is chosen. For the attitude-command system the specifications are:

- Angle Commands: θ, ϕ, ψ

  Rise time criterion: Amplitude >90% of the final value within 1.5 sec

  Overshoot criterion: Overshoot <15% of the final value

  Settling time criterion: Amplitude shall be within 5% of the final value in 5 sec or less

- V_Z Command: same as the velocity system

The most stringent criteria in this application are the rise times. The tradeoff is between exceeding the control rate limits and satisfying the rise time.

5.5.2 Quadratic Response Criteria

Design using quadratic response criteria amounts to choosing Q and R matrices for the cost functions given by each of the controllers. As shown in Eqs. (5.5-2) and (5.5-3), the values of Q and R can be interpreted as specifying maximum allowable values of states and controls.

For the PII controller, the states which can be weighted are

$$\underline{x}^T = [u\ v\ w\ p\ q\ r\ \theta\ \phi\ \psi\ \delta_B\ \delta_C\ \delta_S\ \delta_R\ y_{V_x}\ y_{V_y}\ y_{V_z}\ y_\psi] \tag{5.5-4}$$

and the control rates which can be weighted are

$$\underline{u}^T = [\dot{\delta}_B\ \dot{\delta}_C\ \dot{\delta}_S\ \dot{\delta}_R] \tag{5.5-5}$$

In Eq. (5.5-4), the y states correspond to the integrated error states of the PII control law (called y_I in Chapter 3). The weighted states for the velocity-command PII control law are chosen as follows:

$$\underline{x}^T = [u\ v\ w\ y_{V_x}\ y_{V_y}\ y_{V_z}\ y_\psi] \tag{5.5-6}$$

and the control variables are given by Eq. (5.5-5). The remaining states are not weighted.

For the PI controller, the states which can be weighted are

$$\underline{x}^T = [u\ v\ w\ p\ q\ r\ \theta\ \phi\ \psi\ \delta_B\ \delta_C\ \delta_S\ \delta_R] \qquad (5.5\text{-}7)$$

and the control rates which can be weighted are

$$\underline{u}^T = [\dot{\delta}_B\ \dot{\delta}_C\ \dot{\delta}_S\ \dot{\delta}_R] \qquad (5.5\text{-}8)$$

The following states are chosen to be weighted for the attitude-command PI control law system:

$$\underline{x}^T = [w\ \theta\ \phi\ \psi] \qquad (5.5\text{-}9)$$

and the controls are the same as Eq. (5.5-8). The rest of the state weightings were zero.

The choices for $\underline{x}$ given by Eqs. (5.5-6) and (5.5-9) are obvious by comparing what is weighted and what is commanded for each system. In Eq. (5.5-6), u, v, and w are added for more flexibility. In Eqs. (5.5-6) and (5.5-9), if either ψ or y_ψ is not weighted, the matrices $[F\ Q^{\frac{1}{2}}]$ would not be an observable pair.

5.6 CONTROL GAIN DESIGN

At this point in the control design procedure, the flight conditions have been chosen and the sampling time specified, the classical response criteria have been defined, and the variables which are to be weighted by Q and R have been specified. The next step is the specification of the maximum values, $\underline{x}_{max}$ and $\underline{u}_{max}$ in Eqs. (5.5-2) and (5.5-3), at each flight condition.

5.6.1 Application of Quadratic Design for Velocity-Command PII Controller

The control-rate weighting matrix, R, is defined by the rate-limiting characteristics of the TAGS actuators used on the VALT Research Aircraft. Each actuator is rate-limited at 7.5 in/sec, due to hydraulic constraints. This is a physical limitation which must be avoided to ensure good system response. To provide a margin for error, the value of each limit is placed at

$$\dot{\delta}_{B_{max}} = \dot{\delta}_{C_{max}} = \dot{\delta}_{S_{max}} = \dot{\delta}_{R_{max}} = 2 \text{ in/sec} \qquad (5.6\text{-}1)$$

which is a soft constraint. From Eq. (5.5-2), R becomes

$$R = \begin{bmatrix} .25 & 0 & 0 & 0 \\ 0 & .25 & 0 & 0 \\ 0 & 0 & .25 & 0 \\ 0 & 0 & 0 & .25 \end{bmatrix} \qquad (5.6\text{-}2)$$

The control actuators are displacement-limited to ±5 in. The limits are symmetric about zero for three actuators; the collective control is position-limited from 0 to 10 in. These limits were used in early design phases in the Q matrix, but it was determined that the weightings had little effect on system gains or time histories. In addition, simulated control deflections never approach the limits; therefore, the limits have been neglected in the final design.

The next thing noticed in the design process is that the weightings to meet the velocity step response criteria can be adjusted separately. (This also is true for the attitude system.) This means that the integrator

weightings can be combined with the state weightings as (u, yV_x), (v, yV_y), (w, yV_z), and y_ψ, and each pair can be adjusted to meet the corresponding step response without affecting the step response of other commands.

The noninteracting feature of state weighting leads to a fruitful design methodology. Q matrices are found at extreme flight conditions, then linearly interpolated to determine weightings for the intermediate flight conditions. The first working point chosen is hover, for which the following values are obtained:

$$u_{max} = 6.0 \text{ fps}$$

$$v_{max} = 6.0 \text{ fps}$$

$$w_{max} = 4.0 \text{ fps}$$

$$yV_x max = 10.0 \text{ ft}$$

$$yV_y max = 10.0 \text{ ft}$$

$$yV_z max = 2.0 \text{ ft}$$

$$y_\psi max = 20.0 \text{ deg/sec}$$

The weightings on yV_x, yV_y, yV_z, y_ψ are frozen, and u_{max}, v_{max}, and w_{max} are allowed to change with flight condition. The next extreme design point chosen is V_z = 0 ft/min, V_x = 160 kt. The weightings are adjusted to obtain acceptable step response, and a linear interpolation using u_0 is formed between this point and hover, resulting in

$$u_{max} = 6.0 + \frac{|u_0|}{10.} = 33.02 \text{ fps (at } V_z=0, V_x=160 \text{ kt)} \quad (5.6\text{-}3)$$

$$v_{max} = 6.0 + \frac{|u_0|}{20.} = 19.61 \text{ fps (at } V_z=0, V_x=160 \text{ kt)} \quad (5.6\text{-}4)$$

$$w_{max} = 4.0 + \frac{|u_0|}{80.} = 7.37 \text{ fps (at } V_z=0,\ V_x=160 \text{ kt)} \quad (5.6\text{-}5)$$

The Q and R matrices thus determined, control gains are computed at 19 flight conditions, and acceptable step responses are obtained at every point.

Note that Q and R are chosen for the continuous system, and the step response is observed using the resulting discrete controller. This illustrates the advantages of forming the sampled-data regulator using the techniques presented in Chapter 3. The $\hat{Q}$, M, $\hat{R}$ matrices for the discrete-time controller contain values in every element, and searching directly for these elements would be impractical.

5.6.2 Application of Quadratic Design for Attitude-Command PI Controller

In Section 5.6.1 the Q and R matrices are specified for 19 flight conditions. R is constant and Q is found by linear interpolation between flight conditions. For the attitude-command PI control law, R is constant and is given by Eq. (5.6-2) using the same rate limits. Q must be determined using a different method.

It is necessary to find the state weightings which meet the step response requirements at each flight condition individually. As the attitude commands vertical velocity, maximum value for w is kept in the same format as Section 5.6.1, i.e.,

$$w_{max} = w_1 + \frac{|u_0|}{80} \text{ fps} \quad (5.6\text{-}6)$$

where only w_1 is adjusted. Table 5.6-1 shows the variation

in the maximum values which form Q, as in Eq. (5.6-3), for each flight condition. The maximum values follow a general trend with V_x, although differences resulting from climbing or descending flight can be noted.

TABLE 5.6-1
CRITERIA FOR THE ATTITUDE-COMMAND PI CONTROLLER AT THE FLIGHT CONDITIONS CHOSEN FOR POINT DESIGN

V_x, kt	V_z, ft/min	w_1, fps	θ_{MAX}, deg	ϕ_{MAX}, deg	ψ_{MAX}, deg
-20.0	0.0	.0	3.5	6.0	3.0
0.0	0.0	8.0	3.5	6.0	3.0
20.0	500.0	8.0	3.5	6.0	3.0
20.0	0.0	8.0	3.4	5.9	3.0
20.0	-500.0	8.0	3.3	5.8	2.9
40.0	500.0	8.0	3.1	5.6	2.8
40.0	0.0	9.0	3.1	5.[illegible]	2.8
40.0	-500.0	9.0	3.1	5	2.8
60.0	500.0	9.0	3.1	5.6	2.8
60.0	0.0	9.0	3.1	5.6	2.5
80.0	500.0	9.0	3.1	5.6	2.5
80.0	0.0	9.0	3.1	5.5	2.5
80.0	-1000.0	9.0	3.0	5.2	2.5
120.0	0.0	9.0	2.8	5.3	2.5
120.0	1000.0	9.0	3.0	5.3	2.5
120.0	-1500.0	6.0	1.0	3.5	2.0
120.0	2000.0	9.0	3.0	5.2	2.5
160.0	0.0	6.0	2.3	5.3	2.5

5.7 ESTIMATOR DESIGN

The purpose of this section is to apply the Kalman filter designs presented in Section 4.5 to the VALT Research Aircraft. Aircraft instrumentation is reviewed, and filter gains are computed.

5.7.1 Sensors

A number of different kinds of sensors are available to detect the states of an aircraft. These include gyros, accelerometers, radar, pressure and temperature measuring devices, and others. In this chapter, the VALT Research Aircraft is assumed to use the sensors presented in Table 5.7-1.

TABLE 5.7-1
SENSORS FOR VALT CONTROL SYSTEM DESIGN

SENSOR	LOCATION*		
	Δx_B, in	Δy_B, in	Δz_B, in
Indicated Air Speed	Aircraft Nose		
Barometric Altimeter	280	40	-10
Attitude Gyro (3)	-110	20	30
Angular Rate Gyro (3)	-110	20	30
Accelerometer (3)	10	0	-20

* Locations specified relative to center of gravity

There are three attitude gyro outputs to provide information about Euler angles θ_T, ϕ_T, and ψ_T, three angular rate gyros to measure p_T, q_T and r_T, and three accelerometers which aid in determining body accelerations, $\dot{u}_T$, $\dot{v}_T$, $\dot{w}_T$. The two other sensors are a barometric altimeter, which provides a measurement of the height of the aircraft based on static pressure, and an airspeed indicator, which provides information about forward speed based on dynamic pressure. Acceleration, velocity, and altitude measurements must be processed to provide the appropriate body-axis measurement. Modifications or assumptions for accelerometers, $\ddot{h}_b$, and IAS are shown next.

The accelerometers are not located at the center of gravity, and they sense accelerations arising from angular rotation as well as translational accelerations. Their outputs must be adjusted to give body accelerations, $\dot{u}_T$, $\dot{v}_T$, $\dot{w}_T$.

Let $\Delta\underline{x}_B$ be the location of the accelerometers in the body, measured in the body axes. The position of the accelerometers, $\underline{x}'_E$, expressed in earth-relative axes, is

$$\underline{x}'_E = \underline{x}_E + H_B^E \, \Delta\underline{x}_B \tag{5.7-1}$$

where x_E is the position of the center of gravity of the aircraft in earth-relative axes. Differentiating twice produces the following:

$$\dot{\underline{x}}'_E = \dot{\underline{x}}_E + \dot{H}_B^E \, \Delta\underline{x}_B \tag{5.7-2}$$

$$\ddot{\underline{x}}'_E = \ddot{\underline{x}}_E + H_B^E \, \tilde{\omega}_B^E \, \tilde{\omega}_B^E \, \Delta\underline{x}_B + H_B^E \, \dot{\tilde{\omega}}_B^E \, \Delta\underline{x}_B \tag{5.7-3}$$

In Eq. (5.7-3) $\underline{\omega}_B^E$ represents the angular rate of earth-relative axes expressed in body axes. The expression, $\tilde{\omega}_B^E$, is a matrix equivalent to the vector cross-product. From the definition of $\underline{\omega}_B^E$, $\tilde{\omega}_B^E$ is

$$\tilde{\omega}_B^E = \begin{bmatrix} 0 & -r & q \\ r & 0 & -p \\ -q & p & 0 \end{bmatrix} \tag{5.7-4}$$

The accelerometers are mounted on the body, and their output vector, $\underline{a}_T$, consists of the earth-relative acceleration minus the gravitational acceleration:

$$\underline{a}_T = H_E^B(\ddot{\underline{x}}_E' - \underline{g}_E) = H_E^B(\ddot{\underline{x}}_E - \underline{g}_E) + (\tilde{\omega}_B^E\tilde{\omega}_B^E + \dot{\tilde{\omega}}_B^E)\Delta\underline{x}_B \qquad (5.7\text{-}5)$$

Writing out each individual expression, Eq. (5.7-5) results in

$$a_x = \dot{u} - rv + qw + (-r^2-q^2)x_s + (-\dot{r}+pq)y_s + (\dot{q}+pr)z_s + g\sin\theta \qquad (5.7\text{-}6)$$

$$a_y = \dot{v} + ru - pw + (r^2+pq)x_s + (-r^2-p^2)y_s + (-\dot{p}+qr)z_s - g\sin\phi\cos\theta \qquad (5.7\text{-}7)$$

$$a_z = \dot{w} - qu + pv + (-\dot{q}+pr)x_s + (p+qr)y_s + (-\dot{p}^2-\dot{q}^2)z_s - g\cos\phi\cos\theta \qquad (5.7\text{-}8)$$

where the subscript "T" is implied, and

$$\Delta\underline{x}_B = \begin{bmatrix} x_s \\ y_s \\ z_s \end{bmatrix} = \begin{bmatrix} .8333\ \text{ft} \\ 0.0 \\ -1.66\ \text{ft} \end{bmatrix} \qquad (5.7\text{-}9)$$

The values in Eq. (5.7-9) were obtained from Table 5.7-1. The expressions for a_x, a_y, and a_z above can be simplified by assuming that $\dot{p}$, $\dot{q}$, and $\dot{r}$ small, which is a reasonable assumption in transport aircraft. It can be assumed that current values of u, v, and w are not available at the time the accelerometer outputs are measured, as they are estimated quantities. An approximation can be made, however, by using the previous estimates of total u, v, and w as in the following equations:

$$\dot{u}_k = a_x + \hat{r}_k\hat{v}_{k-1} - \hat{q}_k\hat{w}_{k-1} + (\hat{r}_k^2+\hat{q}_k^2)x_s - (\hat{p}_k\hat{r}_k)z_s - g\sin\hat{\theta}_k \qquad (5.7\text{-}10)$$

$$\dot{v}_k \simeq a_y - \hat{r}_k\hat{u}_{k-1} + \hat{p}_k\hat{w}_{k-1} - (\hat{r}_k^2+\hat{p}_k\hat{q}_k)x_s - (\hat{q}_k\hat{r}_k)z_s + g\sin\hat{\phi}_k\cos\hat{\theta}_k \qquad (5.7\text{-}11)$$

$$\dot{w}_k \simeq a_z + \hat{q}_k\hat{u}_{k-1} - \hat{p}_k\hat{v}_{k-1} - (\hat{p}_k\hat{r}_k)x_s + g\cos\hat{\phi}_k\cos\hat{\theta}_k \qquad (5.7\text{-}12)$$

Equations (5.7-10) through (5.7-12) can be implemented in the computer to provide corrected body acceleration measurements.

The barometric altimeter, corrected for ambient pressure, provides a measurement of height above sea level and is used in the next section in estimating w.

The airspeed indicator provides a value of true airspeed only at sea level, since it is actually a measurement of dynamic pressure. The airspeed indicator is sensitive to angle of attack and sideslip angle through installation-dependent factors. In general, the assumption can be made that

$$u_{IAS} \simeq \left(\frac{\rho_{SL}}{\rho}\right)^{\frac{1}{2}} IAS \qquad (5.7\text{-}14)$$

where ρ is the ambient air density and ρ_{SL} is its sea-level value. The measured value of u_{IAS} can be combined with $\dot{u}$ (Eq. (5.7-10)) to give an estimate for $\hat{u}$, as shown in the next section. The total velocity, V, can be estimated as

$$\hat{V} = \sqrt{\hat{u}^2+\hat{v}^2+\hat{w}^2} \qquad (5.7\text{-}15)$$

The sensors listed in Table 5.7-1 allow the following total measurement vector to be formed:

$$\underline{z}_T^T = [\dot{u}\ \dot{v}\ \dot{w}\ h\ u\ \theta\ \phi\ \psi\ p\ q\ r]_T \qquad (5.7\text{-}16)$$

The associated perturbation measurement vector is obtained by subtracting the related primary and secondary commands as illustrated in Fig. 2.4-3. Another measurement which could be useful is sideslip angle, β. The β measurement would aid in estimating v, and is used in the CH-47B SAS (Ref. 18). The next section suggests that a β sensor could be put to good use.

5.7.2 Application of Kalman Filter Design

The purpose of this section is to show how the available measurements can be processed to provide necessary control information. The state estimation problem could be solved by using a single, full-order Kalman filter of the form illustrated by Fig. 4.5-1. Various simplifications can be made, however, since there are a number of sensors available, and the filter can be partitioned.

The first partition involves estimating the Euler angles and angular rates. The gyro output have reasonably low additive measurement noise, and Eq. (4.5-11) indicates that past values of these states contribute little to their present values. The process equation for each angular state can be approximated as a random walk process (Eq. (4.5-54)). This allows the output of each gyro to be filtered by a low-pass Kalman filter (Section 4.5.4). As an example, the filter equation for roll rate becomes, using Eq. (4.5-55) and (4.5-60),

$$\hat{p}_k = \hat{p}_{k-1} + \frac{2}{1+\sqrt{1+\left(\frac{2\sigma_v}{\sigma_\omega}\right)^2}} \left[p_{g_k} - \hat{p}_{k-1}\right] \qquad (5.7\text{-}17)$$

The variable p_g stands for the gyro perturbation output (i.e., the secondary command is subtracted from the measured value), σ_ν represents the variance of the measurement noise, and σ_ω represents the variance of the process noise. The larger the ratio $(\sigma_\nu/\sigma_\omega)$, the more lag the filter introduces in estimating the state.

The perturbation variables u and w can be estimated separately using complementary filters. There are two measurements which are available to estimate u: u_{IAS} and $\dot{u}_a$. These velocity and acceleration measurements enable the complementary filter, Eq. (4.5-40), to be employed. The filter for estimating axial velocity is

$$\hat{u}_{k+1} = \hat{u}_k + \Delta t \dot{u}_{a_k} + \Delta t \frac{\sigma_\omega}{\sigma_\nu} \left(u_{IAS_k} - \hat{u}_k \right) \qquad (5.7\text{-}18)$$

The two measurements available for determining normal velocity are altitude, z_p, and $\dot{w}_a$. This position and acceleration measurement enable the complementary filter of Eq. (4.5-52) to be used, resulting in

$$\begin{bmatrix} \hat{h} \\ \hat{w} \end{bmatrix}_{k+1} = \begin{bmatrix} 1 & \Delta t \\ 0 & 1 \end{bmatrix} \begin{bmatrix} \hat{h} \\ \hat{w} \end{bmatrix}_k + \begin{bmatrix} \Delta t^2/2 \\ \Delta t \end{bmatrix} \dot{w}_{a_k}$$

$$+ \begin{bmatrix} \Delta t \sqrt{\frac{2\sigma_\omega}{\sigma_\nu}} + \frac{\Delta t^2 \sigma_\omega}{2\sigma_\nu} \\ \Delta t \frac{\sigma_\omega}{\sigma_\nu} \end{bmatrix} (z_{p_k} - \hat{h}_k) \qquad (5.7\text{-}19)$$

The final variable to be estimated is the lateral velocity, v. Information from the lateral accelerometer can be blended with other measurements to form the v estimate. A

complementary filter could be formed if either sideslip angle or navigational cross-track information is available. In lieu of these measurements, a partitioned, reduced-order Kalman filter can be used; this filter has the same form presented in Section 4.6.

5.7.3 Kalman Filter Gains

The estimators in Section 5.7 use various underlying assumptions in order to arrive at their algorithms. Some of the assumptions can be demonstrated using examples of full-order Kalman filters. The first example shows a filter design based on measurements of all the aircraft states (u, v, w, p, q, r, θ, ϕ, and ψ) for the VALT Research Aircraft. The second example provides filter gains with the assumption that v is not measured. The third filter design includes a $\dot{v}$ measurement. The purpose of the last two examples is to indicate the need for a complex filter for estimating v if it is not measured directly (i.e., by means of a sideslip indicator).

The first example is shown in Table 5.7-2, which is a full-order Kalman gain matrix (Eq. (4.5-18)) at the flight condition, V_x = 160 kt, V_z = 0.0. The observation matrix for this case is

$$H = I \tag{5.7-20}$$

i.e., all the states are assumed measured. The discrete plant noise covariance matrix for determining the Kalman filter is

$$\Upsilon = \underline{0}^T I \tag{5.7-21}$$

where the diagonal components of Υ are derived from a vector of assumed standard deviations:

TABLE 5.7-2

DISCRETE KALMAN FILTER GAINS WITH ALL STATES MEASURED.
FLIGHT CONDITION: V_X = 160 KNOTS, V_Z = 0.0

	u	v	w	p	q	r	θ	φ	ψ
$\hat{u}$	.7794	-.000096	-.00264	.02923	1.522	-.00412	-2.668	.000995	.00003
$\hat{v}$	.000143	.7738	.0026	-1.648	.054	-21.35	.00167	2.64	-.0294
$\hat{w}$	.00174	.00134	.76047	.11433	21.27	-.127	.1993	.00593	-.00373
$\hat{p}$	.000064	-.000721	.000243	.863	.0116	.00256	-.000072	-.001	.00002
$\hat{q}$	-.00001	.000079	.00108	.000675	.9047	-.000885	.000217	.000142	-.000008
$\hat{r}$	0.0	-.000134	-.000209	-.01084	.00398	.94	-.000033	-.00029	.000257
$\hat{\theta}$	.000000	.000003	.000046	.000031	.0782	-.000022	.998	.000004	0.0
$\hat{\phi}$	.000003	.000031	.000011	.0754	.000437	-.00519	-.000002	.9986	-.000001
$\hat{\psi}$	0.0	-.000006	-.000009	-.000463	.000209	.0787	-.000001	-.000008	.978

TABLE 5.7-3

DISCRETE KALMAN FILTER GAINS WITH V NOT MEASURED.
FLIGHT CONDITION: V_X = 160 KNOTS, V_Z = 0.0

	u	w	p	q	r	θ	φ	ψ
$\hat{u}$	0.779584	-0.002570	0.035892	1.468305	-0.004267	-2.562004	0.001260	0.000083
$\hat{v}$	0.000085	0.011003	-60.986053	6.860841	-10.499473	0.282085	0.052945	-0.452053
$\hat{w}$	0.001676	0.760882	0.018497	20.479050	-0.129494	0.190925	0.001491	-0.004236
$\hat{p}$	0.000061	0.000224	0.923940	0.004712	0.002521	-0.000329	0.001571	0.000417
$\hat{q}$	-0.000010	0.001041	-0.005268	0.907651	-0.000825	0.000228	-0.000115	-0.000050
$\hat{r}$	0.000000	-0.000202	-0.000681	0.002829	0.940479	-0.000076	0.000184	0.000328
$\hat{\theta}$	-0.000000	0.000043	-0.000218	0.075227	-0.000034	0.996620	-0.000007	-0.000002
$\hat{\phi}$	0.000003	0.000010	0.074973	0.000127	-0.004830	-0.000013	0.978822	0.000016
$\hat{\psi}$	0.000000	-0.000008	-0.000010	0.000149	0.075590	-0.000003	0.000010	0.998637

$$\sqrt{\underline{\theta}^T} = [7.07, 7.07, 7.07, .0872, .0872, .0872, .0872, .0872, .0872] \quad (5.7\text{-}22)$$

The observation noise covariance matrix is

$$\Xi = \underline{\xi}^T \mathbf{I} \quad (5.7\text{-}23)$$

The diagonal elements of Ξ are derived from a vector of measurement noise standard deviations:

$$\sqrt{\underline{\xi}^T} = [4.2, 4.2, 4.2, .0216, .013, .0216, .00332, .013, .00332] \quad (5.7\text{-}24)$$

The values of the observation noise covariance matrix are obtained for the sensors in Table 5.7-1 by using current standards for aircraft instrumentation. The process noise covariance matrix, which represents expected flight motion, is larger than the observation noise covariance matrix. This causes the filter to rely more on the measurements for an estimate than on the updates, particularly for the angles and angular rates. This can be seen in Table 5.7-2, as the elements along the diagonal of the matrix are close to one.

The table shows why the low-pass filters can give adequate results even though they are very simple. For example, examine the $\hat{q}$ row in the gain matrix. One diagonal element (the fifth from the left) is nearly one, and the other gains are much smaller. The off-diagonal gains contribute negligibly to the estimate of q. The predominant gain, $k_{\hat{q}q} = 0.9047$, is close to the gain that would have been obtained if a low-pass filter is designed. If it is claimed that this is the Kalman gain for the low-pass filter, the required σ_ω/σ_ν ratio for the low-pass filter would be 3.8

(using Eq. (4.5-60)). This agrees well with the ratio used in the full-order filter, which is 0.0872/0.0216 ≈ 4.0.

The table also shows why the complementary filter given by Eq. (5.7-18) can give adequate results. The angle, ψ, is obtained by integrating r in the system F matrix. The only two Kalman gains in Table 5.7-2 which contribute significantly in estimating $\hat{\psi}$ are $k_{\hat{\psi}r}$ (= 0.0787) and $k_{\hat{\psi}\psi}$ (=0.978). Therefore, the estimate can be closely approximated by a complementary filter for a variable and its derivative, as demonstrated by Application 1 in Section 4.5.3.

The Kalman gains for estimating the velocity states show considerably more crossfeed among the states than the Kalman gains for estimating the angles. The factor that stands out, however, is the decoupling of longitudinal and lateral-directional cross gains. As an example, the significant states in estimating u are u, q, and θ, while the other states contribute little. The same decoupling feature holds true for v and w.

The next Table 5.7-3 shows a (9x8) Kalman filter gain matrix, in which the v state is assumed to be unmeasured. The individual noise covariance values are the same as in Eq. (5.7-22) and (5.7-24). The primary change occurs in the second row of the Kalman gain matrix. This filter would need a good update equation in order to operate effectively because of the lack of a measurement for v. Comparing this matrix to the previous one, it can be seen that the filter makes up for the absence of lateral velocity information by placing increased emphasis on ψ, p, q, and θ measurements, a surprising result which indicates the importance of considering longitudinal/lateral-directional coupling at high forward speed.

TABLE 5.7-4

DISCRETE KALMAN FILTER GAINS WITH $\dot{v}$ MEASURED.
FLIGHT CONDITION: V_x = 160 KNOTS, V_z = 0.0

	u	$\dot{v}$	w	p	q	r	θ	φ	ψ
$\hat{u}$	.779	.00079	-.00264	.04559	1.52	.199	-2.66	-.024	.00022
$\hat{v}$	.00236	-.7703	.00985	-39.92	3.42	-232.0	.115	26.38	-1.14
$\hat{w}$	.00174	0.00024	.7605	.0663	21.27	-.21	.20	.0113	-.0057
$\hat{p}$	.00006	.00064	.00024	.901	.0084	.179	-.00018	-.0205	.0011
$\hat{q}$	-.00001	-.000079	.0011	-.00327	.9051	-.022	.00025	.0025	-.000124
$\hat{r}$	.000004	-.00188	-.0002	-.0337	.0043	.466	-.0001	.0608	.000706
$\hat{\theta}$	0.0	0.000003	.000046	-.000139	.078	-.00093	.9986	.0001	-.000005
$\hat{\phi}$	.000003	.000039	.000011	.0771	.00029	.0053	-.000006	.9973	.000096
$\hat{\psi}$	0.0	-.000163	-.000009	-.0026	.00025	.0377	-.000006	.0052	.978

The third example of a Kalman filter gain matrix is given by Table 5.7-4 where instead of measuring v, lateral acceleration ($\dot{v}$) is measured. The change in the H matrix given by Eq. (5.7-20) would be that the second row in H is the second row of the system F matrix (which is equal to $\dot{v}$), where the control effect on $\dot{v}$ is considered to be observation noise. Interestingly, the $\dot{v}$ measurement does not decouple the system in the same way that the v measurement did. The v measurement gain has a negative sign, a further indication that system dynamics are important in this estimator. Substantial differences from the previous cases include the increased magnitude of the yaw rate gain and the large gain on roll angle.

A last comparison that can be made between the three tables is the steady-state variance of the estimation error for the v state before the error covariance extrapolation. For the case where v is assumed measured (Table 5.7-2), the estimate variance is 3.7 fps. The variance of the error for a measured quantity should always be less than the observation noise, as it is in this case. When only v is measured (Table 5.7-4), the variance increases to 14.5 fps. Finally, when there is no v measurement as in Table 5.7-3, the variance increases to 35 fps, indicating a poor estimate, as expected.

5.8 SCHEDULED GAINS AND TRIM SETTINGS

The open-loop explicit-adaptive scheme requires that the various gains, trim settings, etc., be scheduled. The correlation coefficient tables and the mean-standard deviation tables of Section 4.4.1 are used on all the available independent variables, resulting in the field of

independent variables being narrowed down to u, w, and V^2. These three are available for simple, polynomial, and multiple regressions and are analogous to using airspeed, angle of attack, and dynamic pressure as independent variables. Table 5.8-1 shows the values of u, w, and V^2 for the nineteen flight conditions chosen in Section 5.3.

The gain and trim schedules for the VALT Research Aircraft are presented for five applications:

- Velocity-Command PII Controller
- Attitude-Command PI Controller
- Static Trim for $\dot{\psi} = 0.0$
- Static Trim for $\dot{\psi} = 0.5$ rad/sec
- F for Linear Dynamic Trim

Velocity-Command PII Controller - Tables 5.8-2 and 5.8-3 show the correlation coefficients obtained for the control gains of the Velocity-Command PII Controller. Table 5.8-2 presents the correlation coefficients for the feedback gains on the perturbation states of the VALT Research Aircraft. Recall that perfect correlation is indicated by a coefficient of 1.0, while a coefficient of zero indicates no correlation. Table 5.8-3 presents the cross-gain correlation coefficients between the controls and presents the correlation coefficients for the gains on the integrator states. An explanation of each block is shown in Table 5.8-2. A blank box indicates that the gain is judged to be constant and does not have to be scheduled. Sixty-six percent of the gains are either judged constant or have a correlation with the chosen flight conditions greater than 0.9. Eighty-six percent have correlations greater than 0.8.

The criterion for deciding which variables should be included in each regression is based on how much

TABLE 5.8-1

FLIGHT CONDITIONS FOR POINT DESIGN: u, w, V^2

V_x, kt	V_z, ft/min	u, fps	w, fps	V^2, $(fps)^2$
160.	0.0	269.65	-17.71	73024.
120.	0.0	202.67	.35	41075.
120.	1000.	202.48	18.8	41350.
120.	-1500.	202.24	-28.27	41700.
120.	2000.	201.72	38.67	42190.
80.	-1000.	135.49	-13.31	18530.
80.	0.0	135.04	4.42	18250.
80.	500.	134.72	13.23	18320.
80.	1000.	134.35	22.01	18530.
60.	0.0	101.17	5.84	10269.
60.	500.	100.65	14.43	10338.
40.	-500.	68.0	-3.16	4633.
40.	0.0	67.35	5.27	4564.
40.	500.	66.67	13.7	4633.
20.	-500.	34.42	-5.09	1210.
20.	0.0	33.62	3.22	1141.
20.	500.	32.82	11.54	1210.
0.0	0.0	0.0	0.0	0.0
-20.	0.0	33.47	-4.56	1141.

TABLE 5.8-2

VELOCITY-COMMAND PII CONTROLLER CORRELATION COEFFICIENTS
FOR VALT RESEARCH AIRCRAFT STATES

$\Delta t N_1$

u	v	w	p	q	r	θ	φ	ψ	CONTROLS
V^2 .943	u w V^2 .918	u V^2 .98	u w V^2 .582	u V^2 .989	u w V^2 .765	u w V^2 .955	u w V^2 .566	u w V^2 .897	δ_B
u w V^2 .964	u w V^2 .929	u V^2 .99	u w V^2 .892	u V^2 .987	u w V^2 .67	u w V^2 .961	u w V^2 .889	u w V^2 .912	δ_C
		u w V^2 .951	u V^2 .432 *	u V^2 .967	u w V^2 .946	u w V^2 .855	u w V^2 .887	V^2 .84	δ_S
u w V^2 .909	u w V^2 .760 *	u w V^2 .889		u w V^2 .978	u w V^2 .963	u w V^2 .904	u w V^2 .956 *	u V^2 .924	δ_R

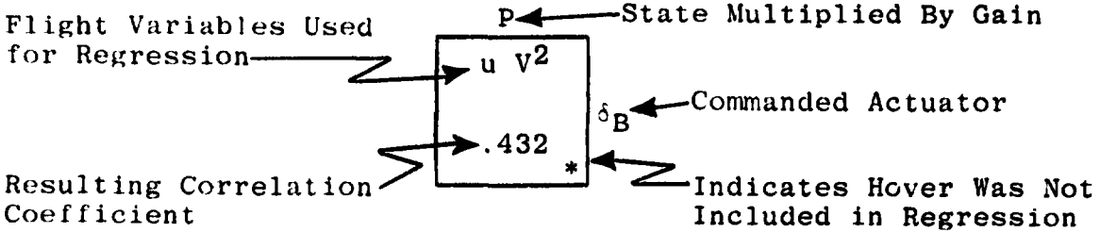

TABLE 5.8-3

VELOCITY-COMMAND PII CONTROLLER CORRELATION COEFFICIENTS

CONTROLS, $\Delta t K_2$				INTEGRATOR STATES, $\Delta t K_3$				
δ_B	δ_C	δ_S	δ_R	y_{V_x}	y_{V_y}	y_{V_z}	y_ψ	
u .964	u V^2 .983	u w V^2 .543	u w V^2 .854	u V^2 .966	u w V^2 .6317 •	u V^2 .993	u V^2 .115	δ_B
u V^2 .983	u V^2 .952	u w V^2 .925	u w V^2 .873	u V^2 .963	u w V^2 .942	u V^2 .93	u w V^2 .908	δ_C
u w V^2 .56 •	u w V^2 .927		u w V^2 .939 •	u w V^2 .832		u .815	u V^2 .918	δ_S
u w V^2 .896	u w V^2 .883 •	u w V^2 .935 •		u w V^2 .921				δ_R

CONTROLS

improvement is obtained by using different combinations, starting from the variable which gives the best simple regression. The fewer number of variables used per gain, the less the computer storage and execution time. Various patterns can be observed in the correlations. For instance, δ_B, which primarily controls pitch, has high correlated gains on u, w, q and θ, while the correlation or cross-coupling gains are lower. The pattern carries over into the other gains for the δ_B command; δ_B, δ_C, y_{V_X}, y_{V_Z} have high correlation, while δ_S, δ_R, y_{V_y} have moderate correlation. Another observed pattern is that the gains at hover lowered the correlation coefficient of the overall regression in some cases. Those regressions which do not use hover as a flight condition are designated with an asterisk.

Tables 5.8-4 and 5 demonstrate the correlation coefficients obtained for the control gains of the attitude-command PI Controller. Table 5.8-4 presents the feedback gains on the states, and Table 5.8-5 lists the control gains for $\Delta t\ N_4$ and $\Delta t\ L$. Fifty-seven percent of the gains have correlation greater than 0.9. Eighty-three percent have correlation greater than 0.8. Four gains have correlation less than 0.5. The first pattern to be noticed is in the ΔtL and ΔtN_4 gains (See Eq. (3.5-56)). Gains which multiply similar integrator error states have similar correlation. The pattern of longitudinal/lateral-directional crossfeeds having lower correlations is not true for this controller. For instance, the (ϕ,δ_S) gain in Table 5.8-2 and Table 5.8-1 show great differences as to which gain in the angle group has the best correlation. Only the gains on ψ were judged constant for the PI controller (and are, in fact, zero); control is turned over completely to the feedforward part of the controller for this variable.

TABLE 5.8-4

ATTITUDE-COMMAND PI CONTROLLER CORRELATION COEFFICIENTS FOR VALT RESEARCH AIRCRAFT STATES

	ΔtN_5								
	u	v	ω	p	q	r	∩	ϕ	ψ
δ_B	$u\ w\ V^2$ .96	$u\ w\ V^2$ .895	$u\ w\ V^2$ .896	$u\ w\ V^2$ .753	$u\ w\ V^2$ .816	$u\ w\ V^2$ .931	$u\ V^2$ .841	$u\ w\ V^2$ .7	
δ_C	$u\ w\ V^2$ .987	$u\ w\ V^2$ 9116 *	$u\ w\ V^2$ .91	$u\ V^2$ .973	$u\ V^2$ .952	$u\ V^2$ .819	$u\ V^2$ .975	$u\ w\ V^2$ .644	
δ_S	$u\ w\ V^2$ 90	$u\ w\ V^2$ .946 *	$u\ w\ V^2$ .631	$u\ w\ V^2$ .971	$u\ V^2$ .983	$u\ w\ V^2$ .81	$u\ V^2$ .955	$u\ V^2$ .42	
δ_R	$u\ w\ V^2$ .473	$u\ w\ V^2$ .582 *	$u\ w\ V^2$ .879	$u\ w\ V^2$ .846	$u\ w\ V^2$ .98	$u\ w\ V^2$ .914	$u\ w\ V^2$ .196	$u\ V^2$ .419	

CONTROLS

TABLE 5.8-5

ATTITUDE-COMMAND PI CONTROLLER
CORRELATION COEFFICIENTS

ΔtL				ΔtN_q				
y_θ	y_ϕ	y_ψ	y_{V_z}	y_θ	y_ϕ	y_ψ	y_{V_z}	
$u\,w\,V^2$ .865	$u\,w\,V^2$ .653	$u\,w\,V^2$ .92	$u\,V^2$ .933	$u\,w\,V^2$ .867	$u\,w\,V^2$ .664	$u\,w\,V^2$ .922	$u\,V^2$ .9255	δ_B
$u\,V^2$ .918	$u\,V^2$ .974	$u\,V^2$ .807	$u\,V^2$ .959	$u\,V^2$ .917	$u\,V^2$ .974	$u\,V^2$ .807	$u\,V^2$ .957	δ_C
$u\,V^2$ .983	$u\,w\,V^2$ .977	$u\,w\,V^2$ .816	$u\,V^2$ .972	$u\,V^2$ .983	$u\,w\,V^2$ .976	$u\,w\,V^2$ .818	$u\,V^2$ .972	δ_S
$u\,w\,V^2$ .981	$u\,w\,V^2$ .843	$u\,w\,V^2$ .929	$u\,w\,V^2$ .817	$u\,w\,V^2$ .981	$u\,w\,V^2$ .844	$u\,w\,V^2$ .928	$u\,w\,V^2$ .816	δ_R

CONTROLS

Controller Gain Regressions - At this point the variables which best correlate with the control gains have been specified. The next phase is to determine the regression coefficients. These are shown in Tables 5.8-6 through 5.8-9 for the PII control law and in Tables 5.8-10 through 5.8-13 for the PI control law. The maximum and minimum values of the true gains for the nineteen flight conditions also are shown. The intercept is the value of the gain at hover produced by the regression.

As an example of the computation involved for determining a gain, consider the pitch-rate differential collective gain for the velocity-command controller. Using the values for the regression coefficients for q in Table 5.8-6 results in the following gain schedule:

$$g = (63.38\text{x}10^{-5})V^2 + (39.3\text{x}10^{-3})u + 14.61 \qquad (5.8\text{-}1)$$

Table 5.8-2 indicates high correlation for this gain schedule, and the value of g is very close to the real value of the gain at all flight conditions.

The gains for the controllers display certain patterns which aid in understanding the gain values and correlation coefficient values. For the PII control law, the most obvious pattern concerns the difference between the longitudinal/lateral cross-gains and the other gains. For instance, in Table 5.8-6 the maximum values of the cross gain (v,p,r,ϕ,ψ) have much smaller values than the other gains (u,w,q,θ). This kind of pattern can be observed in the other tables for the PII controller. In addition, by comparing the correlation coefficients in Table 5.8-2 with the important gains in Table 5.8-6, the large (important) gains have high correlation while the smaller gains have moderate correlation.

Gains for the PI control law also follow discernible trends. Gains between ΔtL and ΔtN_4 which multiply the same type of error variable tend to be opposites of each other. This is a consequence of the weighting on $\dot{\underline{u}}$ in the cost function. The regression coefficients have to be specified to many significant digits because these gains are nearly equal and of opposite sign. The other pattern for the PI control law is that the feedback gains on the states are much smaller than the ΔtL and ΔtN_4 gains. To compare gain values between the PI and PII controllers, the PI gains are already multiplied by Δt while the PII gains are not. The PII regression coefficients are multiplied by Δt in a computer implementation.

Static Trim, $\dot{\psi} = 0.0$ - Maximum and minimum values of the four control positions are given in Section 5.6.1.

Table 5.8-14 lists the trim values of the control positions for the flight conditions chosen in Section 5.4. The relative meaning of the numbers can be explained by taking δ_C as an example. The larger the δ_C position is, the greater the lifting force of the rotors. The largest value of δ_C occurs at V_z = -1500 ft/min, the maximum vertical velocity for the data shown. The values of the control position are scheduled against the u, w, and V^2 flight conditons of Table 5.8-1. In addition, the trim values of θ and ϕ also are scheduled for $\dot{\psi}$ = 0.0. The correlation and regression coefficients are shown in Table 5.8-16. The static trim values of p, q, and r are zero if $\dot{\psi}$ = 0.0. The correlation coefficients for static trim are good, and except for δ_B are greater than 0.9.

Static Trim, $\dot{\psi}$ = 0.5 rad/sec - Table 5.8-16 shows the trim variables and angular rates for the turn rate $\dot{\psi}$ = .05 rad/sec, with the VALT Research Aircraft is in a coordinated turn. In general, it can be concluded that static trim correlates well with flight conditions.

Dynamic Trim - As stated in Section 4.3.2, static trim settings can be aided by linear dynamic trim computations. The equation for dynamic trim (Eq. (4.3-15)) requires the F_2 matrix and the inverse of G_μ. Table 5.8-17 details the correlation coefficients for the upper left 6x6 part of the F matrix, F_2, for the VALT Reserach Aircraft.

5.9 EXAMPLES OF SYSTEM RESPONSE

The previous sections of this chapter detailed the procedure of designing a digital control law using open-loop

TABLE 5.8-6

VELOCITY-COMMAND PII CONTROLLER GAIN REGRESSION
FOR THE δ_B CONTROLLER

K_1

	u	v	w	p	q	r	θ	φ	ψ	
Maximum	.0826	.0017	.941	.1626	71.5	.21	33.31	.298	.319	
Minimum	-.6155	-.006	-.23	.0728	14.01	-.08	-1.39	-.315	-.12	
V^2	.878	.01884	-1.29	.229	63.38	.502	-53.2	-1.025	.741	$\times 10^{-5}$
u		.0295	6.59	-.386	39.3	-2.13	22.37	3.22	-3.11	$\times 10^{-3}$
w		-.85		73.6		94.4	-2857.	-15.9	-3.64	$\times 10^{-4}$
Intercept	-.579	-.00396	.0111	.1097	14.61	.208	28.74	-.213	.2728	

K_2 K_3

	δ_B	δ_C	δ_S	δ_R	y_{V_x}	y_{V_y}	y_{V_z}	y_ψ	
Maximum	6.03	1.735	.0414	.128	.01	.00384	.752	.2036	
Minimum	3.0	-.714	-.0229	-.0359	-.174	-.00365	-.12	-.038	
V^2		7.515	.0481	.04346	.176	-.0135	-1.094	.3973	$\times 10^{-5}$
u	13.9	-13.45	-.09135	-.194	.2145	.034	5.635	-1.813	$\times 10^{-3}$
w			7.069	5.13		-.106			$\times 10^{-4}$
Intercept	2.971	-.1247	.01145	.01141	-.1746	-.00074	.0301	.1867	

TABLE 5 8-7

VELOCITY-COMMAND PII CONTROLLER GAIN REGRESSION FOR THE δ_C CONTROLLER

K_1

	u	v	w	p	q	r	θ	φ	ψ	
Maximum	.165	.045	.109	.5	17.0	.253	54.2	2.07	.319	
Minimum	-.857	-.005	-.871	-.341	-10.19	-.761	-5.5	-.2917	-.12	
v^2	1.279	.0985	.729	2 16	92.93	-2.41	-80.9	4.46	-1.902	$\times 10^{-5}$
u	-5.96	-.149	1.67	-3.67	-188.9	5.12	327.28	-6.69	2.94	$\times 10^{-3}$
w	53.64	-1.3		-1.67		-15.2	-4621.	-32.64	46.5	$\times 10^{-4}$
Intercept	.1025	.00162	-.855	-.0455	-.896	-.1935	-.5037	-.01165	.02385	

K_2 K_3

	δ_B	δ_C	δ_S	δ_R	y_{V_x}	y_{V_y}	y_{V_z}	y_ψ	
Maximum	1.59	3.7	.1284	.01726	.0493	.0154	-.053	.121	
Minimum	-.804	2.02	-0.359	-.103	-.24	-.00214	-.878	-.318	
v^2	7.725	1.99	.362	-.271	.2936	.0038	.65	-1.0	$\times 10^{-5}$
u	-14.5	-11.3	-.564	.482	-1.49	-.0409	1.179	1.6	$\times 10^{-3}$
w			.833	1.54		.0460		14.7	$\times 10^{-4}$
Intercept	-.125	3.68	-.00987	-.00928	-.00402	-.00146	-.846	.0116	

TABLE 5.8-8

VELOCITY-COMMAND PII CONTROLLER GAIN REGRESSION
FOR THE δ_S CONTROLLER

K_1

	u	v	w	p	q	r	θ	φ	ψ	
Maximum	.0159	.478	.033	10.55	2.13	3.053	.379	34.7	2.43	
Minimum	-.00782	.287	-.009	7.94	-.64	.425	-2.79	9.9	.9	
v^2			.071	-4.364	7.832	1.28	-3.11	-1.22	1.604	×10-5
u			-.064	.4126	-12.78	-9.79	2.18	2.44		×10-3
w			.27	-136.8		171.8	171.1	-3666.		×10-4
Intercept	.008	.3857	-.00493	11.12	-.1341	2.65	-.279	20.59	1.22	

K_2 K_3

	δ_B	δ_C	δ_S	δ_R	y_{v_x}	y_{v_y}	y_{v_z}	y_ψ	
Maximum	.0379	.132	3.327	-.0548	.0146	.179	.00085	.919	
Minimum	- 0213	-.0343	2.39	-.1589	-.00218	.171	-.0149	-.457	
v^2	.0679	.366		-.0524	.0286			.37	×10-5
u	-.117	-.562		-.266	-.0387		.05205	.642	×10-3
w	6.46	1.11		-2.71	-.0748				×10-4
Intercept	.011	-.0113	3.068	-.059	.00057	.173	-.01318	.475	

TABLE 5.8-9

VELOCITY-COMMAND PII CONTROLLER GAIN REGRESSION FOR THE δ_R CONTROLLER

	K_1									
	u	v	w	p	q	r	θ	φ	ψ	
Maximum	.0289	.203	.003	-1.21	-.879	16.5	2.36	-1.63	13.2	
Minimum	-.0492	-.083	-.033	-2.23	-2.62	14.14	-2.01	-4.81	11.9	
v^2	-.111	-.0854	.0195		.559		4.53	-1.87	-2.93	$\times 10^{-5}$
u	.0629	.0892	-.1316		4.685		3.71	.14	4.33	$\times 10^{-3}$
w	1.85	1.65	3.8		466.			443.5		$\times 10^{-4}$
Intercept	.0238	-.0468	.00041	-2.01	-2.14	16.03	-1.939	-2.34	13.04	

	K_2				K_3				
	δ_B	δ_C	δ_S	δ_R	y_{v_x}	y_{v_y}	y_{v_z}	y_ψ	
Maximum	.022	.0167	-.0548	2.69	.00796	-.0303	.014	5.106	
Minimum	-.0398	-.109	-.1604	2.52	-.015	-.0139	-.009	4.99	
v^2	.0352	-.278	-.0598		-.0192				$\times 10^{-5}$
u	-.195	.488	-.249		-.0165				$\times 10^{-3}$
w	5.42	1.96	-2.968		.668				$\times 10^{-4}$
Intercept	.0107	-.00853	-.0597	2.55	.00676	-.02047	.00481	5.084	

TABLE 5.8-10

ATTITUDE-COMMAND PI CONTROLLER GAIN REGRESSION
FOR THE δ_B CONTROLLER

	ΔtN_5									
	u	v	w	p	q	r	θ	ϕ	ψ	
Maximum	.000624	.000016	.000202	.141	-16.3	.0887	.325	.0245		
Minimum	-.000485	-.000037	-.000507	-.201	-25.2	-.804	-.931	-.00623		
v^2	.000279	0.000015	-.000133	.06604	-1.26	-.0871	.369	-.00824		$\times 10^{-4}$
u	-.000541	.00004867	.000255	-.1564	2.137	.534	-.736	.02249		$\times 10^{-2}$
w	-.000543	.00006876	.000502	-.2474	5.29	.799		-.02158		$\times 10^{-2}$
Intercept	-.00008	0.0	0.0	-.0438	-18.55	-.822	-.186		0.0	

	ΔtN_4				ΔtL				
	y_θ	y_ϕ	y_ψ	y_{V_z}	y_θ	y_ϕ	y_ψ	y_{V_z}	
Maximum	-181.8	1.138	2.44	.156	300.6098	2.5	7.826	.0123	
Minimum	-299.21997	-2.47	-7.516	-.0129	183.42	-1.17	-2.44	-.1465	
v^2	-18.1	.5649	-1.0558	-.01489	18.17	-.59526	1.0338	.01358	$\times 10^{-4}$
u	25.055	-2.848	5.717	.081157	-25.46	1.41011	-5.746	-.074157	$\times 10^{-2}$
w	60.711	-1.3365	6.6524		-61.282	2.8299	-7.0929		$\times 10^{-2}$
Intercept	-194.93745	-.669	-7.76	.02061	197.11324	.6636	8.0022	-.01979	

TABLE 5.8-11

ATTITUDE-COMMAND PI CONTROLLER GAIN REGRESSION
FOR THE δ_C CONTROLLER

	ΔtN_5									
	u	v	w	p	q	r	θ	φ	ψ	
Maximum	.002339	.000134	.000721	.3168	1.407	1.412	4.315	-.002285		
Minimum	-.000367	-.000112	-.000919	-.6753	-10.19	-.5703	-.191	-.07318		
v^2	0.000191	.000004	.000325	.21136	-1.34	.4728	.51	.01623		$\times 10^{-4}$
u	-0.001416	-.0000424	-.000798	.274	.2864	-.8792	-2.917	.0271		$\times 10^{-2}$
w		-.00010215	.0003486		.5475	-.4119		.0476		$\times 10^{-2}$
Intercept	.00207	.00012	.00019	.2312	-.3975	.1344	3.8	-.03394	0.0	

	ΔtN_4				ΔtL				
	y_θ	y_ϕ	y_ψ	y_{V_z}	y_θ	y_ϕ	y_ψ	y_{V_z}	
Maximum	11.137	3.238	14.11	-.093	76.6	7.06	6.31	.1842	
Minimum	-74.1	-6.97	-6.245	-.2076	-20.89	-3.357	-14.33	.08557	
v^2	-15.79	-2.204	5.225	.00685	16.2	2.245	-5.289	.007215	$\times 10^{-4}$
u	17.018	2.8929	-9.825	.0063814	-18.71	-2.941	9.935	-0.060034	$\times 10^{-2}$
w									$\times 10^{-2}$
Intercept	.67517	2.3729	1.16746	-.20275	3.781	-2.446	-1.17927	.18424	

TABLE 5.8-12

ATTITUDE-COMMAND PI CONTROLLER GAIN REGRESSION
FOR THE δ_S CONTROLLER

	ΔtN_5								
	u	v	w	p	q	r	θ	φ	
Maximum	.000069	.008019	.000016	-11.746	.8417	-3.3939	.1215	.052	
Minimum	0.0	-.00029	-.000047	-14.057	-1.498	-5.64	-.00087	-.1117	
V^2	.000014	-.000052	.000003	.6194	-.6378	-.01	.017	-.000654	$\times 10^{-4}$
u	-.00005227	00.0001	-.00001711	-.9511	1.087	.3021	-.0843	.0324	$\times 10^{-2}$
w	-.00002141	.0000441	.00001898	1.17	-.1529	-2.776		-.0087	$\times 10^{-2}$
Intercept	0.00006	-.00011	0.0	-13.495	.3281	-4.902	.10715	.00415	

	ΔtN_4				ΔtL				
	y_θ	y_ϕ	y_ψ	y_{V_z}	y_θ	y_ϕ	y_ψ	y_{V_z}	
Maximum	9.56	-123.2	-34.165	.0183	20.7	151.63	56.86	.005329	
Minimum	-20.8	-150.1	-56.342	-.00593	-9.543	124.73	34.563	-.01769	
V^2	-7.9875	6.9152	.10573	0.004318	7.986	-6.95	-.001168	-.004109	$\times 10^{-4}$
u	13.4017	-9.822	-5.6804	-0.0040214	-13.466	9.975	5.7758	.0038546	$\times 10^{-2}$
w		13.74	-23.364			-13.722	23.4		$\times 10^{-2}$
Intercept	3.6573	-144.7744	-35.8835	-.00499	-3.5692	146.1612	36.246	.00448	

TABLE 5.8-13

ATTITUDE-COMMAND PI CONTROLLER GAIN REGRESSION
FOR THE δ_R CONTROLLER

ΔtN_5

	u	v	w	p	q	r	θ	φ	ψ	
Maximum	.000047	.026837	.000036	3.19	4.182	-35.916	.0845	.02459		
Minimum	-.000045	-.000084	-.00001	2.4407	-1.693	-28.319	-.0895	-.0186		
v^2	-0.000006	-.000025	.000013	-.2392	-.56	1.79	-.001389	-0.0237		$\times 10^{-4}$
u	0.00000473	.00004954	-.00003151	.575	-.268	-3.575	-.00458	0.09359		$\times 10^{-2}$
w	0.0000188	-.00004337	-.0000186	-.44	-7.31	-4.47	.00516	0.007165		$\times 10^{-2}$
Intercept	.00001	-.00001	.00001	2.797	3.9	-32.61	.01531	-.07945	0.0	

ΔtN_4 ΔtL

	y_θ	y_ϕ	y_ψ	y_{V_z}	y_θ	y_ϕ	y_ψ	y_{V_z}	
Maximum	46.57	34.563	-302.71	0.0	19.0	-27.15	396.41	.02195	
Minimum	18.9	26.944	-393.23	-.022	-46.8	-35.45	305.82	-.000353	
v^2	5.688	-2.6789	20.333	0.001418	5.75	2.6853	-20.745	-0.001459	$\times 10^{-4}$
u	3.5129	6.3473	-38.93	-0.007656	3.485	-6.3819	39.41	0.0075977	$\times 10^{-2}$
w	84.028	-5.4515	-53.096	0.02343	84.295	5.4413	53.092	-0.022396	$\times 10^{-2}$
Intercept	43.35724	30.9595	-357.5947	-.00296	-46.55891	-31.1542	360.2629	.00288	

TABLE 5.8-14

VALUES OF THE CONTROL POSITIONS FOR THE FLIGHT CONDITIONS ($\dot{\psi}$=0.0)

V_x, kt	V_z, ft/min	δ_B, in	δ_C, in	δ_S, in	δ_R, in
160.	0.0	.6826	5.3997	.2111	-.5744
120.	0.0	.2385	3.697	.14548	-.2569
120.	1000.	.03692	2.54	.093079	-.12977
120.	-1500.	.5539	5.4927	.2311	-.52654
120.	2000.	-.1583	1.2963	.032	-.047937
80.	-1000.	-.14407	4.2793	.20728	-.17239
80.	0.0	-.3998	3.1705	.15037	-.051675
80.	500.	-.53026	2.6221	.12292	.000368
80.	1000.	-.66014	2.0766	.09565	.046226
60.	0.0	-.83457	3.2332	.17057	.057614
60.	500.	-1.0332	2.7222	.14572	.11646
40.	500.	-.9222	4.0262	.21861	.081413
40.	0.0	-1.2017	3.5749	.19622	.15071
40.	500.	-1.5439	3.1391	.17677	.23013
20.	500.	-.6885	4.551	.24111	.077484
20.	0.0	-.98058	4.1935	.21948	.11634
20.	500.	-1.1126	3.8648	.20095	.17
0.0	0.0	-.30816	4.6488	.23562	.06542
10.	0.0	.2817	4.2614	.20691	.002694

TABLE 5.8-15

CORRELATION AND REGRESSION COEFFICIENTS FOR δ_B, δ_C, δ_S, δ_R, θ, ϕ STATIC TRIM VALUES, $\dot{\psi}$=0

δ_B, in	δ_C, in	δ_S, in	δ_R, in	θ, deg	ϕ, deg
u w V^2	u w V^2	u w V^2	u w V^2	u w V^2	u w V^2
.8712	.97	.955	.98	.994	.942

TABLE 5.8-15 (Continued)

	δ_B	δ_C	δ_S	δ_R	θ	ϕ	
V^2	4.8137	3.1067	.00236	-.88927	.41906	-.57867	$\times 10^{-5}$
u	-7.0859	-9.441	-.34247	.055997	-34.846	1.6332	$\times 10^{-3}$
w	-1.0486	-6.269	-.3097	.66258	3.452	.6092	$\times 10^{-2}$
Intercept	-.5223	4.345	.2248	.0971	6.562	-.43826	

TABLE 5.8-16

CORRELATION AND REGRESSION COEFFICIENTS FOR
δ_B, δ_C, δ_S, δ_R, θ, ϕ, p, q, r
STATIC TRIM VALUES, $\dot{\psi} = 0.5$ RAD/SEC

	δ_B, in	δ_C, in	δ_S, in	δ_R, in	θ, deg	ϕ, deg	p, rad/sec	q, rad/sec	r, rad/sec	
	u w V^2 .909	u w V^2 .907	u w V^2 .689	u w V^2 .963	u w V^2 .988	u w V^2 .998	u w V^2 .998	u w V^2 .998	u w V^2 .992	
V^2	6.112	.2594	.1102	-1.0503	3.327	4.299	.00286	.00276	-.00825	$\times 10^{-5}$
u	-9.787	-1.4635	-.3623	.6546	-38.77	83.01	.0336729	.07278	.00578	$\times 10^{-3}$
w	-1.57	-6.259	.3056	.957	5.6059	7.7958	-.00489	.006358	-.002265	$\times 10^{-2}$
Intercept	-.505	3.841	.20192	.057	6.446	-.4842	-.00561	-.00037	.04973	

explicit adaption for the VALT Research Aircraft. This section presents examples of system step response that are computed during the design. The responses are obtained for linear-time-invariant system simulations. All of the step responses except the two in Fig. 5.9-1 are simulations of the simplified systems, i.e., the approximations in Section 3.6 are used. The results are obtained using the program DIGADAPT. In each control law, a transformation matrix whose elements depend on the angular orientation of the aircraft (H_B^E) is used. H_B^E is computed for the nominal orientation and not changed in the simulation. H_B^E would be a time-varying matrix in actual implementation.

TABLE 5.8-17

CORRELATION COEFFICIENTS FOR F_2 TO BE USED FOR DYNAMIC TRIM

	u	v	w	p	q	r
u	$u\ V^2$ .845	w^* .718	$u\ w\ V^2$ .972	$u\ V^{2*}$ .802	w .999	$u\ w\ V^{2*}$ .685
v	V^2 .798	$u\ V^{2*}$ .917	$u\ w\ V^2$ .745	w .999	$u\ V^2$ .994	$u\ w\ V^2$ .955
w	$\frac{1}{u}^*\ u\ V^2$ .951 .65	$u\ w\ V^2$ .644	$u\ V^2$ .916	$u\ w\ V^2$ .586	u .999	$u\ w\ V^2$ .762
p	$u\ w\ V^2$ .735	$u\ w\ V^{2*}$ .995	$u\ V^2$ .916	$u\ w\ V^2$ .988	$u\ w\ V^2$ .985	$u\ w\ V^2$ .987
q	$\frac{1}{V^2}^*\ u\ V^2$ .918 .833	$u\ V^2$ .728	$u\ V^2$ .923	$u\ w\ V^{2*}$ .497	$u\ V^2$ .853	$u\ w\ V^2$ .657
r	w^* .73	$\frac{1}{u}^*\ u\ V^2$ .953 .666	$u\ V^2$ .939	$u\ V^2$ .957	$u\ w\ V^2$ .982	$u\ w\ V^2$ .965

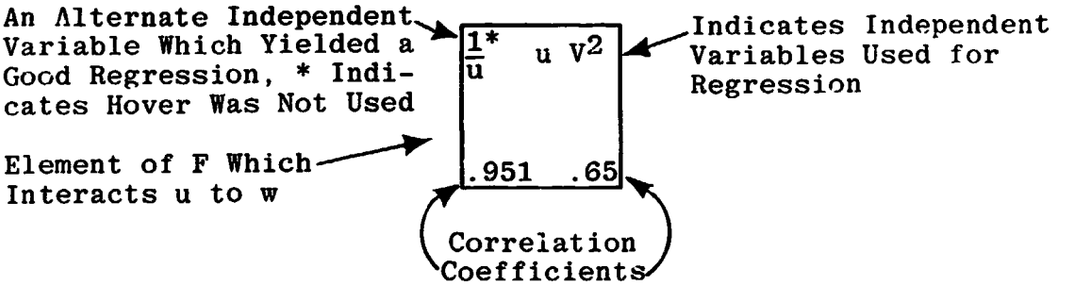

The overall goal of the simulations is to show that the quadratic synthesis control laws meet the step response criteria specified in Section 5.5 for each of the command systems. The velocity-command PII control law simulations are shown in Fig. 5.9-1 to Fig. 5.9-4, and the attitude-command PI control law simulations are shown in Fig. 5.9-5 to Fig. 5.9-7. A comparison between the command-control systems is shown in Fig. 5.9-8. Each of the figures has a second purpose which is detailed in the discussion of the individual simulations. Except for the last figure, each response is obtained by commanding a single component of $\underline{y}_d$, with the other three components commanded to zero.

Figure 5.9-1 - This figure shows the velocity-command PII control law meeting its requirements for a V_z command. One curve is the simplified discrete system response. The continuous response is obtained from the continuous version of the velocity-command PII control law. The discrete system response, which cannot be distinguished in the figure from the continuous system response, is the one that is obtained using the mathematically rigorous discrete system (the second-order assumptions are retained) to simulate a command in V_z. Theory dictates that this rigorously obtained response is the closest to the continuous response which one can achieve using a discrete system. The figure demonstrates the theory and shows the difference in response when the second order simplification is used.

Figure 5.9-2 - This figure shows the velocity-command PII control law meeting its requirements for a command in V_z and for a command in V_x. The responses shown are for the aircraft at hover. The weights in Q were steadily increased until the rise time requirements were exceeded. The requirement is the intersection of the two dotted lines, and the response must be to the left of the intersection as shown.

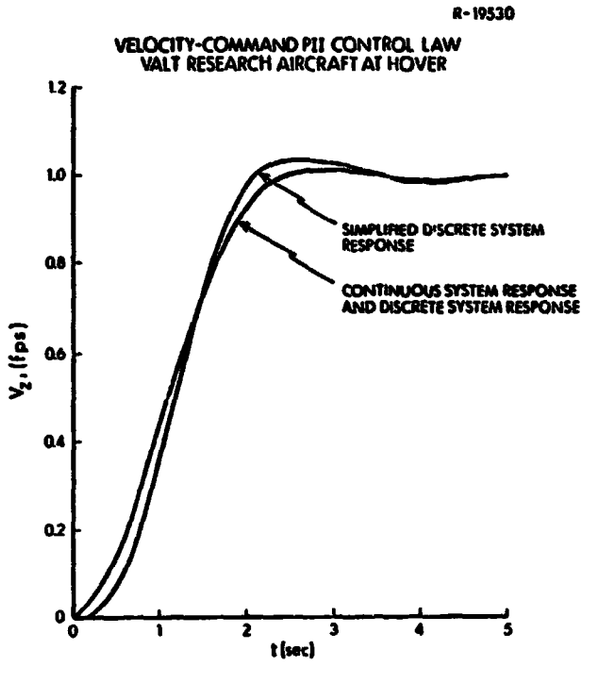

Figure 5.9-1 Comparison Between Continuous, Discrete, and Simplified Discrete Simulations for a Command in V_Z.

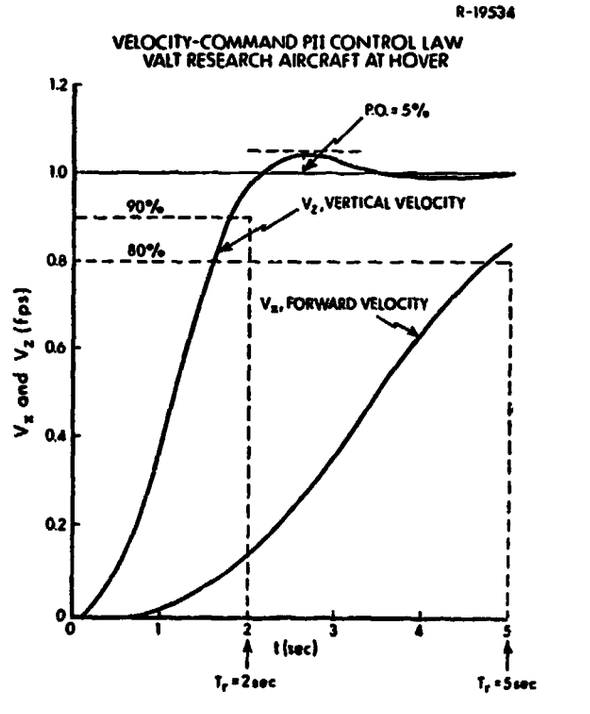

Figure 5.9-2 Simulations for a Command in V_Z and a Command in V_X.

Figure 5.9-3 - This figure shows the velocity-command PII control law meeting its requirements for a command in V_z and a command in V_y for a flight condition different from Fig. 5.9-2 and Fig. 5.9-8. This figures demonstrates the validity of the Q matrix selection procedure detailed in Section 5.6.1. This flight condition is not an extreme point but is an intermediate point in the flight regime chosen for design. The Q weightings are obtained from the interpolated straight line given by Eqs. (5.6-4) through (5.6-6). In this case, the ris times of the responses easily meet the requirements.

Figure 5.9-4 - In Section 5.3, the velocity-command system was paired with the PII control law and the attitude-command system was paired with the PI control law. It was originally intended to use the PII control law for both command systems. As work progressed, it became evident that the PII law did not have sufficient damping to meet the rise time and overshoot requirements of the attitude command system, given the R matrix of Eq. (5.6-2) and weighted variables of the equation below:

$$\underset{\sim}{x}^T = [y_\theta, y_\phi, y_\psi, y_{V_z}, w] \qquad (5.9\text{-}1)$$

This is a result of not allowing large differences in control outputs. The control law is not allowed to pulse the system. The PI law was developed for use in the attitude system because it meets the requirements. There is more damping and there are fewer forward delays in the PI control law. A design for the attitude-command PII control law was developed, however, The following are the maximum criterion values determined in the design. The R matrix values are

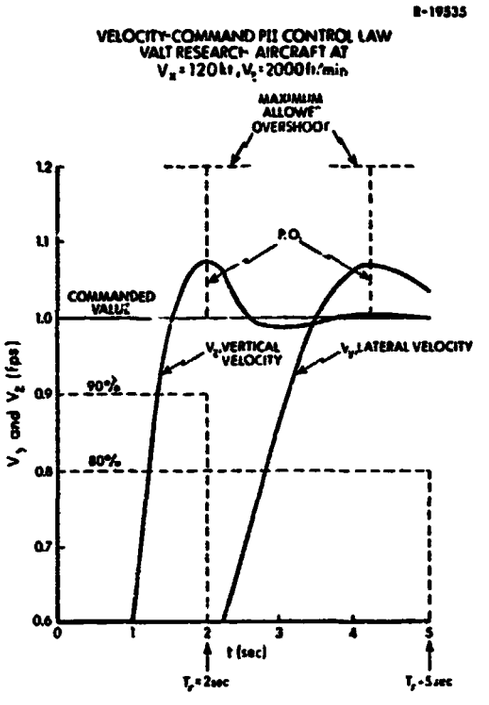

Figure 5.9-3 Simulations for a Command in V_X and a Command in V_Z in Descending Flight

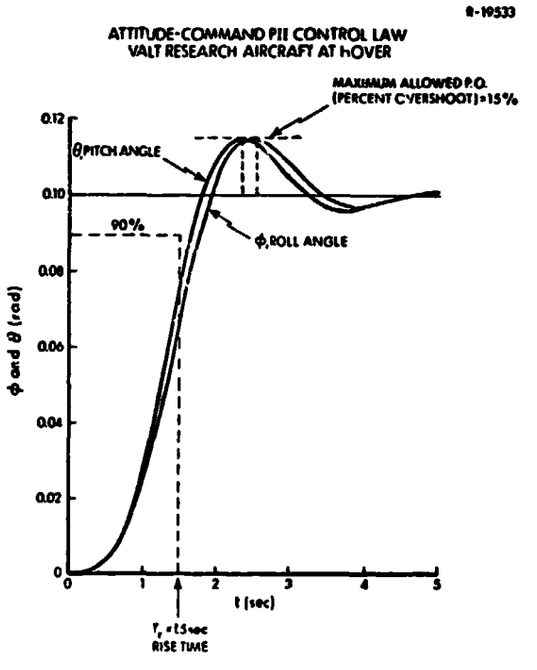

Figure 5.9-4 Simulations for a Command in θ and a Command in ϕ

$$\dot{\delta}_{B_{max}} = 7 \text{ in/sec} \qquad (5.9\text{-}2)$$

$$\dot{\delta}_{C_{max}} = 2 \text{ in/sec} \qquad (5.9\text{-}3)$$

$$\dot{\delta}_{S_{max}} = 3 \text{ in/sec} \qquad (5.9\text{-}4)$$

$$\dot{\delta}_{R_{max}} = 5 \text{ in/sec} \qquad (5.9\text{-}5)$$

and the maximum rtate values for Q are given in Table 5.9-1. The variable, w_1, corresponds to the variable in the following equation:

$$w_{max} = w_1 + \frac{|u_0|}{80} \text{ fps} \qquad (5.9\text{-}6)$$

One can observe the many compromises necessary for this design. The maximum values for R are not all the usual 2 in/sec. Variables that could have been used for damping (θ, ϕ, ψ) are not used because they lower the rise time more than they decrease the overshoot. Figure 5.9-4 shows the attitude-command PII control law step response for separate commands in θ and ϕ. The maximum allowed overshoot is reached before the rise time is satisfied. This behavior also is common for ψ. The V_z command (not shown) met its requirements because the decoupled response feature led to almost the same weights as its cohort in the velocity-command PII system. As seen in the figure, the θ command is closer to meeting its requirements than ϕ, and, in fact, for high forward velocities the requirements are met for θ.

Figure 5.9-5 - This figure shows the attitude-command PI control law meeting its requirements for separate commands in ϕ and V_z. The design methodology for the PI law is to choose Q at each point and not perform an end

TABLE 5.9-1

MAXIMUM DESIGN VALUES FOR ATTITUDE-COMMAND PII CONTROLLER

V_x, kt	V_z, ft/min	$y_1(\theta)$, deg/sec	$y_2(\phi)$, deg/sec	$y_3(\psi)$, deg/sec	$y_4(V_z)$, ft	w_1 fps
-20.0	0.0	2.693	3.151	3.0	2.0	4.0
0.0	0.0	4.0	3.0	3.0	2.0	4.0
20.0	500.0	2.693	3.0	3.0	2.0	4.0
20.0	0.0	4.0	3.0	3.0	2.0	4.0
20.0	-500.0	3.0	3.0	3.0	2.0	4.0
40.0	500.0	2.0	3.151	3.0	2.0	4.0
40.0	0.0	2.292	3.151	3.0	2.0	4.0
40.0	-500.0	2.005	3.151	3.0	2.0	4.0
60.0	500.0	1.1459	3.437	3.0	2.0	4.0
60.0	0.0	1.1459	3.437	3.0	2.0	4.0
80.0	500.0	1.0313	3.437	3.0	2.0	4.0
80.0	0.0	1.0313	3.437	3.0	2.0	4.0
80.0	-1000.0	1.0313	3.437	3.0	2.0	4.0
120.0	0.0	1.0313	3.609	3.0	2.0	4.0
120.0	1000.0	.0859	3.609	3.0	2.0	4.0
120.0	-1500.0	.0916	3.609	3.0	2.0	4.0
120.0	2000.0	.0916	3.609	3.0	2.0	4.0
160.0	0.0	.0916	3.609	3.0	2.0	4.0

point interpolation for the weights on θ, ϕ, and ψ. The figure shows θ just meeting the rise time requirements without exceeding the overshoot, and it shows V_Z, which is weighted as in the PII law, exceeding its requirements slightly.

Figure 5.9-6 - This figure shows the attitude-command PI control law meeting its requirements for separate commands in θ and ϕ at a forward flight condition. The weightings were adjusted until the rise time was achieved. Comparing this figure with Fig. 5.9-5, one can observe that the ϕ response does not vary significantly, while the θ response at the higher forward velocity has more damping. This is one reason that the attitude command PII system was able to meet θ requirements at higher forward velocities.

Figure 5.9-7 - This figure shows the attitude-command PI control law meeting its requirements for a command in ψ. This is compared with a yaw command in the attitude-command PII control law design, explained in the discussion for Fig. 5.9-4. The PII response slightly exceeds the overshoot requirements and does not meet the desired time. Also in the figure are simulations of the corresponding δ_R movements required to yaw the aircraft 0.1 rad (5.73 deg). The PI law allows the controller position to move faster than the PII law. In fact, for this command, the 2 in/sec rate (maximum weighting) is exceeded during the earlier part of the δ_R simulation shown for the PI controller. For the yaw angle command, the VTOL has no preferred yaw angle position. This causes all the other states and controls to return to their original values after the yaw command transients die out. For example, δ_R eventually returns to zero (the original nominal position).

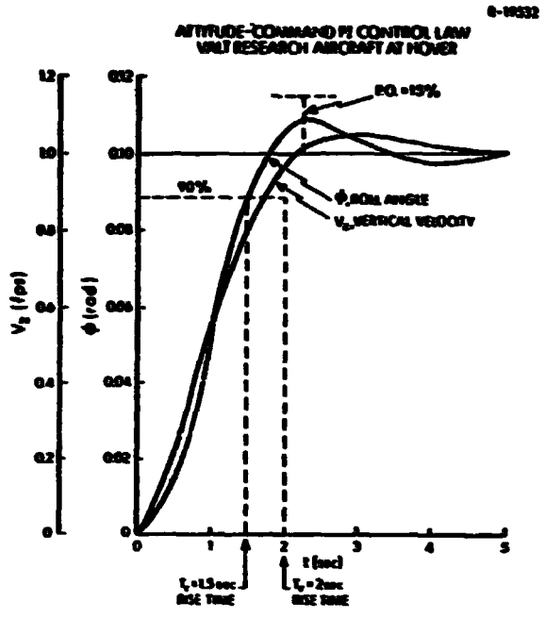

Figure 5.9-5 Simulations for a Command in V_Z and a Command in ϕ

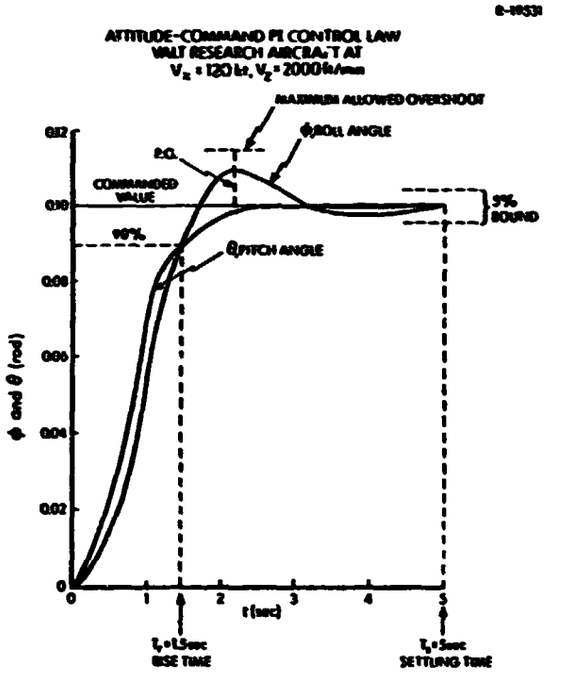

Figure 5.9-6 Simulations for a Command in θ and a Command in ϕ

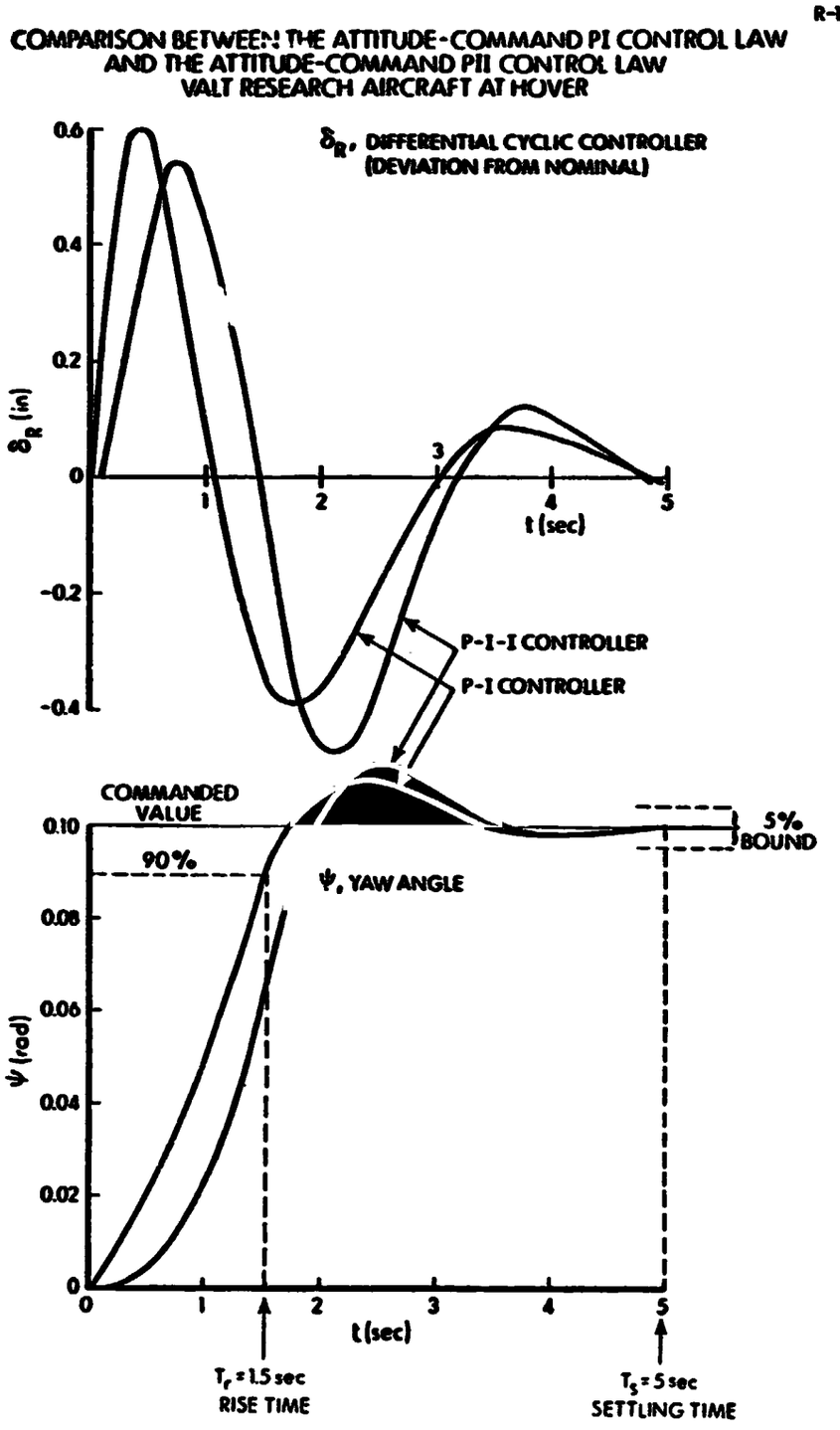

Figure 5.9-7 Simulations for a Command in Yaw

Figure 5.9-8 - This figure shows the velocity command PII control law meeting its requirements for a command in V_y. In the other parts of the figure, the simulations of the corresponding pitch angle transient and δ_S movement also are shown for the PII controller. The steady-state values of θ and ϕ for the PII control law V_y command were observed and recorded. These values then were simultaneously commanded in the attitude-command PI control law. The figure shows the corresponding δ_S, θ, and V_y response which are required to reach the same steady-state values as the PII system. The figure shows that the criteria for the two command systems are different, with the PI law using higher controller rates and larger δ_S deviations to achieve the same result of a V_y = 1 fps increase.

5.10 CHAPTER SUMMARY AND DESIGN PROCEDURE

This chapter has presented applications of several control design techniques to the VALT Research Aircraft and is very successful in doing so. The major developments include the following:

- A sampling time of 12 frames per second was specified based on the worst case of the covariance error propagation and the control structure.
- The transformation matrix was easily found for each command system.
- The velocity-command system was based on the PII control law because the requirements were not stringent and the PII law gives smooth responses.
- The attitude-command system was based on the PI control law because the requirements require fast traisients which the PI law can achieve more easily than the PII law.

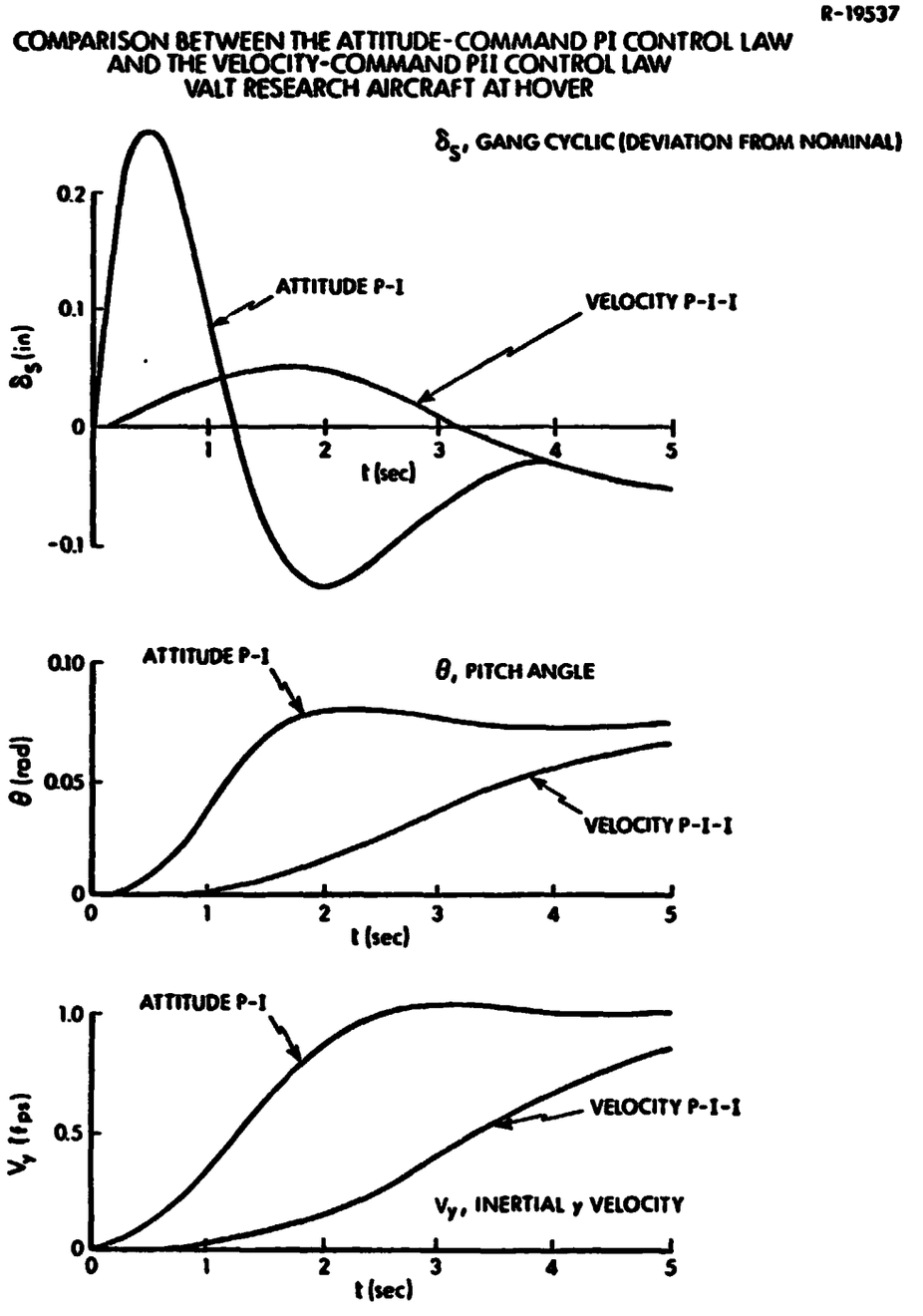

Figure 5.9-8 Simulations for a Command in V_y and a Simultaneous Command in θ and ϕ

- The flight conditions for point design consisted of 19 cases which were systematically chosen to represent the VALT Research Aircraft flight envelope in the vertical plane. The points were biased toward level and low-speed flight, which are considered to be the most common and most demanding conditions, respectively.
- The weighted variables in the cost function were based on the commanded $\underline{y}_d$ variables.
- The state weighting matrix at each flight point was determined based on step response simulations meeting prespecified requirements.
- The velocity-command PII control law system state weighting matrix was successfully found based on determining weighting matrices at extreme flight conditions, then linearly interpolating the weightings.
- The attitude-command PI control law system weighting matrix was determined at each individual flight condition with little change in the weightings. The weightings have a definite pattern if the flight conditions are arranged in ascending forward velocity.
- In both designs, meeting the rise time step response requirement determined when to stop increasing the weights in the state weighting matrix.
- Eighty-five percent of the velocity-command correlation coefficients are greater than 0.8.
- Eighty-three percent of the attitude-command correlation coefficients are greater than 0.8.
- Significant gains in general have correlation coefficients greater than 0.9.
- The longitudinal/lateral-directional cross gains tended to be smaller than the other gains for the PII controller.

- Command-Controller

  Choose the command system and controller type for continuous or discrete case, e.g., Velocity Command (PII Controller), Attitude Command (PI Controller), or Dynamic Controller (Regulator).

- Criteria

  Specify suitable step response requirements, closed-loop eigenvalues, or quadratic weightings.
  Determine the state variables to be weighted by quadratic synthesis.
  Specify Q and R adjustment policy, if required.

- Controller Gain Scheduling

  Obtain control gains from DIGADAPT.
  Iterate Q and R, as required.
  Punch controller gains and flight conditions on computer cards for SCHED input.

  Choose flight conditions for regression (body axes or inertial axes). Reorder punched cards with chosen flight condition type.

  Run SCHED for all combinations of independent variables (flight conditions), printing out correlation coefficients.

  Using SCHED output, choose independent variables for regression based on correlation coefficients and availability of measurements onboard the vehicle.

  Run SCHED for regressions with chosen independent variables.

  Record regression coefficients for use in open-loop explicit-adaptive gain scheduling algorithm.

- Trim Values

  Run DIGADAPT for as many flight conditions as desired, punching control trim positions and state positions for SCHED input.

  Choose body or inertial axes for independent variable conditions.

  Schedule static trim values against flight condition.

  Schedule dynamic trim coefficients against flight condition.

- Low-Pass Filters

  Establish signal and noise variances for measurement states.

  Define filter gains using discrete-time Kalman filter algorithms.

- Complementary Filters

  Choose a sampling interval for the filters if they are to be discrete. Filters are simple enough to be adjusted on line or by full simulation techniques.

- Kalman Filter Design for Unmeasured States

  Define states which are measured, disturbance covariance matrix, and observation noise covariance matrix.

  Run LIGADAPT to obtain Kalman filter gains for flight conditions desired. Run SCHED with Kalman gains as noted above.

6. EVALUATION OF CONTROL SYSTEM DESIGN

The digital-adaptive control systems described in the previous chapters need to be evaluated. An approach for initial evaluation is numerical testing by digital simulation. This chapter presents details of a linear-time-varying simulation technique and simulation results which show the control systems' performance.

6.1 OVERVIEW

The aircraft simulation described in the following sections is designed to test the digital-adaptive control system for representative flight paths. The simulation includes a linear-time-varying vehicle model and guidance and control routines. The aircraft is assumed to follow a nominal flight path, and the computations provide a direct output of trajectory errors arising from various test inputs.

The simulation can incorporate certain nonlinearities, such as actuator position and rate limits, and it relies upon aerodynamic stability derivatives to describe vehicle dynamics.

This linear-time-varying aircraft simulation is flexible, while maintaining a high degree of efficiency and accuracy. The program's flexibility stems from a modular construction which enables the program to deal with various levels of simulation detail. The program's options include:

- Actuator dynamics (first-order lag, displacement limits, and rate limits)
- Rotor dynamics (second-order model)
- Guidance law
- Control law

The linear-time-varying simulation is more efficient than a fully nonlinear model, and computational accuracy is assured by the use of a variable-step-size Runge-Kutta integration routine.

The remaining sections of Chapter 6 discuss the simulation in detail. Section 6.2 describes the nominal flight paths to be flown by the helicopter. Section 6.3 outlines the aircraft simulation and guidance logic. Section 6.4 discusses the digital-adaptive control law and considers implementation and computer loading requirements. Section 6.5 illustrates the control system performance by showing the results of the linear-time-varying simulation, and Section 6.6 is a chapter summary.

6.2 NOMINAL FLIGHT PATH FOR SYSTEM EVALUATION

Aircraft flights can be divided into three phases: takeoff and climb, cruise, and approach and landing. The cruise portion of the flight path is essentially at steady-state, and Chapter 5 has dealt with control system response under these conditions. Because the approach and landing phase of flight is one of the most critical for flight safety, the emphasis of this chapter's evaluation is placed on that phase. The nominal flight path is particularly appropriate as it has features of special interest.

rotor dynamics, and the last four components are the control actuator states. The linear matrices at intermediate states are found at a specific point of the nominal trajectory using linear interpolation between the two waypoints for that segment. Equation (6.3-4) illustrates this procedure for the system matrix F:

$$F(t) = F_n + \gamma(t)(F_{n+1} - F_n) \quad (6.3\text{-}4)$$

where F_n and F_{n+1} are the system dynamics matrices at the previous and next waypoints, respectively. The interpolation value, $\gamma(t)$, varies from 0 to 1 as the vehicle flies from waypoint n to waypoint n+1.

Total values of the states and controls are formed by adding the perturbation states and controls to the trim states and controls, as shown below:

$$\underline{x}_T(t) = \underline{x}_0(t) + \underline{x}(t) \quad (6.3\text{-}5)$$

$$\underline{u}_T(t) = \underline{u}_0(t) + \underline{u}(t) \quad (6.3\text{-}6)$$

For sections of the nominal trajectory which involve translational accelerations or rotations, the nominal states and control should be the dynamic trim states and controls. For most sections of the nominal trajectories discussed in Section 6.2, the differences between static and dynamic trim are small. In Section 4.3, methods for calculating dynamic trim are discussed. The linear simulation results are expressed as perturbations about the nominal trajectory, which is assumed to incorporate dynamic trim.

The approach flight path shown in Fig. 6.2-1 is representative of the terminal portion of the flight of a VTOL vehicle. A steady-turn holding pattern is included to test the guidance and control system's ability in entering and leaving a steady turn. The flight path includes a number of heading changes, perhaps similar to those required by a VTOL vehicle avoiding fixed obstacles. The final section of the flight path exhibits a constant-velocity descent followed by a decelerating descent. This section of the flight path may provide an especially severe test to the digital adaptive controller, due to the rapidly varying vehicle dynamics.

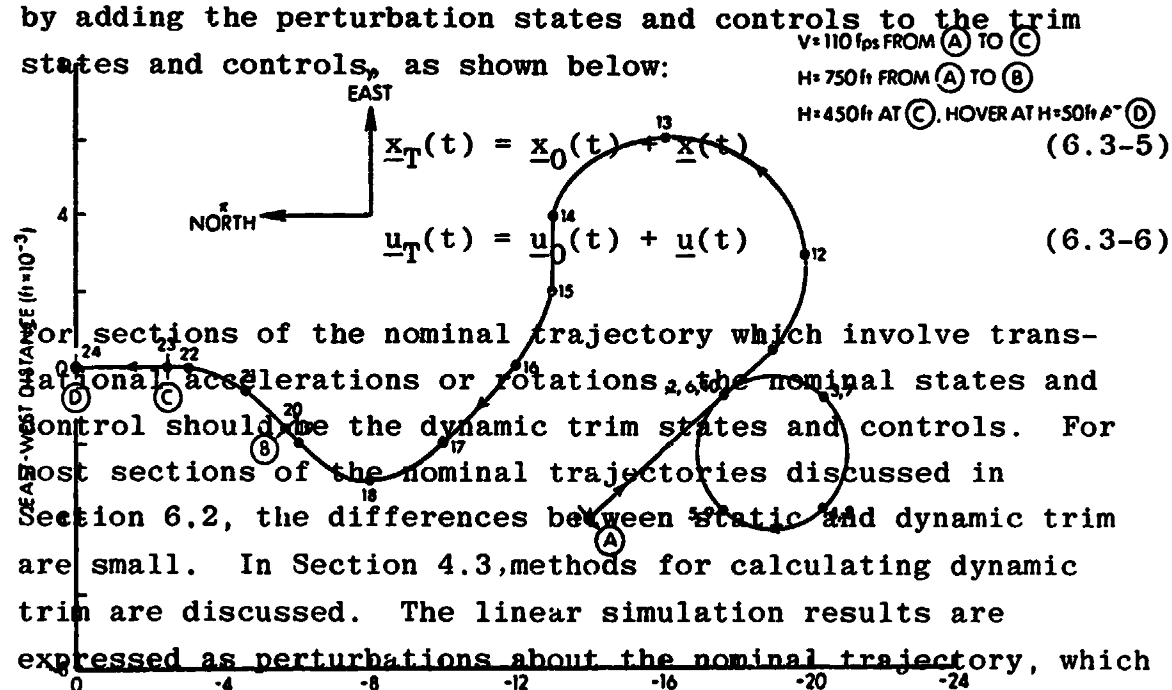

Figure 6.2-1 Approach Flight Path

6.3 LINEAR-TIME-VARYING MODEL FOR SYSTEM SIMULATION

The vehicle equations of motion consist of nonlinear differential equations which describe the behavior of the vehicle states as influenced by the control input and disturbances:

$$\dot{\underline{x}}_T(t) = \underline{f}(\underline{x}_T(t), \underline{u}_T(t), \underline{w}_T(t)) \qquad (6.3\text{-}1)$$

where $\underline{x}_T$ is the total state vector, $\underline{u}_T$ is the total control vector, and $\underline{w}_T$ is the total disturbance vector. As indicated in Section 2.4, this nonlinear equation can be expanded about a nominal trajectory. The result is a nonlinear equation describing the nominal trajectory and a linear equation describing the perturbations about the nominal trajectory:

$$\dot{\underline{x}}_0(t) = \underline{f}(\underline{x}_0(t), \underline{u}_0(t), \underline{w}_0(t)) \qquad (6.3\text{-}2)$$

$$\dot{\underline{x}}(t) = F(t)\underline{x}(t) + G(t)\underline{u}(t) + L(t)\underline{w}(t) \qquad (6.3\text{-}3)$$

In these equations, the subscript "0" indicates a nominal value, while an unsubscripted variable is a perturbation value. The total values of the variables are equal to the sums of the nominal and perturbation values.

When the nominal flight condition is unaccelerated (such as in straight flight at constant velocity), the nominal states and controls are referred to as static trim states and controls. When the nominal flight condition is accelerated the differences between the static trim states and controls (at the same velocity) and the corresponding accelerated values are called the dynamic trim state and control perturbations.

TABLE 6.3-1

STATES OF THE LINEAR-TIME-VARYING SIMULATION

x	Earth x-axis position	[ft]
y	Earth y-axis position	[ft]
z	Earth z-axis position	[ft]
u	Body x-axis velocity	[fps]
v	Body y-axis velocity	[fps]
w	Body z-axis velocity	[fps]
p	Body x-axis angular rate	[rad/sec]
q	Body y-axis angular rate	[rad/sec]
r	Body z-axis angular rate	[rad/sec]
θ	Pitch Euler angle	[rad]
ϕ	Roll Euler angle	[rad]
ψ	Yaw Euler angle	[rad]
δ_B	Differential collective (rotor)	[in]
δ_C	Collective (rotor)	[in]
δ_S	Lateral cyclic (rotor)	[in]
δ_R	Differential cyclic (rotor)	[in]
$\dot{\delta}_B$	Diff. collective rate (rotor)	[in/sec]
$\dot{\delta}_C$	Collective rate (rotor)	[in/sec]
$\dot{\delta}_S$	Cyclic rate (rotor)	[in/sec]
$\dot{\delta}_R$	Diff. cyclic rate (rotor)	[in/sec]
δ_{B_A}	Diff. collective actuator	[in]
δ_{C_A}	Collective actuator	[in]
δ_{S_A}	Cyclic actuator	[in]
δ_{R_A}	Diff. cyclic actuator	[in]

TABLE 6.3-2

CONTROL COMMANDS OF
THE LINEAR-TIME-VARYING SIMULATION

δ_{B_c}	Diff. collective command	[in]
δ_{C_c}	Collective command	[in]
δ_{S_c}	Cyclic command	[in]
δ_{R_c}	Diff. cyclic command	[in]

The dynamic equations are integrated using a variable-step-size, fourth-order Runge-Kutta integration routine. The variable-step-size feature doubles or halves the time step used for integration to minimize errors due to truncation and roundoff, which enhances computational efficiency. Section A.3 of Appendix A contains further details concerning the programming used in the present investigation.

There are a number of options built into the linear-time-varying computer simulation to increase its speed and flexibility. The actuator and rotor states add considerably to the simulation run time, because of the enlarged state vector and because the integration routine must take smaller steps to accurately integrate the relatively fast rotor and actuator dynamics. Consequently, the rotor and actuator dynamics can be excluded from the simulation if desired. Nominal turbulence time histories also can be generated as normal and lateral body-axis velocity disturbances (Section A.3).

6.3.2 Guidance Algorithm

The guidance algorithm used in the present simulation produces total velocity and angle commands. These commands are composed of the nominal velocity and angle values plus perturbations which are intended to null position errors. The guidance laws are based on those derived in Ref. 22. The velocity-command guidance algorithm produces a command vector consisting of three velocity elements and a heading angle command. The attitude-command system (in which the command vector consists of three Euler angle commands and a vertical velocity command) is created by appending the autopilot logic of Ref. 22 to the velocity-command law.

The guidance algorithm contains tables of the position, velocity and guidance gains at each waypoint along the nominal trajectory. The input to the guidance system (from a navigation system) is the true vehicle position, $\underline{x}_E$. From this, the position on the trajectory segment is calculated:

$$\gamma = d/d_0 \tag{6.3-7}$$

$$d = \sqrt{(x_{E+}-x_E)^2 + (y_{E+}-y_E)^2 + (z_{E+}-z_E)^2} \tag{6.3-8}$$

$$d_0 = \sqrt{(x_{E+}-x_{E-})^2 + (y_{E+}-y_{E-})^2 + (z_{E+}-z_{E-})^2} \tag{6.3-9}$$

where the subscript "+" pertains to the position of the waypoint being approached, while the subscript "-" describes the previous trajectory waypoint.

The nominal position, velocity and guidance gains are found from the tables by linear interpolation:

$$\underline{x}_{E_0} = \underline{x}_{E-} + \gamma(\underline{x}_{E+}-\underline{x}_{E-}) \tag{6.3-10}$$

$$\underline{V}_{E_0} = \underline{V}_{E-} + \gamma(\underline{V}_{E+} - \underline{V}_{E-}) \tag{6.3-11}$$

$$K_{G_0} = K_{G-} + \gamma(K_{G+} - K_{G-}) \tag{6.3-12}$$

The nominal heading angle is found from $\underline{v}_{E_0}$ by

$$\xi_0 = \tan^{-1}(V_{E_y}/V_{E_x}) \tag{6.3-13}$$

Velocity-Command Guidance Law - The commands are

$$\underline{V}_{E_C} = \underline{V}_{E_0} + H_G^E(\xi_0)\, K_{G_0}\, H_E^G(\xi_0)(\underline{x}_E - \underline{x}_{E_0}) \tag{6.3-14}$$

$$\psi_c = \xi_0 \tag{6.3-15}$$

where the transformation from earth-relative to guidance axes is

$$H_E^G(\xi) = \begin{bmatrix} \cos\xi & \sin\xi & 0 \\ -\sin\xi & \cos\xi & 0 \\ 0 & 0 & 1 \end{bmatrix} \tag{6.3-16}$$

Thus, the four-element velocity-command guidance output is composed of the three earth-relative velocity commands and the heading angle command.

The guidance gains relate the perturbation guidance frame velocity-commands to the position errors in the guidance frame. Therefore, the feedback relation is

$$\begin{bmatrix} \Delta V_{DR} \\ \Delta V_{CR} \\ \Delta V_H \end{bmatrix}_C = \begin{bmatrix} 0 & K_{12} & K_{13} \\ 0 & K_{22} & K_{23} \\ 0 & K_{32} & K_{33} \end{bmatrix} \begin{bmatrix} \Delta X_{DR} \\ \Delta X_{CR} \\ \Delta X_H \end{bmatrix} \tag{6.3-17}$$

In straight-and-level cruise, every gain is zero except K_{22} and K_{33}, which are chosen to be -0.03 sec^{-1}. This causes position errors to be nulled exponentially with a time constant of 33 sec. Gains for accelerating, turning or climbing flight are time-varying and must be calculated for each trajectory. The recommended method is the use of finite-time optimal control, as is done in Ref. 22.

Attitude-Command Guidance Law - By using the nominal position, velocity and guidance gains, the commands are

$$\phi_c = K_\phi \, \Delta V_{CR_c} \tag{6.3-18}$$

$$\theta_c = K_\theta \, \Delta V_{DR_c} + K_{I_\theta} \int \Delta V_{DR} \tag{6.3-19}$$

$$\psi_c = \xi_0 \tag{6.3-20}$$

$$V_{H_c} = V_{H_0} + \Delta V_{H_c} \tag{6.3-21}$$

where the guidance-frame velocity commands are

$$\begin{bmatrix} \Delta V_{DR} \\ \Delta V_{CR} \\ \Delta V_H \end{bmatrix}_c = K_{G_0} H_E^G(\xi_0)(\underline{x}_E - \underline{x}_{E_0}) \tag{6.3-22}$$

The values of the attitude gains are taken from Ref. 22 and are

$$K_\phi = -0.01 \text{ rad-sec/ft} \tag{6.3-23}$$

$$K_\theta = -0.01 \text{ rad-sec/ft} \tag{6.3-24}$$

$$K_{I_\theta} = -0.001 \text{ rad/ft} \tag{6.3-25}$$

Summary - This section has discussed the linear-time-varying aircraft and guidance simulations. These simulations, defined along a nominal trajectory, capture the essence of the dynamics involved in these systems, and also permit repeated experiments along the same nominal trajectory. Thus, easily comparable results in the form of perturbations about an unchanging nominal flight path can be obtained efficiently. A further advantage of the linear-time-varying simulation is that transient solutions can be obtained without specifying aircraft trim. In the following section, the incorporation of the flight control program in the linear-time-varying simulation structure is discussed.

6.4 FLIGHT CONTROL PROGRAM DESIGN

The aircraft control system is implemented in the linear-time-varying simulation as an independent subroutine, which is functionally similar to on-board control system coding. However, high efficiency of execution and storage, which are important considerations in programming for flight systems, are not simulation design goals here.

In this section, the three functions of the control coding are examined, and estimates of flight computer storage and speed requirements for a digital-adaptive control law are provided.

6.4.1 State Estimation

The state estimation logic produces perturbation values of the states and guidance commands for use in the control calculations. In addition, total state and nominal

control estimates that are needed by the gain calculation or control computation routines are generated. The estimation logic itself is divided into three sections, one for total state estimation from sensor measurements, one for nominal state calculation, and a third section that forms perturbation values by differencing total and nominal values.

The total state estimation routine, as described in Section 5.6, is composed of fixed low-pass and complementary filters that operate on sensor outputs. Assuming sideslip measurements are not available, this state can be estimated by using lateral acceleration and angular rates. The total value of the output vector, $\underline{y}_T$, in Fig. 6.4-1 is simply a function of the total state, and it is formed by a transformation based on nominal state values.

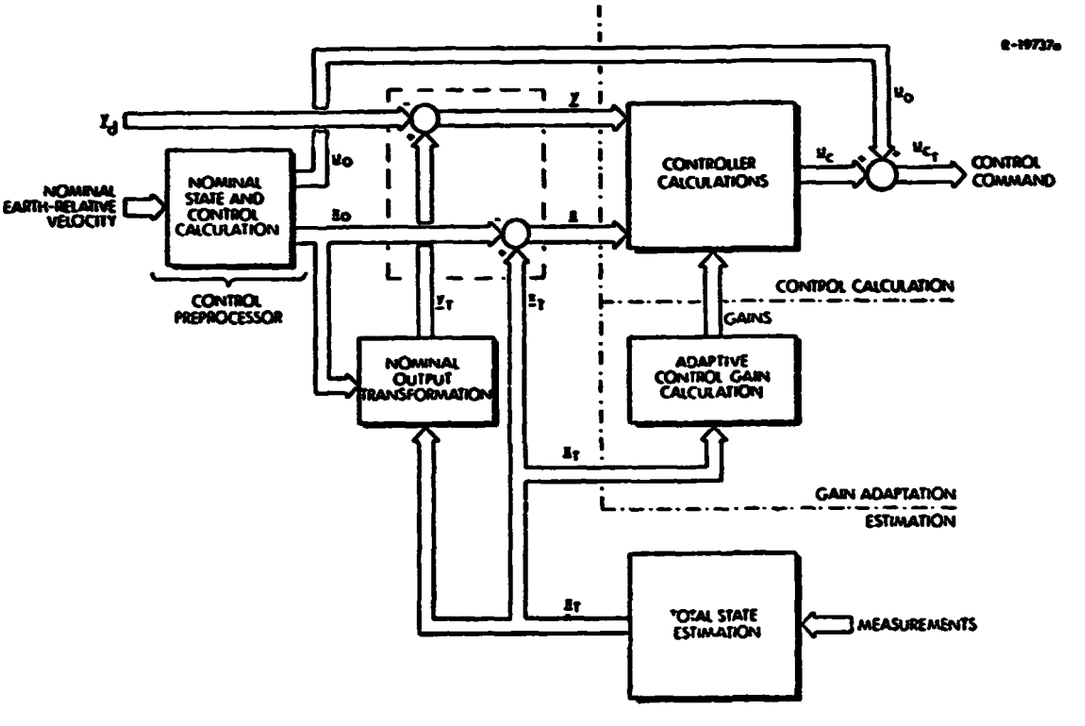

Figure 6.4-1 Complete Controller Diagram

The nominal state and control calculation represents the guidance-control interface, and may be termed a control preprocessor (See Section 2.4). As shown in Fig. 6.4-1, the nominal state and control calculations use the nominal velocity, which is stored in the guidance section. This velocity is used to calculate static trim controls and Euler angles with the scheduling algorithms described in Section 5.7. The static trim body-axis velocities are derived from the nominal velocities and the static trim Euler angles. Nominal states and controls are formed by adding the corrections due to dynamic trim as derived in Section 4.3. It should be noted that errors due to neglecting dynamic trim (i.e., assuming the static trim is the nominal value) are not great unless the nominal trajectory exhibits high state rates. Furthermore, the control system's integral compensation should cause the vehicle to follow the nominal trajectory even if dynamic trim is neglected.

The perturbation states and outputs are formed by differencing the total and nominal values. The perturbation state and output values are used by the control algorithm to calculate perturbation control commands.

In addition to producing perturbation states and outputs for the controller algorithm, the estimation logic must supply the control gain calculation algorithm (described in Section 6.4.2) with total state estimates. It also provides the control computation algorithm (discussed in Section 6.4.3) with nominal control values.

6.4.2 Control Gain Calculation

The control gains are found from a gain schedule derived in Section 5.7. This schedule, which relates control

gains to the body-axis u and w velocities and the velocity magnitude squared (V^2), has been derived by regression analysis. The gain-scheduling coefficients would be stored in the flight computer memory to form the basis of a digital feedback control law using open-loop explicit adaptation. The gain update interval is chosen to be equal to the control sampling period in the present simulation, although less frequent updates could be acceptable in practice. This is possible because the gains are functions of velocity, which is slowly varying. Implementation of these control laws in a flight computer should include gain limits and consistency checks of the gains to ensure that gross errors have not occurred. These flight-safety-related checks are not necessary in a simulation such as that described here.

6.4.3 Primary Control Calculations

The primary control calculation uses the perturbation states and guidance commands to calculate the perturbation control command. The controller uses the gains produced by the gain calculation algorithm. These operations are illustrated in Fig. 6.4-2.

There are two time delays between the desired system output, $\underline{y}$, and the control command, $\underline{u}_c$, in the PII controller. These delays serve three useful purposes. They provide the controller with an integrating action that should reduce the controller sensitivity to noise in the state feedback terms. The integration of desired output provided by the first delay gaurantees the zero steady-state error property discussed above. Finally, the "inner" delay of the PII controller (Fig. 3.6-2) can eliminate the effective computation lag in real-time implementation. This occurs because the control command to be applied at a given sample

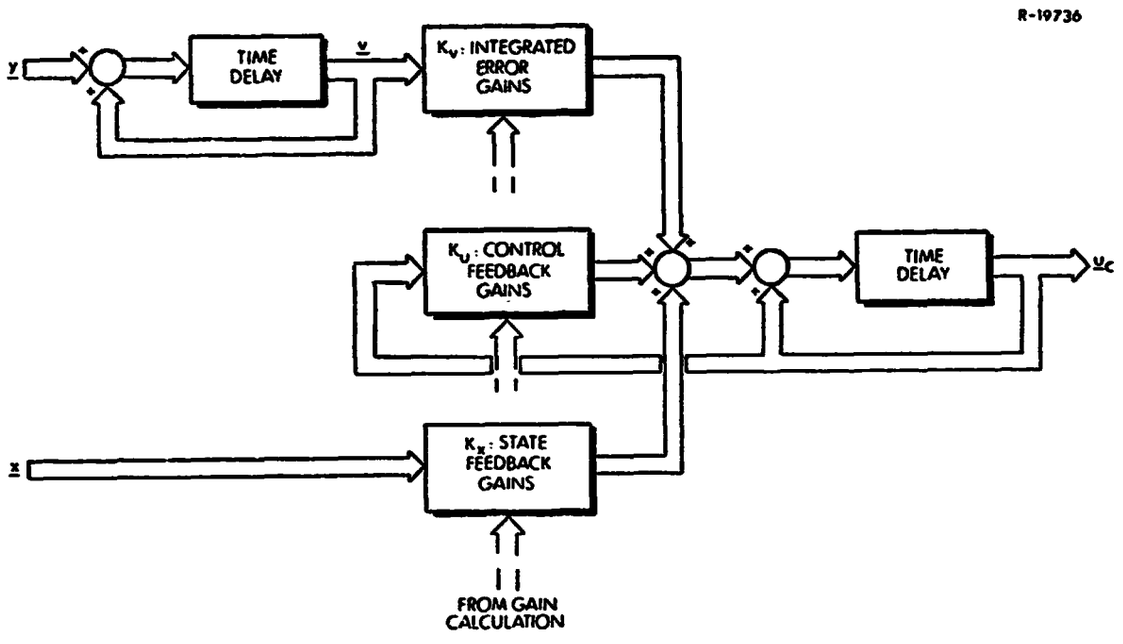

Figure 6.4-2 Discrete-Time PII Controller Contained in the Linear-Time-Varying Simulation

time is calculated during the previous control sample period, and is thus ready to be applied at the correct time. In the PI controller, computation delay effects are not entirely eliminated, as about half of the feedback terms do not pass through the integrator delay element (Fig. 3.6-1).

As discussed in Section 6.3.2, two guidance systems are considered in the simulation, and each produces its own desired output vector. In the PII velocity-command system, the desired output vector consists of the three components of earth-relative velocity and the yaw angle. This vector must be transformed into the guidance reference frame because the control algorithm was designed in this reference frame. This transformation (which is given by Eq. (6.3-16)) is part of the K_v gains of Fig. 6.4-2. The desired output vector for a PII attitude-command system consists of the

three body Euler angles and the vertical velocity. The same controller structure is used for both velocity-command and attitude-command guidance systems, and only the gains are changed from one system to another. Alternate controller structures, such as the PI controller, are not discussed further here.

6.4.4 Computer Storage and Speed Requirements

Estimation of the number of computer operations necessary to execute each section of the complete control algorithm can be performed by examining the detailed specifications of Chapters 4 and 5. Storage for data and program instructions also can be estimated in the same way.

Table 6.4-1 lists estimates of the operations per cycle which would be required to execute the velocity-command control law. These operations and data storage estimates are somewhat conservative, as they do not take into account the savings in operations that may occur when all zero adds and multiplys are excluded. The total computer duty cycle, i.e., the percentage of time which is required to perform control-related computations, depends upon the control sampling and gain update intervals. Using the 12-per-sec control rate established in Chapter 5 and assuming that the gains are recomputed at the same frequency, the control duty cycle for the computer described in Section 2.3.2 is about 15 percent. This estimate accounts for transfer of information to and from storage. It does not allow for the scaling operations normally required in fixed-point computation, which could increase the timing estimate by several percentage points. It also may be possible to lengthen the gain update interval, which would decrease the timing estimate by several points.

TABLE 6.4-1
COMPUTER TIMING AND SIZE ESTIMATES

FUNCTION	MEMORY (WORDS)		OPERATIONS PER CYCLE	
	INSTRUCTIONS	DATA	ADD	MULT.
Total and Nominal State and Control Calculation (No Dynamic Trim)	450	160	70	75
Dynamic Trim	850	150	135	145
Control Gain Calculation	900	310	155	155
Control Calculation	600	35	90	110

6.5 RESULTS OF EVALUATION

The linear-time-varying simulation described in the earlier sections of this chapter has been programmed, (as described in Section A.3), and it has been used to test the performance of the digital-adaptive controller along selected portions of the nominal trajectories. These tests illustrate the capabilities of the controller in straight flight and along a decelerating descent.

The first demonstration tests indicate the gain scheduling capability of the controller along a straight-and-level section of the approach flight path -- from Waypoint 1 to Waypoint 2 in Fig. 6.2-1. A comparison of the gains calculated by linear-optimal control at a fixed flight condition near this trajectory segment and the gains found along this trajectory indicates less than 10 percent error in

all significant gains and less than 5 percent error in most of them. The perturbation trajectories of earth-relative velocity, shown in Fig. 6.5-1, bear this out. This figure illustrates the control system's response to a V_{y_E} guidance command of 1 fps. The V_{y_E} response is fast, accurate, and well damped. The V_{z_E} response (due to dynamic coupling) is larger than for the optimal gains at this flight condition, but the correct steady-state value is quickly reached.

The performance of the guidance and control algorithms operating together is illustrated in Fig. 6.5-2. The vehicle is flying along the approach trajectory segment taken from Fig. 6.2-1. In this case, there is an initial cross range error of -11 ft. This error causes the guidance system to command a velocity perturbation to correct the position error, and the control system responds smoothly to this command. The magnitude of the response is small, due to the small values of the guidance gains during cruise.

The response of the digital-adaptive controller during a decelerating descent is shown in Fig. 6.5-3. (This represents the segment between Waypoints 23 and 24 in Fig. 6.2-1). This figure shows the response to two sequential guidance commands. The first is a perturbation earth-relative velocity command of 1 fps for V_{y_E}, and the second is a 1 fps V_{z_E} command. The x-axis response is small in this case, and the y-axis response is quick and accurate. It is disturbed somewhat by the subsequent V_{z_E} command, but it is moving towards the correct steady-state value at the end of the 15-sec simulation. The V_{z_E} response to the V_{z_E} command is offset somewhat due to the previous V_{y_E} command, but it is moving toward the correct steady-state value at the end of the run. It is important to note that these responses occur along a nominal trajectory where the dynamic

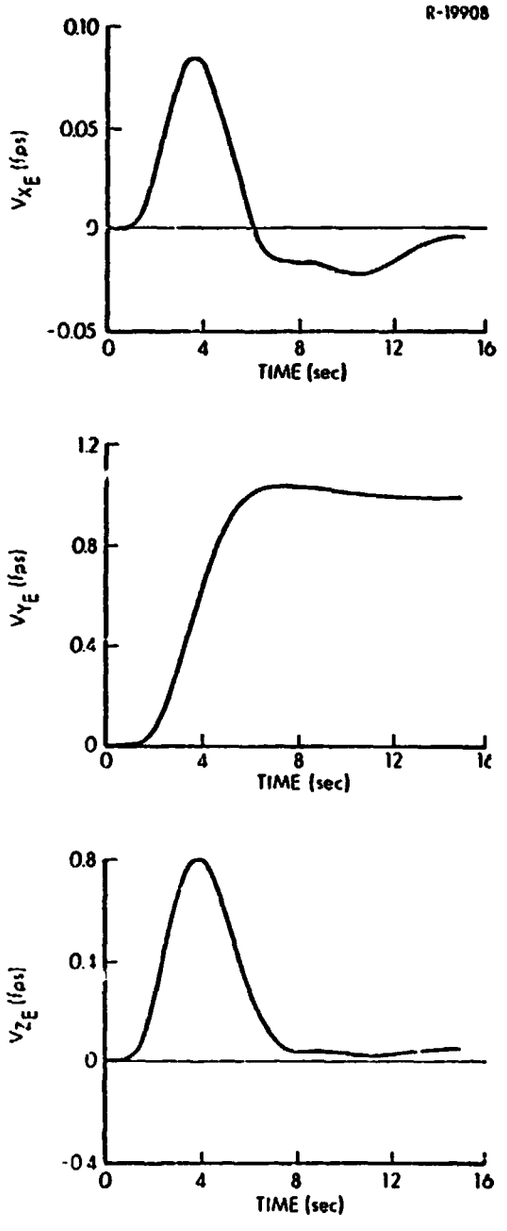

V_0 = 110 FPS ψ = 2.409 RAD

V_{Y_E} COMMAND = 1.0 FPS

APPLIED AT 0.5 SEC

CONTROLLER GAINS FOUND FROM REGRESSION COEFFICIENTS

STEP RESPONSE CRITERIA SATISFIED

Figure 6.5-1 Earth-Relative Velocity Response Along Approach Flight Path -- Waypoint 1 to 2 (Controller Only)

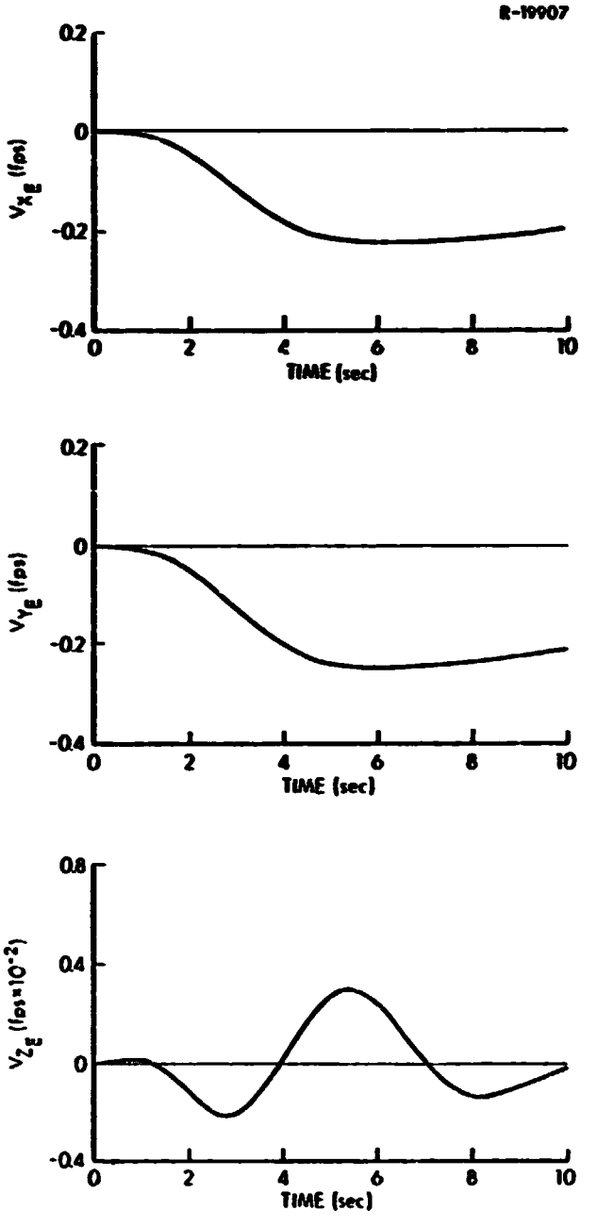

V_0 = 110.0 FPS ψ = 2.409 RAD

INITIAL CROSS RANGE ERROR

−11.0 FT.

AFTER 5 SECONDS: −10.4 FT
AFTER 10 SECONDS: −8.8 FT

CRUISE GUIDANCE GAINS

CONTROLLER GAINS FOUND FROM REGRESSION COEFFICIENTS

Figure 6.5-2 Earth-Relative Velocity Response Approach Flight Path -- Waypoint 1 to 2 (Guidance and Control on)

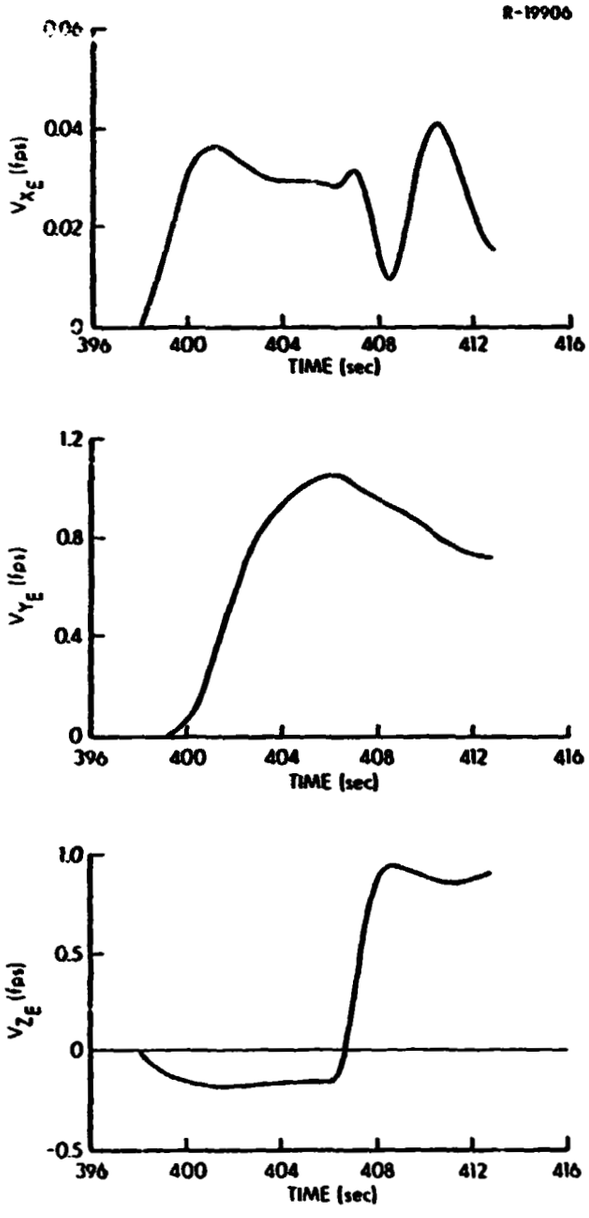

DECELERATING DESCENT (ψ_0 = 0.0 RAD)

AT T = 398.0 SEC. V_{X_0} = 110.0 FPS

V_{Z_0} = 8.55 FPS

AT T = 413.0 SEC. V_{X_0} = 73.7 FPS

V_{Z_0} = 5.73 FPS

V_{Y_E} COMMAND = 1.0 FPS

APPLIED AT 398.5 SEC.

V_{Z_E} COMMAND = 1.0 FPS

APPLIED AT 406.0 SEC.

CONTROLLER GAINS FOUND FROM REGRESSION COEFFICIENTS

Figure 6.5-3 Earth-Relative Velocity Response Approach Flight Path-- Waypoint 23 to 24 (Controller Only)

pressure drops by more than 50 percent in 15 sec. The velocity drops from 110 fps at Waypoint 23 to 74 fps at Waypoint 24. The gain calculation by means of the regression coefficients compensates well for this change.

6.6 CHAPTER SUMMARY

Chapter 6 has described the linear-time-varying simulation of the VALT Research Aircraft and its guidance and control algorithms. This type of simulation is useful because it eliminates the difficult and time consuming trim calculation problem by assuming a realistic nominal flight path. At the same time, the linear simulation preserves the essential vehicle, guidance, and control dynamics. Results are produced in easily usable form as perturbations about the nominal trajectory.

Test results presented in Section 6.5 illustrate the adaptive controller performance along significant sections of a nominal flight path. These initial results lead to the conclusion that the controller produces good closed-loop response along straight trajectories, even when the vehicle is in a decelerating descent.

7. CONCLUSIONS

Methods for designing digital-adaptive control systems for VTOL aircraft have been developed using the comprehensive methods of linear-optimal estimation and control theory. This work is drawn together in the establishment of a recommended design procedure which contains the following major tasks:

- System Definition - Define the flight envelope of the aircraft. Choose flight conditions within this envelope that represent the normal flight regime of the aircraft and which provide enough data for correlating (mathematically) control system gains with flight variables. Generate linear-time-invariant dynamic models of the aircraft at these flight conditions.

- Design Criteria - Define command-response and stability augmentation objectives of the control system. Establish performance criteria for the closed-loop response of the aircraft. Determine allowable ranges of the displacements and rates of the control effector mechanization, including all actuator dynamics, mechanical linkage and gearing, control surface stops, etc.

- Continuous Control System Design - Use continuous cost function weighting matrices (Q and R) in the discrete controller design algorithm, as discussed in Chapter 3. (The equivalent continuous-time controller need not be designed in order to obtain the discrete-time controller; however, the former could be useful as an aid to choosing weighting matrices, to determining control effects on sampling interval, or to providing reference response histories for evaluating the digital system.)

- Sampling Interval Determination - Define state-vector and control-command uncertainty bounds. Establish covariance matrices of disturbance inputs, state estimate errors, and aircraft dynamic model uncertainties. Propagate the state covariance matrix at representative working points in the flight envelope until error bounds are reached at each working point, defining the longest acceptable sampling interval at that point (See Chapter 4). Choose the shortest of these for implementation in the digital control law.

- Discrete Control System Design - Choose either the PI or PII control structure for implementation. (As a rule of thumb, the PI structure is preferred if there is a premium on fast response. The PII structure is preferred for smooth, precise response. Computational requirements are virtually identical for the two controllers.) Compute control gains at several extremes of the flight envelope, adjusting Q and R as required to obtain control objectives. (If flight variable measurements are particularly noisy, feedback information may be lagged by low gains in the estimators described below. In this case, evaluation of control objectives should be carried out with estimators "in the loop.") Establish simple interpolation rules for adjusting Q and R at intermediate flight conditions and compute requisite control gains. If acceptable response is not obtained at all flight conditions, adjust Q and R until response is satisfactory.

- Estimator-Observer Design - Define sensor characteristics and locations for flight variable measurements. Determine approximate signal and noise variances for measurements. Partition the state estimation problem into parallel reduced-order problems, if possible. Design reduced-order, constant-gain filters (e.g., discrete-time low-pass or complementary filters) for states with low measurement noise and/or little dynamic coupling with other states. Estimate unmeasured states with simplified, constant-gain Kalman filters. (Estimator design

should be largely independent of control design, although the converse may not be true. The Separation Theorem indicates that the stability of estimation and control systems can be determined independently; however, meeting closed-loop response criteria with noisy feedback measurements could require simultaneous evaluation of estimation and control logic, as mentioned in the previous paragraph.)

- Trim Commands - Establish trim objectives (static trim, longitudinal axes only, etc.). Identify the control effectors which can be used to regulate trim equilibrium. If there are fewer control effectors than are required to meet trim objectives, choose kinematic flight variables to be used as trim parameters. Compute static trim settings for each flight condition. Define a linear dynamic trim compensation algorithm, if quickened transient response is desired.

- Gain and Trim Scheduling - Compute means and standard deviations of all control gains, estimator gains, static trim settings, and linear dynamic trim coefficients (summed and averaged over all design flight conditions). Identify those quantities which can be assumed constant (or zero) and those which should be scheduled. Correlate all quantities to be scheduled against functions of flight variables to determine candidate groupings for gain scheduling. Perform regression analysis to generate the gain and trim schedules for the open-loop explicit adaptation.

- Control Law Evaluation - Implement gain and trim schedules for digital simulation. Simulate performance of the adaptive control law to establish command response, disturbance response, and measurement error rejection, as appropriate. Use linear-time-invariant and linear-time-varying simulations for initial testing. Simulate selected control nonlinearities and on-board computation delays as testing progresses. Perform "all-up" testing of the digital control law using a fully nonlinear simulation.

This design procedure is intended to make best use of engineering judgment and to avoid unnecessary complexities in the control system which ultimately is implemented on board a VTOL aircraft. An attempt is made to eliminate details which contribute much to mathematical rigor but little to vehicle control. The procedure presented here provides the control system designer with analytical tools which aid control law development. It is clear that the designer retains an important role in system development, for there are many points at which intermediate results must be reviewed and decisions must be made before proceeding.

The significance of this investigation is indicated by several observations regarding linear-optimal design of digital flight control laws:

- The complexity of the linear-optimal system is not significantly different from a classically designed system - Comparison with the TAGS flight controller indicates that computer instruction and memory requirements and use of feedback information is similar for modern and conventional command-response systems.

- The necessary control structure is visible at an early stage of the design process - The linear-optimal control design begins by defining all reasonable state-control paths, allowing the designer to evaluate the relative importance of each control path and to eliminate those which contribute little to system response.

- Computational duty cycle can be minimized with a linear-optimal design - The sampling rate of 12 frames per sec, although conservatively chosen, is one-third less than the TAGS sampling rate and more than 90 percent smaller than other classically designed digital flight controllers.

- Computational (transport) lag effects are eliminated in the PII controller and are modest in the PI controller - The PII controller contains a pure delay between the control command and its transmittal to the control actuators; hence, all computations can be completed in the interval between making a measurement and issuing a command (assuming that the flight computer itself is fast enough to complete the calculations within a single sampling interval). Approximately half of the PI computations are subject to a pure time delay and, thus, do not contribute to control transport lag.

- Tradeoffs between response criteria and control constraints form an integral part of the design process - Quadratic synthesis provides the "best" response which can be obtained for specified limitations on control displacement and rate. If response criteria cannot be satisfied within the control constraints, the designer can use optimal control theory to learn what improvements in control actuation are required to obtain the desired response.

- Linear-optimal methods allow the designer to specify the smallest possible gain magnitudes - The Q and R matrices provide complete control of overshoot, rise time, settling time, and disturbance response when the PI or PII control structures are used. Furthermore, quadratic synthesis provides stable closed-loop response as a starting point. The designer has the flexibility to adjust cost function weighting to the point that some or all criteria are just barely satisfied, implicitly specifying the lowest acceptable gains.

- Pulsing of control actuators by discrete-step commands of the digital system can be moderated by control-rate weighting - Control position difference is the discrete-time equivalent of the control rate of a continuous-time system; hence, control-rate weighting tends to minimize the command steps produced by the digital control, thereby reducing pulsing of the control actuators.

- **Open-loop explicit adaptation of control gains is adequate for adjusting the gains of a known aircraft to varying flight condition, is computationally efficient, and is consistent with current flight control design practice** - Comprehensive gain and trim scheduling provides all the adaptation required for a vehicle with well-defined characteristics, and the adaptation process itself is predictable. Thus, it is appropriate for application to operational aircraft. On-board implementation of gain scheduling involves simple algorithms which can be executed rapidly. Gain scheduling has been an operational flight control technique on many aircraft types for more than a decade.

Digital-adaptive controllers can contribute to the development and operation of future VTOL aircraft. This report has presented a design procedure for such control laws, and it has substantiated the recommended techniques through development and evaluation of command-response control laws for the VALT Research Aircraft.

APPENDIX A
FLIGHT CONTROL DESIGN PROCEDURES

This appendix describes three computer programs to be used in the analysis, design, and evaluation of flight control laws.* Design techniques for analog (continuous-time) and digital (discrete-time) control systems are implemented in Program DIGADAPT using Linear-Quadratic-Gaussian (LQG) Synthesis. Program SCHED computes correlations between flight conditions and control system gains and trim settings, indicating possible relationships for scheduling control functions in the actual system. This program also generates the gain scheduling functions by regression analysis. Program TVHIS is a linear-time-varying simulation of flight motions in the neighborhood of a reference flight path. It is a useful tool for evaluating the performance of control systems alone or in combination with predetermined guidance laws.

Several options for estimation and control logic are provided in DIGADAPT. Control laws which can be generated include dynamic, proportional-integral (PI), and proportional-double integral (PII) command-response controllers. Estimation logic is based upon the Kalman filter, and the sampling interval for digital systems is determined using a state covariance propagation technique. Once system gains have been computed at several flight conditions, the gain scheduling provides open-loop explicit adaptation of the control law.

---

*These programs are described in detail in Ref. 1.

These design programs have been developed for a specific application, the control of a tandem-rotor helicopter. They can be extended to a variety of aircraft configurations, including other VTOL designs, as well as conventional transport, fighter, and general aviation aircraft. Application to reentering spacecraft, missiles, and submarines also is straightforward. The basic routines and subroutines have been programmed to handle systems of arbitrary dimension, so they are generally applicable to a wide variety of vehicle control laws. In each case, details of control effectors and elastic modes must be specified by the designer. Figure A-1 illustrates the data flow for this system of programs.

A.1 PROGRAM DIGADAPT

DIGADAPT is comprised of seven program chapters: the main executive, system matrix computation, sampling interval determination, linear-optimal gain design, calculation of eigenvalues, and time history simulations. These program chapters are discussed below.

Main Executive - The main program reads the data for a given run and calls all subsequent program chapters (Fig. A.1-1). On the first case for a given execution of DIGADAPT, the program reads a header card and then reads data via NAMELIST to override the BLOCK DATA initialization. On subsequent cases of a multiple case run, only the header card is needed. The program terminates when the last case input has been processed. The output from the main executive consists of an abstract of the DIGADAPT program along with a listing of initialization parameters.

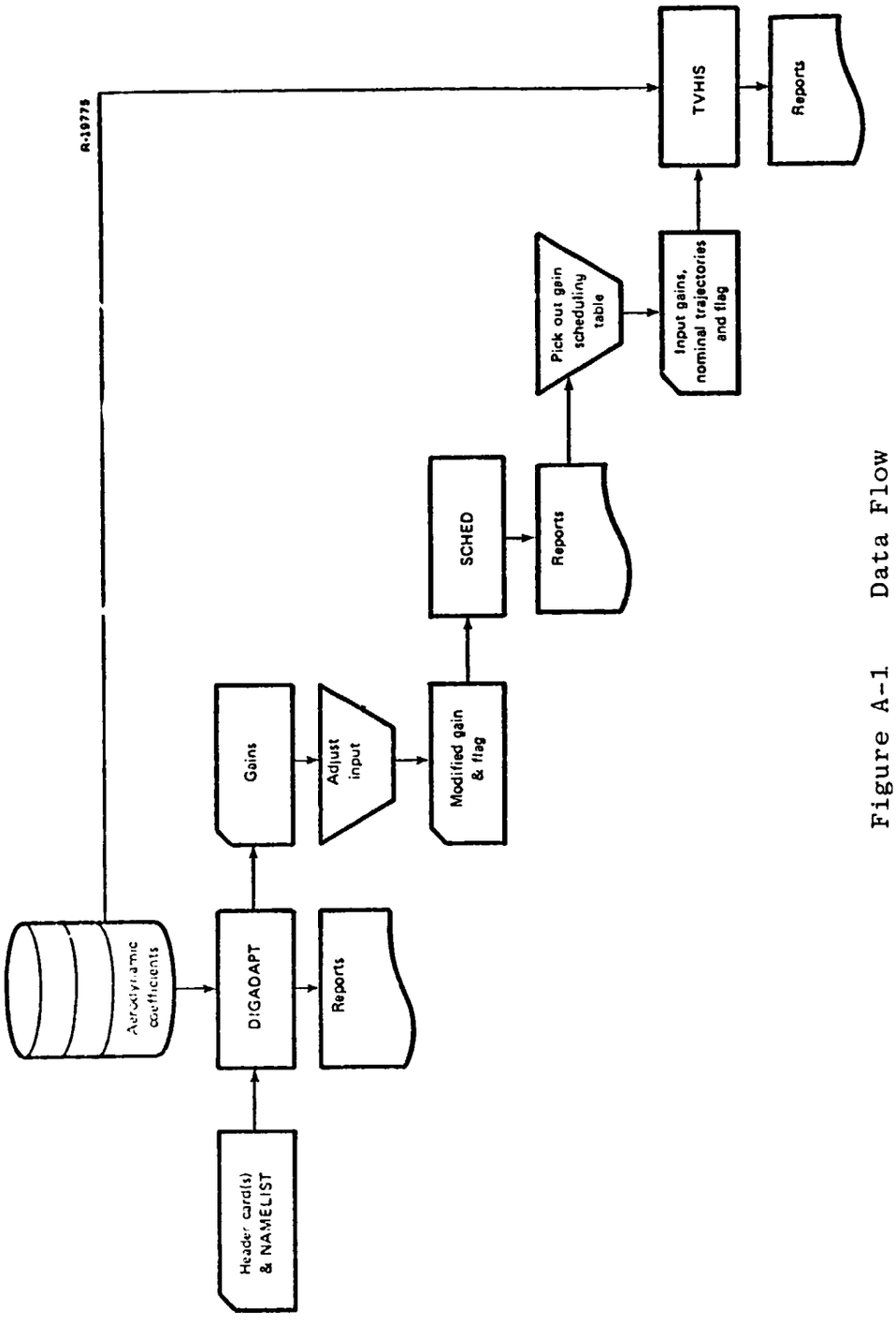

Figure A-1 Data Flow

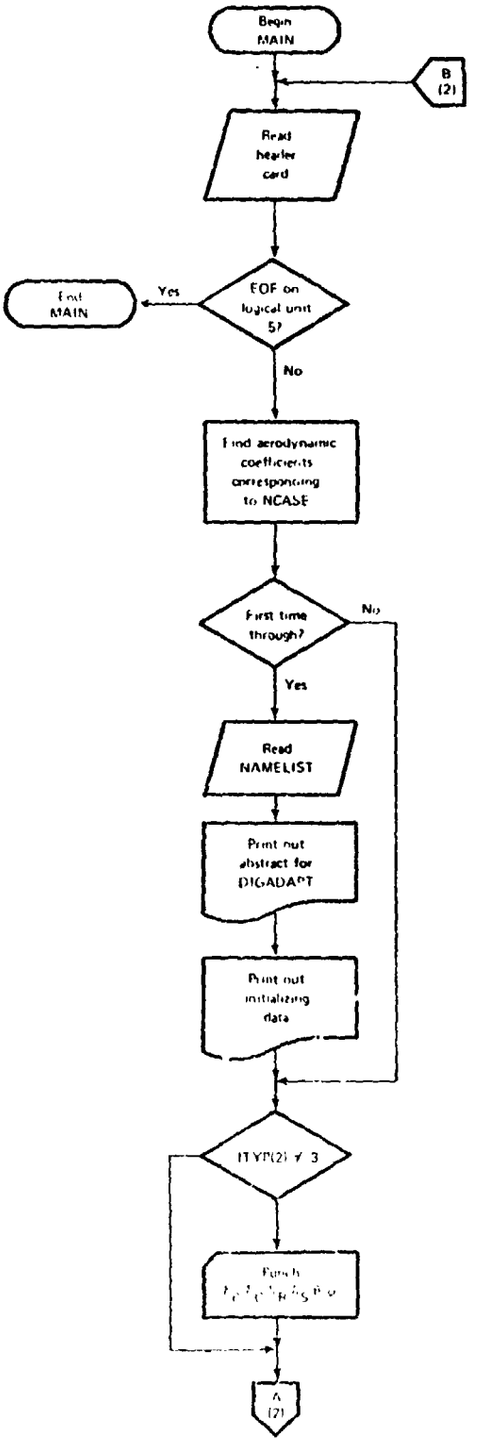

Figure A.1-1 Flowchart of DIGADAPT Executive (Segment 1 of 2)

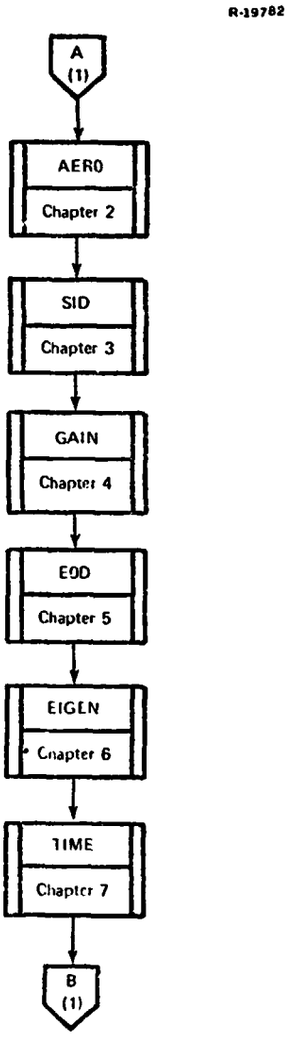

Figure A.1-1 Flowchart of DIGADAPT Executive (Segment 2 of 2)

System Matrix Computation (AERO) - The purpose of subroutine AERO is to place the stored aerodynamic coefficients into the correct positions of the system matrices F and G.

Sampling Interval Determination (SID) - The purpose of subroutine SID is to aid in the determination of the

sampling interval of a continuous linear-time-invariant system. In this program chapter, the state covariance matrix is propagated until an error bound is reached, specifying the sampling interval, as described in Chapter 4.

Linear-Optimal Control Gains (GAIN) - The purpose of this program chapter is to design various linear-optimal controllers. GAIN is divided into continuous and discrete modes of design, with and without integrators.

Estimator - Observer Design (EOD) - EOD is used to perform the estimator-observer design calculations. Steady-state discrete-time Kalman filter gains for a continuous-time system are found.

Eigenvalue Computation (EIGEN) - EIGEN is used to calculate the eigenvalues of various modes of motion of the given vehicle system matrix. The corresponding natural frequencies, damping rates, periods, and times to half amplitude are calculated.

Time History Simulations (TIME) - Subroutine TIME computes the time response of continuous-time and discrete-time systems.

A.2 PROGRAM SCHED

SCHED performs a regression analysis between independent (flight condition) and dependent (gain) variables. The program can perform simple, polynomial, or multiple regressions, and it calculates means and standard deviations of the dependent variables. Other dependent variables can be the F and G matrices, the Kalman Filter gains, and the

trim values at particular flight conditions. Figure A.2-1 illustrates the program flow.

SCHED performs data storage and retrieval for four subroutines from the IBM Scientific Subroutine Package, (GDATA, MULTR, CORRE, ORDER), which produce the regression results (Ref. 83). At the outset, one has the options of performing regressions, or determining correlation coefficients. Next, the program computes simple functions of the independent variable (no change, square, inversion, inversion and square, and square with sign preservation). Other functions can be added if necessary. Any of the independent variables (and functions) can be used to obtain a polynomial regression of order one or two. The process can be repeated for any number of independent variables. In addition, the program has the option of performing a simple regression between the dependent variables. Each dependent variable can be scheduled against other dependent variables. Multiple regressions also are possible. SCHED outputs are correlation coefficients, regression coefficients, and a table of residuals.

A.3 PROGRAM TVHIS

Program TVHIS is designed as a realistic yet efficient aircraft simulation. The simulation is based on a linear-time-varying vehicle model, including actuator and rotor dynamic models. The capability of simulating actuator rate and displacement limits is incorporated.

Program TVHIS includes a guidance subroutine which calculates total velocity commands by summing the nominal velocity and a velocity correction due to crossrange and altitude errors. The control algorithm can be tested in TVHIS with or without the guidance law.

The inputs to program TVHIS consist of the aircraft specifications, the nominal trajectory, the gain scheduling coefficients and executive commands. Figure A.3-1 illustrates the program calling sequence. The program output consists of plots of the vehicle states, controls and other variables of interest.

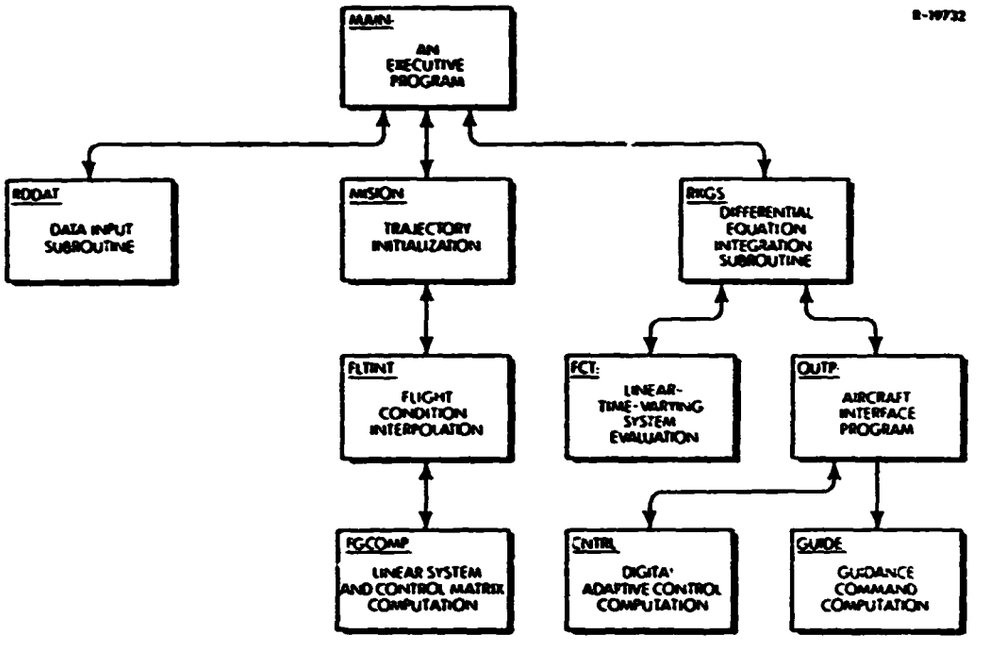

Figure A.3-1 Program TVHIS Subroutine Calling Sequence

APPENDIX B
MATHEMATICAL MODEL OF THE VALT RESEARCH AIRCRAFT

The mathematical model of the VALT Research Aircraft used in this report consists of three parts. The major portion is composed of the rigid-body dynamics (12 states) and control inputs, while the two other parts are rotor dynamics and actuator dynamics. The relationship between these three parts is indicated in Fig. B-1. The lower- and upper-boost actuators are not modeled in this report because of their high bandwidth, but these could be added to the helicopter simulation as required.

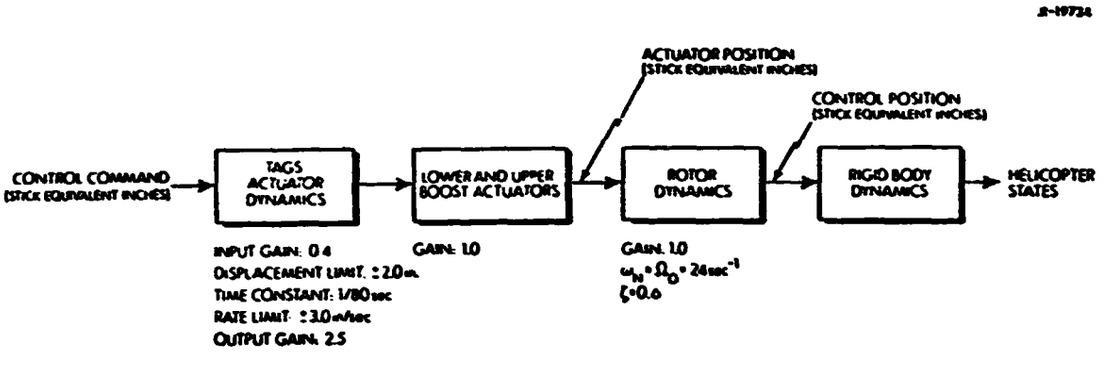

Figure B-1 Organization of the Mathematical Model for the VALT Research Aircraft

The rigid-body dynamics represent the response of the helicopter to small disturbances and inputs in the neighborhood of trim. These aerodynamic and inertial effects are modeled by using standard linear equations of motion, such as those found in Ref. 2. The dimensional stability derivatives at the appropriate flight condition are taken

directly from data tables supplied by the NASA Langley Research Center, as are the static trim states and controls. These data tables consist of sixty dimensional stability derivatives, four static trim control settings and two static trim Euler angles at each flight condition. The sixty dimensional stability derivatives are the partial derivatives of specific forces and moments with respect to motion variables and control deflections. The specific forces (X/m, Y/m, and Z/m) and moments (L/I_x, M/I_y, and N/I_z) are differentiated with respect to the translational velocities (u,v, and w), the rotational velocities (p, q, and r) and the control deflections (δ_B, δ_C, δ_S, and δ_R). (For notational simplicity, the mass and moment-of-inertia divisors are dropped.) For example, the sensitivity of longitudinal specific force to variations in longitudinal velocity is expressed as X_u. A full list of stability derivatives at representative flight conditions is included in Table B-1.

All of the control values are expressed in "CH-47 stick equivalent inches" (except those in the TAGS actuators), i.e., the position of the CH-47 stick that would cause that control value. The stick position limits are -5.0 to +5.0 in. for differential collective, cyclic and differential cyclic displacement, and 0.0 to 10.0 in. for collective displacement. The actuator position is expressed in "TAGS actuator inches," which is 0.4 times the corresponding "CH-47 stick equivalent" position. Consequently, TAGS actuators have position limits of -2.0 to +2.0 in. for differential collective, cyclic and differential cyclic, commands and a range of 0.0 to 4.0 in. for collective commands.

The TAGS actuator model consists of a first-order system with a time constant of 1/80 sec in each of the four control channels. In addition, each TAGS actuator contains a rate limit of 3.0 in./sec and a displacement limit as given above.

TABLE B-1

TYPICAL AERODYNAMIC DATA

	HOVER	60 KT, 1000 FPM UP	60 KT, 1000 FPM DOWN	160 KT, LEVEL FLIGHT
X_u	-0.01993	-0.02307	-0.01807	-0.05614
X_v	0.02903	-0.00011	0.00026	-0.00262
X_w	0.02857	0.03484	0.04039	-0.05575
$X_{\delta B}$	0.11838	0.13104	0.12317	0.12616
$X_{\delta C}$	0.95437	0.36094	0.49068	-1.66085
$X_{\delta S}$	0.00001	-0.00009	0.00008	0.00031
$X_{\delta R}$	0.00000	-0.00011	0.00008	-0.00019
X_p	0.00842	0.00096	0.00152	0.00695
X_q	2.65543	2.43266	2.28595	3.81414
X_r	-0.08009	-0.03151	-0.04746	-0.08738
Y_u	-0.00125	0.00013	-0.00068	0.00300
Y_v	-2.26822	-0.08301	-0.06739	-0.17666
Y_w	0.00248	0.00412	0.00281	0.00340
$Y_{\delta B}$	0.01356	0.04004	0.06322	-0.18189
$Y_{\delta C}$	0.07311	0.06667	0.03340	0.08421
$Y_{\delta S}$	1.17256	1.14416	1.09882	1.49437
$Y_{\delta R}$	-0.05346	-0.03793	-0.06752	-0.04303
Y_p	-1.42261	-1.56230	-2.50848	-2.90554
Y_q	0.00659	0.04349	-0.03710	0.99333
Y_r	-0.15448	-0.16880	-0.26958	-0.31177
Z_u	0.01559	-0.04789	-0.09016	0.02964
Z_v	0.00409	0.00107	0.00702	0.00121
Z_w	-0.26342	-0.58473	-0.51847	-0.52210
$Z_{\delta B}$	0.03577	0.37286	0.59022	-0.00462
$Z_{\delta C}$	-8.36930	-9.69911	-8.93235	-8.03202
$Z_{\delta S}$	-0.00005	0.00165	-0.00105	0.00229
$Z_{\delta r}$	0.00000	-0.00037	0.00028	-0.00009
Z_p	0.03885	-0.06678	0.30291	0.03493
Z_q	0.29197	-0.65483	-1.70958	0.72745
Z_r	0.05558	-0.63779	0.78808	-0.42549
L_u	-0.00037	-0.00012	-0.00051	0.00101
L_v	-0.00625	-0.00627	-0.00476	-0.01072
L_w	0.00041	0.00116	0.00237	0.00513
$L_{\delta B}$	-0.02512	-0.00814	0.01567	-0.04001
$L_{\delta C}$	-0.01348	-0.01506	0.00038	0.03951
$L_{\delta S}$	0.41894	0.41112	0.40075	0.50032
$L_{\delta R}$	-0.14029	-0.13330	-0.13595	-0.17220
L_p	-0.67698	-0.69571	-0.93966	-1.00670
L_q	0.10369	0.04995	-0.04961	0.07261
L_r	-0.04916	-0.05242	-0.07989	-0.06690
M_u	0.00489	-0.00289	-0.00639	-0.00019
M_v	-0.00025	-0.00037	-0.00013	0.00126
M_w	0.00199	0.01517	0.02041	0.01761
$M_{\delta B}$	0.34017	0.39000	0.39728	0.27608
$M_{\delta C}$	0.02221	0.13137	0.18675	0.21187
$M_{\delta S}$	0.00000	-0.00001	0.00003	-0.00005
$M_{\delta r}$	0.00001	-0.00033	0.00025	-0.00041
M_p	0.00047	-0.02774	0.03703	0.00858
M_q	-1.15454	-1.64610	-1.73690	-1.15498
M_r	-0.00444	-0.01806	0.02445	0.00509
N_u	0.00049	0.00025	0.00054	-0.00007
N_v	0.04218	0.00001	-0.00018	-0.00113
N_w	0.00023	0.00005	-0.00106	-0.00357
$N_{\delta B}$	0.04928	0.04299	0.01298	0.00206
$N_{\delta C}$	0.00118	0.01029	-0.00302	-0.02719
$N_{\delta S}$	0.00929	0.01003	0.00777	0.01269
$N_{\delta r}$	0.20620	0.20136	0.19317	0.26262
N_p	0.00054	-0.02288	-0.01351	-0.06381
N_q	-0.16659	-0.14334	-0.01175	0.08280
N_r	-0.04268	-0.04306	-0.03787	-0.07566
δB_0	-0.30816	-0.47876	-1.24186	0.68263
δC_0	4.64881	4.27130	2.21473	5.39970
δS_0	0.23562	0.22403	0.12170	0.21111
δR_0	0.06542	-0.06339	0.17357	-0.57441
θ_0	6.48795	2.96632	3.61291	-3.75758
ϕ_0	-0.49490	-0.40330	-0.15149	-0.54619

The rotor dynamics represent the response of the rotors to changes in actuator position. They are physically caused by the rotor blades pitching and flapping into the new equilibrium position. Rotor dynamics are modeled as linear second-order systems with unity gain. The undamped natural frequency is 24 rad/sec, and the damping ratio is 0.6.

The data is available for all possible combinations of 11 forward speeds (-40 to +160 kt in 20-kt increments), 9 vertical speeds (+2000 ft/min to -2000 ft/min in 500 ft/min increments), and 3 turn rates ($\dot{\psi}$ = ±0.05 rad/sec and $\dot{\psi}$ = 0.0). Interpolation of data between flight conditions makes it possible to find the aerodynamic derivatives and trim controls at any desired flight condition within the CH-47B flight envelope. Four typical sets of dimensional stability derivatives and static trim controls are shown in Table B-1. Note that the subscript "0" indicates static trim and that the static trim pitch and roll Euler angles are measured in degrees.

The perturbation states and controls of the helicopter rigid body motions are given in Table B-2. The first three rows of the system dynamics matrix, F, account for the transformation from body-axis velocity perturbations to earth-axis velocity perturbations, and they include the effects of Euler angle perturbations on this transformation. The first three states do not affect the dynamics of the remaining nine. Table B-3 lists the non-zero elements of the last 9 rows of F and of G.

Rows 7 and 9 of the F and G matrices in Table B-3 are primed to indicate that the roll and yaw moment dimensional stability derivatives have been transformed to account

TABLE B-2

PERTURBATION STATES AND CONTROLS

x_E	Earth x-axis position	[ft]
y_E	Earth y-axis position	[ft]
z_E	Earth z-axis position	[ft]
u	Body x-axis velocity	[fps]
v	Body y-axis velocity	[fps]
w	Body z-axis velocity	[fps]
p	Body x-axis angular rate	[rad/sec]
q	Body y-axis angular rate	[rad/sec]
r	Body z-axis angular rate	[rad/sec]
θ	Pitch Euler angle	[rad]
ϕ	Roll Euler angle	[rad]
ψ	Yaw Euler angle	[rad]
δ_B	Differential collective	[in]
δ_C	Collective	[in]
δ_S	Cyclic	[in]
δ_R	Differential cyclic	[in]

TABLE B-3

F AND G MATRIX COMPONENTS

$F(4,4)$	$= X_u$	$F(7,6)$	$= L'_w$
$F(4,5)$	$= X_v - r_o$	$F(7,7)$	$= L'_p$
$F(4,6)$	$= X_w - q_o$	$F(7,8)$	$= L'_q$
$F(4,7)$	$= X_p$	$F(7,9)$	$= L'_r$
$F(4,8)$	$= X_q - w_o$	$F(8,4)$	$= M_u$
$F(4,9)$	$= X_r + v_o$	$F(8,5)$	$= M_v$
$F(4,10)$	$= -g\cos(\theta_o)$	$F(8,6)$	$= M_w$
$F(5,4)$	$= Y_u = r_o$	$F(8,7)$	$= M_p + r_o(I_z - I_x)/I_y$
$F(5,5)$	$= Y_v$	$F(8,8)$	$= M_q$
$F(5,6)$	$= Y_w + p_o$	$F(8,9)$	$= M_r + p_o(I_z - I_x)/I_y$
$F(5,7)$	$= Y_p + w_o$	$F(9,4)$	$= N'_u$
$F(5,8)$	$= Y_q$	$F(9,5)$	$= N'_v$
$F(5,9)$	$= Y_r - u_o$	$F(9,6)$	$= N'_w$
$F(5,10)$	$= -g\sin(\theta_o)\sin(\phi_o)$	$F(9,7)$	$= N'_p$
$F(5,11)$	$= g\cos(\theta_o)\cos(\phi_o)$	$F(9,8)$	$= N'_q$
$F(6,4)$	$= Z_u + q_o$	$F(9,9)$	$= N'_r$
$F(6,5)$	$= Z_v - p_o$	$F(10,8)$	$= \cos(\phi_o)$
$F(6,6)$	$= Z_w$	$F(10,9)$	$= -\sin(\phi_o)$
$F(6,7)$	$= Z_p - v_o$	$F(10,11)$	$= -\dot{\psi}_o\cos(\theta_o)$
$F(6,8)$	$= Z_q + u_o$	$F(11,7)$	$= 1.0$
$F(6,9)$	$= Z_r$	$F(11,8)$	$= \sin(\phi_o)\tan(\theta_o)$
$F(6,10)$	$= -g\sin(\theta_o)\cos(\phi_o)$	$F(11,9)$	$= \tan(\theta_o)\cos(\phi_o)$
$F(6,11)$	$= -g\cos(\theta_o)\sin(\phi_o)$	$F(11,10)$	$= \dot{\psi}_o\sec(\theta_o)$
$F(7,4)$	$= L'_u$	$F(12,8)$	$= \sin(\phi_o)/\cos(\theta_o)$
$F(7,5)$	$= L'_v$	$F(12,9)$	$= \cos(\phi_o)/\cos(\theta_o)$
		$F(12,10)$	$= \dot{\psi}_o\tan(\theta_o)$
$G(4,1)$	$= X_{\delta B}$	$G(7,1)$	$= L'_{\delta B}$
$G(4,2)$	$= X_{\delta C}$	$G(7,2)$	$= L'_{\delta C}$
$G(4,3)$	$= X_{\delta S}$	$G(7,3)$	$= L'_{\delta S}$
$G(4,4)$	$= X_{\delta R}$	$G(7,4)$	$= L'_{\delta R}$
$G(5,1)$	$= Y_{\delta B}$	$G(8,1)$	$= M_{\delta B}$
$G(5,2)$	$= Y_{\delta C}$	$G(8,2)$	$= M_{\delta C}$
$G(5,3)$	$= Y_{\delta S}$	$G(8,3)$	$= M_{\delta S}$
$G(5,4)$	$= Y_{\delta R}$	$G(8,4)$	$= M_{\delta R}$
$G(6,1)$	$= Z_{\delta B}$	$G(9,1)$	$= N'_{\delta B}$
$G(6,2)$	$= Z_{\delta C}$	$G(9,2)$	$= N'_{\delta C}$
$G(6,3)$	$= Z_{\delta S}$	$G(9,3)$	$= N'_{\delta S}$
$G(6,4)$	$= Z_{\delta R}$	$G(9,4)$	$= N'_{\delta R}$

for the inertial effects in these terms. The F and G matrices with the primed rows, F' and G', are found by forming the F and G matrices with rows 7 and 9 as given in Table B-4, and then premultiplying as in Eqs. B-1 and B-2:

$$F' = H\,F \tag{B-1}$$

$$G' = H\,G \tag{B-2}$$

where

$$H = \left[\begin{array}{c|c|c} I(6x6) & 0 & 0 \\ \hline 0 & H_1 & 0 \\ \hline 0 & 0 & I(3x3) \end{array}\right] \tag{B-3}$$

and

$$H_1 = \begin{bmatrix} \dfrac{I_x I_z}{\left[I_x I_z - I_{xz}^2\right]} & 0 & \dfrac{I_z I_{xz}}{\left[I_x I_z - I_{xz}^2\right]} \\ 0 & 1 & 0 \\ \dfrac{I_x I_{xz}}{\left[I_x I_z - I_{xz}^2\right]} & 0 & \dfrac{I_x I_z}{\left[I_x I_z - I_{xz}^2\right]} \end{bmatrix} \tag{B-4}$$

TABLE B-4

ROW 7 AND 9 COMPONENTS

$F(7,4) = L_u$

$F(7,5) = L_v$

$F(7,6) = L_w$

$F(7,7) = L_p$

$F(7,8) = L_q + r_o(I_y - I_z)/I_x$

$F(7,9) = L_r + q_o(I_y - I_z)/I_x$

$F(9,4) = N_u$

$F(9,5) = N_v$

$F(9,6) = N_w$

$F(9,7) = N_p + q_o(I_x - I_y)/I_z$

$F(9,8) = N_q + p_o(I_x - I_y)/I_z$

$F(9,9) = N_r$

$G(7,1) = L\delta_B$

$G(7,2) = L\delta_C$

$G(7,3) = L\delta_S$

$G(7,4) = L\delta_R$

$G(9,1) = N\delta_B$

$G(9,2) = N\delta_C$

$G(9,3) = N\delta_S$

$G(9,4) = N\delta_R$

REFERENCES

1. Nalbandian, J.Y., "User's Manual for Flight Control Design Programs," The Analytic Sciences Corporation, TR-640-2, Reading, Mass., 24 September, 1975.

2. Seckel, E., Stability and Control of Airplanes and Helicopters, Academic Press, New York, 1964.

3. Helicopter Guidance and Control Systems, AGARD-CP-86-71, Neuilly-sur-Seine, September 1971.

4. Konig, H., and Schmitt, H., "Optimization of Automatic Flight Control Concepts for Light Helicopters Witn All-Weather Capability," in Ref. 3, pp. 2-1 to 2-13.

5. Wellern, W., "Some Problems in the Development of an Automatic Flight Control System for Light Helicopters," in Ref. 3, pp. 7-1 to 7-15.

6. Sweeting, D., "Some Design Aspects of the Stability Augmentation System for the WG13 Rigid Rotor Helicopter," in Ref. 3, pp. 15-1 to 15-12.

7. Dukes, T.A., "Helicopter IFR Flight Path Control System," in Ref. 3, pp. 18-1 to 18-10.

8. Gallagher, J.T., et al., "A Model-Following Variable Stability System for the NASA ARC X-14B," Journal of Aircraft, Vol. 9, No. 7, July 1972, pp. 461 to 469.

9. Kelly, J.R., et al., "A Manual-Control Approach to Development of VTOL Automatic Landing Technology," American Helicopter Society Preprint No. 761, May 1973.

10. Deardorff, J.C., et al., "Flight Test Development of the Tactical Aircraft Guidance System," American Helicopter Society Preprint No. 761, May 1973.

11. Gossett, T.D. and Corliss, L.D., "A Quadratic Performance Index for a VTOL Aircraft Prefilter Model Reference Attitude Control System," NASA TN D-6231, Washington, March 1971.

REFERENCES (Continued)

12. Osder, S.S., et al., "Navigation, Guidance, and Control Systems for V/STOL Aircraft," Sperry Technology, Vol. 1, No. 3, 1973, pp. 34 to 41.

13. Gaul, J.W., et al., "Application of Optimal Control Theory to VTOL Flight Control System Design," AFFDL-TR-67-102, September 1967.

14. Murphy, R.D. and Narendra, K.S., "Design of Helicopter Stabilization Systems Using Optimal Control Theory," Journal of Aircraft, Vol. 6, No. 2, March-April 1969, pp. 129 to 136.

15. Hall, W.E., Jr. and Bryson, A.E., Jr., "Inclusion of Rotor Dynamics in Controller Design for Helicopters," Journal of Aircraft, Vol. 10, No. 4, April 1973, pp. 200 to 206.

16. Carlock, G.W. and Sage, A.P., "VTOL Flight-Control System Design Using Sensitivity Analysis," IEEE Transactions on Aerospace and Electronic Systems, Vol. AES-11, No. 2, March 1975, pp. 155 to 161.

17. Gupta, N.K. and Bryson, A.E., Jr., "Automatic Control of a Helicopter With a Hanging Load," Stanford University Report SUDAAR-459, June 1973.

18. Davis, J.M., "Stability and Control Analysis -- Model CH-47B, CH-47C," Boeing Report 114-AD-603, Philadelphia, November 1966.

19. Anon., "Tactical Aircraft Guidance System Advanced Development Program," USAAMRDL TR-71-57, Ft. Eustis, Va. (prepared by CAE Electronics, Ltd., Montreal) February 1972.

20. Anon., "Tactical Aircraft Guidance System Advanced Development Program Flight Test Phase Report," Vols. I and II, USAAMRDL TR-73-89A,B, Ft. Eustis, VA, (prepared by CAE Electronics Ltd., Boeing Vertol Co., and IBM Federal Systems Division), April 1974.

21. Anon., Fundamentals of Helicopter Stability and Control, Boeing Vertol Report No. R242, Bureau of Naval Weapons Contract No. NOW 60-0469-f, February 1961.

REFERENCES (Continued)

22. Hoffman, W.C., Zvara, J., Bryson, A.E., Jr., and Ham, N.D., "An Automatic Guidance Concept for VTOL Aircraft," AIAA Paper No. 70-1035, New York, August 1970.

23. Lee, H.Q., McLean, J.D, and Erzberger, H., "Guidance and Control Techniques for Automated Air Traffic Control," Journal of Aircraft, Vol. 9, No. 7, July 1972, pp. 490 to 496.

24. Erzberger, H. and Pecsvaradi, T., "4-D Guidance System Design With Application to STOL Air Traffic Control." Proceedings of the 1972 Joint Automatic Control Conference, Stanford, August 1972.

25. Holley, W.E. and Bryson, A.E., Jr., "Multi-Input, Multi-Output Regulator Design for Constant Disturbances and Non-Zero Set Points With Application to Automatic landing in a Crosswind," Stanford University Report SUDAAR - 465, August 1973.

26. Price, C.F., and Koenigsberg, W.D., "Adaptive Control and Guidance for Tactical Missiles," Vols., I and II, TR-170-1, The Analytic Sciences Corp., 30 June 1970.

27. DeRusso, P.M., Roy, R.J., and Close, C.M., State Variables for Engineers, J. Wiley & Sons, New York, 1965.

28. Patel, R.V., "On the Computation of Numerators of Transfer Functions of Linear Systems," IEEE Transactions on Automatic Control, Vol. AC-18, August 1973, pp. 400 to 401.

29. Ragazzini, J.R., and Franklin, G.F., Sampled-Data Control Systems, McGraw-Hill Book Company, New York, 1958.

30. Tou, J.T., Digital and Sampled-Data Control Systems, McGraw-Hill Book Company, New York, 1959.

31. Horowitz, I.M., Synthesis of Feedback Systems, Academic Press, New York, 1963.

32. Horowitz, I.M., "Optimum Linear Adaptive Design of Dominant-Type Systems With Large Parameter Variations," IEEE Trans. on Automatic Control, June 1961, Vol. AC-14, No. 3.

REFERENCES (Continued)

33. McRuer, D., Ashkenas, I., and Graham, D., "Aircraft Dynamics and Automatic Control, Princeton University Press, Princeton, 1973.

34. Bryson, A.E., Jr., and Ho, Y.C., Applied Optimal Control, Blaisdell Publishing Company, Waltham, Massachusetts, 1969.

35. Sage, A.P., Optimum Systems Control, Prentice-Hall, Inc., Englewood Cliffs, New Jersey, 1968.

36. Gelb, A., Ed., Applied Optimal Estimation, MIT Press, Cambridge, Massachusetts, 1974.

37. Luenberger, D.G., "An Introduction to Observers," IEEE Transactions on Automatic Control, Vol. AC-16, No. 6, December 1971, pp. 596 to 602.

38. Kalman, R.E., "When is a Linear Control System Optimal?", Trans. of the ASME, Journal of Basic Engineering, Vol. 86, 1964.

39. Kreindler, E., "On Performance Sensitivity of Optimal Control Systems," Int. Journal of Control, Vol. 15, No. 3, March 1972.

40. Tiroshi, I., and Elliott, J.R., "A 'Type One' Servo Explicit Model Following Adaptive Scheme," AIAA Paper No. 73-852, New York. August 1973.

41. Stengel, R.F., "Digital Flight Control Design Using Implicit Model Following," AIAA Paper No. 73-841, New York, August 1973.

42. Tyler, J.S., Jr. "The Characteristics of Model-Following Systems as Synthesized by Optimal Control," IEEE Trans. on Automatic Control, Vol. AC-9, October 1964.

43. Anon., "Parameter Estimation Techniques and Applications in Aircraft Flight Testing," NASA TN D-7647, Washington, April 1974.

44 Brown, C.M., Jr., and Monopoli, V.R., "Linear System Identifications: The Application of Lion's Identification S · me to a Third Order System with

REFERENCES (Continued)

Noisy Input-Output Measurements," 1973 Allerton Conference, University of Illinois.

45. Jazwinski, A.H., Stochastic Process and Filtering Theory, Academic Press, New York, 1970.

46. Maybeck, P.S., "Combined State and Parameter Estimation for On-Line Applications," Ph.D. Thesis, Massachusetts Institute of Technology, February 1972.

47. Landau, I.D., and Courtiol, D.B., "Adaptive Model Following Systems for Flight Control and Simulation," Journal of Aircraft, Vol. 9, No. 9, September 1972.

48. Gilbart, J.W., Monopoli, R.V., and Price, C.F., Improved Convergence and Increased Flexibility in the Design of Model Reference Adaptive Control Systems," 1970 IEEE Symposium on Adaptive Processes and Control, The University of Texas, 7-9 December 1970.

49. Staff of the Flight Research Center, "Experience With the X-15 Adaptive Flight Control System," NASA TN D-6208, Washington, March 1971.

50. Stear, E.B., and Gregory, P.C., "Adaptive Flight Control-Past, Present, and Future," Flight Control Laboratory, Aeronautical Systems Division, Air Force Systems Command Report N63-10008.

51. Ehlers, H.L., and Smyth, R.K., "Survey of Adaptive Control Applications to Aerospace Vehicles," AIAA Paper No. 68-970, New York, August 1968.

52. Buscher, R.G., "Self-Adaptive Flight Control without Test Signals," Space/Aeronautics, December 1961.

53. Gelb, A., and Vander Velde, W.E., Multiple-Input Describing Functions and Nonlinear System Design, McGraw-Hill Book Company, 1968.

54. Thompson, M.O., and Welsh, J.R., "Flight Test Experience with Adaptive Control Systems," Advanced Control System Concepts, AGARD-CP-58, Neuilly-sur-Seine, January 1970, pp. 139 to 1 7.

REFERENCES (Continued)

55. Anderson, B.D.O. and Moore, J.B., Linear Optimal Control, Prentice Hall, New Jersey, 1971.

56. Brockett, R.W., Finite Dimensional Linear Systems, J. Wiley and Sons, New York, 1970.

57. Perkins, W.R. and Cruz, J.B., "Feedback Properties of Linear Regulators," IEEE Trans. Automatic Control, Vol. AC-16, No. 6, December 1971, pp. 659 to 664.

58. Kwakernaak, H. and Sivan, R., Linear Optimal Control Systems, Wiley-Interscience, New York, 1972.

59. Athans, M., "On the Design of P-I-D controllers Using Optimal Linear Regulator Theory," Automatica, Vol. 7, 1971.

60. Power, H.M., and Porter, B., "Necessary Conditions for Controllability of Multivariable Systems Incorporating Integral Feedback," Electron. Letters, Vol. 6, No. 25, 1970.

61. Sandell, N. and Athans, M., "Design of a Generalized P-I-D Controller by Optimal Linear Control Theory," Decision and Control Sciences Group of the M.I.T. Electronic Systems Laboratory, 1972.

62. Young, P.C. and Willems, J.C., "An Approach to the Linear Multivariate Servomechanism Problem," International Journal of Control, Vol. 15, No. 5, May 1972.

63. Dorato, P. and Levis, A.H., "Optimal Linear Regulators: The Discrete Time Case," IEEE Trans. Automatic Control, Vol. AC-16, No. 6, December 1971, pp. 613 to 620.

64. Smith, C.L., Digital Computer Process Control, International Textbook Co., Pennsylvania, 1972.

65. Berman, H. and Gran, R., "Design Principles for Digital Autopilot Synthesis," Journal of Aircraft, Vol. 11, No. 7, July 1974, pp. 414 to 422.

66. Hall, W.E., Jr. and Bryson, A.E., Jr., "Synthesis of Hover Autopilots for Rotary-Wing VTOL Aircraft," Guidance and Control Lab., Stanford University, SUDAAR-446, June 1972.

REFERENCES (Continued)

67. Higgins, W.T., "A Comparison of Complementary and Kalman Filtering," IEEE Trans. Aerospace and Electronic Sy., Vol. AES-11, No. 3, May 1975, pp. 321 to 325.

68. Hall, B.A., and Trainor, W.V., et. al., "Modular Digital Missile Guidance System Study," Raytheon Co. Missile Systems Division, Report No. BR-8C73, June 1973.

69. Kleinman, D.L., "On an Iterative Technique for Riccati Equation Computation," IEEE Trans Automatic Control (Corresp.), Vol. AC-13, February 1968, pp. 114 to 115.

70. Kleinman, D.L., "Stabilizing a Discrete, Constant, Linear System With Application to Iterative Methods for Solving the Riccati Equation," IEEE Trans. Automatric Control (Corresp.), Vol. AC-13, June 1974, pp. 252 to 254.

71. Kleinman, D.L., "An Easy Way to Stabilize a Linear Constant System," IEEE Trans. Automatic Control (Corresp.), Vol. AC-15, December 1970, pp. 692.

72. Lee, T.H., Adams, G.E. and Gaines, W.M., Computer Process Control: Modeling and Optimization, John Wiley & Sons, Inc., New York, 1968.

73. Kalman, R.E., "A New Approach to Linear Filtering and Predication Problems," Trans. ASME, J. Basic Eng., Vol. 82, March 1960, pp. 34 to 45.

74. Kalman, R.E. and Bucy, R.S., "New Results in Linear Filtering and Prediction Theory," Trans. ASME, J. Basic Eng., Vol. 83, December 1961, pp. 95 to 107.

75. Athans, M., "The Role and Use of the LQG Problem in Control System Design," IEEE Transactions on Automatic Control. Vol. AC-16, No. 6, December 1971, pp. 529 to 552.

76. Brown, R.G., "Integrated Navigation Systems and Kalman Filtering: A Perspective," Navigation, Vol. 19, No. 4, Winter 1972-1973, pp. 355 to 362.

77. Rhodes, I.B., Dynamic Systems, Control and Optimization, to be published.

REFERENCES (Continued)

78. Sandell, N., Jr., and Athans, M., "On Type-L Multivariable Linear Systems," Automatica, Vol. 9, No. 1, January 1973, pp. 131 to 136.

79. Davison, E.J., "Comments on Optimal Control of the Linear Regulator With Constant Disturbances," IEEE Trans. on Automatic Control, Vol. AC-15, April 1970, pp. 264.

80. Schwartz, M., Information Transmission, Modulation, and Noise, McGraw-Hill, New York, 1970.

81. Mrazek, J.G. and Rubertus, D.P., "Considerations in the Design of a Digital Flight Control Function for a High Performance Aircraft," NAECON '74 Record, Dayton, June 1974.

82. Powell, D. and Katz, P., "Sample Rate Selection for Aircraft Digital Control," AIAA, Paper No. 74-885, New York, August 1974.

83. Anon., "System/360 Scientific Subroutine Package, Version III, Programmer's Manual," GH20-0205-4, IBM Corporation, August 1970.